

WAVE IMPACT FORCES ON A HORIZONTAL CYLINDER

by

Sundar Prasad

B.Eng., University of Delhi, 1986

M.Tech., Indian Institute of Technology, Madras, 1988

A THESIS SUBMITTED IN PARTIAL FULFILLMENT OF
THE REQUIREMENTS FOR THE DEGREE OF
DOCTOR OF PHILOSOPHY

in

THE FACULTY OF GRADUATE STUDIES
DEPARTMENT OF CIVIL ENGINEERING

We accept this thesis as conforming
to the required standard

THE UNIVERSITY OF BRITISH COLUMBIA

July 1994

© Sundar Prasad, 1994

In presenting this thesis in partial fulfilment of the requirements for an advanced degree at the University of British Columbia, I agree that the Library shall make it freely available for reference and study. I further agree that permission for extensive copying of this thesis for scholarly purposes may be granted by the Head of the Department or by his or her representatives. It is understood that copying or publication of this thesis for financial gain shall not be allowed without my written permission.

Department of Civil Engineering
The University of British Columbia
2324 Main Mall
Vancouver, B.C. V6T 1Z4
Canada

JULY 18, 1994

Abstract

Impact forces due to wave slamming on structural elements of offshore platforms have been known to reach very high magnitudes and contribute to accelerated fatigue of members and joints due to the resulting dynamic response. Results of previously reported theoretical analyses vary by as much as 100% with regards to the peak value of the slamming coefficient, and experimental verification of these results has been difficult due to the significant amount of scatter in the data reported by several investigators. The present thesis investigates the slamming force due to non-breaking and breaking wave impact on a fixed horizontal circular cylinder located near the still water level.

A numerical model which is based on a combination of slamming, buoyancy, drag, and inertia force components has been developed in order to predict the time history of the vertical force on a fixed horizontal cylinder in waves. The model has also been modified to include the effects of dynamic response and cylinder inclination. In addition, an approach based on an impulse coefficient is proposed for estimating the maximum dynamic response of an elastically supported cylinder.

Experiments have been carried out in the wave flume of the Hydraulics Laboratory of the Department of Civil Engineering at the University of British Columbia in order to measure the vertical force on a horizontal test cylinder for a range of regular (non-breaking) wave conditions and cylinder elevations. The data has been analyzed to obtain the corresponding slamming and impulse coefficients, as well as the impulse rise-time and duration. Corrections to the measured coefficients to account for buoyancy, dynamic response and free surface slope are indicated. The coefficients exhibit a considerable degree of scatter, even when the various corrections are taken into account. However, the degree of scatter of the impulse coefficient is notably less than that

of the slamming coefficient. The results for the maximum slamming coefficient C_{s0} agree with those of recent studies which observe that C_{s0} may be closer to 2π than the generally accepted value of π . A limited number of tests have also been performed for the case of an inclined cylinder, and the effect of tilt on the maximum slamming force and rise-time is examined.

The numerical model for the rigid horizontal cylinder has been used to determine the variation of the maximum non-dimensional vertical force in regular waves as a function of the governing non-dimensional parameters. Statistics of the maximum force obtained from simulations in random waves are compared to corresponding results derived from available analytical expressions, and indicate reasonable agreement in the case of a narrow-band spectrum. The temporal variation of the vertical force predicted by the numerical model is also compared to that of the measured force in regular non-breaking waves. In general, the agreement is quite good for both a horizontal and inclined cylinder. The application of the numerical model to an estimation of a member's response in a prototype situation is illustrated. It is seen that the approach based on the impulse coefficient is relatively simple, and appears to be effective in estimating maximum responses for conditions under which the method is applicable.

Experiments have also been carried out in order to measure the impact forces due to plunging wave action on a horizontal circular cylinder located near the still water level. The vertical and horizontal components of the impact force on the cylinder due to a single plunging breaker have been measured for three elevations of the cylinder, and six locations of wave breaking relative to the horizontal location of the cylinder. A video record of the impact process has been used to estimate the kinematics of the wave and plunging jet prior to impact. The force measurements have been corrected for the dynamic response of the cylinder, and analyzed to obtain slamming coefficients and rise times. It is observed that the cylinder elevation and the wave breaking location relative to the cylinder have a significant effect on the peak impact force. The magnitude of the impact force due to a breaking wave is 4 to 20 times greater than that due to a regular non-breaking wave of similar height and period. In addition to the fluid velocity, the curvature of the water surface has a noticeable effect on the peak impact force.

Table of Contents

Abstract	ii
Table of Contents	iv
List of Tables	viii
List of Figures	ix
List of Principal Symbols	xv
Acknowledgements	xix
INTRODUCTION	1
1.1 General	1
1.2 Literature Review	4
1.2.1 Wave Force on a Horizontal Cylinder in the Splash Zone	4
1.2.2 Forces on Horizontal Cylinders due to Breaking Waves	10
1.3 Scope of Present Investigation	11
1.3.1 Numerical Modelling	12
1.3.2 Experiments on Slamming in Regular Waves	13
1.3.3 Experiments on Slamming in Breaking Waves	13
THEORETICAL FORMULATION	15
2.1 Dimensional Analysis	15

2.2	Hydrodynamic Force on a Rigid Horizontal Cylinder	18
2.2.1	Buoyancy Force	18
2.2.2	Slamming Force	19
2.2.3	Inertia Force	25
2.2.4	Drag Force.....	26
2.2.5	Combination of Force Components	27
2.3	Hydrodynamic Force on an Elastically Supported Horizontal Cylinder	30
2.3.1	Response of an SDOF System to Impact Loading	30
2.3.2	Cylinder Response to Wave Impact Loading	35
2.3.3	Modelling Slamming as an Impulse.....	39
2.4	Slamming Force on an Inclined Cylinder	42
2.5	Water Particle Kinematics in Waves	45
2.5.1	Regular Waves	45
2.5.2	Effects of Free Surface Slope.....	46
2.5.3	Random Waves	48
2.6	Computational Considerations	50
EXPERIMENTAL STUDY		53
3.1	Test Facilities	53
3.1.1	Wave Flume	54
3.1.2	Wave Generation.....	54
3.1.3	Cylinder model	56
3.1.4	Data Acquisition and Control	58

3.2	Dynamic Characteristics of the Test Cylinder	61
3.3	Horizontal Cylinder in Non-Breaking Waves	63
3.4	Data Analysis	65
3.4.1	Noise Filtering Techniques	65
3.4.2	Determination of the Instant of Slamming	67
3.4.3	Analysis of Wave and Force Records	69
3.5	Inclined Cylinder in Non-Breaking Waves	71
3.6	Horizontal Cylinder in Breaking Waves	72
3.6.1	Generation of the Breaking Wave	72
3.6.2	Measurement of Force and Breaking Wave Profiles	73
3.6.3	Analysis of Breaking Wave Impact Force	74
RESULTS AND DISCUSSION		78
4.1	Slamming Forces in Non-Breaking Waves	79
4.1.1	Raw Data from Horizontal Cylinder Experiments	79
4.1.2	Slamming Coefficients from Horizontal Cylinder Experiments.....	82
4.1.3	Impulse Coefficients from Horizontal Cylinder Experiments	86
4.1.4	Tests on Inclined Cylinder	88
4.2	Numerical Simulation	89
4.2.1	Regular Waves	90
4.2.2	Random waves	92
4.2.3	Comparison with Experimental Observations	95
4.2.4	Practical Application	98

4.3	Breaking Wave Impact.....	100
4.3.1	Cylinder Elevation I	101
4.3.2	Cylinder Elevation II	102
4.3.3	Cylinder Elevation III	104
4.3.4	Slamming Coefficients due to Breaking Wave Impact	105
CONCLUSIONS		107
5.1	Wave Slamming on a Horizontal Cylinder	107
5.1.1	Experimental Study	107
5.1.2	Numerical Modelling	110
5.2	Plunging Wave Impact on a Horizontal Cylinder	111
5.3	Recommendations	112
References		115
Tables		120
Figures		127

List of Tables

- 1.1 Peak slamming coefficient C_{s0} reported in earlier experimental studies.
- 4.1 Properties of regular waves used in slamming experiments.
- 4.2 Peak slamming coefficients and related parameters estimated from multiple slamming events in a regular wave test. $T = 1.5$ sec, $H = 18.4$ cm, $h = 0.5$ cm.
- 4.3 Summary of test conditions and principal results from slamming tests in regular waves.
- 4.4 Summary of impulse coefficients and related parameters estimated from slamming tests in regular waves.
- 4.5 Summary of observations from impact tests in breaking waves.

List of Figures

- 1.1 Photograph of non-breaking wave impact on horizontal test cylinder.
- 1.2 Photograph of plunging wave impact on horizontal test cylinder.
- 1.3 Comparison of analytical and experimental results for the slamming coefficient C_s as a function of relative submergence s/a (Greenhow and Li, 1987). 1, experiments of Campbell and Weynberg (1980); 2, ellipse theory of Fabula (1957); 3, von Karman (1929); 4, semi-Wagner; 5, Wagner's flat plate approach (1932); 6, Taylor (1930); 7, semi-von Karman; 8, semi-Wagner; 9, Wagner's exact body approach.
- 2.1 Definition sketch for a fixed cylinder.
- 2.2 Regimes of cylinder submergence.
- 2.3 Variation of dimensionless buoyancy force with relative submergence s/a .
- 2.4 Variation of C_s with submergence s/a - selected results. - - - - -, von Karman; — - - —, Wagner; —————, Taylor; — - - - -, Campbell and Weynberg; -----, Miao; — — —, Armand and Cointe.
- 2.5 Variation of inertia coefficient C_m with relative submergence s/a . —————, Taylor's solution ($C_{m0} = 2.0$); — — —, approximations for $C_{m0} = 2.0$ and 1.7.
- 2.6 Sketch of free surface elevation and corresponding vertical wave force over one wave cycle. —————, model I; — — —, model II. (a) complete submergence, (b) partial submergence.
- 2.7 Proposed variation of combined $C_s + C_d$ coefficient with relative submergence s/a for $C_d = 0.8$. —————, $C_s + C_d$; - - - - -, Taylor's solution for C_s .
- 2.8 Definition sketch of a single degree of freedom (SDOF) system.
- 2.9 Representation of an idealized impact force with $T_d/T_r = 1.0$.

- 2.10 Response F_t/F_o of SDOF system to an applied impulsive force with different values of T_r/T_n . ———, applied force and response for impact with $T_d/T_r = 1.0$; - - - - -, applied force and response for impact with $T_d/T_r = 2.0$. (a) $T_r/T_n = 0.2$, (b) $T_r/T_n = 2.0$.
- 2.11 Dynamic amplification factor F_{to}/F_o and relative rise time T_t/T_r as functions of T_r/T_n for an applied impulsive force with different values of T_d/T_r . ———, $\zeta = 0$; - - - - -, $\zeta = 0.02$; — - — - -, $\zeta = 0.05$. (a) and (b), $T_d/T_r = 1.0$; (c) and (d), $T_d/T_r = 2.0$.
- 2.12 Definition sketch for dynamically responding cylinder.
- 2.13 Definition sketch for the computation of the impulse coefficient. ———, combined impulsive and residual force; - - - - -, residual force.
- 2.14 Definition sketch for wave impact on an inclined circular cylinder.
- 2.15 Definition sketch for impact due to a sloping water surface.
- 2.16 Variation of the free surface slope correction factors C'_s/C_s (·····) and C_i^*/C_i (— - — -) for an experimentally measured wave (————) of period $T = 1.1$ sec, and height $H = 17$ cm.
- 3.1 Photograph of wave flume in the Hydraulics Laboratory.
- 3.2 Photograph of computer controlled wave generator.
- 3.3 (a) Photograph of test cylinder assembly, (b) Sketch of the experimental setup.
- 3.4 Block diagram of wave generation and data acquisition equipment.
- 3.5 Record of the vertical force due to free vibration of the cylinder induced by an applied step force of -19.6 N (2 kg).
- 3.6 Spectral density of free vibration record in Fig. 3.5.
- 3.7 Early stages of the measured vertical force on the test cylinder due to a typical wave slamming event. •, indicates individual force samples.
- 3.8 Time histories of free surface elevation and vertical force during a slamming event. $T = 1.4$ sec, $H = 22.8$ cm, $h = 0.5$ cm.

- 3.9 Time series of vertical force (·····) and corresponding local variance (————) used to detect the onset of slamming.
- 3.10 Flow chart showing steps in analysis of experimental data.
- 3.11 Frame of video record defining the wave breaking location x_b .
- 3.12 Record of the horizontal force due to free vibration of the cylinder induced by an applied step force of 9.8 N (1 kg).
- 3.13 Spectral density of free vibration record in Fig. 3.12.
- 3.14 Comparison of corrected horizontal force (————), with recorded horizontal force (·····), and applied step force (— — — —).
- 3.15 Impact force on the horizontal test cylinder due to plunging wave ($h = 8.7$ cm, $x_b = 36$ cm). (a) —————, recorded vertical force component; ·····, recorded horizontal force component. (b) —————, recorded vertical force component; ·····, corrected horizontal force component.
- 4.1 Time histories of the free surface elevation and vertical force over a 10 sec duration for a wave of low steepness. $T = 1.8$ sec, $H = 13.5$ cm, $h = 0.5$ cm.
- 4.2 Time histories of the free surface elevation and vertical force over a 10 sec duration for a wave of medium steepness. $T = 1.5$ sec, $H = 18.4$ cm, $h = 0.5$ cm.
- 4.3 Time histories of the free surface elevation and vertical force over a 10 sec duration for a wave of large steepness. $T = 1.1$ sec, $H = 17$ cm, $h = 0.5$ cm.
- 4.4 Time histories of free surface elevation and vertical force during a slamming event. $T = 1.1$ sec, $H = 17.5$ cm, $h = 0.5$ cm.
- 4.5 Time histories of free surface elevation and vertical force during a slamming event. $T = 1.4$ sec, $H = 16.5$ cm, $h = 0.5$ cm.
- 4.6 Time histories of free surface elevation and vertical force during a slamming event. $T = 1.6$ sec, $H = 16.8$ cm, $h = 0.5$ cm.
- 4.7 Time histories of free surface elevation and vertical force during a slamming event. $T = 1.5$ sec, $H = 13.9$ cm, $h = 0.5$ cm.

- 4.8 Time histories of free surface elevation and vertical force during a slamming event. $T = 1.5$ sec, $H = 18.4$ cm, $h = 0.5$ cm.
- 4.9 Time histories of free surface elevation and vertical force during a slamming event. $T = 1.5$ sec, $H = 22.9$ cm, $h = 0.5$ cm.
- 4.10 Time histories of free surface elevation and vertical force during a slamming event. $T = 1.5$ sec, $H = 18.4$ cm, $h = 4.5$ cm.
- 4.11 Time histories of free surface elevation and vertical force during a slamming event. $T = 1.5$ sec, $H = 18.4$ cm, $h = -4.5$ cm.
- 4.12 Correction factors for peak slamming force and rise time as a function of the observed rise time ratio T_t/T_n . ———, F_{10}/F_0 ; - - - - -, T_t/T_r .
- 4.13 Probability density histogram of C_{s0} (·····) based on data collected from entire set of experiments. ———, log-normal probability density.
- 4.14 Probability density histogram of C_{s0}'' (·····) based on data collected from entire set of experiments. ———, log-normal probability density.
- 4.15 Probability density histogram of C_i^* based on data collected from entire set of experiments.
- 4.16 Comparison of slamming force time histories for different cylinder inclinations, $T = 1.2$ sec, $H = 19.3$ cm. ———, $\theta = 0^\circ$; ·····, $\theta = 4.8^\circ$; — - — - , $\theta = 9.6^\circ$.
- 4.17 Comparison of slamming force time histories for different cylinder inclinations, $T = 1.8$ sec, $H = 17.8$ cm. ———, $\theta = 0^\circ$; ·····, $\theta = 4.8^\circ$; — - — - , $\theta = 9.6^\circ$.
- 4.18 Time histories of free surface elevation and simulated vertical force for $\omega^2 a/g = 0.05$, $\omega^2 H/g = 0.6$, and different cylinder elevations. ———, Model I; — - — - , Model II.
- 4.19 Distribution of the non-dimensional maximum vertical force as a function of cylinder elevation and $\omega^2 H/g$. ———, Model I; - - - - -, Model II. (a) $\omega^2 a/g = 0.005$, (b) $\omega^2 a/g = 0.01$, (c) $\omega^2 a/g = 0.05$, (d) $\omega^2 a/g = 0.1$.
- 4.20 Variation of the non-dimensional maximum vertical force as a function of $\omega^2 a/g$ for different values of $\omega^2 H/g$. ———, Model I; - - - - -, Model II.

- 4.21 Spectral density (————) and corresponding amplitude spectrum (Δ) with $H_s = 10\text{m}$, and $T_p = 14.3$ sec, used in the numerical simulation of random waves. (a) Narrow-band spectrum, (b) Pierson-Moskowitz spectrum.
- 4.22 Segment of numerically simulated time series of (a) free surface elevation and, (b) non-dimensional vertical force for a narrow-band spectrum.
- 4.23 Segment of numerically simulated time series of (a) free surface elevation and, (b) non-dimensional vertical force for a two-parameter Pierson-Moskowitz spectrum.
- 4.24 Comparison of probability density of force maxima on a horizontal cylinder located at $h = 0$. — — — —, analytical prediction (Isaacson and Subbiah, 1990); —————, numerical simulation, method A; —————, numerical simulation, method B. (a) narrow-band spectrum, (b) two-parameter Pierson-Moskowitz spectrum.
- 4.25 Comparison of vertical force predicted by rigid cylinder model (————) with the measured force (······). $T = 1.2$ sec, $H = 15.2$ cm, $h = 0.5$ cm.
- 4.26 Early stages of slamming force predicted by dynamic cylinder model (————) compared with rigid cylinder model estimate (— — — —) and the measured force (······). $T = 1.2$ sec, $H = 15.2$ cm, $h = 0.5$ cm, $T_n = 290$ Hz, $T_r = 20$ msec.
- 4.27 Comparison of vertical force predicted by rigid cylinder model (————) with the measured force (······). $T = 1.5$ sec, $H = 18.4$ cm, $h = 0.5$ cm.
- 4.28 Photograph showing mass of water suspended from test cylinder after recession of incident wave.
- 4.29 Comparison of vertical force predicted by rigid cylinder model (————) with the measured force (······). $T = 1.5$ sec, $H = 18.4$ cm, $h = -4.5$ cm.
- 4.30 Early stages of slamming force predicted by dynamic cylinder model (————) compared with the measured force (······). $T = 1.5$ sec, $H = 18.4$ cm, $h = -4.5$ cm, $T_n = 290$ Hz, $T_r = 18$ msec.
- 4.31 Comparison of force on inclined cylinder predicted by numerical model (————) with the measured force (······). $T = 1.8$ sec, $H = 17.8$ cm, $\theta = 4.8^\circ$.
- 4.32 Comparison of force on inclined cylinder predicted by numerical model (————) with the measured force (······). $T = 1.2$ sec, $H = 15.2$ cm, $\theta = 9.6^\circ$.

- 4.33 Predicted time history of the vertical force on the cylinder for the example application. —————, total force on rigid cylinder; - - - - -, buoyancy force component; — - — - -, mid-span cylinder response for fixed end condition; ·········, mid-span cylinder response for pinned-end condition.
- 4.34 Sequence of video frames showing plunging wave impact on horizontal test cylinder. $h = 4.7$ cm, $x_b = 25.5$ cm.
- 4.35 Digitized profiles of plunging wave in the vicinity of the horizontal test cylinder. $h = 4.7$ cm, $x_b = 36$ cm.
- 4.36 Time histories of recorded vertical force (—————) and corrected horizontal force (········) on horizontal test cylinder due to breaking wave impact. $h = 4.7$ cm, $x_b = 25.5$ cm.
- 4.37 Sequence of video frames showing plunging wave impact on horizontal test cylinder. $h = 8.7$ cm, $x_b = -3.5$ cm.
- 4.38 Sequence of video frames showing plunging wave impact on horizontal test cylinder. $h = 8.7$ cm, $x_b = 25.5$ cm.
- 4.39 Digitized profiles of plunging wave in the vicinity of the horizontal test cylinder. $h = 8.7$ cm, $x_b = 25.5$ cm.
- 4.40 Time histories of recorded vertical force (—————) and corrected horizontal force (········) on horizontal test cylinder due to breaking wave impact. $h = 8.7$ cm, $x_b = 25.5$ cm.
- 4.41 Sequence of video frames showing plunging wave impact on horizontal test cylinder. $h = 8.7$ cm, $x_b = 49$ cm.
- 4.42 Sequence of video frames showing plunging wave impact on horizontal test cylinder. $h = 12.7$ cm, $x_b = 25.5$ cm.
- 4.43 Digitized profiles of plunging wave in the vicinity of the horizontal test cylinder. $h = 12.7$ cm, $x_b = 17$ cm.
- 4.44 Time histories of recorded vertical force (—————) and corrected horizontal force (········) on horizontal test cylinder due to breaking wave impact. $h = 12.7$ cm, $x_b = 25.5$ cm.

List of Principal Symbols

a	cylinder radius.
A_c	cross-section area of the cylinder.
A_i	immersed area of cylinder cross-section.
α	angle subtended at the cylinder axis by the water surface.
c	wave celerity.
C	damping coefficient of single-degree-of-freedom system.
C_d	drag coefficient.
C_i	impulse coefficient.
C_i^*	impulse coefficient corrected for effects of free surface slope.
C_m	inertia coefficient.
C_{m0}	inertia coefficient for large value of cylinder submergence.
C_s	slamming coefficient.
C_{s0}	maximum value of the slamming coefficient.
C'_{s0}	maximum slamming coefficient corrected for effects of free surface slope.
C''_{s0}	maximum slamming coefficient corrected for effects of free surface slope and buoyancy.
C^*_{s0}	maximum slamming coefficient corrected for effects of free surface slope, buoyancy, and dynamic amplification.
C_{s+d}	combined slamming and drag coefficient.
d	water depth.

D	diameter of cylinder.
δ	angle of inclination of the free surface during impact.
f_0	peak frequency of wave spectrum.
\hat{F}	maximum value of the vertical force due to non-breaking wave impact.
F_b	buoyancy force.
F_d	drag force.
F_i	inertia force.
F_o	maximum value of the applied force.
Fr	Froude number.
F_s	slamming force.
F_t	measured force.
F_{to}	maximum value of the measured force.
\hat{F}_r	maximum value of the resultant force due to breaking wave impact.
\hat{F}_x	maximum value of the horizontal force component due to breaking wave impact.
\hat{F}_z	maximum value of the vertical force component due to breaking wave impact.
ϕ	direction of the maximum resultant force due to breaking wave impact.
g	gravitational acceleration.
h	elevation of cylinder measured from the still water level.
H	wave height.
H_s	significant wave height of wave spectrum.
η	free surface elevation.
$\dot{\eta}$	vertical velocity of free surface.

$\ddot{\eta}$	vertical acceleration of free surface.
k	wave number.
K	stiffness of single-degree-of-freedom system.
L	cylinder length.
m	added mass.
M	mass of single-degree-of-freedom system.
ν	kinematic viscosity of water.
θ	inclination of the cylinder axis.
r	displacement response of the cylinder.
\dot{r}	velocity of the cylinder.
\ddot{r}	acceleration of the cylinder.
Re	Reynolds number.
r_w	radius of curvature of the breaking wave-front prior to impact.
ρ	density of water.
s	cylinder submergence.
$S_{\eta}(f)$	spectral density of free surface elevation.
T	wave period.
T_d	decay-time of the applied force.
T_i	duration of the impulse.
T_n	natural period of vibration.
T_r	rise-time of the applied force.
T_t	rise-time of the measured force.

- v_n water particle velocity normal to the free surface.
- ω angular frequency of non-breaking wave .
- ω_d damped natural angular frequency of vibration.
- ω_n natural angular frequency of vibration.
- x_b location of wave breaking.
- ζ non-dimensional damping ratio.

Acknowledgements

The author would like to acknowledge several individuals who assisted in various phases of the project. The author would like to thank his research advisor, Dr. Michael Isaacson, for his help and encouragement throughout the course of this study, and his invaluable insight and critical appraisal during the preparation of the thesis. The expertise of Mr. Kurt Nielsen, Mr. Ron Dolling and Mr. John Wong of the Department of Civil Engineering, in assembling the test cylinder, and setting up the instrumentation and signal cables is gratefully acknowledged. The advice of Mr. Dan Pelletier of the Hydraulics Laboratory at the National Research Council of Canada in the customization of the real-time control and data acquisition systems and software for the purposes of this study is deeply appreciated. The author would also like to thank his colleagues and friends for their help and support.

Financial support in the form of a University of British Columbia Graduate Fellowship and a research assistantship from the Department of Civil Engineering is gratefully acknowledged.

Chapter 1

INTRODUCTION

1.1 General

The phenomenon of hydrodynamic impact or ‘slamming’ manifests itself in many forms. These usually involve either a rapidly moving body entering a water surface, or a moving water surface striking a body. One of the earliest reported studies of this phenomenon was prompted by the occurrence of impact on the floats of seaplanes during landing (von Karman, 1929). A similar type of impact can cause snatch loading of crane hoisting cables during the installation of subsea modules. Ships are subjected to impact when the bottom of the vessel hits the water with a high velocity, or when oncoming waves slam the bow above the waterline. Wave slamming can occur on the underside of the deck between the two hulls of a catamaran or semisubmersible platform, and on horizontal piers and docks. Members of jacket platforms which would normally not be situated in the splash zone during the operating life of the structure may still be subjected to slamming forces during towing and launch operations. In addition to impact due to regular waves on horizontal or near-horizontal structures near the water surface, vertical structures such as the columns of offshore platforms and sea-walls are also subjected to impact loads due to breaking waves. Sloshing of fluid inside a storage tank can lead to very high slamming pressures on the walls of the tank.

Wave impact forces are highly dynamic and are characterized by their large magnitudes and short durations. In cases where the entire length of a horizontal bracing is simultaneously struck by a rising wave, the impact forces can be much higher than the hydrodynamic force experienced

by the member when it is fully submerged and subjected to a flow of similar velocity. Such forces can cause local damage to structural elements. Even in cases where impact forces may not be larger than the static loads on the structural element, dynamic stresses due to impact and the possibility of increased fatigue stressing of joints due to such loads may contribute to structural failure and consequently determine design criteria for the member.

A common case of hydrodynamic impact corresponds to a horizontal cylinder located near the water surface which undergoes intermittent submergence due to incident waves, and attention is focussed on this particular case. An example of wave slamming on a horizontal cylinder is illustrated in Figure 1.1. Some of the readily observable features of this phenomenon are the significant distortion of the free surface adjacent to the cylinder and air entrainment due to the effects of the accompanying splash. The wave slamming force on a horizontal member is generally taken as proportional to the square of the water impact velocity and involves the use of a slamming coefficient C_s which varies with cylinder submergence. The usual approach to estimating wave slamming force on horizontal members is given by:

$$F_s = \frac{1}{2} C_s \rho D w^2 \quad (1.1)$$

where ρ is the fluid density, F_s is the wave slamming force per unit length of the member, C_s is a slamming coefficient, w is the water particle velocity normal to the surface of the member and D is the diameter of the member. In fact C_s may vary with time after the onset of slamming, and its maximum value, which occurs after a very short rise-time subsequent to water-cylinder contact, is of primary interest in design. This value is designated here as C_{s0} . A number of theoretical and experimental studies have been carried out in order to establish appropriate values of the slamming coefficient for the common case of a horizontal circular cylinder. Experimental observations have yielded values of C_{s0} which exhibit a considerable degree of scatter, ranging from about 1.0 to 6.4, although a value of π is generally recommended in design codes (Miller, 1977, Sarpkaya, 1978, Campbell and Weynberg, 1980, Miao, 1988). There are a number of difficulties in carrying out experimental studies on slamming. The very short durations involved

make it a highly dynamic process, and the response of the member due to the load can change the magnitude of the impact. Furthermore, the rise-time associated with the slam force depends on various factors such as air entrainment, compressibility, cylinder roughness, cylinder inclination and motion of the cylinder. The variability of the rise-time can cause a significant variation in the dynamic amplification of the impact force resulting in appreciable scatter in the observed force.

A theoretical basis for the slamming force formulation has also been investigated by several authors. During the early stages of impact, the slamming force is associated with the rate of change of momentum of the fluid, and can thereby be expressed in terms of the added mass of the partially submerged member. However, there are a number of complications in extending such a development beyond the initial stages of impact, due in part to water level variations around the partially submerged member.

In addition to the slamming force, other force components also contribute significantly to the vertical force after the onset of impact. These are the buoyancy force, an inertia force associated with the fluid's acceleration, and a drag force component associated with flow separation effects and dependent on the fluid's velocity. The coefficients used to determine the magnitude of the inertia and drag forces may vary with the extent of submergence, the cylinder size and the water particle kinematics.

Figure 1.2 illustrates a typical plunging wave impact on a horizontal test cylinder. The mechanism of plunging wave impact is quite different from a regular wave impact, with larger horizontal water particle velocities, increased air entrainment and turbulence. It is well known that breaking wave impact on a structure in the splash zone gives rise to higher local pressures and forces in comparison to the impact due to non-breaking waves of comparable height and period. A theoretical or numerical treatment of the dynamics of breaking waves and their interaction with structures presents significant difficulties due to the strongly nonlinear nature of the problem which is essentially a transient two-phase turbulent process. Carefully conducted

experiments are a source of useful data that can aid in understanding the breaking wave impact process, and help to estimate forces that could occur under similar conditions in the field.

The objectives of the present study are to examine existing models of wave slamming on a slender horizontal cylinder, conduct experimental investigations to observe the impact force on an instrumented cylinder subjected to non-breaking regular waves and compare the observed data with previously reported values. It is intended that the influence of variables such as cylinder elevation and orientation with respect to the water surface will also be studied in the experiments. This thesis also presents the results from an experimental study of the forces due to the impact of a plunging or deep-water breaking wave on a slender horizontal cylinder. The intent of these objectives is to help verify or suggest modifications to analytical models in order to enable designers to predict more accurately operating and design conditions to which an offshore structure and its structural components may be exposed.

1.2 Literature Review

1.2.1 Wave Force on a Horizontal Cylinder in the Splash Zone

Theoretical Studies

The impact force on a horizontal cylinder due to a rising water surface is given by the rate of change of momentum of this flow, which in turn depends on the properties of the cylinder's vertical added mass. The added mass varies with the level of submergence up to the stage when the cylinder is submerged 3 to 4 diameters below the free surface. This quantity also depends on the frequency associated with the flow, and in the case of impulsive flows, it is the infinite frequency limit that is of interest in determining the magnitude of the impact force. An expression for the added mass may be developed on the basis of potential flow theory. Taylor (1930) solved the above problem using a conformal mapping technique and thereby derived a closed-form expression for the vertical added mass of a partially submerged cylinder. Numerical techniques such as a source distribution method (Garrison, 1978) and the Frank close-fit method

(Faltinsen et al., 1977) may also be used to provide estimates of the added mass. These methods yield a C_{s0} value of about 3.1.

Several theoretical techniques have been used to modify the above approaches in order to account for the local deformation of the free-surface near the cylinder during the early stages of penetration. Wagner (1931) and Fabula (1957) proposed modifications, which include a 'wetting correction', in order to account for the piled up water when calculating the wetted width of the body, and a 'drag correction' which include quadratic terms in the expression for pressure. Both approaches yield a C_{s0} value of 2π , although Fabula's (1957) technique predicts a more rapid decay of the slamming force with submergence. Detailed numerical and experimental results concerning the water impact of a circular cylinder were given in an EPRI report (1978) based on research connected with boiling water reactors. The four numerical models described in this report correspond to; an explicit Lagrangian method (Gross, EPRI 1978), a boundary integral method (Geers, EPRI 1978), a finite element method (Marcal, EPRI 1978), and an incompressible Eulerian fluid method (Nichols and Hirt, EPRI 1978). The results of three of the numerical simulations were in good agreement with the experimental results and indicated a C_{s0} value of 2π .

Cointe and Armand (1987) used the method of matched asymptotic expansions to solve the boundary value problem for water-cylinder impact. They too conclude that C_{s0} is 2π rather than π as given by some of the earlier theories. Greenhow and Li (1987) reviewed a number of different formulations for evaluating the added mass of a horizontal circular cylinder moving near the free surface and conclude that the effects of free surface deformation on the slamming coefficient is significant and must be included in any theoretical treatment. They recommend two different methods to calculate the added mass for small and large cylinder submergence respectively which both indicate a C_{s0} value of $4\pi/3$. Figure 1.3 shows a comparison of C_s predicted by a number of theoretical and experimental results presented in their paper wherein the abscissa corresponds to the relative submergence of the cylinder and is denoted by s/a where s

and a are the submergence and cylinder radius respectively. It is seen that there are considerable differences between the various models, especially with respect to the value of C_{so} .

In addition to the impact force on the cylinder, other components contributing to the vertical force include the buoyancy, drag and inertia forces. The buoyancy force at any instant is associated with the submerged volume of the cylinder and can be readily determined. In contrast, the drag force due to separation effects cannot be easily quantified, especially during the initial stages of submergence. In addition, both the drag and impact force components are functions of the square of the relative velocity between the water and the cylinder, and hence cannot be differentiated in any experimental data. The inertia force component is a function of the relative water acceleration and is a function of the added mass of the cylinder.

The vertical hydrodynamic force on a horizontal cylinder subjected to wave slamming may be simulated numerically by the use of a suitable model which incorporates the four force components identified above without introducing abrupt changes in either the magnitude or rate of change of the total hydrodynamic force. Although the rise-time of the slamming force is not important if the cylinder is assumed rigid, a realistic situation will involve an elastically supported structure which will respond to the applied force. The magnitude of response depends on the dynamic characteristics of the structure and determines the force transmitted by the structure to its supports. Since the rise-time of the slamming force is not accounted for in the current added mass models it is usually introduced by increasing the slamming force linearly from zero at the instant of impact, to a peak value after a specified delay.

The Morison equation (Morison et al., 1950) is a numerical model for estimating fluid forces on a fixed body in an unsteady flow. It is based on the assumption that the force can be given by the linear superposition of a drag force which is dependent on the square of the velocity and acts on the projected frontal area, and an inertia force which is dependent on the acceleration and the volumetric displacement. The formula estimates the magnitude of these force components by using two parameters known respectively as the drag coefficient C_d and the inertia coefficient

C_m , whose values must be chosen mainly on the basis of empirical data. In the case of surface piercing vertical cylinders, the flow regime over which this formulation is applicable generally corresponds to the case where the diameter of the cylinder is less than 20% of the wavelength.

A modified form of the Morison equation which includes the buoyancy force component on a partially submerged horizontal cylinder was proposed by Dixon et al. (1979a) and expressions to describe the force spectra in narrow-band and wide-band Gaussian seas were also formulated (Dixon et al., 1979b, Easson et al., 1981). These studies neglect the effect of slamming forces on the cylinder. Kaplan and Silbert (1976) described a mathematical model for slamming on a rigid cylinder and presented impact force statistics from a simulation in random waves. Miller (1977) developed a computer model for the vertical wave force on an instrumented cylinder which behaves as a two degree-of-freedom dynamic system. The slamming force was assumed to increase linearly to a peak value over a specified rise-time, and to decrease linearly to zero over a specified decay-time. The drag and inertia components were assumed to act only when the cylinder was fully submerged and were computed from constant drag and inertia coefficients. The resulting combined force exhibits discontinuities in magnitude and the buoyancy component had to be reduced when the water surface was receding in order to avoid an unrealistic dynamic response during that stage.

Arhan et al. (1978) modelled the response of a horizontal elastic cylinder with clamped ends subjected to wave slamming. They assumed that the slamming force rises instantaneously upon impact to a peak value and then decreases linearly to zero when the cylinder was partially submerged by half its radius. The maximum deflection and stress on the cylinder were computed by numerically integrating the equation of motion. Miao (1990) computed the bending stress on a flexible cylinder subjected to water impact. The hydrodynamic force was computed as the sum of the momentum, drag and buoyancy forces and the equation of motion was solved for various end fixity conditions using the mode superposition approach. Computed bending stresses compared well with his experimental observations of slamming on a cylinder driven into still water. Isaacson and Subbiah (1990) considered the application of a suitable

force formulation to the case of a cylinder subjected to wave impact in random waves. By restricting the analysis to force maxima in waves with narrow-band spectra, they were able to provide analytical results for the probabilistic properties of the force maxima.

Experimental Studies

Experimental investigations on slamming have been conducted in a variety of ways. Different methods have been used to induce slamming -- a model cylinder driven at a constant velocity through a still water surface; a fixed horizontal cylinder subjected to slamming forces in a U-Tube; or a fixed horizontal cylinder subjected to slamming forces due to waves. In addition, field observations of impact forces have included measurements from a horizontal brace of the Ocean Test Structure (Kaplan, 1979), and full-scale slamming on British Petroleum's West Sole platform (Miller, 1980).

Dalton and Nash (1976) conducted tests to observe impact forces on a horizontal cylinder in a wave tank and reported values of C_{s0} ranging from 1.0 to 4.5. However, they report that these values are derived from force peaks that occur after the cylinder has been submerged by 8 to 12 diameters and observed that significant wave forces associated with regular wave trains are not of an impulsive nature, which indicates that their measurements may not have included the early stages of the slamming force.

Miller (1977) identified loading regimes associated with wave slamming and described slamming tests on a cylinder in waves. Tests conducted for 3 cylinder elevations indicated an average value of C_{s0} of 3.6, although there was appreciable scatter in the results. Miller concluded that this was consistent with the theoretical value of π and attributed the observed higher value to dynamic amplification effects. The effects of the slamming force rise-time on the dynamic response were illustrated by simulating numerically the vertical wave force using a dynamic analogue and comparing the computed force traces with the experimental records.

Faltinsen et al. (1977) conducted experiments with elastic horizontal circular cylinders that were driven with constant velocity through an initially calm free surface and reported C_{s0} values ranging from 4.1 to 6.4. The experimental data was compared with results from a dynamic model which computed the slam load from potential theory, and it was observed that theoretical predictions were lower than the experimental values. Sarpkaya (1978) measured the hydrodynamic force on a cylinder subjected to slamming in a U-Tube. He observed that the dynamic characteristics of the measuring system play a significant role in the observed impact force. He reported experimental observations for C_{s0} as 3.17 ± 0.05 , and so concluded that C_{s0} was essentially equal to the theoretical value of π .

Campbell and Weynberg (1980) measured spanwise and circumferential pressures in addition to the vertical force on horizontal and inclined cylinders driven through a still water surface. They observed that the slamming force was predominant for tests involving a Froude number ($Fr = w/\sqrt{gD}$, where w is the fluid velocity, g is the gravitational acceleration, and D is the cylinder diameter) higher than 0.6. They also indicated that the slamming force was masked by the dynamic response of the force transducer and that scatter in the observed data was the result of variable rise-times that were sensitive to small variations in the slope of the cylinder. It was also noted that drips from the cylinder had a significant effect on the response. They summarized their results by proposing an empirical equation that relates the slamming coefficient and cylinder submergence, and which uses $C_{s0} = 5.15$. This equation is independent of the Froude number and was not corrected for buoyancy effects.

Kaplan (1979) presented results from an analysis of impact force data collected from a horizontal brace of the Ocean Test Structure in the Gulf of Mexico. The force measurements were recorded at a time interval of 0.1 sec. after being low-pass filtered using a 3 Hz cutoff frequency. The low sampling rate and high degree of filtering make it difficult to perform a quantitative analysis of the slamming force characteristics. The data was analyzed by comparing it to a synthetically generated slamming force record that had also been low-pass filtered at 3 Hz. C_{s0} values between 1.88 and 5.11 with a mean value of 2.98 were reported.

Miller (1980) reviewed the results of slamming tests done by various investigators who used a variety of experimental techniques. The reported values of C_{s0} varied from 0.4 to 6.9. Miao (1990) reported results from experiments on a 1.52 m long flexible horizontal cylinder which was driven at a constant velocity through a stationary water surface. He proposed an expression for the variation of C_s with submergence which indicates a C_{s0} value of 6.1, and also concluded that for typical truss members in heavy seas, the dynamic amplification of the response and the induced stresses ranged from 0.3 to 0.6 due to the short impulse times observed in the experiments. Table 1.1 provides a summary of results from earlier experimental studies on slamming forces on a horizontal cylinder.

1.2.2 Forces on Horizontal Cylinders due to Breaking Waves

Studies of breaking wave impact on structures are especially pertinent to the design of offshore platforms since these may give rise to the largest environmental loads during the operating life of the structure. The complex nature of the problem and the difficulty of obtaining precise control over wave breaking in laboratory experiments has been the main reason for the scarcity of literature available on this topic. Impact forces due to a breaking wave have been observed to be two to four times larger than those due to non-breaking wave of comparable amplitude, and the force rise-time is significantly smaller.

Studies of wave impact forces due to breaking waves have largely related to vertical piles and walls, and vertical plates (e.g. Kjeldsen and Myrhaug, 1979, Kjeldsen, 1981, Sawaragi and Nochino, 1984, Kjeldsen et al., 1986, Basco and Niedzwecki, 1989, Chan and Melville, 1989, and Zhou et al., 1991). These have shown that the most severe impulsive forces are due to plunging waves and that these act at elevations above the mean water level. Measurements of impact pressures on vertical plates due to plunging waves have shown that impulsive pressures may occur over a range of horizontal locations relative to the plunging wave location (Chan and Melville, 1988, Chan et al. 1991a, Chan et al. 1991b, and Zhou et al., 1991). These pressures

may be spread over a vertical distance of about half the wave height, and peak impulsive pressures range from $3\rho c^2$ to $30\rho c^2$, where c is the wave celerity.

Vinje and Brevig (1981) used a numerical time-stepping procedure to simulate breaking wave impact on a horizontal cylinder and a vertical wall. Since their study did not include the effects of air entrainment, it is not possible to apply their model to most situations where the dynamics of trapped air plays an important role in determining the impact pressures. Based on experiments with vertical and inclined plates, Kjeldsen (1981) observed that the magnitude of shock pressures is a function of the steepness of the wave-front, and that a plate tilted forward at 45° to the horizontal which is struck from below experienced larger impact pressures than a vertical plate. He also noted that scaling laboratory results to prototype conditions may be difficult due to the differing magnitudes of air entrainment in the wave crest for the two cases. Easson and Greated (1984) performed experiments with plunging wave impact on a horizontal cylinder located at different elevations above the still water level. They observed that the peak impact force and rise-time changes with the vertical location of the cylinder. The influence of the measuring system's dynamic response on the impact force was not examined in their study. In a recent work related to plunging wave impact on a large horizontal cylinder, Chan (1993) measured pressures on the upwave face of the cylinder for different cylinder elevations and wave breaking locations relative to the cylinder axis. Peak pressures were found to vary from $4\rho c^2$ to $33\rho c^2$ and were affected by factors such as the local wave profile and the amount of entrained air.

1.3 Scope of Present Investigation

This study addresses three areas relating to wave impact on a slender horizontal cylinder located near the still water level which undergoes intermittent submergence in the presence of waves. These are, (i) Development of a numerical model to estimate the vertical force on a horizontal cylinder using available expressions for the different force components, and proposing modifications to include the effect of dynamic response and cylinder inclination; (ii) Conducting

slamming experiments in regular non-breaking waves in order to determine C_{s0} as well as related parameters, and to compare the experimental observations with the estimates of the numerical model; and (iii) Conducting experiments on slamming due to a plunging wave in order to determine the maximum impact force and corresponding slamming coefficients.

1.3.1 Numerical Modelling

The vertical component of the wave force on a horizontal cylinder located in the zone of intermittent submergence is made up of four components: the impact force, the inertia force, the drag force and the buoyancy force. Although previous studies have dealt with the nature of these components, a numerical model which involves a combination of these components in a consistent manner and in varying ways is presented in this investigation. The simulation of the total wave force variation without slope discontinuities during the different stages of cylinder submergence is one of the main features of this model.

In addition to estimating the applied force on a rigid cylinder in regular and random waves, the model is suitably modified so as to predict the applied and transmitted force in the case of a cylinder that responds dynamically to the applied force. This dynamic force model includes the effect of the finite rise-time associated with the slamming force. The effect of cylinder inclination on the hydrodynamic force is also examined.

Results from regular wave simulations are used to obtain typical traces of force variation in a wave cycle for various cylinder locations, and to also provide the non-dimensional peak force in a wave cycle as a function of the other governing non-dimensional variables of the problem. In the case of random waves, statistics of peak force due to waves synthesised from narrow-band and Pierson-Moskowitz spectra are computed and compared with corresponding results derived from closed-form expressions.

1.3.2 Experiments on Slamming in Regular Waves

As already indicated, alternative theoretical predictions of the slamming coefficient show significant differences, especially with respect to C_{s0} . In the offshore industry, the recommended value of C_{s0} is 3.5 although several theories indicate that C_{s0} is as high as 6.3 (2π). Since both safety and economy are primary concerns in design, it is important that either value of C_{s0} be backed up by reliable experimental observations.

The value of the peak slamming coefficient C_{s0} and related parameters have been determined by conducting experiments on a slender horizontal cylinder subjected to slamming in regular non-breaking waves. Tests are conducted for a range of wave heights and periods, and different cylinder elevations. The vertical force on the cylinder and the water surface elevation at the cylinder location have been measured and subsequently analyzed to provide the value of the peak slamming coefficient immediately after impact, the impact force rise-time, as well as other relevant parameters. A new approach to the prediction of wave slamming effects is developed. This is based on an impulse coefficient C_i , and values of C_i are obtained from the experimental records. Experimental tests which are intended to examine the effect of cylinder inclination on the slamming force are also presented.

The experimental force records are compared with the predictions of the alternative numerical models for the cases of a rigid horizontal cylinder, a dynamically responding horizontal cylinder, and a rigid inclined cylinder. Suitable modifications to theory are suggested so that results from the numerical model more closely match the experimental data.

1.3.3 Experiments on Slamming in Breaking Waves

The test cylinder has also been used to study the impact force due to a breaking wave, which is also referred to as a 'plunging' wave in this study. Impact pressures due to a plunging wave are known to be the highest among the various types of breaking waves. A single breaking wave is generated using a frequency and amplitude modulated wave packet consisting of 30 prescribed

sinusoidal components. Tests are carried out for 3 cylinder elevations, and 6 different locations of wave breaking. Both the horizontal and vertical components of the impact force are measured, and are analyzed to determine the resultant peak force and the corresponding rise-time. A video record of the wave impact is used to estimate the kinematics of the wave-front prior to impact. The video records are also used to examine the influence of the geometry of the plunging wave on the characteristics of the impact force. The impact forces are compared with those obtained due to a regular non-breaking wave impact. The issues governing the applicability of these results to large scale situations are also discussed.

The importance of wave slamming in offshore design is aptly illustrated by Attfield (1975) who refers to the case of British Petroleum's WB West Sole platform in the southern North Sea:

“Wave slam on horizontal members in the splash zone was underestimated on the West Sole platforms to be more than three times the normal wave loads allowed These factors caused overstress of members in the splash zone and in fact one horizontal brace just below water level fell off in September 1972.”

He also notes that inspection of tubular members in West Sole's other structures revealed fatigue cracks, and that design faults were more apparent in the splash zone than underwater.

In this context, the present thesis is intended to provide relevant numerical and experimental results of wave slamming on horizontal cylinders and consequently contribute to a better understanding of the problems associated with wave slamming.

Chapter 2

THEORETICAL FORMULATION

Various considerations influence the force on a horizontal cylinder subjected to impact in waves. This chapter identifies these and describes a suitable formulation in order to simulate numerically the variation of hydrodynamic force for a given regular or random wave train.

2.1 Dimensional Analysis

A definition sketch of the problem which is initially under investigation is shown in Fig. 2.1. Uni-directional waves propagate past a fixed slender horizontal circular cylinder of radius a , whose lower surface is at a distance h above the still water level (SWL). The water surface elevation at any instant is given by η which subtends an angle α at the cylinder axis, and the corresponding cylinder submergence and immersed cross-section area are given by s and A_i respectively.

It is appropriate initially to examine the vertical force on the basis of dimensional considerations. The maximum force per unit length \hat{F} acting on the cylinder in regular waves depends on the cylinder radius a , the cylinder elevation h , the wave angular frequency ω , the wave height H , the gravitational constant g , the still water depth d , the fluid density ρ , the kinematic viscosity ν , and the bulk modulus E . A dimensional analysis indicates that the non-dimensional vertical force can then be expressed as a function of dimensionless parameters in the following manner:

$$C_F = \frac{\hat{F}}{\rho g a^2} = f\left(\frac{h}{H}, \frac{\omega^2 a}{g}, \frac{\omega^2 H}{g}, kd, Re, Ca\right) \quad (2.1)$$

h/H is a dimensionless cylinder elevation, $\omega^2 a/g$ is a frequency parameter, $\omega^2 H/g$ is similar to the wave steepness, kd is a depth parameter, where k is the wave number related to ω by the dispersion relationship, Re is a Reynolds number, and Ca is a Cauchy number based on the impact velocity and E . Alternatives to Eq. 2.1 are of course possible. In particular, it may also be useful to consider the wave height to cylinder radius ratio H/a , which is similar to the Keulegan-Carpenter number, and if required this may be adopted in place of the steepness parameter. Equation 2.1 may be simplified by assuming deep water waves and ignoring the influence of viscosity and compressibility so that:

$$\frac{\hat{F}}{\rho g a^2} = f\left(\frac{h}{H}, \frac{\omega^2 a}{g}, \frac{\omega^2 H}{g}\right) \quad (2.2)$$

The vertical force per unit length acting on the cylinder is generally modelled as the combination of components corresponding to an impulsive slamming force; a time-varying buoyancy force; and drag and inertia forces based on the vertical fluid velocity and acceleration respectively. The hydrodynamic force per unit length on the cylinder is thus expressed as the sum of four contributions:

$$F = F_b + F_s + F_d + F_i \quad (2.3)$$

where F_b is the buoyancy force, F_s is the slamming force, F_d is the drag force, and F_i is the inertia force. It is instructive to consider the ratios of the magnitudes of these four force components in the context of the dimensionless parameters given in Eq. 2.2, by examining the usual representation of each component in terms of empirical coefficients and the different variables describing the wave train and the cylinder. The ratios of the magnitudes of the slamming, drag and inertia forces to the buoyancy force are thereby given respectively as:

$$\left. \begin{aligned} \frac{F_i}{F_b} &= O[\omega^2 H/g] \\ \frac{F_d}{F_b} &= O\left[\frac{(\omega^2 H/g)^2}{\omega^2 a/g}\right] = O\left[(\omega^2 a/g) \left(\frac{H}{a}\right)^2\right] \\ \frac{F_s}{F_b} &= O\left[\frac{(\omega^2 H/g)^2}{\omega^2 a/g}\right] = O\left[(\omega^2 a/g) \left(\frac{H}{a}\right)^2\right] \end{aligned} \right\} \quad (2.4)$$

The buoyancy force on a fully submerged member is proportional to the volume of fluid displaced by the member and is independent of the wave conditions. The inertia to buoyancy force ratio depends primarily on the wave steepness; while the drag and slamming force components both depend in a similar way on the wave steepness and frequency parameters.

It is also useful to consider the values of the dimensionless parameters which may occur in typical situations. For waves with periods varying from 5 to 20 sec, wave heights extending to 20 m and the cylinder diameter varying from 0.1 to 2 m, the parameter ranges are approximately:

$$\frac{\omega^2 a}{g} \approx 0.001 - 0.2$$

$$\frac{\omega^2 H}{g} \approx 0 - 0.9$$

$$\frac{H}{a} \approx 0 - 200$$

Furthermore, h/H within the range between ± 0.5 is of interest in the present context, so that slamming on the cylinder does occur. More specifically, on the basis of a sinusoidal wave profile, the conditions under which no submergence, only partial submergence, partial and complete submergence, and only complete submergence occur, can be expressed in terms of h/H and H/a as follows:

No submergence: $\frac{h}{H} > 0.5$

Only partially submerged: $\frac{h}{H} \leq 0.5$, and $\frac{h}{H} + 2 \frac{a}{H} > 0.5$

Partial and complete submergence: $-0.5 < \frac{h}{H} + 2 \frac{a}{H} \leq 0.5$

Completely submerged: $\frac{h}{H} + 2 \frac{a}{H} \leq -0.5$

For convenience, this is indicated in Fig. 2.2, which shows the ranges of h/H and H/a for which no submergence, partial submergence and complete submergence occur. The figure indicates how partial submergence is less likely to occur for larger values of H/a .

2.2 Hydrodynamic Force on a Rigid Horizontal Cylinder

The various components comprising the vertical force on a horizontal cylinder have been identified in the preceding section, and each of these is now examined in detail.

2.2.1 Buoyancy Force

The buoyancy force per unit length of the cylinder is given by:

$$F_b(t) = \begin{cases} \rho g A_i(s) & \text{for } 0 \leq s/a < 2 \\ \rho g A_c & \text{for } s/a \geq 2 \end{cases} \quad (2.5)$$

where $A_i(s)$ is the sectional area of the immersed portion of the cylinder, $s = \eta - h$, as indicated in Fig. 2.1, and $A_c = \pi a^2$ is the sectional area of the cylinder. $s/a \geq 2$ corresponds to complete submergence. $A_i(s)$ may be expressed as:

$$A_i(s) = 0.5 a^2 (\alpha - \sin \alpha) \quad (2.6)$$

where α is as shown in Fig. 2.1. The buoyancy force for partial submergence can thus be expressed as:

$$F_b(t) = \frac{1}{2} \rho g a^2 (\alpha - \sin \alpha) \quad (2.7)$$

The angle α and s are related by:

$$\alpha = 2 \cos^{-1} \left(1 - \frac{s}{a} \right) \quad \text{for } 0 \leq s/a \leq 2 \quad (2.8)$$

The variation of the dimensionless buoyancy force $F_b/\rho g a^2$ with the relative submergence s/a is shown in Fig. 2.3. It is noted that the above expressions are valid under the assumption that the free surface is horizontal and there is no run-up on the sides of the cylinder.

2.2.2 Slamming Force

The earliest treatment of the water impact problem was by von Karman (1929) who examined the impact force on the floats of seaplanes during landing. The basic simplifying assumptions used for a theoretical treatment of this problem are that the fluid is incompressible and inviscid, the flow is irrotational, the body is rigid, and that surface tension is negligible. The force on a stationary object subjected to impact from a rising water surface is given by the rate of change of momentum of the fluid in the vicinity of the object. The impact force is thereby expressed as:

$$F_m(t) = \frac{\partial}{\partial t} (m w) \quad (2.9)$$

where $F_m(t)$ is the force due to the change of momentum, m is the added mass of the body and w is the vertical fluid particle velocity. The added mass m is a hydrodynamic property of the body and the flow geometry such that an acceleration \ddot{x} of the body gives rise to a hydrodynamic force $m\ddot{x}$ resisting this acceleration.

In the case of a horizontal cylinder, von Karman (1929) suggested that the effects of spray and water rise up the sides of the cylinder during the initial stages of impact were negligible, and that the flow-field about the cylinder is similar to that for a flat plate of the same width as the instantaneous waterplane section (shown as a dashed line in Fig. 2.1). For a two-dimensional flow around a flat plate, the flow field is symmetric both fore and aft of the plate. For a plate of width $2b$ and length L , the added mass is given by $\rho\pi b^2 L$. However, since there is no fluid above the equivalent flat plate in the case of the cylinder, the added mass per unit length of the cylinder is half that of the plate and is given by:

$$m = \frac{1}{2} \rho \pi b^2 \quad (2.10)$$

where b is the immersed half-width of the cylinder. Eq. 2.10 can be expressed in terms of the submergence s as:

$$m = \frac{1}{2} \rho \pi s (2a - s) \quad (2.11)$$

Instead of treating the above problem as equivalent to flow around a flat plate, Taylor (1930) used the method of conformal mapping to solve for the unbounded flow around a circular lens. This solution can be used to derive an expression for the vertical added mass m per unit length of a partially submerged cylinder ($0 \leq s/a \leq 2$), and is given as:

$$m = \frac{1}{2} \rho a^2 \left[\frac{2\pi^3 (1 - \cos \alpha)}{3 (2\pi - \alpha)^2} + \frac{\pi}{3} (1 - \cos \alpha) + \sin \alpha - \alpha \right] \quad (2.12)$$

After full submergence ($s/a > 2$), the added mass of the cylinder can still be evaluated using potential flow theory but using different methods. The velocity potential for irrotational flow in an inviscid unbounded fluid due to a body (a horizontal cylinder near the free surface in the present case) undergoing small amplitude harmonic oscillations may be expressed as:

$$\Phi(x,y,z,t) = \sum_{j=1}^6 \xi_j \phi_j(x,y,z) e^{i\omega t} \quad (2.13)$$

where ξ_j is a complex amplitude with respect to the j -th mode of motion ($j = 1, \dots, 6$, corresponding to surge, sway, heave, roll, pitch and yaw, respectively), ϕ_j is the potential function associated with each mode of motion, and ω is the oscillation frequency. The linearized boundary condition at the free surface is given by:

$$\frac{\omega^2}{g} \phi_j = \frac{\partial \phi_j}{\partial z} \quad \text{at } z = 0 \quad (2.14)$$

For the case of slamming considered here, the hydrodynamic loading is a high frequency phenomenon so that the free surface boundary condition can be expressed as the high frequency limit of Eq. 2.14:

$$\phi_j = 0 \quad \text{at } z = 0, \omega \rightarrow \infty \quad (2.15)$$

The corresponding potential flow problem can be solved by a source distribution method, or a Frank close-fit method as described by Faltinsen et al. (1977). The solution can in turn provide the added mass of the cylinder. Greenhow and Li (1987) have given results for the vertical

added mass of a cylinder when it enters or exits a free surface. Their expression, which is also valid when the cylinder is partially submerged is given by:

$$m(s) = \rho \pi a^2 \left\{ \frac{(1-q^2)^2}{q^2} \left[\frac{1}{12} + \frac{(1+m_1') K^2(m_1)}{3 \pi^2} - \frac{E(m_1) K(m_1)}{\pi^2} \right. \right. \\ \left. \left. - \frac{1}{6} - \frac{2(1+m_2') K^2(m_2)}{3 \pi^2} + \frac{2 E(m_2) K(m_2)}{\pi^2} \right] - 1 \right\} \quad (2.16)$$

where $E(m_1)$ and $K(m_1)$ are the complete elliptic integrals of the first and second kinds respectively (see Abramowitz and Stegun, 1970), m_1 is the elliptic integral parameter, and m_1' , m_2 and m_2' are related to m_1 through:

$$\left. \begin{aligned} m_1' &= 1 - m_1 \\ m_2' &= 1 - m_2 \\ \frac{K(m_2)}{K(m_2')} &= \frac{1}{2} \frac{K(m_1)}{K(m_1')} \end{aligned} \right\} \quad (2.17)$$

Also:

$$q = \exp \left[-\pi \frac{K(m_1')}{K(m_1)} \right] = \exp[-\sigma_0] \quad (2.18)$$

σ_0 is a parameter describing the cylinder position and is given as:

$$\sinh^2 \sigma_0 = \frac{s(s-2a)}{a^2} = \frac{(1-q^2)^2}{4q^2} \quad (2.19)$$

Reverting to the definition of the impact force as the rate of change of fluid momentum as given in Eq. 2.9, it is possible to expand the expression as:

$$F_m(t) = m \frac{\partial w}{\partial t} + w \frac{\partial m}{\partial t} \quad (2.20)$$

Equation 2.20 can be rewritten as:

$$F_m(t) = m \dot{w} + \frac{\partial m}{\partial s} w^2 \quad (2.21)$$

since $s = wt$. Eq. 2.21 has two terms which are a function of the fluid acceleration and velocity respectively. The acceleration term is a component of the inertia force which is discussed in the next section. For a situation where the flow is non-accelerating, the only force component is due to the velocity-squared term. This term is designated as the slamming force and is also expressed in terms of a slamming coefficient C_s as:

$$F_s(t) = \frac{1}{2} C_s \rho D w^2 \quad (2.22)$$

where $D (= 2a)$ is the diameter of the cylinder. C_s may hence be expressed as a function of the rate of change of added mass:

$$C_s = \frac{2}{\rho D} \frac{\partial m}{\partial s} \quad (2.23)$$

Expressions for the added mass m , given by Eqs. 2.11 or 2.12 for partial submergence and by Eq. 2.16 for both partial and complete submergence, may be used to develop corresponding expressions for the slamming coefficient. In the case of von Karman's added mass model, C_s is given by:

$$C_s = \frac{2}{\rho D} \rho \pi (a - s) = \pi \left(1 - \frac{s}{a}\right) \quad (2.24)$$

Wagner (1931) used a technique similar to the above, but he proposed that the equivalent flat plate be extended between the spray roots at the sides of the cylinder. He determined the location of the spray roots by using the vertical velocity of the upwash predicted by potential flow theory for a flat plate. Wellicome (Campbell et al., 1977) used Wagner's model to integrate the pressure distribution over a flat plate, and derived an expression for the variation of C_s :

$$C_s = \frac{2\pi}{(1 + 1.5 s/a)} \quad (2.25)$$

The expression for C_s on the basis of Taylor's model is given by:

$$C_s = \frac{1}{\sin \frac{\alpha}{2}} \left[\frac{2\pi^3}{3} \left(\frac{\sin \alpha}{(2\pi - \alpha)^2} + \frac{2(1 - \cos \alpha)}{(2\pi - \alpha)^3} \right) + \frac{\pi}{3} \sin \alpha + \cos \alpha - 1 \right] \quad (2.26)$$

which is applicable for α between 0 and 2π ($s/a = 0$ to 2). Figure 2.4 shows a comparison of the behaviour of C_s predicted by the above expressions. According to von Karman's model, the slamming coefficient at impact has a value of π which decreases linearly with increasing submergence till it drops to 0 when the cylinder is half submerged and remains zero as s/a increases beyond 1 since the flow is past a constant projected width ($= D$). Wagner's wetting correction doubles the value of C_{s0} to 2π , but predicts a very gradual rate of decay for C_s . The features of Taylor's solution are that $C_s = \pi$ at the instant of impact, $s/a = 0$; C_s reaches a minimum value of 0.298 at $s/a = 1.555$; and C_s increases to a value of 1.351 ($= \pi^3/9 - 2\pi/3$) at the instant of complete submergence, $s/a = 2$. Previous experimental data (e.g. Sarpkaya, 1978, Campbell and Weynberg, 1980) indicate that a maximum in C_s near the instant of complete submergence as predicted by Eq. 2.26 is unrealistic.

In comparison, expressions for the variation of C_s with cylinder submergence estimated from tests involving a horizontal cylinder impacting calm water at a constant velocity have been given by Campbell and Weynberg (1980), and Miao (1988) respectively:

$$C_s = \frac{5.15}{1 + 9.5 s/a} + 0.275 (s/a) \quad (2.27)$$

$$C_s = 6.1 \exp(-6.2 s/a) + 0.4 \quad (2.28)$$

The variation of the above expressions is also shown in Fig. 2.4. The expressions in Eqs. 2.27 and 2.28 have not been corrected for buoyancy effects which were estimated to be less than 5% of the total force during the initial high load phase of the slam. It is seen that the above experimental curves for C_s predict a value of C_{s0} which is larger than the generally accepted value of π and which also exhibits a faster rate of decay with increasing submergence than do the analytical expressions.

In an extensive review of several analytical methods to determine the added mass of a cylinder moving near the free surface, Greenhow and Li (1987) present results for the variation of C_s with cylinder submergence which are shown in Fig. 1.3. They emphasize that the assumptions

entailed in the derivation of Eq. 2.16 become unreliable after the initial stages of impact ($s/a \geq 1$) due to the possibility of local particle accelerations no longer being large compared with g and significant displacement of the free surface from $z = 0$ for high entry speeds. The methods which use corrections to account for the deformation of the free surface during impact, and the exact shape of the wetted cylinder, yield different estimates of the peak value C_{s0} ranging from π to 2π .

In the most recent analytical treatment of the impact problem, Cointe and Armand (1987) use the method of matched asymptotic expansions to derive a second-order solution for the slamming force on a cylinder. They justify the wetting correction proposed by Wagner (1931) which modifies the first-order estimate of C_s from π to 2π .

As mentioned in Chapter 1, experiments have indicated a finite rise-time during which the slamming force increases from zero to a peak value, though the theoretical models for C_s imply that the peak force occurs instantaneously. The compressibility of the air between the cylinder and the water surface, aeration, and compressibility of water are some of the factors which can influence the rise time of the slamming force. The presence of air bubbles also decreases the effective density of the water, and the corresponding velocity of sound in water, which in turn may lead to reduced hydrodynamic pressure in vicinity of the cylinder and a smaller slamming force. In the absence of a suitable model to account for these effects, the peak impact force on an infinitely rigid cylinder entering an incompressible fluid is assumed to have a zero rise-time since this does not affect the magnitude of the transmitted force.

It is not possible to use Eq. 2.22 in the case of cylinder exit, i.e. when the water surface is receding from the cylinder. Greenhow (1988) analyzed the cylinder entry and exit problems, and presented results from a numerical model based on potential flow theory with exact nonlinear free surface boundary conditions. He observed that while forces predicted by conventional slamming theory showed fair agreement with his results in some cases, there was a 'wide and fascinating' diversity of free-surface flows for various values of Froude number and starting

positions of the cylinder. These results thus preclude the general use of added mass theory. In the case of cylinder exit, the simulations predicted the lifting of water above the cylinder and the subsequent formation of thin layers; the draw-down and rush-up of the free surface beneath the cylinder, and the rush-up terminating in localized breaking (also seen in his experiments); and the formation of large regions of strong negative pressure on the cylinder surface. A large increase in upward force on the cylinder due to the rush-up was predicted by one of the calculations, and was also observed in pressure measurements in a corresponding experiment, though the author states that further experimental work is needed to confirm this effect.

In the absence of an accepted theoretical model or sufficient experimental data, the force due to added mass effects when the wave recedes from the cylinder has not been considered in this study.

2.2.3 Inertia Force

The inertia force F_i acting on the cylinder is associated with the vertical fluid acceleration \dot{w} and is expressed as:

$$F_i(t) = \rho A_i \dot{w} + m \dot{w} \quad (2.29)$$

where m is the added mass of the partially submerged cylinder (Eq. 2.12 or 2.16). The first term in Eq. 2.29 is referred to as the Froude-Krylov force which corresponds to the inertia of the fluid volume displaced by the cylinder, and the second term is the momentum component as derived in Eq. 2.21. The inertia force can be written in terms of an inertia coefficient C_m as:

$$F_i(t) = C_m \rho A_c \dot{w} \quad (2.30)$$

where $C_m = A_i/A_c + m/\rho A_c$ is the corresponding inertia coefficient based on the area A_c rather than A_i .

On the basis of Eq. 2.16, the corresponding variation of C_m with immersion s/a based on m given by Taylor (i.e. Eq. 2.12) is shown in Fig. 2.5. At complete immersion, $s/a = 2$, the inertia

coefficient reaches a value of 1.645 ($= \pi^2/6$), and for a deeply submerged cylinder, $s/a \rightarrow \infty$, the inertia coefficient approaches a value of 2.0 corresponding to the case of an unbounded fluid. C_m is within 2% of this value for $s/a \geq 4.1$. The value of C_m at $s/a = \infty$ is designated as C_{m0} .

2.2.4 Drag Force

The fourth component in Eq. 2.3 is the drag force. For a completely submerged cylinder, the drag force component of the Morison equation is given by:

$$F_d(t) = \frac{1}{2} C_d \rho D w |w| \quad (2.31)$$

where C_d is the drag coefficient and w is the vertical fluid velocity.

The drag force acting during partial submergence is less well known, and corresponding values of the drag coefficient are not available. During the early stages of impact, flow separation should not occur and the drag force rises from a value of zero at the instant of impact to the magnitude given by Eq. 2.31 after full submergence. It may be possible to extend this to the case of partial submergence by utilising the instantaneous immersed width of the cylinder in place of D , but the variation of the corresponding drag coefficient would still be unknown. It is noted that Eq. 2.31 has the same form as the slamming force in Eq. 2.22, both being proportional to the square of the water particle velocity, and it is expected that these two components will undergo a smooth transition from one to the other during partial submergence, and from the partially submerged stage to the fully submerged stage.

The semi-von Karman method of determining the slamming coefficient (Greenhow and Li, 1987) indicates that beyond $s/a = 0.6$, C_s is approximately constant at a value of 0.7, which is the recommended value for $s/a > 0.15$. They justify this conclusion based on the agreement of the semi-von Karman method with the experimental data of Campbell and Weynberg (1980). However, experimental data obtained by measuring the vertical force on a horizontal cylinder subjected to slamming cannot directly distinguish between the contributions of the slamming and drag components during the stage of partial submergence ($0 < s/a < 2$). For this stage, it may

thus be useful to consider the drag and slamming coefficients in combination, $C_d + C_s$, rather than separately.

2.2.5 Combination of Force Components

There are a number of difficulties in attempting to superpose the four force components described above in order to describe the variation of the total force with time. Firstly, a suitable model for the slamming coefficient has to be selected. If present industry practice of adopting $C_{s0} = \pi$ is considered, Taylor's model (Eq. 2.26) may be a possible choice. However, the variation of C_s indicated in Fig. 2.4 is clearly unreasonable beyond the initial stages of impact. Likewise, the theoretical variation of the inertia coefficient with submergence indicates a value of $C_m = 2.0$ for a fully submerged cylinder far from the free surface, which may not be consistent with values of C_m observed in experimental studies. Furthermore, the variation of the drag force due to partial submergence is also unclear, although it is expected that in combination with the slamming force, the variation is continuous.

Certain options are possible for describing the force variation with time and two such models are adopted here. Model I is based on the approach used by Isaacson and Subbiah (1990), who were concerned only with the force maxima during any particular wave. They assume that the variation of the vertical force from the instant of impact to the instant of complete submergence is linear with time. This leads to considerable simplicity in the force formulation since the slamming force contribution is evaluated only at the instant of impact using Eq. 2.22 with a specified value of C_{s0} ; and the Morison equation with constant drag and inertia coefficients, together with the buoyancy force, is used during the fully submerged stage. The time variation of the vertical force over one wave is indicated as a solid line in Fig. 2.6(a) for the cases of partial and complete submergence. As an aid to interpreting the behaviour of the force, the figures include horizontal and vertical lines which indicate the cylinder location and corresponding instants of impact and complete submergence. This shows how the total vertical force varies linearly with time from the maximum slamming force at the instant of wave-cylinder

contact to the value at the instant of complete submergence. In a similar fashion, as the free surface recedes from the cylinder, the total vertical force drops with a linear variation from the value at the instant of complete submergence to zero. Isaacson and Subbiah avoided the case when the cylinder is only partially submerged during the passage of the wave ($h < H/2 < h + 2a$), and it is appropriate here to extend their model to include this range also. In order to do so in a reasonably simple manner, a corresponding approximation is made for this range, which leads to the force variation shown in Fig. 2.6(b). The vertical force at the instant of maximum submergence ($\eta = H/2$), corresponds to inertia and buoyancy only. However, although the magnitude of the inertia force at maximum submergence is unclear, it is assumed that the inertia force at this instant can be determined from the specified value of C_m used in conjunction with the submerged cross-sectional area of the cylinder. The vertical force is then assumed to vary linearly from the instant of impact, where the force is due to slamming and is given by Eq. 2.22, to the instant of maximum submergence, where the force is made up of buoyancy and inertia components only, and then to vary linearly again from this instant to zero at the instant when the cylinder is no longer in contact with the wave.

An alternative approach, denoted here as Model II, attempts to model the variation of the vertical force during the stage of partial submergence using modified expressions for the inertia, drag and slamming force as indicated below. As mentioned in Section 2.2.4, it may be useful to consider the combined slamming and drag forces in order to account for the velocity-squared based force during partial submergence. This is achieved by assuming that the sum, $C_s + C_d$, varies as Eq. 2.23 from the instant of impact to the point at which this combined coefficient reaches a specified value of C_d . After this point, the combined coefficient remains constant at the value of C_d until the wave recedes from the cylinder. A possible variation of $C_s + C_d$, henceforth designated as C_{s+d} , is shown by the solid line in Fig. 2.7 for the case when C_s is determined using Taylor's model (dashed line), and $C_d = 0.8$. The division of this combined force into slamming and drag components need not be of concern, but for convenience one may consider this to account for C_s decreasing from its initial peak value of C_{s0} to C_d , whereupon it continues decreasing to zero and the drag coefficient then begins increasing from zero to the

specified value in such a way that the sum of the two coefficients remains constant. For typical values of C_d (0.6 to 1.0), this transition occurs near $s/a = 1$, when the cylinder is approximately half submerged, which might be expected, as the use of C_s based on potential theory is then prone to inaccuracy, while the drag force builds up as flow separation commences. The velocity-squared force is then evaluated using Eq. 2.22 with C_{s+d} used in place of C_s . When the free surface recedes from the cylinder, it is assumed that slamming force is absent and as the cylinder becomes partially submerged, the drag force is computed by using the maximum immersed width of the cylinder in place of D in Eq. 2.31 together with the specified value of C_d .

The inertia force is evaluated using Eq. 2.30. Instead of using a constant value of C_m after complete submergence as in Model I, the inertia coefficient is now assumed to vary with submergence as a function of the added mass, as indicated earlier. Eq. 2.12 is used to obtain values of added mass during partial submergence. However, in order to facilitate the computation of the dimensionless added mass $m/\rho a^2$ after complete submergence, and also in order to incorporate a variation which approaches an empirical inertia coefficient other than the theoretical value of 2.0, a three parameter exponential curve has been adopted to describe the variation of inertia coefficient with s/a . The dimensionless added mass variation after full submergence is expressed as:

$$\frac{m}{\rho a^2} = \lambda_1 - \lambda_2 \exp(-\lambda_3 \frac{s}{a}) \quad 2 \leq \frac{s}{a} \leq \infty \quad (2.32)$$

where λ_1 , λ_2 and λ_3 are parameters which are chosen such that the inertia coefficient $C_m (= 1 + m/\rho A_c)$ reaches a specified value C_{m0} at $s/a = \infty$, and the variation of added mass and its gradient with respect to s/a are continuous at $s/a = 2$, on the basis of Eq. 2.12. The parameters may thereby be derived as:

$$\left. \begin{aligned} \lambda_1 &= \pi(C_{m0} - 1) \\ \lambda_2 &= \frac{\pi(C_{m0} - \pi^2/6)}{\exp(-2\lambda_3)} \\ \lambda_3 &= \frac{(\pi^2/9 - 2/3)}{(C_{m0} - \pi^2/6)} \end{aligned} \right\} \quad (2.33)$$

In the particular case of potential theory when $C_{m0} = 2$, the parameters λ_1 , λ_2 and λ_3 are approximately π , 12.57 and 1.21 respectively. Fig. 2.5 shows the predicted variation of C_m with s/a as dashed lines for cases corresponding to $C_{m0} = 1.7$ and 2.0.

The above expressions for the variation of C_m after full submergence are valid for $C_{m0} \geq 1.645$. If a simulation requires that the value of C_{m0} be less than 1.645, the model uses an approach similar to that in the case of the variation of C_{s+d} with increasing submergence. Once the value of C_m predicted on the basis of Eq. 2.12 reaches the value of C_{m0} during partial submergence, it is held constant at that value with increasing submergence. A similar method is used when the free surface recedes from the cylinder.

2.3 Hydrodynamic Force on an Elastically Supported Horizontal Cylinder

The hydrodynamic vertical force on a rigid cylinder subjected to wave slamming has been formulated in Section 2.2. The expressions for the various force components have been derived on the assumption that the cylinder and its support structure do not respond to the applied wave force. In the case of an elastically supported cylinder subjected to wave slamming, the dynamic response alters the magnitude of the applied force since the fluid particle kinematics relative to the cylinder are modified due to the cylinder vibration. The force transmitted by the cylinder to its supports is also affected due to its dynamic response and this force may be higher or lower than the applied force, depending on the length of the slamming impulse and the natural frequency of the cylinder. The governing variables and the modified numerical model for wave slamming on an elastically supported cylinder are examined in the following sections.

2.3.1 Response of an SDOF System to Impact Loading

The cylinder and its support structure can be modelled as a single-degree-of-freedom (SDOF) system with a mass M , a stiffness K and a damping coefficient C . The schematic representation

of such a system is shown in Fig. 2.8. The equation of motion of this system when subjected to a time varying force $F(t)$ is given by:

$$M \ddot{r} + C \dot{r} + K r = F(t) \quad (2.34)$$

where r , \dot{r} and \ddot{r} are the time varying cylinder displacement, velocity and acceleration respectively. The natural frequency of this system, denoted by ω_n and the damping coefficient C can be expressed in terms of a non-dimensional damping ratio denoted ζ as:

$$\omega_n = \sqrt{\frac{K}{M}}$$

$$\zeta = \frac{C}{2M\omega_n} \quad (2.35)$$

The applied force $F(t)$ in Eq. 2.34 has the same general form as given in Eq. 2.3. In the present study, it is assumed that the force transducer in the support structure determines the dynamic characteristics of the cylinder. If the applied force were to be measured by such a configuration, the measured force which is also termed as the transmitted force is given by:

$$F_t(t) = K r(t) \quad (2.36)$$

In cases where the damping force component is also assumed to be a part of the transmitted force, the right-hand side of Eq. 2.36 is given by $Kr(t) + C\dot{r}(t)$. The measured force is hence a function of the natural frequency and damping of the system. For the case of an applied load $F(t)$, the response of an SDOF system starting from rest is given by:

$$r(t) = \frac{1}{\omega_d} \int_0^t F(\tau) \exp[-\zeta\omega_n(t - \tau)] \sin[\omega_d(t - \tau)] d\tau \quad (2.37)$$

where ω_d is the damped natural frequency of the system and is given by $\omega_n\sqrt{1 - \zeta^2}$ and τ is a dummy variable of integration.

Let us consider the idealized case of an impact load $F(t)$ which increases linearly from 0 to a peak value F_0 in a rise-time T_r and then drops linearly to 0 in a decay-time T_d as shown in Fig. 2.9. During the stage when the force is increasing, $F(t)$ can be expressed as:

$$F(t) = \frac{F_0 t}{T_r} \quad 0 \leq t \leq T_r \text{ [Stage A]} \quad (2.38)$$

The response of the system to this load can be determined using Eq. 2.37. If the system is initially at rest, the response during the stage when the force is increasing ($0 \leq t \leq T_r$), is given by:

$$\begin{aligned} r(t) &= \frac{F_0}{K T_r} \left[t - \frac{2\zeta}{\omega_n} + \exp(-\zeta\omega_n t) \left(\frac{2\zeta}{\omega_n} \cos(\omega_d t) + \frac{(2\zeta^2 - 1)}{\omega_d} \sin(\omega_d t) \right) \right] \\ \dot{r}(t) &= \frac{F_0}{K T_r} \left[1 - \exp(-\zeta\omega_n t) \left(\cos(\omega_d t) + \frac{\zeta\omega_n}{\omega_d} \sin(\omega_d t) \right) \right] \end{aligned} \quad (2.39)$$

When the force is decreasing (Stage B), the system response can be evaluated in terms of $t' = t - T_r$, since that simplifies the expression for the applied force to:

$$F(t) = F_0 \left[1 - \frac{t'}{T_d} \right] \quad T_r \leq t \leq T_r + T_d \text{ [Stage B]} \quad (2.40)$$

The response in Stage B can now be given as the sum of the the free vibration due to r and \dot{r} (at $t = T_r$) from Eqs. 2.39, designated as r_0 and \dot{r}_0 respectively and the forced response due to the applied force in Eq. 2.40. The displacement $r(t')$ in Stage B is hence:

$$\begin{aligned} r(t') &= \exp(-\zeta\omega_n t') \left(r_0 \cos(\omega_d t') + \frac{(\dot{r}_0 + \zeta\omega_n r_0)}{\omega_d} \sin(\omega_d t') \right) + \\ &\frac{F_0}{K T_d} \left[\left(\frac{2\zeta}{\omega_n} + T_d \right) \left(1 - \exp(-\zeta\omega_n t') \cos(\omega_d t') \right) - t + \right. \\ &\left. \frac{(1 - 2\zeta^2 - \zeta\omega_n T_d)}{\omega_d} \exp(-\zeta\omega_n t') \sin(\omega_d t') \right] \end{aligned} \quad (2.41)$$

The motion of the system after the force has dropped to zero, shown as Stage C in Fig. 2.9, can be evaluated in a manner similar to that for Stage B, wherein the system displacement and velocity at the end of Stage B (at $t' = T_d$) are used to determine the free vibration response in Stage C.

It can be seen from Eqs. 2.39 and 2.41, that the transmitted force $F_t(t)$ given by Eq. 2.36 is a function of the dynamic characteristics of the system and that its magnitude at any instant may not be the same as that of the applied force. Since the initial stages of the wave slamming force are similar to the impact force analyzed above, it is useful to compare the transmitted force (which would be measured by a typical force transducer) with the actual applied force. The two main parameters of interest are the measured peak force F_{t0} immediately after impact and the corresponding rise-time T_t . The ideal measuring system should report the same force as the applied force at every instant and an examination of Eqs. 2.39 and 2.41 indicates that such a measuring system would have a natural frequency ω_n such that $\omega_n T_r$ is very large. The effect of the damping ratio ζ on the measured force using systems with high natural frequency is not significant, especially for typical damping values between 5% and 10%.

As mentioned earlier, measurements indicate that there is a finite rise-time during which the slamming force increases from zero to a maximum value. Sarpkaya (1978) showed that the rise-time and the natural frequency of an elastic cylinder can cause the apparent maximum value of C_s to vary between 0.5π and 1.7π . In order to examine the influence of the dynamic characteristics of the system and the rise-time of the slamming force on the transmitted (or measured) force F_t , two idealized types of impact force are considered. In the case of the first impact, the rise-time T_r is the same as the decay time T_d , and in the second case, $T_d = 2 T_r$. Fig. 2.10(a) illustrates both load cases and the corresponding force measured by a system with $T_r/T_n = 0.2$ (where the natural period $T_n = 2\pi/\omega_n$) and $\zeta = 0.05$. Fig. 2.10(b) shows the results for the case when $T_r/T_n = 2.0$. It is observed that there is a significant difference between the applied and recorded force for the case where $T_r/T_n = 0.2$. The measured force maximum is higher than the applied force peak due to dynamic amplification and the apparent rise-time to

reach the force maximum is larger than T_r . Obviously this is not a desirable configuration for an experimental study of impact force. For the case where $T_r/T_n = 2.0$, Fig. 2.10(b) shows that the measured force is a better estimate of the applied force, though there are differences due to the oscillatory nature of the response.

The effect of the variation of T_r/T_n for various values of ζ (0, 0.02, 0.05) on the dynamic magnification factor F_{t0}/F_0 and the relative rise-time T_t/T_r are summarized in Fig. 2.11 for both aforementioned loading cases. The desirable properties of a measurement system for recording impact forces can be interpreted from these figures. It is observed in Fig. 2.11(a) that for T_r/T_n smaller than 0.1, F_{t0}/F_0 is less than 0.6 and decreases to 0 as T_r/T_n approaches 0. This is because a system that has a large natural period in comparison to the rise and decay time of the impact force does not have adequate time to 'see' the force. Consequently the response is smaller than that for a static load and the measured force is lower than the applied force. It is seen that F_{t0}/F_0 approaches a value of 1 in an oscillatory manner as T_r/T_n increases beyond 1. Hence if a system is chosen such that T_r/T_n is at least 2 and preferably greater than 3, the measured force maximum will be a fairly good estimate of the applied force maximum. A similar requirement is evident in Fig. 2.11(b) which shows that the relative rise-time T_t/T_r also approaches a value of 1 as T_r/T_n becomes large. It is also observed that the effect of damping on the measured peak force and rise-time diminishes with increasing values of T_r/T_n .

Figures 2.11 (c) and (d) illustrate the variation of F_{t0}/F_0 and T_t/T_r for the case where $T_d = 2T_r$. The trends are seen to be similar to those in Figs. 2.11 (a) and (b) respectively. Although the duration of the impact is longer in this case, the amplification factor F_{t0}/F_0 is seen to increase marginally by about 7% at $T_r/T_n \approx 0.5$. Consequently, a method which corrects the measured force for the effects of dynamic amplification, based on the assumption that the slamming force component can be represented as an impact where $T_d = T_r$ will be reasonably accurate even if the actual decay time T_d is 100% larger than its assumed value.

2.3.2 Cylinder Response to Wave Impact Loading

The slamming, inertia and drag forces on the cylinder are functions of the water particle velocity and acceleration. In the case of a cylinder which responds dynamically to the applied load, the nature of the loading changes since the motion of the cylinder modifies the relative velocity and acceleration between the water and the cylinder. The problem has to be solved iteratively, since the response at any instant is a function of the applied force which in turn is a nonlinear function of the relative water particle velocity (and thus a nonlinear function of the response). A numerical model which accounts for the dynamic behaviour of the cylinder and expresses the applied hydrodynamic load as a function of the relative water particle kinematics is described.

A definition sketch for the case of an elastically supported horizontal cylinder subjected to wave slamming is shown in Fig. 2.12. The equilibrium height of the cylinder axis from the still water level (SWL) is given by h . The cylinder displacement from its equilibrium position due to an applied force is denoted by r . Both h and r are measured positive upwards. If the cylinder is subjected to hydrodynamic forces due to an incident wave train, the equation of motion of the cylinder is given by:

$$M \ddot{r} + C \dot{r} + K r = L (F_b + F_s + F_i + F_d) \quad (2.42)$$

where the terms on the left side of Eq. 2.42 are as in Section 2.3.1, the 4 force terms on the right side have been described for the case of a rigid cylinder in Sections 2.2.1 - 2.2.4, and L is the length of the cylinder. For the case of a dynamically responding cylinder, the buoyancy force F_b is given by Eq. 2.5 where the cylinder submergence:

$$s = \eta - (h + r) \quad (2.43)$$

Since the cylinder is located near the still water level, the following relations for the applied force are based on the assumption that the vertical components of water particle velocity and acceleration are given by $\dot{\eta}$ and $\ddot{\eta}$ respectively (see Section 2.5.1). Equation 2.9 can be rewritten

to account for the relative water particle velocity and hence the force per unit length of the cylinder due to the rate of change of fluid momentum is given by:

$$F_m(t) = \frac{\partial}{\partial t} [m (\dot{\eta} - \dot{r})] \quad (2.44)$$

Equation 2.44 can be expanded in a form similar to Eq. 2.21:

$$F_m(t) = m (\ddot{\eta} - \ddot{r}) + (\dot{\eta} - \dot{r}) \frac{\partial m}{\partial s} \frac{\partial s}{\partial t} \quad (2.45)$$

which can be further simplified to:

$$F_m(t) = m (\ddot{\eta} - \ddot{r}) + (\dot{\eta} - \dot{r})^2 \frac{\partial m}{\partial s} \quad (2.46)$$

The first term in Eq. 2.46 is the momentum component of the inertia force and the second term is the slamming force which can be written in terms of the slamming coefficient C_s as:

$$F_s(t) = \frac{1}{2} C_s \rho D (\dot{\eta} - \dot{r})^2 \quad (2.47)$$

Equation 2.29 for the inertia force per unit length is rewritten to account for the relative acceleration:

$$F_i(t) = \rho A_i \ddot{\eta} + m (\ddot{\eta} - \ddot{r}) \quad (2.48)$$

The drag force is similarly given by:

$$F_d(t) = \frac{1}{2} C_d \rho D (\dot{\eta} - \dot{r}) |\dot{\eta} - \dot{r}| \quad (2.49)$$

Equation 2.42 can now be expressed as:

$$M \ddot{r} + C \dot{r} + K r = L \left[F_b + \frac{1}{2} C_s \rho D (\dot{\eta} - \dot{r})^2 + \rho A_i \ddot{\eta} + m (\ddot{\eta} - \ddot{r}) + \frac{1}{2} C_d \rho D (\dot{\eta} - \dot{r}) |\dot{\eta} - \dot{r}| \right] \quad (2.50)$$

As described in Section 2.2.5, Model II combines the hydrodynamic force due to the slamming and drag components into a single force that is proportional to the square of the relative velocity and a combined coefficient C_{s+d} . Equation 2.50 can be rewritten for Model II as:

$$(M + m l) \ddot{r} + C \dot{r} + K r = L \left[F_b + C_m \rho \frac{\pi D^2}{4} \ddot{\eta} + \frac{1}{2} C_{s+d} \rho D (\dot{\eta} - \dot{r}) |\dot{\eta} - \dot{r}| \right] \quad (2.51)$$

The variations of the coefficients C_m and C_{s+d} have been discussed in Section 2.2.5.

Equation 2.51 is nonlinear and can be solved in the time domain using any suitable numerical technique. The Newmark iteration method with a linear acceleration formulation has been used in this study. The solution begins at a time step when the water surface is below the initially stationary cylinder, since the applied force and the response are known to be zero. The acceleration \ddot{r} at the next time step is assumed to be the same as that at the previous time step (i.e. $\ddot{r}_{t+\Delta t} = \ddot{r}_t$) and this value is used in the first step of the iteration to obtain the velocity \dot{r} and displacement r at $t+\Delta t$:

$$\begin{aligned} \dot{r}_{t+\Delta t} &= \dot{r}_t + \ddot{r}_t \Delta t + \gamma \Delta t (\ddot{r}_{t+\Delta t} - \ddot{r}_t) \\ r_{t+\Delta t} &= r_t + \dot{r}_t \Delta t + (\Delta t)^2 \left[\frac{\ddot{r}_t}{2} + \beta (\ddot{r}_{t+\Delta t} - \ddot{r}_t) \right] \end{aligned} \quad (2.52)$$

where Δt is the time step size and γ and β are coefficients which have the values 0.5 and $\frac{1}{6}$ respectively for the linear acceleration method. Since the values of $\dot{\eta}$, $\ddot{\eta}$ and η are known at time $t+\Delta t$, the right hand side of Eq. 2.51 can now be evaluated and is designated as $F_{t+\Delta t}$. A revised estimate for $\ddot{r}_{t+\Delta t}$ is calculated using Eq. 2.51:

$$\ddot{r}_{t+\Delta t} = \frac{1}{(M + m l)} [F_{t+\Delta t} - C \dot{r}_{t+\Delta t} - K r_{t+\Delta t}] \quad (2.53)$$

This value of $\ddot{r}_{t+\Delta t}$ is used in Eq. 2.52 to obtain more accurate values of $\dot{r}_{t+\Delta t}$ and $r_{t+\Delta t}$ and the iteration continues until the value of $\ddot{r}_{t+\Delta t}$ calculated by Eq. 2.53 converges.

The choice of Δt is very important in order to run a simulation and interpret results correctly. The time interval chosen should be small enough such that all quantities which are functions of time are accurately modelled (i.e. frequency components in the input wave force and in the output response oscillation are represented without aliasing) and the Newmark iteration process converges, and large enough to avoid lengthy computation times and redundant data. The criteria used to select a suitable value of Δt are discussed in Section 2.5.3.

In the case of a cylinder which does not respond to an applied force, the rise-time of the impact force has not been considered in the analysis since it does not influence the magnitude of the transmitted force. It has been shown in Section 2.3.1 that in the case of a compliant cylinder, the transmitted force is a function of the cylinder's natural frequency and the rise-time of the applied force. Consequently, the assumption that the slamming coefficient reaches a peak value of C_{s0} ($= \pi$ or higher value depending on the choice of model for C_s) at the instant of impact may lead to unrealistic predictions of the transmitted force. A numerical model which can simulate varying impact force rise-times allows for a more realistic simulation of the wave slamming force and consequent dynamic response of compliant cylinders. There is no explicit formulation for the force rise-time in Eq. 2.50 and unlike the case of a rigid cylinder wherein it is possible to simulate a linear variation of force using interpolation between known force magnitudes at any two points in time, the hydrodynamic force on a vibrating cylinder is not known beyond one time step due to the interdependent nature of the force and cylinder response.

However, it is known that the dominant contribution to the total force on the cylinder during the initial stages of impact is due to slamming. Consequently a pseudo-linear (since the buoyancy and inertia force components add a little nonlinearity in the early stages of immersion and the relative velocity changes slightly during the rise-time) increase of the applied impact force can be introduced by modifying the coefficient C_{s+d} , such that it increases linearly from 0 at the instant of impact to the peak value of C_{s0} over a specified rise-time T_r :

$$C_{s+d} = C_{s0} \frac{(t - t_i)}{T_r} \quad t_i \leq t \leq t_i + T_r \quad (2.54)$$

where t_i is the instant of impact. After $t = t_i + T_r$, C_{s+d} varies in the same manner as it would for a rigid cylinder, wherein the submergence s/a is assumed to increase from 0 after $t = T_r$. The value of T_r chosen for a simulation should be such that C_{s+d} reaches its peak value of C_{s0} before significant immersion of the cylinder ($s/a \leq 0.4$) and is typically between 5 and 30 msec.

2.3.3 Modelling Slamming as an Impulse

Sections 2.3.1 and 2.3.2 have shown possible techniques of numerically modelling wave slamming on a horizontal cylinder which responds to the rapidly varying load, and of determining effects such as the dynamic amplification of the applied force. This treatment requires detailed information on the characteristics of the slamming force variation with time during the early stages of impact. However, past experimental evidence has proven that it is quite difficult to obtain reliable estimates of the slamming coefficient due to several factors such as air entrainment, cylinder inclination, and dynamic response. These cause appreciable scatter in the peak value of the slamming coefficient reported by several investigators.

The time scale of the slamming force on horizontal members of offshore platforms is in the range of 0.01 - 0.2 sec. If the natural period of such a member is in the range 0.5 - 1 sec, the maximum response of the member is usually governed by the magnitude of the slamming impulse, rather than the precise form of the applied load itself. Hence, as an alternative to the conventional approach involving the slamming coefficient, it may be more convenient to define the slamming event using an impulse coefficient which combines the impact force and rise-time into a single dimensionless quantity.

A typical time history of the measured slamming force is sketched in Fig. 2.13. As indicated in the figure, the force F may be considered to be made up of two components: an impulsive force F_i , which rises rapidly to a maximum and then falls to zero over a duration T_i ; and a residual force F_r which may be taken to increase steadily over this duration, starting from zero, and which is associated approximately with drag, inertia and buoyancy components. For convenience, T_i may be taken to correspond to the instant at which the overall force F reaches a

minimum as indicated in the figure. The measured force record using a test cylinder, usually includes oscillations at the natural frequency of the cylinder. In such a case, the minimum force which is used to define the end of the impulse should be identified after the record is first filtered so as to remove these oscillations, since this would correspond more closely to the applied force. On the basis of the above representation, the impulse I on the cylinder, which is associated with the impulsive force F_i , may be written as:

$$\begin{aligned} I &= \int_0^{T_i} F_i dt \\ &= \int_0^{T_i} F dt - \frac{1}{2} T_i F(T_i) \end{aligned} \quad (2.55)$$

The second term on the right-hand side of Eq. 2.55 corresponds to the area of the shaded triangle shown in Fig. 2.13. An impulse coefficient may now be defined as:

$$C_i = \frac{I}{\rho a^2 w L} \quad (2.56)$$

where w is the vertical water particle velocity at the instant of impact, and L is the length of the cylinder.

Since it is assumed that the impulsive force F_i is due to the slamming force discussed in Section 2.2.2, it is possible to estimate a theoretical impulse coefficient from the closed-form expression for C_s . It is seen in Figs. 1.3 and 2.4 that the more plausible models derived for the variation of C_s reach a minimum value by the stage when the cylinder has been submerged by half, i.e. $s/a = 1$. As discussed in Section 2.2.5, this is consistent with the notion that conventional added mass theory can provide a fair estimate of the slamming coefficient only during the early stages of impact. As the submergence increases, flow separation effects begin to influence the hydrodynamic force, and it is difficult to separate the drag force component from the impulsive force. Hence it is assumed that the theoretical impulse coefficient can be

estimated between the limits of $0 \leq s/a \leq 1$. The theoretical impulse is expressed in a manner similar to Eq. 2.55:

$$I = \int_0^{T_i} 0.5C_s \rho D w^2 L dt = \rho a^2 w L \int_0^1 C_s(s/a) d(s/a) \quad (2.57)$$

The theoretical impulse coefficient corresponds to the area under the C_s curve between $s/a = 0$ and 1. The expressions for C_s given in Section 2.2.2 have been integrated to yield the following values of C_i :

$$C_i = 1.571 \quad \text{von Karman (based on Eq. 2.24)}$$

$$C_i = 3.833 \quad \text{Wagner (based on Eq. 2.25)}$$

$$C_i = 1.571 \quad \text{Taylor (based on Eq. 2.26)}$$

These can be compared to C_i obtained from experimentally derived expressions for C_s :

$$C_i = 1.412 \quad \text{Campbell and Weynberg (based on Eq. 2.27)}$$

$$C_i = 1.382 \quad \text{Miao (based on Eq. 2.28)}$$

It is important to note that the above definition of C_i is based on the slamming force which is a function of the square of the velocity. This must be kept in mind when interpreting the above values of C_i derived from experimental observations which include buoyancy effects. The contribution of buoyancy to the impulse, denoted I_b , is a function of the square of the Froude number, and is given by:

$$I_b = \frac{1}{3} \frac{\rho a^2 w L}{w^2/gD} \quad (2.58)$$

This indicates a decrease of 0.1 to 0.2 in the C_i values derived from the expressions given by Campbell and Wenberg (1980) and Miao (1988), leading to an average estimate of about $C_i = 1.2$.

The response r of an SDOF system with mass M and natural period T_n to an impulse I of duration T_i ($\ll T_n$) is given as (e.g. Clough and Penzien, 1975):

$$r = \frac{I}{M\omega_n} \sin(\omega_n t') \quad (2.59)$$

where $\omega_n = 2\pi/T_n$ and t' is time measured after the end of the impulse. Thus the maximum response due to the impulse I is given as $I/M\omega_n$ and this occurs at time $t' = T_n/4$. In order to obtain the overall maximum response, the response at this instant due to the residual force F_r is also required. However, such a calculation may itself require a time-stepping procedure in order to account for the dynamic response of the cylinder. Once the two component responses have been obtained, they may then be summed to obtain the overall maximum response. This can in turn be used to determine quantities such as the maximum transmitted force or stress.

It is expected that the impulse coefficient derived from experimental observations will exhibit less scatter since it is not dependent on a single observation of the peak force. However, the applicability of the impulse coefficient in the context of engineering design is confined to situations where the impulse duration T_i is reasonably small in relation to the natural period T_n of the cylinder (e.g. a brace), such that the dynamic response and stresses may be determined by the impulse magnitude rather than the precise time history of the loading.

2.4 Slamming Force on an Inclined Cylinder

The previous sections have described the specific case of a horizontal cylinder subjected to wave impact. In general, the member's axis or the water surface may not be exactly horizontal which leads to an oblique impact. The flow in this situation is no longer two-dimensional and is more complex. Miller (1977) modelled this case using a strip approach wherein the slamming force is determined by adding the contributions of several incremental slamming loads on thin elements of the cylinder. The definition sketch for inclined impact is shown in Fig. 2.14. A cylinder of length L is inclined at an angle θ to the still water level and its axis is oriented normal

to the direction of wave propagation. The height of the lower edge of the cylinder from the still water level is denoted by h .

When the cylinder is subjected to an incident wave train, the initial contact is made at the lower edge and as the water level rises, its submerged length increases from 0 to L . This leads to a more gradual increase in the hydrodynamic force in comparison to the case of a horizontal cylinder. The submerged length of the cylinder is given by:

$$L_s = \begin{cases} \frac{\eta - h}{\sin\theta} & \text{for } 0 \leq \eta \leq (h + L \sin\theta) \\ L & \text{for } \eta > (h + L \sin\theta) \end{cases} \quad (0^\circ < \theta < 90^\circ) \quad (2.60)$$

The submergence normal to the cylinder axis varies along the submerged length and is expressed as:

$$s(y) = (L_s - y) \tan \theta = \frac{\eta - h - y \sin \theta}{\cos \theta} \quad (0 \leq y \leq L_s) \quad (2.61)$$

where y is measured from the lower edge of the cylinder.

The force on the cylinder is determined by analysing the force on a strip of width dy submerged by an amount $s(y)$ (see Fig. 2.14). The buoyancy force component normal to the cylinder axis on the strip is:

$$dF_b = \rho g A_i(s) \cos \theta dy \quad (2.62)$$

where $A_i(s)$ is given by Eq. 2.6. The water particle velocity and acceleration normal to the cylinder axis are given by $w \cos \theta$ and $\dot{w} \cos \theta$ respectively. The slamming force on the strip can be expressed as:

$$dF_s = \frac{1}{2} C_s(s) \rho D (w \cos \theta)^2 dy \quad (2.63)$$

where $C_s(s)$ is the slamming coefficient. Similarly, the expression for the inertia force on the strip is given by:

$$dF_i = C_m(s) \rho \pi \frac{D^2}{4} (\dot{w} \cos \theta) dy \quad (2.64)$$

where $C_m(s)$ is the inertia coefficient. The elemental drag force may be expressed as:

$$dF_d = \frac{1}{2} C_d(s) \rho D (w \cos \theta)^2 dy \quad (2.65)$$

The four force components on the strip can be integrated along the submerged length of the cylinder to yield the total force at any instant:

$$F = \int_0^{L_s} dF_b + dF_s + dF_i + dF_d \quad (2.66)$$

Eq. 2.60 can be rewritten in a summation form to yield:

$$F = \sum_{j=1}^N \left(\rho g A_i(s) \cos \theta + \frac{1}{2} [C_{s+d}(s)] \rho D (w \cos \theta)^2 + C_m(s) \rho \frac{\pi D^2}{4} (\dot{w} \cos \theta) \right) \frac{L_s}{N} \quad (2.67)$$

where N is the number of strips into which the length L_s is divided, the submergence s is determined from Eq. 2.61, and $y = (j L_s)/N$. The variations of the coefficients C_{s+d} and C_m with submergence have been discussed in Section 2.2.5.

Wave impact on an inclined cylinder results in a smaller peak force and longer rise-time in comparison to the case where the cylinder is horizontal. The effect of the longer rise-time is inconsequential for rigid cylinders, but may actually lead to a larger dynamic response in the case of a compliant cylinder if its natural period is comparable to the rise-time as seen in Section 2.3.1. Hence it may be necessary for a designer to determine whether the decrease in peak impact load due to the inclination of a cylinder has been offset by increased dynamic amplification caused by a corresponding increase in the rise-time.

It is noted that in reality, wave impact on an inclined cylinder results in a three-dimensional flow problem which is not being solved here. The flow in the vicinity of the cylinder, and the associated hydrodynamic force change significantly with increase in cylinder inclination, and the strip method described above is not expected to result in good estimates of the force for values of θ greater than 20° .

2.5 Water Particle Kinematics in Waves

The hydrodynamic force due to wave impact has been expressed in terms of the water particle velocity and acceleration at the free surface during the early stages of impact, and at the cylinder axis after complete submergence of the cylinder. Linear wave theory is used to determine the free surface elevation η and the corresponding water particle kinematics.

2.5.1 Regular Waves

For a regular wave train the water surface elevation η at the cylinder location is given by:

$$\eta = \frac{H}{2} \cos \omega t \quad (2.68)$$

where H is the wave height, ω is the wave angular frequency ($= 2\pi/T$ where T is the wave period) and t is time. The linear dispersion relation, which relates ω and the wave number k , is given by:

$$\omega^2 = gk \tanh(kd) \quad (2.69)$$

where d is the water depth.

The hydrodynamic force in the vertical direction is associated with the vertical water particle velocity and acceleration. On the basis of linear wave theory, these may be expressed as:

$$\left. \begin{aligned} w &= -\omega \frac{H}{2} G(z) \sin \omega t \\ \dot{w} &= -\omega^2 \frac{H}{2} G(z) \cos \omega t \end{aligned} \right\} \quad (2.70)$$

where

$$G(z) = \frac{\sinh[k(d+z)]}{\sinh[kd]} \quad (2.71)$$

and z is measured upwards from the still water level. In the present case, the value of z corresponds to the vertical location of the cylinder axis. Since Eqs. 2.70 are valid only for z between $-d$ and 0 , several methods have been described to evaluate the water particle kinematics in the vicinity of the free surface based on alternative extensions to the expressions given by linear wave theory. Chakrabarti (1988) has summarized various modifications to Eqs. 2.70 in order to extrapolate the evaluation of water particle kinematics above the still water level. For the present investigation, the kinematics above the still water level are taken as the values at the still water level itself. This assumption is valid for small amplitude waves since elevations relative to the still water level of the order of wave height are considered and thus it is reasonable to assume that $G(z) \approx 1$ within the precision of linear wave theory. Hence w and \dot{w} are replaced by $\dot{\eta}$ and $\ddot{\eta}$ respectively.

2.5.2 Effects of Free Surface Slope

The development of the slamming force which has been described in the previous sections is strictly valid only for a horizontal free surface. If instead the free surface is assumed to impact the cylinder at an angle δ to the horizontal as shown in Fig. 2.15, the water particle velocity normal to the free surface is $v_n = \dot{\eta} \cos \delta$, and the vertical component of the slamming force per unit length is then given by:

$$\begin{aligned} F_s &= \frac{1}{2} C_s \rho D v_n^2 \cos \delta \\ &= \frac{1}{2} C_s \rho D \dot{\eta}^2 \cos^3 \delta \end{aligned} \quad (2.72)$$

On the basis of a wave train which is assumed to propagate steadily, it can be shown that the angle δ is a function of the vertical velocity of the free surface:

$$\frac{\partial \eta}{\partial x} = -\tan \delta = -\frac{1}{c} \dot{\eta} \quad (2.73)$$

where c is the wave celerity and x is measured along the direction of wave propagation.

Suitable corrections to the slamming and impulse coefficients obtained from measurements of the vertical force can now be developed by applying the result for $\tan \delta$ in Eq. 2.73 to Eq. 2.72. On this basis, it may be shown that the slope correction factor for the slamming coefficient is given by:

$$\frac{C_s'}{C_s} = \left[1 + \left(\frac{\dot{\eta}}{c} \right)^2 \right]^{3/2} \quad (2.74)$$

where C_s' is a slamming coefficient derived on the basis of v_n instead of $\dot{\eta}$. A similar correction factor can be obtained for the impulse coefficient in Eq. 2.56 to provide:

$$\frac{C_i^*}{C_i} = 1 + \left(\frac{\dot{\eta}}{c} \right)^2 \quad (2.75)$$

Figure 2.16 illustrates the behaviour of these correction factors for the case of the steepest non-breaking wave used in the experiments which has a period $T = 1.1$ sec, and height $H = 17$ cm. Only the portion of the wave record varying from the lowest point in the wave trough to the highest point in the wave crest is shown since the correction factors are applicable for a rising water surface which causes slamming forces. It is seen that the factors deviate significantly from the value of 1.0 in the zero-crossing zone of the wave where $\dot{\eta}$ reaches a maximum. The maximum value of C_s'/C_s is about 1.17 and that of C_i^*/C_i is 1.11.

It has been pointed out earlier that the slamming process is governed by a variety of factors, many of which are difficult to control, and which account for considerable scatter in experimental data. Because of this, it may well turn out that the above corrections for the free surface slope effects in general may be an unnecessary refinement.

2.5.3 Random Waves

The extension of the numerical simulation to the case of random waves described by a specified spectrum may also be made. The two cases considered here correspond to a narrow-band spectrum and the two parameter Pierson-Moskowitz spectrum.

The form of the narrow-band spectrum adopted here is given by:

$$S_{\eta}(f) = \begin{cases} \frac{\pi H_s^2}{32f_r} \cos\left[\frac{\pi}{f_r}(f - f_0)\right] & \text{for } f_0 - \frac{f_r}{2} \leq f \leq f_0 + \frac{f_r}{2} \\ 0 & \text{otherwise} \end{cases} \quad (2.76)$$

where H_s is the significant wave height, f_0 is the peak frequency, and f_r represents the frequency range over which the spectrum is non-zero.

The two-parameter Pierson-Moskowitz spectrum is instead given as:

$$S_{\eta}(f) = \frac{5H_s^2}{16f_0} \left(\frac{f_0}{f}\right)^5 \exp\left[-\frac{5}{4}\left(\frac{f}{f_0}\right)^{-4}\right] \quad (2.77)$$

For either spectrum, a time record of the free surface elevation may be represented as a superposition of regular wave trains with different amplitudes, frequencies and phases:

$$\eta(t) = \sum_{i=1}^{N_f} A_i \cos(2\pi f_i t - \varepsilon_i) \quad (2.78)$$

where A_i , f_i and ε_i are respectively the amplitude, frequency and phase of the i -th regular wave component, and N_f is the number of frequencies used in generating the random wave record.

The randomness in $\eta(t)$ can be incorporated in various ways. The method adopted here, known as the deterministic spectral amplitude model (Tuah and Hudspeth, 1982), or the random phase spectrum method (Funke and Mansard, 1984), assumes that the the phases ε_i in Eq. 2.78 are random and uniformly distributed between 0 and 2π , while the amplitudes A_i are determined from the discretized spectral density as:

$$A_i = \sqrt{2 S_{\eta}(f_i) \Delta f} \quad (i = 1 \text{ to } N_f) \quad (2.79)$$

The spectrum of the resulting time series of η will then exactly match the target spectrum.

Analogous to Eqs. 2.70, expressions for the vertical velocity w and acceleration \dot{w} for the case of a random wave train are given respectively by:

$$\left. \begin{aligned} w &= \dot{\eta} = - \sum_{i=1}^{N_f} 2\pi f_i A_i \sin(2\pi f_i t - \varepsilon_i) \\ \dot{w} &= \ddot{\eta} = - \sum_{i=1}^{N_f} (2\pi f_i)^2 A_i \cos(2\pi f_i t - \varepsilon_i) \end{aligned} \right\} \quad (2.80)$$

There are a number of interrelated parameters which must be selected in order to carry out a numerical simulation of η , $\dot{\eta}$, and $\ddot{\eta}$. These include the frequency interval Δf , the number of frequency values N_f , the time step size ΔT_w , the duration of the wave record T_w , and the number of data points in the wave record N . Relations between these parameters are:

$$\Delta f = \frac{1}{T_w} \quad (2.81)$$

$$\Delta T_w = \frac{1}{2N_f \Delta f} \quad (2.82)$$

$$N = \frac{T_w}{\Delta t_w} + 1 \quad (2.83)$$

Eq. 2.82 represents the Nyquist criterion which relates the maximum frequency $N_f \Delta f$ that can be resolved from a signal which is discretized with a time interval ΔT_w .

T_w must be sufficiently large to ensure that the number of waves in the record is sufficient for carrying out a probability distribution analysis; and Δf is determined directly from Eq. 2.81. In the case of a narrow-band spectrum, the frequency range of the spectrum f_r also needs to be selected and may be related to the spectral width parameter of the wave record. The number of discretized frequencies with non-zero coefficients is approximately $f_r/\Delta f$.

2.6 Computational Considerations

The numerical simulation of slamming force deals with an event which occurs over very small time scales in comparison to the wave period. The time step size Δt_s between successive values of the computed vertical force should be chosen so as to represent accurately the variation of the force with time and simultaneously minimize the computational effort required. Although the frequency components in a typical wave train giving rise to the vertical force may be relatively low, there is a very rapid variation of the vertical force in every wave cycle associated with the onset of slamming. This corresponds to the presence of significant high frequency components in the force record. The choice of a particular time step size depends in part on the specific problem under consideration i.e. whether the cylinder is rigid or compliant, the cylinder is horizontal or inclined and whether the waves are regular or random.

In the case of regular waves interacting with a rigid horizontal cylinder, the choice of Δt_s to be used in the simulation is influenced mainly by the need to model the rapid variation in vertical force immediately after the instant of impact. The maximum slamming force is assumed here to occur instantaneously, so that it is important that the instant of slamming be present in the sample values since the vertical force reaches a critical value at this point. The value of Δt_s is determined so as to ensure that the partially submerged stage of the cylinder is adequately represented in the simulation. Specifically, the difference in wave elevations between two successive time steps in the simulation when the free surface is travelling the fastest, is taken as $0.1D$. Thus for deep water waves:

$$\Delta t_s = \frac{DT}{10\pi H} \quad (2.84)$$

Typically this choice leads to between 50 and 2500 time steps in each wave period. The instant of impact can be determined by linear interpolation between successive time steps for which the cylinder is above the water surface at the former instant and partially submerged at the latter. The hydrodynamic force on the cylinder is then computed at this time step also.

A random wave record synthesized using the Nyquist criterion of Eq. 2.82 may not have sufficient resolution to determine the instant of slamming using linear interpolation described for regular waves, since in cases where the cylinder diameter is appreciably smaller than the significant wave height, it is possible that successive values of η might correspond to no submergence and complete submergence respectively. In order to treat such occurrences, and since a smaller Δt_s interval is required only for periods of partial submergence, a cubic spline interpolation technique is used to introduce additional sample points within the corresponding time interval. The cubic spline method preserves rapid changes in slope especially in the velocity and acceleration records. Once values at smaller intervals have been obtained, linear interpolation is used to obtain the instants at which slamming occurs.

When a computation of the dynamic response of the cylinder to the wave force is required, the factors that govern the choice of Δt_s are the frequency components in the incident wave train, the natural frequency of the system, the Newmark iteration convergence criterion and the frequency components in the hydrodynamic force. The chosen value of Δt_s is the smallest obtained from a consideration of these four factors and is usually governed by the need to correctly represent the rapid variation of the hydrodynamic force immediately after impact. Unlike the case of the rigid cylinder, the technique of interpolation to determine the exact instant of slamming cannot be applied since the position of the cylinder is not fixed. The value of Δt_s should be sufficiently small so that successive samples when the cylinder is dry and then partly submerged are such that $s/a \approx 0$ for the latter sample and the slamming force peak that occurs immediately after water-cylinder contact is not underestimated by a large amount. In addition, if the slamming force is assumed to reach its peak value instantaneously, the value of Δt_s used in the simulation will imply a rise-time of Δt_s . Hence a zero rise-time condition cannot be simulated in the case when the dynamic response of the cylinder is considered.

It has however been shown in Section 2.3.1 that a zero (or near zero) rise-time condition for a typical slamming event will not produce significant dynamic response implying that the magnitude of the dynamic stresses will be low and not be of interest in design situations. For

typical rise-times between 5 and 25 msec, a value of Δt_s that ensures at least 2 samples within the rise-time duration is adequate to accurately compute the dynamic response. The simulation is conducted at equally spaced points in time in contrast to the rigid cylinder case wherein the Δt_s value varies depending on the stage of the cylinder submergence.

The above techniques are applied in a similar way for the case of the inclined cylinder, where only the rigid cylinder case has been examined.

Chapter 3

EXPERIMENTAL STUDY

A significant component of this study on wave slamming relates to an experimental investigation in which an instrumented cylinder has been subjected to slamming forces in non-breaking and breaking waves. The horizontal test cylinder was fixed at different elevations near the still water level and the vertical force was measured for incident regular waves of various heights and periods. The same test set-up was also used to measure the horizontal and vertical impact forces due to a plunging wave which could be generated to break at different locations along the wave flume. The tests have been conducted in the wave flume of the Hydraulics Laboratory of the Department of Civil Engineering at the University of British Columbia. This flume is equipped with a wave generator which is capable of producing regular and random waves.

The following sections describe the equipment and methods used in the experimental set-up for wave generation and data acquisition. The techniques of signal conditioning and data analysis used to derive pertinent information from the measurements are also discussed.

3.1 Test Facilities

The apparatus used for the experimental study of the slamming force can be classified under three separate functional headings. These are: the wave generation equipment, the instrumented cylinder which is subjected to wave slamming, and the equipment used for data acquisition.

3.1.1 Wave Flume

A photograph of the wave flume in which the experiments have been conducted is shown in Fig. 3.1. The flume is 40 m long, with a 15 m long test section, 0.62 m wide, and operates at a nominal water depth of 0.55 m. The flume has a plywood beach of 7.7 m length set at a slope of 1:14, and which is covered by a mat of synthetic hair. A large holding tank at the end of the beach also helps to absorb and dissipate incident wave energy. The reflection of wave energy from this beach is quite low, although it has not been measured in this study.

3.1.2 Wave Generation

A photograph of the wave generator is shown in Fig. 3.2. The generator consists of an electrically powered servo-motor which drives a linear actuator connected to a hinged wave paddle. The rotation of the servo-motor shaft is converted to a translatory motion of a thrust rod by the linear actuator which has a usable operating stroke of ± 25 cm. The wave paddle can be configured to operate in three modes, namely a hinged flapper, a combination flapper-piston and a piston articulation. These enable the reproduction of velocity profiles ranging from shallow to deep water waves. Waves with periods between 0.8 and 2.5 sec and wave heights of up to about 25 cm can be generated in this flume.

The wave generator is controlled by a Digital Equipment Corporation (DEC) VAXstation 3200 computer running the VMS operating system. The GEDAP (Generalized Experiment control, Data acquisition and Analysis Package) library of software and the associated RTC (Real Time Control) programs developed at the Hydraulics Laboratory of the National Research Council of Canada (Miles, 1989, Pelletier, 1989) allow the user to control the wave generation and data acquisition processes. The software allows for three regular wave generation options: a sinusoidal wave train with specified height and period; a sinusoidal wave train of maximum steepness for a specified wave height and a sinusoidal wave train of maximum steepness for a specified wave period. Random waves can also be generated either from a target wave spectrum based on a theoretical parametric spectral model (e.g. Pierson-Moskowitz, JONSWAP etc.) or

from a prototype spectrum obtained from either a wave hindcasting procedure or from full-scale measurements at sea.

Synthesis of Wave Generator Drive Signals

The computer programs for the synthesis of the wave generator control signals are based on linear theory (Havelock, 1929) which relates the rotation or displacement of the waveboard to the water surface elevation at the front of the waveboard. Factors such as the propagation of the wave train from the waveboard to the test section, the articulation mode of the wave paddle, and the dynamics of the servo-system are all taken into account in the creation of the driving signal.

The process involves the generation of a desired free surface elevation time series at a specified location in the wave flume. This wave record is generated at a sampling interval of 0.05 sec (20 samples/sec). The transfer function between the paddle motion and the resulting water surface elevation, along with the wave generator calibration relating the paddle motion to the applied voltage are used to compute another time series which is subsequently used as the drive signal. A DEC AAV11 digital-to-analog (D/A) converter combined with an analog active low-pass filter is used to convert the drive signal to a continuous voltage which is sent to the controller of the servo-motor. The highest frequency of waves (with a minimum wave height of 5 cm) that can be generated in this flume is limited to about 3.5 Hz due to the maximum velocity of 0.61 m/sec which can be achieved by the actuator thrust rod.

If the water surface elevation at the test area in the wave flume is measured with a wave probe when waves are generated with the above signal, the variation of the free surface elevation with time will usually not be the same as that of the desired wave train. Some of the factors that cause the differences include limitations of the transfer function used to approximate the servo-dynamics of the wave machine controller, limitations of linear wave theory in calculating the waveboard motion and nonlinear wave propagation effects which may occur as the wave travels from the wave machine to the wave probe. In the case of regular waves, the generated signal can be modified with a suitable amplification factor given by H_d/H_m , where H_d is the desired wave

height, and H_m is the measured wave height. This amplification factor is applied to generate another time series of the driving signal, and the procedure is repeated until the desired wave height is obtained at the test location.

3.1.3 Cylinder model

A photograph of the test cylinder assembly is shown in Fig. 3.3(a), and a corresponding schematic diagram is shown in Fig. 3.3(b). The PVC cylinder has an external diameter of 4.2 cm and is 30 cm long. It is expected that the low length/diameter ratio of 7.14 will reduce the likelihood of errors due to wave skew and also limit the flexural response of the cylinder. The sealed ends of the cylinder are connected by aluminium tubes to the sensing plate of the force transducer which is located 34 cm above the cylinder axis. Since the aluminium tubes transmit the force on the cylinder to the dynamometer, they have to be shielded from the effects of the incident waves in order for the dynamometer to read the force on the cylinder only. This is achieved by means of plastic tubes which are connected to the back face of the dynamometer, and which act as sleeves in keeping the force transmitting members dry.

The dynamometer is attached to a large frame spanning the width of the flume and fixed to the laboratory floor. The connection of the dynamometer to the frame is via a solid steel rod such that the cylinder-transducer assembly can be easily moved vertically and also pivoted about the vertical and horizontal planes. In this position, the cylinder axis is located 8.7 m from the wave paddle.

Measurement of Hydrodynamic Impact Forces

The variables which affect the vertical force on a horizontal circular cylinder in waves have been discussed in Section 2.1. Some of these can be readily quantified and controlled in a laboratory. However, other factors such as air entrainment in the water surface, compressibility of the fluid on impact with the cylinder, water run-up on the sides of the cylinder, the possibility of not having a perfectly smooth cylinder surface or a perfectly circular cylinder cross-section,

minor deviations in cylinder alignment in the horizontal and vertical planes, and residual vibration from the laboratory floor due to the wave generator are difficult to measure and their influence on the hydrodynamic force is unknown. It is expected though, that the relative deviations in the measured force due to these factors will be small, and that the results from this experimental study will be useful from an engineering standpoint.

Section 2.3 examines the requirements of the force measuring system for this particular application and points to the necessity of making an assumption regarding the nature of the rise-time of the slamming force. This is difficult since the rise-time is one of the unknowns in this study. Various methods can be used to measure hydrodynamic impact on a cylinder. One possibility is to measure the dynamic response of the test cylinder with an accelerometer; compute the velocity and displacement of the cylinder from the acceleration record and then use Eq. 2.34 to determine the applied force on the cylinder. This method may suffer from difficulties relating to noise, and the unknown effects of the added mass and hydrodynamic damping with increasing cylinder submergence. The use of several pressure transducers located on the surface of the test cylinder has been reported in previous studies. The measurements of pressure on the cylinder surface are integrated to determine the total force on the cylinder. The advantages of this method include the relative absence of dynamic effects, and extremely fast response times. However among the limitations are the requirements for elaborate instrumentation and significant data storage capacity. A dynamometer can be used to obtain good measurements of slamming forces in waves if the experimental rig is designed to meet the necessary dynamic criteria. The total force on the cylinder is available as a single signal, and it is possible to carry out longer tests in waves and generate smaller amounts of data in comparison to an experiment involving pressure transducers.

The most important factor to be considered when designing a model to measure impulsive forces is that the system should have a very high natural frequency of vibration in comparison to the dominant frequencies which are present in the dynamic force. There are two different modes of vibration that can influence the measured slamming force in the above cylinder-dynamometer

configuration. The cylinder may vibrate in a flexural mode between its end supports and the overall cylinder and force transmitting member assembly may oscillate as a lumped mass with the dynamometer providing the stiffness component. The flexural mode of vibration can be reduced to a very large extent by using a rigid cylinder with a low length-to-diameter ratio. The reduction of the overall dynamic response necessitates that the cylinder and force transmitting members be light and the dynamometer have a high stiffness in order to accurately measure the rapidly varying applied force. The damping of the model should also be low in order to minimize phase errors between the applied and measured force.

There are contradictory requirements in the need for a model that is quite stiff, so that the dynamic amplification of the impulsive force is minimal, and the rise-time is measured correctly. In order for the system to be stiff, the dynamometer must have a high stiffness, which for low load levels implies that the strain gauges in the dynamometer will not produce a significant change in voltage, leading to a weak signal which is not much higher than the background noise. Conversely, if a dynamometer with a lower stiffness is employed so that a high level signal is obtained for the applied force, the natural frequency of the system is low and will lead to the measured slamming force being significantly influenced by dynamic effects.

In this study, the careful use of high-gain signal amplifiers, low-noise cables and judicious numerical filtering techniques have made it possible to use a reasonably stiff dynamometer and obtain good results from the force measurements.

3.1.4 Data Acquisition and Control

In addition to the physical factors which affect the magnitude of the slamming force, the accuracy with which this highly dynamic force is measured and stored is dependent on the instrumentation, which includes the dynamometer, amplifiers, power supplies, signal carrying cables, analog to digital conversion hardware and the controlling computer. After the force is converted to a voltage by the dynamometer, the signal is amplified, digitized and stored as numerical data for further analysis. The accuracy of the sampled data corresponding to the force

depends on the linearity of the transducer and amplifiers and their ability to remain drift free between calibration and the actual tests. Furthermore, noise due to stray electromagnetic fields and the AC power line frequency of 60 Hz can get mixed with the signal from the dynamometer stage, and during signal amplification and transmission. Standard low-pass noise filtering of this data is not possible because the slamming force may have significant frequency components in the same range as the interfering noise.

Figure 3.4 shows a block diagram of the apparatus used for acquiring water surface elevation and force data during the experiments. The main components are the wave probe, force transducer, amplifiers, signal cables, analog-to-digital (A/D) converter and the computer used to control the experiment and simultaneously acquire data.

The wave probe is based on a design of the Hydraulics Laboratory of the National Research Council of Canada. It is a capacitance-type 'bow-string' sensor consisting of a loop of wire stretched on one side of a metal frame. The wire loop sensor is connected to an amplifier designed to convert the change of capacitance to a measurable change in voltage. This device has a linearity better than 98.5% and a resolution better than 1 mm, the latter being limited mainly by the meniscus, and under wave action, by the run-up.

The dynamometer used for measuring the force on the cylinder is a single-ring multi-component transducer (Advanced Mechanical Technology Inc. SRMC3A-100) with six output channels. These channels correspond to the forces in three orthogonal directions (F_x , F_y and F_z) and moments about those three axes (M_x , M_y and M_z). The instrument uses strain gauges to perform the force and moment measurements. The gauges are configured in four-arm bridges to provide high thermal stability. The F_x channel of the dynamometer is used for the measurement of the vertical force in this study. At a rated stiffness of 2.63×10^6 N/m, the peak load capacity of this channel is 225 N and the sensitivity is $54 \mu\text{V/N}$ for an excitation of 10 V.

The output voltage from the F_x channel of the dynamometer is very low level for typical wave slamming forces and has to be amplified before it can be recorded. The amplifier used for this

application is a Pacific Instruments Model 8255 Transducer Conditioning Amplifier which provides excitation, balance, calibration, amplification and filtering functions. The switch selectable low-pass filter provides steps of 1 Hz, 10 Hz, 100 Hz, 1 kHz, 10 kHz and wideband (no filtering). The amplifier can be set for a maximum gain of 2500. However, it was found that a gain of 2500 was not adequate to obtain a good signal to noise ratio for the experiments. The force signal is hence amplified in two stages. The first stage consists of an amplifier built in-house which is powered by lead-acid batteries and provides a gain of 1000. By virtue of its running from a DC power source, this amplifier adds very little noise to the signal from the transducer. This preamplified signal is then further amplified by a factor of 5 using the Pacific Instruments amplifier. The amplified force signal is transmitted by shielded cable to the A/D converter.

The analog-to-digital converter is used to discretize a continuously varying voltage to a series of digital values spaced at a pre-determined time interval. The two properties of the converter which determine how accurately the digitized force signal represents the original continuous waveform are the resolution and the sampling rate. The resolution of the converter is defined as the smallest difference in input voltage which can be measured. The DEC ADQ32 12 bit A/D converter used in this study has a maximum input range of ± 10 V and programmable gains $G = 1, 2, 4$ or 8 . The usable input voltage range is hence determined from the gain setting for any particular channel as $V_{\text{range}} = \pm 10/G$ V. The objective is to maximize the resolution and hence minimize the quantization noise in the sampled signal. In the experiments with non-breaking waves, the force signal did not exceed ± 2 V, and the gain for that channel was set to 4 yielding a V_{range} of ± 2.5 V. The resolution in this case is given by $\Delta V = 5/2^{12} = 0.00122$ V. This corresponds to a resolution of 1.26×10^{-3} N, based on the calibration constant of the dynamometer.

The sampling rate which is defined as the number of analog-to-digital conversions made in one second is determined on the basis of the frequency components in the input force signal. The A/D converter used in this study is capable of a peak sampling rate of 200,000 samples/sec when

using only one channel. However, the sampling rate should be chosen so that the input force is correctly recorded, and the size of the data files obtained from the experiments are not unnecessarily large. The sampling interval has to satisfy the Nyquist criterion which states that $\Delta t_{\max} = 1/(2 f_{\max})$, where Δt_{\max} is the maximum allowable time difference between successive samples to prevent aliasing and f_{\max} is the highest frequency component in the signal. This implies that there must be at least 2 samples per cycle of the highest frequency component present in the acquired signal. It has been noted earlier that the slamming force signal has significant high frequency components and that low-pass filtering of the signal should be done at a cut-off frequency beyond which no force information is present. In order to determine the sampling rate for the measurement of the force signal, it is necessary to know the highest frequency which must be retained in order to accurately describe the variation of the slamming force.

A preliminary measurement of the slamming force was made in which the cylinder was placed just touching the still water level, the amplifier low-pass filter cut-off was set to 10 kHz and the sampling rate was 20 kHz. It was observed that the rise-time for a slamming event due to a wave of 1.2 sec period and 0.2 m height was typically 8 msec. The rise-time and magnitude of the slamming force peak were not modified when the low-pass filter on the amplifier was reduced from the 10 kHz setting to a 1 kHz cut-off. There however was a noticeable difference in the force trace when the filter setting was further decreased to 100 Hz. It was thus decided to operate the amplifier filter using a 1 kHz cut-off. The sampling rate was then fixed at 2.5 kHz to satisfy the Nyquist criterion and prevent aliasing errors.

3.2 Dynamic Characteristics of the Test Cylinder

The dynamic characteristics of the cylinder were examined using a free vibration test which involved applying a step load on the test cylinder using a weight suspended by a steel wire that was then cut using an acetylene torch. The resulting force transmitted to the dynamometer was measured and is shown in Fig. 3.5. The cylinder-dynamometer combination oscillates at the

predominant frequency of 290 Hz as can be seen from the spectral density of the record shown in Fig. 3.6. The other minor vibration components present at frequencies of 75 Hz, 130 Hz and 190 Hz which do not seem to be related to the dominant frequency, may be caused by vibration of the support structure and cross-talk from the other channels of the dynamometer. Quantitative measurements of these effects including the level of background noise were not obtained. The first force peak is reached in 2.4 msec which provides an indication of the transient response capabilities of the test cylinder assembly. The damping factor is evaluated from the free vibration trace using the following relationships:

$$R_f = \ln \left[\frac{f_m}{f_{m+n}} \right] \quad (3.1)$$

$$\zeta = \sqrt{\frac{R_f^2}{R_f^2 + 4\pi^2 n^2}}$$

where f_m and f_{m+n} are amplitudes of the free vibration force trace after m cycles and $m+n$ cycles respectively. The average damping factor in air was determined to be about 2%.

Figure 3.7 shows the early stages of a typical wave slamming record which has only been filtered with a 1 kHz low-pass filter at the amplifier stage. It can be seen that when the free surface is below the cylinder, the measured force is not zero but consists of background electromagnetic noise and vibration. At the instant of slamming, the force on the cylinder begins to increase rapidly and reaches a maximum after 15 msec. This rise-time is not the same for all slamming events and varies to quite an extent. The individual digitized samples are also shown as dots on the force trace. It is evident that the sampling rate is high enough to record accurately the increase of the slamming force. It is also seen that there are some oscillations superposed on the force trace as it increases to the first maximum, which is comparable to the simulated behaviour shown in Fig. 2.10(b). This indicates that the cylinder-dynamometer assembly is able to respond quickly to the applied force (see Section 2.3.1), and that the measured peak force and rise-time are good estimates of the actual values.

3.3 Horizontal Cylinder in Non-Breaking Waves

The computer used for data acquisition runs software which controls the A/D converter in terms of setting up the channels to be used, the gain for each channel, the sampling rate and the length of time for which data is collected. The wave probe and dynamometer were calibrated by a program which relates known values of water surface elevation or force to corresponding voltages read by the A/D converter. Since both the devices showed linear characteristics over the range of interest, the calibration constant and zero offset were the only parameters determined from the calibration process.

The computer runs two intercommunicating processes concurrently. One of the processes sends the control signal to the wave machine and the other acquires data from the A/D converter. This allows for wave generation and data acquisition to be synchronized so that sampling is started at a specified time interval after the wave machine is activated. The delay between activating the generator and starting measurements is usually set between 15 to 20 sec which allows for the generator to ramp up to full amplitude and the wave train at the test site to stabilize. It is hence possible to conduct an experiment and store the measured wave record at the test site, and repeat the experiment to store the corresponding slamming force on the cylinder, with both records having the same starting time with reference to the instant that the wave generator was activated.

The experiments were carried out in two stages. The first stage consisted of generating regular waves of different heights (10 to 23 cm) and periods (1 to 1.8 sec) in the flume and storing the measured wave train at the test site at a sampling rate of 2500 samples/sec. Although this sampling rate is very high for acquiring data from a wave probe, it is necessary to sample the water surface elevation at the same rate as the wave force due to a data acquisition software and hardware limitation which introduces a varying phase difference between observed values of the same signal which has been sampled at different rates. This error is not important in cases where data with low frequency content is being digitized, but it is not acceptable when events are

occurring which have time scales in milliseconds. Once the wave record was acquired, it was converted to physical units (metres) using the calibration information, numerically filtered to remove noise, and resampled at a lower rate of 50 samples/sec to conserve storage space on the computer.

The cylinder model was not present at this stage and the wave probe was placed coincident with the axis of the cylinder. It is noted here that the wave record measured at the cylinder location in the absence of the cylinder will be different from the wave record observed when the cylinder is present in the flume. The wave field in the vicinity of the experimental cylinder is slightly modified due to runup and reflection effects which influences the water surface elevation and hence the computed water particle kinematics. However, the experimental results obtained for the force coefficients should be applicable in design situations where the incident, undisturbed wave conditions are used to estimate the water particle kinematics. Consequently the incident, undisturbed water surface elevation at the cylinder location has been measured in this experimental study. To ensure that a particular wave train was repeatable over separate experiments, multiple measurements of the same wave train were obtained and analyzed for variability. The repeatability was excellent. Data for each test run for a particular wave height and period was recorded for 20 sec.

In the second stage, the wave probe was removed and the cylinder was placed in the flume. The orientation and elevation of the cylinder were checked to ensure that the axis was perpendicular to the walls of the flume, and that the lower surface of the cylinder was horizontal. The waves corresponding to the stored regular wave trains were generated again and the vertical force on the cylinder was measured at a sampling rate of 2500 Hz and stored. Tests were performed for 3 different elevations of the cylinder, $h = 0.5$ cm, -4.5 cm, and 4.5 cm.

3.4 Data Analysis

The following section describes the techniques used to analyze the wave record and corresponding slamming force records obtained from the tests in regular waves in which the cylinder axis was horizontal and oriented parallel to the wave crests. Section 3.4.1 examines the effects of noise in the force record and the techniques used to filter unwanted components out of the signal. Sections 3.4.2 and 3.4.3 describes how the filtered wave and force records are analyzed to determine quantities such as the slamming coefficient and the rise-time.

3.4.1 Noise Filtering Techniques

Most analyses of experimental data usually involve filtering the data to remove unwanted noise which can affect the results. This is a fairly simple procedure which can either be implemented in the form of analog filtering by dedicated circuits during the data collection stage, or by using digital filtering algorithms after the data has been digitized and stored. The treatment of correct noise removal is especially important in this study since the slamming force typically has frequency information which is in the same range as some electrical noise. Any filtering technique used for analyzing such data must ensure that valid force information is not removed along with the interfering noise.

A variety of sources can produce noise. The power supply lines that run in the laboratory generate electromagnetic noise which shows up as a 60 Hz signal of unknown magnitude mixed with the main signal. Electromagnetic noise is also generated from other devices (e.g. motors) within the laboratory. Thermal noise of a random nature and spread over a range of frequencies is generated within the transducers and circuitry of the amplifiers. The dynamometer which is quite sensitive picks up mechanical noise from its floor supports. In addition, quantization noise is introduced during the analog-to-digital conversion process, but can be mitigated to a large extent by using the full range of the A/D converter for a given signal.

A significant amount of effort has been spent in this study in attempting to minimize the pick-up and transmission of noise during the experiments. A high signal-to-noise ratio cannot be achieved in this study since the stiffness requirements for the dynamometer result in low output voltages as discussed earlier in Section 3.1.3 and 3.1.4. Although the dynamometer output is amplified by a factor of 5000, any noise present before amplification is also increased and the advantages of amplification are evident only in the case of noise picked up during transmission of the signal from the amplifiers to the A/D converter. The objective in the present set-up has been to minimize noise before and after amplification by using stable power supplies, high quality transducers, amplifiers and shielded signal cables.

It has been stated in Section 3.1.4 that the slamming force is not modified if the low-pass filter on the amplifier is set at a cut-off of 1 kHz. This enables the removal of all noise components in the force signal which have frequencies greater than about 1100 Hz, since the filter has a finite roll-off slope.

Figure 3.8(a) shows the variation of the water surface elevation due to a regular wave of height $H = 22.6$ cm and period $T = 1.4$ sec, and also indicates the location of the test cylinder. The slight difference between the actual elevation of the cylinder, $h = 0.5$ cm, and the elevation indicated in Fig. 3.8(a) is due to the wave record being measured in the absence of the cylinder, whereas the presence of the cylinder causes local variations of 3 to 5 mm in the water surface which can cause impact to occur slightly earlier or later than the instant in the wave record when $\eta = 0.5$ cm. The corresponding vertical force on the cylinder is shown in Fig. 3.8(b). It can be seen that the signal-to-noise ratio is much higher for the wave record than for the force record. The analysis of these records begins with numerical (digital) filtering in order to remove those components of noise that have not been removed by the analog filters in the amplifiers of the dynamometer and the wave probe.

Digital filtering of time series data can be done in two ways. A non-recursive filtering technique using an FFT-based algorithm provides low-pass, high-pass, band-pass or band-stop

(notch) filtering capabilities. The other method, known as polynomial filtering is recursive and is based on simple interpolating polynomials which act as low-pass filters. Polynomial filtering is carried out by fitting a curve of a chosen order to a window of data within the main data series. This method weights the individual datum by its neighbouring data to substantially reduce noise. The polynomial filter used to process the water surface elevation and force data is a GEDAP program LP_K_FILT which provides low-pass filtering of an input time series by convolving the data with a 41 point Kaiser filter that allows for variable ripple attenuation levels. The attenuation is inversely related to the roll-off slope of the filter. Convolution in the time domain rather than multiplication in the frequency domain saves on computer memory requirements since the frequency domain technique needs a filter of length equal to the size of the input time series.

3.4.2 Determination of the Instant of Slamming

The slamming event shown in Fig. 3.8(a) shows that the vertical force begins to increase rapidly at about $t = 18.25$ sec. This estimate is made visually and is based on the rapid rise of the force beyond the ambient noise component which itself ranges from -0.05 N to 0.05 N. The correct determination of the instant of slamming is important in this study since it affects the correct estimation of parameters such as the cylinder submergence and the associated buoyancy force component, as well as the rise-time of the slamming force. Due to the volume of data to be processed, it is not efficient to fix visually the instants of slamming in a force record, and hence an accurate and stable slamming detection algorithm is developed which can be used to process the measured force.

Since the elevation of the cylinder h is known for every experiment, and the wave record corresponding to the measured slamming force is also known, the instant of slamming can be fixed as that when the water surface elevation becomes greater than the value of h . This technique was tried unsuccessfully, as it was observed that the force signal was sometimes still

zero or was already rising rapidly when a slamming event was indicated by the wave record as seen earlier in Fig. 3.8.

It is also not possible to associate the onset of slamming when the measured force increases beyond a small threshold value, due to the significant ambient noise level when the cylinder is above the free surface. Consequently it is necessary to use some property of the force record which is not affected by the noise, but which changes when slamming occurs. One such parameter is the local variance which is a measure of the variance of the sampled data over a chosen interval of time in the force record. The local variance of the force as a function of time t , with a sampling window of width t_w , is given by:

$$\sigma^2(t, t_w) = \overline{F^2}(t, t_w) - (\overline{F})^2(t, t_w) \quad (3.2)$$

where $\overline{F^2}(t, t_w)$ is the moving average of the square of the force record, $(\overline{F})^2(t, t_w)$ is the square of the moving average of the record and $\sigma^2(t, t_w)$ is the local variance. The behaviour of the local variance of a small section of the slamming force record in Fig. 3.8(b) is shown in Fig. 3.9. It can be seen that while the force record is affected by background noise, the local variance is quite stable and begins to increase only with the onset of slamming. The window size and the threshold beyond which an increase in the local variance indicates the onset of slamming were chosen after analysing several slamming records with various values of t_w . A window size $t_w = 0.004$ sec (10 samples) and a variance threshold of 0.01 N^2 has been used to detect slamming events in this study.

The method has been optimized in the case of a force record for regular waves. A visual inspection is first used to determine the points in time within which the first slamming event occurs. The algorithm scans this region of the record, determines the instant when the variance threshold is exceeded and marks that point as the beginning of a slamming event. The search is then moved ahead by one wave period and the procedure is repeated for all the slamming events until the end of the force record.

3.4.3 Analysis of Wave and Force Records

Figure 3.10 shows a flow diagram of the various stages involved in the analysis of the force and wave records. The records are initially subject to digital low-pass filtering to remove high frequency noise components which were not removed by the amplifier. The cut-off frequency for the force record has been set at 400 Hz since a spectral analysis of the slamming force indicates that there is no significant energy component in the record beyond 400 Hz. The filtering does not affect the peak magnitude or the rise-time of the slamming force. The wave records which have already been stored at a lower sampling rate of 50 Hz are then low-pass filtered at a cut-off frequency of 6 Hz to remove any stray data points in the record which may affect the water particle velocity values. The filtered force record is then processed using the local variance algorithm (see Section 3.4.2) in order to identify the slamming events in the record. Since the wave record has only 50 samples per second as compared to 2500 samples/sec for the force, a cubic spline based representation of the record is used to determine the free surface elevation and velocity at any instant corresponding to a given point in the force record.

The resulting time histories of the water surface elevation and the corresponding vertical force on the cylinder are analyzed to obtain the slamming coefficients and other relevant parameters. The main parameter of interest is the peak slamming coefficient which corresponds to the maximum force observed immediately after impact and is estimated as:

$$C_{so} = \frac{F_{to}}{0.5\rho LD\dot{\eta}^2} \quad (3.3)$$

where F_{to} is the peak value of the total force immediately after impact, and $\dot{\eta}$ is the corresponding vertical water particle velocity at the free surface. There are possible corrections which may be applied to the above estimate of the maximum slamming coefficient.

The value of $\dot{\eta}$ is corrected for the effects of the free surface slope as discussed in Section 2.5.2 (Eq. 2.74) and used to obtain a modified value of the peak slamming coefficient designated as

C'_{s0} . This is generally expected to result in an increase in the value of C_{s0} by 5% to 10%, depending on the steepness of the wave train used in the test.

Secondly, because of the finite rise-time taken to reach the the maximum slamming force, the buoyancy force component is not zero at that instant. This may be estimated by assuming that the cylinder submergence at any instant is $s = \eta - h$, and may thereby be subtracted from the measured maximum force prior to estimating the slamming coefficient, which is now denoted as C''_{s0} . It is noted that the assumption of a level free surface after impact is implicit in this operation. In reality, the actual contribution of the buoyancy force component will be less than the computed estimate since photographs of wave impact have shown that the free surface in the vicinity of the cylinder is disturbed to a certain extent depending on the velocity of the impact.

The dynamic response of the cylinder may be accounted for approximately using the results presented in Section 2.3.1 for a triangular impulse having equal rise and decay times. A corrected estimate of the rise-time T_r of the applied force is determined using the observed value of the rise-time for a particular slamming event T_t , and the known natural period T_n and damping ζ of the measuring system. The ratio of T_r/T_n is then used to determine the dynamic amplification factor to obtain a corrected value of the slamming coefficient. This coefficient which has been corrected for the effects of free surface slope, buoyancy and dynamic effects is denoted by C^*_{s0} .

The impulse coefficient C_i defined in Eq. 2.56 (see Section 2.3.3) is also evaluated for the various tests. Since the correction for the free surface slope can also be applied in this case, a modified value of the impulse coefficient denoted as C^*_i is determined using Eq. 2.75.

Additional parameters of interest which are reported include the Froude number at impact based on the vertical velocity of the free surface $\dot{\eta}/\sqrt{gD}$, the Froude number based on the slope-corrected free surface velocity v_n/\sqrt{gD} , the observed rise-time T_t , the rise-time corrected for

dynamic effects T_r , the relative cylinder submergence at the instant of peak impact force ($v_n T_r/a$), and the relative cylinder submergence at the end of the impulse ($v_n T_i/a$).

Since the vertical force on the cylinder is measured over a duration of 20 sec, there may be 10 to 20 slamming events in each force record, depending on the wave period. A statistical analysis of the above parameters is therefore carried out, after removing the highest and lowest values of the peak slamming force from that record. The mean, standard deviation, minimum and maximum quantities for the parameters are determined for every combination of wave height and period.

The wave records are analyzed separately by a zero-crossing method to determine the exact wave height and period that is realized during the tests.

3.5 Inclined Cylinder in Non-Breaking Waves

In addition to the slamming tests on the horizontal cylinder in regular waves, a number of experiments were performed in which the cylinder axis was tilted by rotating the cylinder-dynamometer assembly in the vertical plane. The cylinder axis was aligned normal to the direction of wave propagation as in the case of the horizontal cylinder tests.

The objective of these tests is to observe the behaviour of the slamming force on the inclined cylinder and to compare this to that for the horizontal cylinder for the same wave condition. In addition, the predictions of the theoretical model for slamming on inclined cylinders (see Section 2.4) are also compared with the experimental results.

Tests were conducted for two inclinations of the cylinder axis, $\theta = 4.8^\circ$ and 9.6° . The corresponding height of the lower edge of the cylinder measured from the still water level was $h = 0.5$ cm and -2.0 cm respectively. The force normal to the cylinder axis (in the vertical plane) was measured in regular waves with the same heights and periods used in the horizontal cylinder tests.

3.6 Horizontal Cylinder in Breaking Waves

The last phase of the experimental study on wave slamming consists of a set of tests on the forces due to breaking wave impact on a fixed, horizontal circular cylinder located near the free surface. The two-dimensional case of uni-directional waves propagating in a direction orthogonal to the cylinder axis is considered. The vertical and horizontal components of the impact force on the cylinder due to a single breaking or ‘plunging’ wave were measured for three elevations of the cylinder, and six locations of wave breaking relative to the horizontal location of the cylinder. The measurements have been corrected for the dynamic response of the cylinder, and analyzed to obtain impact coefficients and rise-times. A video record of the impact process was also obtained in order to estimate the kinematics of the wave and plunging jet prior to impact, and provide information on the effects of the shape of the wavefront on the observed impact force.

3.6.1 Generation of the Breaking Wave

The experimental facilities and the test cylinder have been described in Section 3.1. A single plunging wave was generated during each run of the experiments, using a procedure similar to that described by Chan and Melville (1988). This involves the generation of a frequency and amplitude modulated wave packet consisting of a number of prescribed sinusoidal components. The phases of the individual wave components were chosen on the basis of linear wave theory to give rise to a summation of crest elevations at a desired wave breaking location. In the present study, the wave components have been generated with the following characteristics:

Period of centre frequency component	1.1 sec
Length of centre frequency component	1.81 m
Frequency bandwidth	1.11 Hz
Number of frequency components	30

Due to nonlinear interactions between the various components, the wave crest breaks approximately 1 m before the estimated location of breaking based on linear theory. The wave

generation program was hence used to compute a wave which would break 1 m downwave of the cylinder location, so that the actual wave breaking in the experiments occurred in the vicinity of the cylinder. The actual location of breaking is determined by video records made in the absence of the cylinder, which would otherwise interfere with the plunging crest of the wave. The horizontal location of wave breaking is characterized by x_b which is defined as the distance between the cylinder axis and the point in the wave flume where the plunging jet from the crest of the breaking wave touches down on the free surface. The value of x_b is negative if the jet touches down before reaching the cylinder. The determination of the wave breaking location depends on a visual estimate from video records of the experiments, and consequently reported values of x_b may have an error of ± 2 cm. A typical example is shown in Fig. 3.11 for $x_b = -3.5$ cm.

The experiments were carried out for 6 values of x_b ranging from -3.5 cm to 49.0 cm, which cover a variety of impact conditions, ranging from a wave that has already broken before reaching the cylinder, to one that is in the early stages of steepening when it impacts the cylinder.

3.6.2 Measurement of Force and Breaking Wave Profiles

Since it is well known that breaking waves cause significantly higher impact forces than regular waves, and that the horizontal force is a major component of the total force due to breaking wave impact, the test cylinder assembly was modified to ensure that the larger forces did not interfere with the proper operation of the dynamometer. The plastic sleeve tubes which shield the connecting members between the cylinder and dynamometer were disconnected from the support frame, and rigidly clamped to the walls of the wave-flume. This ensured that the large horizontal forces would not cause the sleeve tubes to move and disturb the force transmitting members.

In addition to the vertical force channel of the dynamometer which was already configured for the non-breaking wave slamming tests, another channel of the dynamometer was connected to an independent amplifier in order to measure the horizontal force. The channel which senses the

moment about the dynamometer's Y-axis (parallel to the cylinder axis) was calibrated to measure the horizontal force on the cylinder. A free vibration test was conducted to determine the dynamic characteristics of the cylinder in the horizontal direction. Figure 3.12 shows the trace of the horizontal force measurement made by applying a step load in the horizontal direction using the method described in Section 3.2. A comparison of Figs. 3.5 and 3.12 indicates that the cylinder-dynamometer assembly has different dynamic characteristics in the vertical and horizontal directions. Figure 3.13 shows the spectrum of the horizontal free vibration record which indicates the presence of only one dominant component at 29 Hz. The average damping determined from the free vibration trace was about 2%.

Experiments were conducted for 3 cylinder axis elevations above the still water level, $h = 4.7$, 8.7 , and 12.7 cm, and for each of these elevations, tests were carried out for 6 horizontal locations of wave breaking. The slamming force due to a regular non-breaking wave of period $T = 1.2$ sec and height $H = 20.5$ cm was also measured for each cylinder elevation. For each test, the force records were sampled at the rate of 10,000 samples/sec over a duration of 2 sec. The signals were obtained after low-pass filtering at a high cut-off frequency (1000 Hz) to ensure that transient force components were not lost.

The tests were recorded on videotape at 30 frames/sec and a shutter speed of 1/1000 sec in order to estimate parameters such as the breaking wave location, the wave kinematics immediately prior to impact, and also to provide a visualization of the impact process.

3.6.3 Analysis of Breaking Wave Impact Force

The effect of the dynamic response of the cylinder-dynamometer system on the measured force is expected to be more severe in the case of the horizontal force component, due to the low natural frequency of the measurement system in comparison to the higher frequency components that are present in the rapidly varying impact force. Typical traces of the variation of the measured vertical and horizontal components of the impact force ($h = 8.7$ cm, $x_b = 25.5$ cm) are shown in Fig. 3.15(a) which indicates that while the vertical force rises rapidly immediately after

impact, the corresponding horizontal force increases more gradually and shows a strong oscillatory component during and after the initial stages of impact. This causes the measured maximum horizontal force to differ from that of the applied force and also introduces a phase difference between the applied and measured force as discussed in Section 2.3.1.

In order to correct the measured horizontal force for dynamic effects, the equation of motion of the cylinder and its support structure in the horizontal direction can be expressed as:

$$M' \ddot{x} + C' \dot{x} + K' x = F' \quad (3.4)$$

where M' , C' , and K' are the effective mass, damping, and stiffness respectively in the horizontal direction; x , \dot{x} and \ddot{x} denote respectively the horizontal displacement, velocity and acceleration, and F' is the horizontal component of the applied force. The natural frequency for the horizontal mode of vibration, and damping ratio are defined as $\omega'_n = \sqrt{K'/M'}$ and $\zeta' = C'/2M'\omega'_n$ respectively. For a known time history of the applied force, $F'(t)$, the response $x(t)$ of the SDOF system which is initially at rest is given by Eq. 2.37 and is repeated here for convenience:

$$x(t) = \frac{1}{M'\omega'_d} \int_0^t F'(\tau) \exp[-\zeta'\omega'_n(t - \tau)] \sin[\omega'_d(t - \tau)] d\tau \quad (3.5)$$

where $\omega'_d = \omega'_n \sqrt{1 - \zeta'^2}$, and τ is a variable of integration. The force measured by the dynamometer is given by $F'_t(t) = K' x(t)$ and can therefore be expressed as:

$$F'_t(t) = \frac{\omega'_d}{1 - \zeta'^2} \int_0^t F'(\tau) \exp[-\zeta'\omega'_n(t - \tau)] \sin[\omega'_d(t - \tau)] d\tau \quad (3.6)$$

It is now possible to determine the unknown applied force $F'(t)$ from the measured force $F'_t(t)$ and the dynamic characteristics of the measuring system, using a numerical method which expresses the integral in Eq. 3.6 as a summation and solves for $F'(t)$ at every time step.

If the measured force is digitally recorded at a pre-determined sampling rate such that the time interval between successive samples is Δt , the applied force may be derived from Eq. 3.6 as:

$$F'(0) = \frac{F_t(\Delta t) (1 - \zeta'^2)}{\omega'_d \Delta t \exp(-\zeta' \omega'_n \Delta t) \sin(\omega'_d \Delta t)} \quad (3.7)$$

$$F'(i\Delta t) = \frac{F_t((i+1)\Delta t) (1 - \zeta'^2)}{\omega'_d \Delta t \exp(-\zeta' \omega'_n \Delta t) \sin(\omega'_d \Delta t)} - \frac{\sum_{j=0}^{i-1} F'(j\Delta t) \exp(-\zeta' \omega'_n (i-j)\Delta t) \sin(\omega'_d (i-j)\Delta t)}{\exp(-\zeta' \omega'_n \Delta t) \sin(\omega'_d \Delta t)} \quad \text{for } i = 1 \text{ to } N-1 \quad (3.8)$$

where N is the total number of points in the measured force record.

The method has been verified by its application to the time series of $F_t(t)$ generated by the free vibration test described earlier, and the results are shown in Fig. 3.14. Values of $\omega_n = 182.2$ rad/sec ($f_n = 29$ Hz) and $\zeta = 2\%$ have been used. The applied step loading is shown by the dashed line, and the corresponding recorded horizontal force is shown by the thin dotted line. It is seen that although the corrected force trace shown by the solid line in Fig. 3.14 is affected by the presence of residual dynamic components, it is still a reasonable estimate of the applied step load. The correction method is also applied to the horizontal force measured due to breaking wave impact as shown in Fig. 3.15(a). Figure 3.15(b) shows the corrected horizontal force component derived from the recorded force time series, and also repeats the vertical force trace shown in Fig. 3.15(a) for the purpose of comparison. The corrected force trace in Fig. 3.15(b) shows an oscillation before the beginning of the actual impact which is associated with the numerical low pass filtering (125 Hz cut-off) performed on the recorded horizontal force record. This was applied in order to remove high frequency noise before the application of the dynamic correction method, since there was a tendency for noise components in the recorded force to amplify and add to the predicted maximum force. The cut-off frequency of 125 Hz was selected after examining the predicted value of the maximum applied horizontal force using progressively lower cut-off frequencies (e.g. 400, 250, 150 Hz). The predicted maximum was significantly affected when a cut-off of 100 Hz was used.

Although the free vibration record of the vertical force indicates a dominant frequency of 290 Hz, the presence of other frequency components at 75, 130 and 190 Hz rules out the application of the above correction method to the recorded vertical force, since these will be amplified by varying degrees and result in an incorrect estimate of the maximum slamming force. The peak value of the recorded vertical force has been corrected using the same technique described in Section 3.4.3 for the regular wave tests. The peak values of the corrected vertical and horizontal force are used to obtain the magnitude and direction of the maximum resultant force on the cylinder due to the breaking wave, which is reported along with the corresponding rise-time.

There are certain assumptions implicit in the application of the above technique to the present problem. The response $x(t)$ and its derivatives modify the applied hydrodynamic force $F(t)$, whereas it is assumed here that the influence of cylinder motion on the applied force is minimal, and that the results derived from the above method will be usable from an engineering standpoint. The treatment of the cylinder-dynamometer assembly as an SDOF system also represents a simplification, but this is not expected to have a significant effect on the estimate of the applied force.

The water particle velocity in the plunging wave immediately prior to impact is estimated by analyzing a series of still images digitized from a video record of the impact. A series of 4 successive images with a time interval of 1/30 sec are captured over a duration spanning approximately 1/15 sec before impact to 1/30 sec after impact. The profile of the wave-front in each image is digitized for further analysis. The celerity of the wave which is constant for all the tests is a representative quantity which is determined from the wave profiles. The velocity normal to the moving water surface adjacent to the cylinder is also determined for cases where the surface is relatively undisturbed. Since the impact force on the test cylinder is dependent on the contact area between the water surface and the cylinder during the early stages of impact, the radius of curvature of the wave surface adjacent to the cylinder is also determined from the video records.

Chapter 4

RESULTS AND DISCUSSION

The results of the experimental and numerical investigations which have been described are presented and discussed in this chapter. The first part of this chapter focuses on the experimental results from slamming tests in non-breaking waves of various heights and periods, and different elevations of the cylinder axis near the still water level. The parameters of interest estimated from the measured force records include the maximum value of the slamming coefficient immediately after impact, the corresponding rise-time, the impulse coefficient, and the corresponding impulse duration. The various corrections applied to these coefficients due to the effects of buoyancy, free surface slope, and dynamic amplification are also presented. Statistical properties of these estimates from different experiments are indicated. The effects of cylinder inclination on the maximum force and rise-time are examined by comparison with the forces observed on a horizontal cylinder subjected to the same incident waves.

The application of numerical models to estimate the vertical wave force acting on a section of a fixed, rigid horizontal cylinder located near the free surface, and the effect of variations of the governing non-dimensional parameters on the magnitudes of the maximum vertical force are discussed. Numerical simulations for a horizontal cylinder subjected to slamming in random waves have been used to estimate the probability density of the maximum force and the result is compared with analytical predictions. Time series of the numerically predicted force are compared with experimentally observed data for the cases of both horizontal and inclined cylinders. An example application of the slamming model to practical situations is also presented.

The final section of this chapter discusses the experimental results for impact forces due to a breaking wave. The maximum horizontal and vertical force components, along with the resultant force and the rise-time are presented for several cases which involve different elevations of the cylinder and various wave breaking locations. The geometry of the wave profile in the vicinity of the cylinder immediately prior to impact is shown and its effect on the impact force is examined. Slamming coefficients based on the local particle velocity and the wave celerity are indicated. The issues of applying these results at prototype scales are also discussed.

4.1 Slamming Forces in Non-Breaking Waves

Tests have been conducted in non-breaking regular waves for a horizontal cylinder at three different elevations and an inclined cylinder at two different tilt angles. The component of the hydrodynamic force normal to the cylinder axis in the vertical plane was measured, along with the water surface elevation at the cylinder location in the absence of the cylinder. In the case of the tests on the horizontal cylinder, the force data has been analyzed to obtain various parameters such as the peak slamming coefficient. The force data obtained from the inclined cylinder tests are used to illustrate the effects of axis tilt on the magnitude and temporal variation of the slamming force.

4.1.1 Raw Data from Horizontal Cylinder Experiments

Tests have been conducted for 16 regular wave conditions with a range of wave periods ($T = 1.0$ to 1.8 sec) and wave heights ($H = 9.8$ to 22.9 cm). The wave conditions along with the corresponding wave steepness and celerity for all the tests are listed in Table 4.1. For the case where the cylinder elevation $h = 0.5$ cm, the water particle velocity at the instant of impact is nearly a maximum and the corresponding acceleration is close to zero. Six additional tests have been conducted for cylinder elevations $h = -4.5$ cm and 4.5 cm.

Since the vertical force on the cylinder was measured over a duration of 20 sec, there are multiple slamming events in each force record, and Fig. 4.1 shows an example of the free surface elevation and corresponding vertical force traces over a duration of 10 sec for an incident wave having a low steepness $H/L = 0.036$, and for $h = 0.5$ cm. Similar traces are shown in Figs. 4.2 and 4.3 for incident waves of moderate ($H/L = 0.063$) and large steepness ($H/L = 0.102$) respectively. When the cylinder is out of the water, the measured force is seen to consist of background electromagnetic noise which is present even at frequencies below the 1 kHz cut-off setting of the amplifier. These figures indicate that the slamming force maxima vary somewhat from one event to the next. This variation is caused by random disturbances on the water surface due to reflection, splashing and drips after each cylinder submergence event, and tends to increase with wave steepness. It is observed that this influences only the slamming force and corresponding rise-time, and that the vertical force after the initial stages of slamming is essentially the same for every submergence event. The variability of the slamming force maxima observed in Figs. 4.1 - 4.3 emphasizes the difficulty in obtaining consistent estimates of the slamming coefficient.

Figures 4.4 - 4.11 show time histories of the vertical force and corresponding water surface elevation over a single slamming event for 8 different tests. As an aid to interpreting these results, the figures include horizontal and vertical lines which indicate the cylinder location and corresponding instants of impact and complete submergence. Figures 4.4, 4.5, and 4.6 correspond to three tests characterized by a change in wave period (with a slight difference in wave height); Figs. 4.7, 4.8 and 4.9 correspond to a change in wave height for the same wave period; and Figs. 4.8, 4.10 and 4.11 correspond to changes in cylinder elevation for the same wave height and period.

A comparison between Figs. 4.4, 4.5, and 4.6 for the case of waves with $H \approx 17$ cm, and $T = 1.1, 1.4,$ and 1.6 sec respectively, indicates that the slamming force maximum which occurs immediately after wave impact, decreases with increasing wave period, whereas the subsequent maximum in the force which occurs after full submergence is less variable. It is also observed

that the magnitude of the peak slamming force drops rapidly from a value that is more than double the maximum force which occurs after full submergence due to a combination of buoyancy, inertia and drag force contributions, to one which is about half of the overall maximum force. The change in the maximum slamming force is expected on account of a reduction in the water particle velocity at impact. Figures 4.7, 4.8 and 4.9, for impact due to waves with $T = 1.5$ sec, and $H = 13.9, 18.4$ and 22.9 cm respectively, show that both the peak slamming force and the maximum force after complete submergence increase with an increase in wave height which also corresponds to a larger impact velocity at the same cylinder location. The nature of the force variation after impact changes since the magnitude of the drag force relative to the inertia force is affected by the change in wave height. Finally, Figs. 4.8, 4.10, and 4.11 are used to illustrate the distinctly different force records obtained with a wave of $T = 1.5$ sec, $H = 18.4$ cm, and cylinder elevations $h = 0.5, 4.5$ and -4.5 cm respectively. When the cylinder is lowered from $h = 0.5$ to -4.5 cm, Fig. 4.11 shows that there is a marked reduction in the peak impact force, since the impact velocity is reduced, and the significant hydrodynamic forces occur after full submergence. In contrast, there is a smaller reduction in the peak slamming force when $h = 4.5$ cm due to a relatively smaller decrease in impact velocity near the upper portion of the wave which displays vertical asymmetry in the form of shallow troughs and steep crests.

All the time histories of the vertical force show the presence of residual vibration components after the initial wave impact. The nature of the oscillation is very similar to that shown in Fig. 3.5. The slamming force contains components at frequencies which are higher than those present in the case of the force on a continuously submerged member. In the case of structural elements of offshore platforms, slamming forces may induce dynamic response of the member resulting in dynamic stresses. These stresses may be significant especially if the frequency content of the force is close to the natural frequency of the member, and consequently indicates the need for dynamic analysis of the member during its design. In addition to the magnitude of the dynamic stress, the occurrence of frequent stress reversals will lead to fatigue damage of the member and its support connections, and must also be considered as a design criterion.

4.1.2 Slamming Coefficients from Horizontal Cylinder Experiments

The time histories of the water surface elevation and the corresponding vertical force on the cylinder have been analyzed to obtain the slamming coefficients and other relevant parameters. Since the vertical force on the cylinder was measured over a duration of 20 sec, the number of slamming events for any one test ranges from 10 to 20, depending on the wave period. Every force record was analyzed after removing the highest and lowest values of the peak slamming force from the data. As discussed in Section 3.4.3, a maximum slamming coefficient C_{so} can be estimated from the observed value of the peak slamming force F_{to} and the corresponding value of $\dot{\eta}$ at that instant. The various corrections to this value of C_{so} , namely the free surface slope, buoyancy, and dynamic amplification corrections have also been described in Section 3.4.3.

Table 4.2 illustrates the effects of the different corrections applied to the data obtained from a typical experiment using a wave with $T = 1.5$ sec, $H = 18.4$ cm, and cylinder elevation of $h = 0.5$ cm. The value of $\dot{\eta}$ realized for the successive slamming events is seen to be reasonably constant at about 0.39 m/sec. However, the corresponding peak slamming coefficient C_{so} shows a larger degree of scatter. The coefficient of variation (C.O.V.), which is defined as the ratio of the standard deviation to the mean, is used to quantify the degree of scatter in the data. The individual values of C_{so} vary from 4.36 to 6.63, and it has a mean value and C.O.V. of 5.16 and 0.16 respectively. The effect of the free surface slope correction is reflected in the values of the water particle velocity normal to the free surface v_n and the corresponding slamming coefficient C'_{so} which is determined on the basis of v_n . It is seen that in comparison to $\dot{\eta}$ and C_{so} , there is a minor reduction of about 2.5% in the value of v_n and the mean value of C'_{so} increases by 6% to 5.47 respectively. The degree of scatter remains unaffected. The contribution of the buoyancy force to the above estimates of the peak slamming coefficient can be determined by the relative submergence of the cylinder $(s/a)_o$ at the instant of occurrence of the maximum force. The value of $(s/a)_o$ varies between 0.29 and 0.44, and has a mean and C.O.V. of 0.35 and 0.14 respectively. This indicates that the cylinder is submerged to approximately one-sixth of its diameter when the peak slamming force occurs. It is noted that photographic studies of cylinder entry into water

have shown that the free surface is significantly displaced during the early stages of impact, and that the assumption of a level free surface will generally lead to an overestimation of the buoyancy force contribution. The modified slamming coefficient C_{so}'' which is derived after removing the buoyancy force component is also shown in Table 4.2. It is seen that the average value of C_{so}'' decreases by about 10% to 4.91 in comparison to C_{so}' , while its C.O.V. of 0.18 is about the same, and individual values vary from 3.96 to 6.51.

Finally, the dynamic response of the cylinder may be accounted for approximately using the results presented in Section 2.3.1 for a triangular impulse and which is shown in Fig. 4.12 in a modified form. The correction is carried out as follows: by assuming a natural period $T_n = 3.45$ msec ($f_n = 290$ Hz) and a damping ratio $\zeta = 2\%$, the observed rise-time T_t is used with the results in Fig. 4.12 to estimate the corresponding actual rise-time T_r of the applied force. This is then used with the measured force maximum F_{to} (with the buoyancy component removed) to obtain the corresponding applied force maximum F_o . Since the natural frequency of the test cylinder is quite high, it is able to respond quickly to the rapidly increasing slamming force. Consequently the corrections to the observed rise-time and vertical force are small for the case shown in Table 4.2, and vary between 0 and 5%. The value of T_t varies between 17.2 and 25.6 msec, and has an average of 20.1 msec. The corrected value T_r has an average value of 19.4 msec. The C.O.V. for these parameters is 0.13. The slamming coefficient C_{so}^* which includes the dynamic correction is seen to decrease slightly in comparison to C_{so}'' , and varies from 3.87 to 6.43 with a mean value of 4.81. The cumulative effect of the 3 corrections is thus seen to reduce the average value of the peak slamming coefficient by about 7% in this particular example. However, the magnitude of the correction varies with the wave conditions used in the test. It is also noted that the various corrections do not contribute to any significant change in the degree of scatter exhibited by the different slamming coefficients.

A summary of the results from all 22 experiments with non-breaking waves incident on the horizontal cylinder located at 3 different elevations is presented in Table 4.3. Since the water particle velocity at impact is the primary quantity which determines the magnitude of the

slamming force, the non-dimensional values of $\dot{\eta}/\sqrt{gD}$ that were observed in the various tests are indicated. The mean value of this parameter varies from 0.37 for the wave with the least steepness, $T = 1.8$ sec, $H = 13.5$ cm, to 0.78 for the case of the relatively steep wave of $T = 1.2$ sec, and $H = 19.3$ cm. The C.O.V. of $\dot{\eta}/\sqrt{gD}$ is the lowest among all the other quantities measured in this study, and varies from 0.02 to 0.14. This indicates that the waves generated in the flume showed good repeatability, with the steeper waves displaying slightly larger variation in the impact velocity for successive slamming events.

The mean value of C_{so} for each of the 22 cases varies from 3.04 to 7.79, and has been plotted in turn as a function of different combinations of the parameters indicated in Eq. 2.2. These reveal no apparent trend of C_{so} with these parameters. However, it is possible that the absence of any such trend may be due to the limited range of values of the parameters, the relatively low number of observations made, and the possibility of a complex dependence on several of the parameters.

The C.O.V. of C_{so} varies from 0.09 to 0.36 and increases with the steepness of the incident wave. This trend is explained by the likelihood of increased disturbances on the water surface due to the higher water particle kinematics in steeper waves. Individual values of C_{so} vary from 1.86 to 11.7 and the overall mean of C_{so} is 4.87. It is noted that Campbell and Weynberg (1980) reported a value of $C_{so} = 5.15$ based on their experiments. Figure 4.13 shows the probability density histogram of C_{so} based on a total of 311 slamming events recorded in the 22 tests. The data is seen to follow a log-normal distribution which is shown as a solid line in the figure. The expression for the log-normal probability density for C_{so} is based on its median value, \tilde{C}_{so} , and the standard deviation of $\ln(C_{so})$, denoted σ :

$$p(C_{so}) = \frac{1}{C_{so} \sigma \sqrt{2\pi}} \exp\left[-0.5 \left(\frac{\ln(C_{so}/\tilde{C}_{so})}{\sigma}\right)^2\right] \quad (4.1)$$

where $\tilde{C}_{so} = \mu \exp(\sigma/2)$, and $\sigma^2 = \ln(\gamma^2 + 1)$. Here μ is the mean of C_{so} (≈ 4.87 in the present study), and γ is the coefficient of variation of C_{so} (≈ 0.38 in the present study). Führböter (1986)

observed that the maximum pressure due to plunging wave impact on a sloping beach also follows a log-normal distribution.

The impact velocity corrected for the slope of the free surface is shown as v_n/\sqrt{gD} and its magnitude is always smaller than the corresponding value of $\dot{\eta}/\sqrt{gD}$. As expected, the magnitude of correction is generally small ($\leq 9\%$) and increases with wave steepness. The mean value of this quantity varies from 0.36 to 0.75. The corresponding mean value of C'_{s0} is 3 - 12% larger in comparison to C_{s0} , and varies from 3.14 to 8.26, with its C.O.V. expected to be the same as that for C_{s0} .

The measured rise-time T_t is an important parameter since it provides an estimate of the dynamic amplification of the impact force. The average value of T_t for the tests varies from 11.6 to 37.1 msec and its C.O.V. ranges from 0.13 to 0.36. For the case $h = 0.5$ cm, T_t tends to increase with v_n/\sqrt{gD} , which may be attributed to the slower rise of impact pressures due to increased presence of entrained air and local disturbances as a consequence of larger impact velocities. Based on the mean value of T_t observed in each test, the ratio T_t/T_n varies from 3.36 to 10.8, and the corresponding correction factors T_t/T_r vary between 1.07 and 1. The corrected rise-time T_r varies from 10.8 to 37.1 msec for the 22 tests.

Miller (1980) indicated that, under ideal conditions of water impact on a horizontal cylinder, the rise-time of the slamming force may be associated with the propagation of a pressure wave within the water, and is of the order of the time taken for the wave to travel a distance $0.2D$, i.e. $T_r = O[0.2D/c]$, where D is the cylinder diameter and c is the velocity of sound in water. For the case of water with no entrained air, $c \approx 1500$ m/s. This corresponds to a rise-time of order 0.005 msec, based on the above estimate. Lundgren (1969) has shown that the speed of sound in water is strongly affected by the presence of air bubbles and decreases to about 40 m/s for 10% entrained air content, which would lead to a longer rise-time of 0.2 msec. These rise-time estimates are significantly shorter than those observed in the present study as reported above, which indicate that the effects of compressibility may be relatively minor in comparison to other factors which influence the rise-time.

The cylinder submergence $v_n T_r/a$ when the slamming force reaches a maximum is seen to be nearly the same as the quantity $(s/a)_o$ determined from the water surface elevation record for the tests, where $s = \eta - h$. The value of $v_n T_r/a$ ranges from 0.13 to 0.80, and its C.O.V. varies from 0.11 to 0.41 which is very similar to the scatter shown by T_t . This quantity also exhibits an increasing trend with respect to v_n/\sqrt{gD} for reasons similar to those attributed to the trend shown by T_t (and hence T_r). Although not shown in Table 4.3, the quantity $v_n T_t/a$ which was evaluated for every slamming event (311 samples) indicates an overall mean cylinder submergence $(s/a)_o$ of 0.36. This corresponds to an average cylinder submergence of 7 mm when the peak slamming force occurred.

The mean value of the maximum slamming coefficient corrected for buoyancy effects C_{so}'' ranges from 3.07 to 7.72, with its C.O.V. varying from 0.07 to 0.44. Figure 4.14 shows the probability density histogram of C_{so}'' values based on 311 slamming events observed in 22 tests. The overall mean of C_{so}'' is 4.68 which is 4% smaller than the corresponding value of C_{so}' , and its C.O.V is 0.44. Figure 4.14 also shows the log-normal probability density variation for C_{so}'' based on its mean and C.O.V as defined in Eq. 4.1. It is seen that the comparison between the histogram and the theoretical curve for C_{so}'' is fair, although not as good as that shown for C_{so} (Fig. 4.13).

Finally, the effect of the measuring system's dynamic response on the slamming coefficient is estimated using the mean value of T_t observed in the 22 tests, which yields corresponding values of the peak force correction factor F_{t0}/F_o that vary from 1 to 1.04. The peak slamming coefficient corrected for dynamic effects C_{so}^* varies between 2.92 and 7.60.

4.1.3 Impulse Coefficients from Horizontal Cylinder Experiments

The use of an impulse coefficient to describe slamming has been discussed in Section 2.3.3. The data obtained from the non-breaking regular wave tests on the horizontal cylinder has been analyzed to obtain estimates of the impulse coefficient C_i and related parameters which are summarized in Table 4.4. The mean value of C_i estimated from each of the 22 tests using $\dot{\eta}$ as

the impact velocity, varies from 0.26 to 1.36, with an overall mean of 0.73; and the C.O.V. of C_i varies from 0.04 to 0.41. The mean value of the impulse coefficient based on the impact velocity corrected for free surface slope C_i^* varies from 0.26 to 1.47, and is higher than the corresponding value of C_i by between 1% and 9%. In general, C_i^* exhibits trends which are similar to those of C_i , and has similar C.O.V.s. Figure 4.15 shows a probability density histogram based on estimates of C_i^* from every slamming event, and these observations do not appear to fit any of the common probability distribution models. The overall mean of C_i^* is 0.77. The degree of scatter for C_i^* in relation to that for C_{s0} is of particular interest, and the present results indicate that the C.O.V. of C_i^* is less than that for C_{s0} by about 25% on average. In some cases (e.g. for $T = 1.2$ sec, $H = 12.1$ cm; and for $T = 1.4$ sec, $H = 16.5$ cm) the C.O.V. is reduced by as much as 76%. There were only 4 tests in which the C.O.V. of C_i^* shows an increase. The estimates of the impulse coefficient did not show any observable trend with respect to incident wave conditions or cylinder elevation.

The dimensionless impulse duration $v_n T_i/a$ indicates the relative submergence of the cylinder when the impact is assumed to have ended. Its mean value varies from 0.29 to 1.15, and exhibits less scatter than the dimensionless rise-time $v_n T_r/a$. The C.O.V. of $v_n T_i/a$ ranges from 0.05 to 0.21, which on average is less than the C.O.V. of $v_n T_r/a$ by about 54%. The overall mean value of $v_n T_i/a$ is 0.69 which corresponds to a submergence of about one-third of the cylinder's diameter at the end of the slamming impulse.

The reduction in scatter of the impulse coefficient in comparison to that of the slamming coefficient suggests that the former quantity may be relatively useful in estimating the dynamic response of cylindrical elements subjected to wave slamming. However, it is emphasized that this approach is only useful for cases where the impulse duration T_i is reasonably small in relation to the natural period T_n of the system, such that the system's response may be determined by the impulse magnitude rather than the precise time history of the loading.

4.1.4 Tests on Inclined Cylinder

A number of tests have been conducted by tilting the test cylinder's axis at different angles with respect to the still water level and measuring the hydrodynamic force normal to the cylinder axis in the vertical plane. The objective of these tests is solely to observe the changes in the characteristics of the impact force due to the slope of the cylinder's axis, and an exhaustive analysis of the measured force has not been conducted in this study.

Tests have been conducted for two inclinations of the cylinder axis $\theta = 4.8^\circ$ and 9.6° and three wave conditions. In the case where $\theta = 4.8^\circ$, the height of the lowest edge of the test cylinder from the still water level was $h = 0.5$ cm (see Fig. 2.14), and for $\theta = 9.6^\circ$ this was instead $h = -2.0$ cm. It is expected that the initial impact velocity for these 2 cases is similar to those observed during the horizontal cylinder tests with $h = 0.5$ cm. In general, the force records measured during these tests confirm the experimental observations of Campbell and Weynberg (1980) who conducted impact measurements on a circular cylinder which was driven into a still water surface at various angles of inclination. They found that the slamming force increased more gradually and that the corresponding peak load decreased with inclination, although the presence of disturbances on the water surface sometimes tended to induce significant dynamic response.

Figure 4.16 compares the slamming force on the test cylinder for $\theta = 0^\circ$, 4.8° and 9.6° , and a non-breaking regular wave with $T = 1.2$ sec, and $H = 19.3$ cm which is one of the relatively steep waves used in this study. The dynamic response of the cylinder is still evident in the force traces, although it is less severe for the case of $\theta = 9.6^\circ$. In comparison to the case of the horizontal cylinder where the impact force reaches a maximum of 11.3 N in 12.6 msec, the peak force drops to 7.9 N and the corresponding rise-time increases to 36 msec when $\theta = 4.8^\circ$. There is no evidence of any slamming force maximum in the case where $\theta = 9.6^\circ$, and the rate of increase of the normal force is quite gradual. In the case of a wave with medium steepness, $T = 1.5$ sec, $H = 18.4$ cm, the peak impact force decreases from 6.2 N to 2.5 N, and the rise-time

increases from 18 msec to 55 msec when θ changes from 0° to 4.8° . There is no evidence of slamming in the case of $\theta = 9.6^\circ$. The final test was conducted with a wave of $T = 1.8$ sec, and $H = 17.8$ cm which has relatively low steepness, and the force traces for the 3 inclinations are compared in Fig. 4.17. The dynamic effects are less severe due to the reduced wave steepness. It is seen that the slamming force is not the dominant component of the hydrodynamic force, and that it is barely evident even in the case of $\theta = 4.8^\circ$. An interesting feature of these measurements is that although the rise-time of the slamming force increases to 40 msec when $\theta = 4.8^\circ$, compared to 10 msec for the horizontal cylinder case, the corresponding peak force has nearly the same value of 2 N in the two cases. This may be caused by the buoyancy force becoming the dominant component after the early stages of impact, and offsetting any differences in the relatively small slamming force seen in this case. In the case of $\theta = 9.6^\circ$, the force rises very gradually in a manner similar to the other wave conditions.

The observations discussed above are for individual cases taken from multiple slamming events observed in an experiment. These also tend to show scatter in a manner similar to horizontal cylinder tests due to the presence of disturbances on the water surface, although the scatter decreases with increasing cylinder inclination which results in reduced slamming forces. However, the trends for the reduction in the slamming force and increase of rise-time are quite repeatable.

4.2 Numerical Simulation

The numerical method for estimating the various components which make up the vertical wave force acting on a section of a rigid horizontal circular cylinder located near the free surface, taking account of wave slamming and intermittent submergence has been discussed in Chapter 2. Two numerical models, namely Models I and II which essentially differ in their treatment of the vertical force during the partially submerged phase, have been used to obtain time histories of the vertical force on a cylinder in simulated regular and random waves. The effect of variations

of the governing non-dimensional parameters on the magnitudes of the maximum force are examined, and results from alternative models for evaluating the time histories of the force in regular waves are compared. Corresponding results for random waves are also shown.

The force predicted by the numerical model is compared with experimental observations for both cases of a rigid and dynamically responding cylinder. A practical application of the various methods described is also illustrated.

4.2.1 Regular Waves

As indicated in Chapter 2, the governing non-dimensional parameters in this study are $\omega^2 a/g$, $\omega^2 H/g$ and h/H , since deep-water conditions are assumed and the influence of Reynolds number is only considered through the choice of the empirical force coefficients. The influence of these parameters on the vertical force is investigated. Force coefficient values of $C_{s0} = \pi$, $C_d = 0.8$, and $C_m = 1.7$ ($C_{m0} = 1.7$ for Model II) have been adopted for this investigation. Although recent studies and the results of the present experimental investigation indicate a higher value of C_{s0} , a value of π is being used to examine the properties of the dimensionless maximum vertical force. The variation of the inertia coefficient, and the combined slamming and drag coefficient (C_{s+d}) with submergence in Model II is assumed to be as shown in Figs. 2.5 and 2.7 respectively.

Figure 4.18 shows the variation of the dimensionless vertical force $F/\rho g a^2$ over one wave cycle for $\omega^2 a/g = 0.05$, $\omega^2 H/g = 0.6$ and two cylinder elevations, $h/H = -0.3$ and 0.3 , and compares the predictions of Models I and II. It can be observed that significant differences in the force predicted by the two models occur in the partially submerged stage, with Model I predicting a larger force than Model II. This is due to the different assumptions made in the two models with respect to the variation of the hydrodynamic force during partial submergence. In Model II, the combined slam and drag coefficient used to determine the velocity-squared force decreases rapidly after the instant of slamming, while the inertia coefficient begins increasing from zero. The hydrodynamic force determined using these varying coefficients is less than the linear variation of the force given by Model I. Model II also predicts a negative force as the wave

recedes from the cylinder which is not shown by Model I. This difference is associated with the inertia and drag forces computed in Model II when the cylinder is partially submerged as the free surface recedes. The force due to this contribution is significant when the cylinder is above the mean water level since both the inertia and drag loads are downward and oppose the buoyancy force.

From the aspect of engineering design, the maximum force \hat{F} on the cylinder over a wave cycle is of particular interest. This has been computed for a range of wave conditions and is shown in dimensionless form in Figs. 4.19(a)-(d) as a function of the dimensionless cylinder elevation h/H , for four values of steepness $\omega^2 H/g$ (0.2, 0.4, 0.6 and 0.8) and for four values of the frequency parameter $\omega^2 a/g$ (0.005, 0.01, 0.05 and 0.1). The values of H/a are also indicated in the figure. The solid and dashed lines correspond to the predictions of Models I and II respectively. The close agreement overall between the two predictions provides some justification for the use of the simpler Model I by Isaacson and Subbiah (1990). The maximum force with respect to cylinder elevation is seen to occur at $h/H = 0$ for most values of the steepness and frequency parameters. Consequently, a designer should avoid placing horizontal structural elements in close proximity to the still water level.

A number of features of Fig. 4.19 can be explained by considering the stage of the wave cycle which gives rise to the peak force. For the largest values of H/a , which are contained in Figs. 4.19(a) and 4.19(b), the peak force over most of the elevation range is due to slamming. This gives rise to the parabolic-type variation of peak force with h/H , with maxima near $h/H = 0$. This is because $\dot{\eta}$ at the instant of impact is greatest at $h/H = 0$. At lower values of h/H (< -0.4), the slamming force is absent, or is small since $\dot{\eta}$ at the instant of impact is then also small. The peak force then occurs after full submergence, at a phase which does not vary with h . Since the flow kinematics are assumed to be constant with elevation near the mean water level, this maximum force is seen not to vary with cylinder location.

For the lowest values of H/a , which are contained in Figs. 4.19(c) and 4.19(d), a slight disparity in the peak force predictions of the two models is apparent. This discrepancy arises

because the force maxima then occur mostly during partial submergence, where the predictions of the two models differ the most. Furthermore, both models then predict the maximum force to increase fairly uniformly with decreasing h/H . This is because for this range of conditions (large $\omega^2 a/g$ and small $\omega^2 H/g$ or H/a), the buoyancy force becomes significant in comparison with the other components (see Eq. 2.4), and for incomplete submergence this increases with decreasing h/H . The curves in Fig. 4.19(d) do not reach a maximum value since partial submergence still occurs until $h/H < -0.5 - 2a/H$, which is below the range of h/H shown in the figure.

The largest maximum force with respect to variations in cylinder elevation was seen in Fig. 4.19 to occur in most cases near $h = 0$, and is of particular interest. Figure 4.20 shows this largest force in non-dimensional form as a function of the frequency parameter $\omega^2 a/g$ for two values of wave steepness $\omega^2 H/g$ (0.2 and 0.6). The predictions of both Models I and II are included, but are virtually indistinguishable so that the agreement between the two models predictions of this largest peak force is very good.

The figure indicates that the non-dimensional maximum force becomes constant for smaller values of H/a , corresponding to increasing values of $\omega^2 a/g$ for any particular value of $\omega^2 H/g$. By comparing these results with those of Fig. 4.19, it may be seen that for larger values of H/a the largest force occurs at $h/H = 0$ and is associated with slamming, whereas for lower values of H/a the largest force occurs at lower elevations of the cylinder and is associated with buoyancy, inertia and drag during partial or full submergence. In fact, for the selected values of the empirical coefficients C_{s0} , C_d and C_m , the largest force for $H/a < 6.7$ is due to buoyancy and inertia only, and these give rise to a non-dimensional force which is independent of $\omega^2 a/g$. This corresponds to the observed ranges in Fig. 4.20 over which the nondimensional force is constant with respect to $\omega^2 a/g$.

4.2.2 Random waves

As discussed in Section 2.5.3, results for random waves have been obtained both for a narrow-band spectrum as well as for a two-parameter Pierson-Moskowitz spectrum. For both cases,

conditions corresponding to a significant wave height $H_s = 10$ m, a peak period $T_p = 14.3$ sec, and a cylinder diameter $D = 40$ cm have been used. On the basis of the results shown for regular waves, it is expected that both Models I and II will give similar predictions of the force maxima, and consequently only Model II has been used throughout.

The spectral density and corresponding amplitude spectrum for both the narrow-band and Pierson-Moskowitz spectra are shown in Fig. 4.21. For the narrow-band spectrum, the simulated wave and force time series were obtained with a record length $T_r = 2860$ sec, a time interval $\Delta t = 0.559$ sec, a frequency range corresponding to $f_r/f_0 = 0.1$ (see Eq. 2.76) and a frequency interval $\Delta f = 0.00035$ Hz. These values correspond to approximately 200 waves, and a total number of data points $N = 5120$. However, this is increased to approximately 8000 points because of additional points used for durations of partial submergence. In the case of the Pierson-Moskowitz spectrum, the time series were obtained with $T_r = 1500$ sec, $\Delta t = 0.25$ sec, and $N_f = 1500$.

Portions of the simulated time series of the free surface elevation and the corresponding vertical force for the cylinder located at the still water level, $h = 0$, are shown in Fig. 4.22 for the case of the narrow-band spectrum, and in Fig. 4.23 for the case of the Pierson-Moskowitz spectrum. In the latter case, the vertical force is seen to contain a relatively large number of peaks for each period of cylinder immersion. Furthermore, for this case the largest force maxima are not necessarily associated with waves which have the largest individual heights taken in the same order. Indeed, the largest dimensionless peak force is 34.5, and corresponds to a wave height of 12.8 m, based on successive zero-upcrossings, or a height of 17.2 m based on successive zero down-crossings. The dimensionless maximum force for regular waves with these two heights would be 26.1 and 51.5 respectively. Thus the extension of regular wave results to the random wave case, which may well be appropriate for a narrow-band spectrum, may not be applicable for a broad-band spectrum.

Various statistics of the maximum force can be obtained from time series such as those described above. In this study, the simulated data corresponding to Figs. 4.22 and 4.23 have

simply been used to obtain the corresponding probability densities of the peak force, and these densities are compared to the analytical predictions of Isaacson and Subbiah (1990) in Fig. 4.24. Isaacson and Subbiah's results are based on the assumption of a narrow-band spectrum, but it is of interest to examine the adequacy of their predictions for spectra of more general shape so that the comparison for the broader band spectrum is also given. A possible limitation of their approach may be the assumption of a single force peak within each wave. In order to attempt accounting for this, the probability densities from the simulations have been obtained on the basis of all the force maxima in each record, denoted method A and shown as a solid thin line in Fig. 4.24; and a single (largest) force maximum for every wave (defined by successive zero upcrossings), denoted method B and shown as a solid thick line in Fig. 4.24. These two methods yield quite different probabilities, since the latter omits the smaller secondary force peaks within each wave which may be present.

Figure 4.24(a) indicates that for the case of the narrow-band spectrum the agreement between the analytical prediction and the simulation results based on a single force maximum for each wave is quite reasonable; whereas the simulation results based on all the peak forces yields poorer agreement. This is because the simulated force record contains secondary peaks for some waves, as indicated in Fig. 4.22(b), and the analytical predictions do not apply to these. Discrepancies between the predictions and either of the simulation results also arise because of sample variability, in that the simulation results pertain to only one force record, whereas the analytical predictions correspond to the average of many force records.

Figure 4.24(b) indicates that for the case of the broader band spectrum the agreement between the analytical prediction and the simulation results based on either method is generally poor, in that the theory predicts a relatively large number of force peaks within a relatively narrow peak force range. As before, some of this discrepancy arises partly because of the secondary peaks which occur within each wave, and partly because of sample variability. Even so, the poor agreement indicates that the analytical model cannot be extended directly to the case of a broad-band spectrum. This is consistent with the numerical illustration given earlier which relates to the single largest peak force.

4.2.3 Comparison with Experimental Observations

It is of interest to compare the vertical force predicted by the numerical model for the case of the test cylinder in regular waves with corresponding experimental observations. This makes it possible to test the validity of the various assumptions made in the formulation of Model II which relate to the variation of the combined slamming and drag coefficient, and the inertia coefficient during partial submergence. The predictions of the models for both the rigid and dynamically responding horizontal cylinder are presented.

Preliminary results from the rigid cylinder model simulations indicate that the variation of the slamming coefficient during the early phases of partial submergence corresponds more closely to Campbell and Weynberg's (1980) expression derived from their experimental observations (Eq. 2.27), which is based on a C_{s0} value of 5.15 and has a faster rate of decay in comparison to Taylor's model as seen in Fig. 2.4. It is also simpler to use in comparison with Taylor's model and allows straightforward changes to the value of C_{s0} used in the simulation. The implementation of this expression is similar to that described in Section 2.2.5 wherein the combined C_{s+d} coefficient is initially determined using Eq. 2.27 during partial submergence of the cylinder, until it reaches a value of C_d whereupon it remains constant at the value of C_d for the remainder of the wave cycle. The variation of C_s predicted by Eq. 2.27 reaches a minimum value of 0.74 at $s/a = 1.3$ and then begins rising gradually with increasing submergence. This prevents the use of the combined C_{s+d} model for values of C_d lower than 0.74, and Eq. 2.27 has been modified to accommodate lower values of C_d . This is achieved by assuming that the value of C_s reaches the value of C_d at the instant of complete submergence ($s/a = 2$). The modified version of Eq. 2.27 for this criterion is hence given by:

$$C_s = C_{s0} \left[\frac{1}{1 + 9.5s/a} + \left(\frac{0.5C_d}{5.15} - 0.025 \right) s/a \right] \quad (4.2)$$

where C_{s0} is the desired value of the peak slamming coefficient, and C_d is the drag coefficient which is less than 0.74.

The inertia coefficient is taken to increase from zero to the desired value of C_m and is then held constant. The values of C_d and C_m used in the numerical model are based on estimates derived from a least squares fit method applied to the fully submerged portion of the experimental vertical force record. The corresponding experimental wave record is used to obtain the water particle velocity and acceleration values which are used in the numerical model.

Horizontal Cylinder

Figure 4.25 compares the measured vertical force on the test cylinder located at $h = 0.5$ cm, for the case of incident waves with period $T = 1.2$ sec and height $H = 15.2$ cm, with the prediction of the numerical model for a rigid cylinder based on $C_{s0} = 5.15$, $C_d = 0.7$, and $C_m = 0.6$. It is seen that the significant differences between the predicted and observed force occur during the partially submerged stage. The predicted slamming force reaches a maximum instantaneously, while the experimental record shows a rise-time of 20 msec. However, the nature of the predicted vertical force variation compares very well over the entire length of the experimental record. The dynamic model described in Section 2.3.2 incorporates the effects of cylinder response to the applied force and also allows the inclusion of a specified rise-time. The result from a simulation which uses the test cylinder's natural frequency of 290 Hz, a damping value of 2%, and a rise-time of 20 msec, for the same cylinder location, wave conditions, and force coefficients as above, is illustrated in Fig. 4.26. Only the initial 0.25 sec of impact are shown for better detail, along with the segment of the corresponding measured force record. It is seen that the predicted force matches the measured force quite accurately. While the former quantity shows an oscillation at the natural frequency superposed on the general trend of the force, the latter shows seemingly random oscillations which are due to the presence of other modes of vibration (see Fig. 3.6). The oscillations in the predicted force trace are damped out approximately 0.3 sec after impact, and the subsequent behaviour of the force is the same as that predicted by the rigid cylinder model.

Figure 4.27 compares the predicted and measured vertical force for incident waves with $T = 1.5$ sec, and $H = 18.4$ cm, and the cylinder located at $h = 0.5$ cm. The values of the force

coefficients chosen are $C_{so} = 5.15$, and $C_d = C_m = 0.8$. It is seen that while the trends of the predicted and measured force agree quite well during the initial phase of slamming and partial submergence, they show markedly different behaviour after full submergence of the cylinder. This is possibly due to the choice of the inertia coefficient which is seen to have values which are close to zero or negative in some cases when estimated using the least squares fit method. In the present case, the least squares method estimates of C_d and C_m are 0.7 and -0.1 respectively. The discrepancy in the predicted force consequently arises since a C_m value of 0.8 is used.

It is also seen in Figs. 4.25 and 4.27 that the vertical force is generally overpredicted by the numerical model during the early stages of slamming. This may be due to the larger buoyancy force estimated by the numerical model based on the assumption of an undisturbed free surface in the vicinity of the cylinder while the actual submergence of the cylinder is usually lesser due to the formation of spray roots. There are indications of a slightly larger negative (downward) force which persists for a longer duration in the observed force record as the free surface recedes from the cylinder. Video records of the slamming event show that even after the free surface drops below the level of the cylinder, there is a mass of water which remains suspended from the cylinder for a longer length of time as seen in Fig. 4.28. This may be the cause of the observed behaviour of the negative force which is not predicted by the numerical model.

Figures 4.29 and 4.30 present comparisons of the measured force record for the case of the cylinder located at $h = -4.5$ cm, in incident waves of $T = 1.5$ sec, and $H = 18.4$ cm, with the predictions of the rigid and dynamic cylinder models respectively. The values of C_{so} , C_d , and C_m used in the simulation are 5.15, 1.25 and 0.5 respectively. A rise-time of 18 msec is also used in the dynamic model. It is seen that the correspondence between the observed and predicted force is very good.

Inclined Cylinder

The numerical model for the force on an inclined cylinder located near the still water level has been described in Section 2.4. The behaviour of the various force components is modelled in a

manner similar to the above case of a horizontal cylinder and the components of the water particle kinematics normal to the cylinder axis in the vertical plane are used to estimate the slamming, drag and inertia force.

Figure 4.31 compares the early stages of the measured and predicted force due to a slamming event in waves of period $T = 1.8$ sec, and height $H = 17.8$ cm, on the test cylinder which was inclined at $\theta = 4.8^\circ$, and had a clearance $h = 0.5$ cm. The force coefficients used in the simulation are $C_{s0} = 6.18$, $C_d = 0.8$, and $C_m = 0.5$. It is seen that there is an indication of a small force peak approximately 0.08 sec after the instant of slamming, and the force rises gradually until the cylinder is fully submerged. The predicted values agree fairly well with the observed force, although the numerical model predicts a slightly larger maximum at the instant when the cylinder becomes fully submerged.

Figure 4.32 presents another comparison of the measured and predicted force over one wave cycle for the case of the test cylinder inclined at $\theta = 9.6^\circ$, located at $h = -2.0$ cm and subjected to waves with $T = 1.2$ sec, and $H = 15.2$ cm. Force coefficients $C_{s0} = 5.15$, $C_d = 0.7$ and $C_m = 0.6$ are used in the simulation. The two force records are seen to compare very well, although the observed force is seen to rise slightly faster during the early stages of cylinder immersion.

The examples shown above indicate that the numerical models for predicting the vertical force on a horizontal or inclined cylinder located near the free surface generally yield results which compare well with experimental data. The method for combining the slamming, buoyancy, drag, and inertia force components works reasonably well when used with appropriate values of the force coefficients.

4.2.4 Practical Application

In order to illustrate the various approaches indicated here in the context of a typical ocean engineering application, consideration is given to an example corresponding to a cylinder of diameter 40 cm, length 16.0 m, and wall thickness of 12.5 mm, located with its lower surface at

the still water level, $h = 0$ cm, and subjected to a wave train of period $T = 12$ sec and height $H = 8$ m. Two configurations of the cylinder have been analyzed based on different end fixity conditions. It is also assumed that the dynamic response of the cylinder due to the applied slamming force is predominantly in its fundamental mode.

The first case in which the cylinder is assumed to have both ends rigidly fixed yields a modal stiffness value of 7.16 MN/m, and a modal mass of 1906 kg. This corresponds to a natural period of 0.1 sec. Force coefficients have been assumed as follows: $C_d = 0.8$, $C_m = 1.2$, $C_{so} = 4.5$. Figure 4.33 shows the predicted time series of the applied vertical force on the cylinder assuming it to be rigid (shown as a solid line), where it is seen that the maximum vertical force of 63.1 kN occurs at the instant of impact. The buoyancy component of the force (dashed line), and the mid-span response of the cylinder (chain-dashed line) to the applied force are also shown in Fig. 4.33. The maximum mid-span displacement of the cylinder due this applied force is estimated to be 12.1 mm. If the maximum force of 63.1 kN is treated as a static load, the corresponding mid-span deflection for the cylinder with both ends fixed is seen to be 11.5 mm. This indicates that in this example, the severity of the impact force is amplified due to the dynamic response of the cylinder. It is also noted that the mid-span displacement of the cylinder due to its self-weight would be 3.4 mm.

The second case involves the treatment of the above cylinder with pinned supports. The corresponding modal stiffness decreases to 0.67 MN/m, and the modal mass is also reduced to 953 kg, which results in a larger natural period of 0.23 sec. The static mid-span displacement due to the cylinder's self weight is 17.0 mm. The dynamic response of this system to the applied force described above is also shown in Fig. 4.33 as a dotted line. The maximum mid-span response in this case is estimated at 38.7 mm. If the maximum force of 63.1 kN is treated as a static load, the corresponding mid-span deflection for the cylinder with pinned end conditions is seen to be 57.4 mm. This indicates that the effect of the impact force is attenuated by about 33% since some of the applied force is being resisted by the inertia of the cylinder.

Since the natural period of the cylinder in the second case is sufficiently large in comparison to the duration of the impulse, it is possible to estimate the maximum mid-span response of the cylinder as the sum of the maximum dynamic response due to the slamming impulse, and the static displacement due to the more gradually varying vertical force after the end of the impulse. Although the maximum response of a single degree of freedom system to an applied impulse occurs at $T_n/4$ sec after the end of the impulse, where T_n is the natural period of the system, the maximum response of a cylinder subjected to wave impact will usually occur later due to the presence of the increasing buoyancy, drag, and inertia force components, and in general may be assumed to occur between $T_n/4$ and $T_n/2$ sec after the end of the impulse. This is evident in the above example where the maximum response of 38.7 mm occurs 0.12 sec after impact which is slightly larger than $T_n/2$ sec. On the basis of an impulse coefficient $C_i = 0.7$, which corresponds closely to the predicted applied force time series, and the vertical force on the cylinder at $T_n/3$ or 0.08 sec after the end of the impulse, which is seen to be 24 kN at $t = 3.12$ sec in Fig. 4.33, the maximum displacement is instead predicted to be 43.7 mm. This shows that the impulse response approach may be used to obtain a quick estimate of the member response under certain conditions. It is emphasized that the present example relates to fundamental mode motions only, and that higher mode motions, with relatively high natural frequencies, would also be excited by the wave slamming.

4.3 Breaking Wave Impact

Results from the experimental study of breaking wave impact on a horizontal cylinder are presented in this section. Tests have been conducted for three different elevations of the cylinder, and six different horizontal locations of wave breaking. Both horizontal and vertical components of the force on the cylinder were recorded, and then analyzed to obtain the peak force and rise-time after applying corrections for dynamic response of the cylinder. Although the force records illustrated in this section show the corrected horizontal force trace, the corresponding vertical force records are uncorrected since the dynamic correction is carried out only for the peak value of the vertical force.

The corrected rise-time for the peak horizontal force component is within 1 msec of the rise-time for the vertical force component in all the tests. This is evident in the force traces shown in Figs. 4.36, 4.40, and 4.44 where the vertical and horizontal force peaks are seen to occur nearly simultaneously. This allows the estimation of the peak resultant force from the vertical and horizontal force components by assuming that they occur at the same time. The peak values of the corrected horizontal and vertical components of the impact force, the peak resultant force and its direction, and the corresponding rise-time are presented in Table 4.5.

4.3.1 Cylinder Elevation I

The first set of tests were carried out with the lowest cylinder position ($h = 4.7$ cm). Figure 4.34 presents a series of images that show breaking wave impact for the case $x_b = 25.5$ cm. The first two frames show the plunging jet of the wave in the formative stage. The 3rd frame shows the initial impact to be due to the lower face of the wave and not the spilling front of the wave. The last frame shows the cylinder just after complete submergence. Although the jet has started collapsing and there is evidence of splash, the water in the vicinity of the cylinder is relatively undisturbed. The wave profiles have been digitized and a typical example corresponding to the case where the wave breaks at $x_b = 36$ cm is shown in Fig. 4.35 which also indicates the location of the cylinder with respect to the breaking wave. The horizontal and vertical axes of Fig. 4.35 correspond to the horizontal and vertical dimensions in the vicinity of the test cylinder, and the four curves which represent the wave-front are spaced at time intervals of 1/30 sec from left to right. These curves are used to estimate quantities such as the impact velocity and curvature of the water surface.

The observed vertical force and the corrected horizontal force record obtained for the test where $x_b = 25.5$ cm are shown in Fig. 4.36, where it is seen that the peak horizontal force component of 17 N, and the peak vertical component of 21 N (16.9 N after correction) occur nearly simultaneously at 3.8 msec after impact. The normal velocity of the water surface prior to impact is estimated from Fig. 4.35 to be 0.63 m/sec and the radius of curvature of the surface is quite large (> 20 cm). The vertical force component shows a temporal variation similar to that

obtained from regular wave impact, although the horizontal force component in the present case is also quite significant on account of the slope of the water surface at the instant of impact. Table 4.5 summarizes the peak forces observed for 6 different values of x_b . For all the tests (except for $x_b = -3.5$ cm), the peak horizontal and vertical force components show an increasing trend as the wave breaking location progresses from upwave to downwave of the cylinder. The peak resultant force increases from 12.6 N to 30.5 N as the breaking location advances from 7.5 cm to 49 cm. The direction of the resultant peak force also changes from 53° to 36° , as the horizontal force component becomes more significant. This trend is possibly due to the increasing steepness of the lower face of the wave at the location of the cylinder with an increasing value of x_b . The rise-time to the peak force is quite similar for all these cases and varies from 2.6 msec to 4.4 msec. The test for the case of $x_b = -3.5$ cm is different from the other cases in this set as the wave has already broken before the occurrence of impact. There is a large amount of splash and disturbance on the water surface and consequently it is difficult to obtain a good estimate the water surface velocity in this case. The peak horizontal force component has a magnitude of 15 N, but the peak vertical component is directed downward and has a magnitude of 4.5 N. The resultant force of 15.7 N is higher than the peak force in the case of $x_b = 7.5$ cm. This force is directed 17° below the horizontal indicating that the downward velocity component of the plunging jet contributes to the impact force. The peak impact force due to a regular wave ($T = 1.2$ sec, $H = 20.5$ cm) is mainly due to the vertical force component, while the horizontal component has a more gradual rate of increase. The peak resultant impact force of 7.2 N is significantly lower than the breaking wave impact forces seen in these tests, and also shows a larger rise-time of 15.1 msec.

4.3.2 Cylinder Elevation II

The impact forces for this location of the cylinder ($h = 8.7$ cm), were the highest among all the tests. Figures 4.37, 4.38 and 4.41 show a series of images which illustrate the 3 different types of breaking wave impact that occur in this set. Figure 4.37 shows the impact for the case of $x_b = -3.5$ cm. It can be seen in the 1st frame that the plunging jet of the wave has already broken

onto the lower face of the wave, and that there is significant amount of splash. The 2nd and 3rd frames show the onset of impact which appears to be initially due to the jet and the accompanying splash. The last frame shows that even after complete submergence, there is a lot of residual air entrainment and disturbance in the vicinity of the cylinder. It is not possible to estimate the kinematics of the wave from the video records in this case.

The next series of images shown in Fig. 4.38 are for the most severe impact case corresponding to wave breaking at $x_b = 25.5$ cm. The first three frames show the development of the jet of the breaking wave, and indicate evidence of slight air entrainment in the upper concave face of the wave. The 4th frame indicates that the impact is quite strong and that it arises from the main body of the wave after the forward tip of the wave has passed over the cylinder. The digitized profiles corresponding to this case are shown in Fig. 4.39, and it is seen that the radius of curvature of the wave under the jet is approximately 1.7 cm which is comparable to the cylinder radius of 2 cm. This leads to a larger contact area at the instant of impact, and consequently a larger force. The time series of the force components for this test are shown in Fig. 4.40.

The impact due to a wave breaking at $x_b = 49$ cm is shown in Fig. 4.41. In contrast with the two previous examples, the jet in the wave crest has not developed prior to impact, the impact itself does not disturb the flow significantly, and the presence of splash and air entrainment is evident only after the cylinder is fully submerged. The radius of curvature (9.7 cm) of the water surface at the instant of impact is also noticeably larger than in the previous case, $x_b = 25.5$ cm. There is a decrease in the peak horizontal force observed in this test.

A summary of the results obtained from the 6 breaking wave tests for this cylinder elevation is included in Table 4.5. The peak resultant force increases from 32.1 N to 63.7 N as the wave breaking location advances from -3.5 cm to 25.5 cm. It is observed that this increase in the peak force is associated with a decrease in the radius of curvature of the wave-front, and a less disturbed water surface prior to impact. The peak force decreases as x_b increases beyond 25.5 cm, even though there seems to be a slight increase in velocity at impact. This could possibly be attributed to the increasing radius of curvature of the water surface at impact. The

horizontal force component is dominant for all the tests in this set, and consequently the direction of the peak force is between 14° and 18° above horizontal for all the tests. The case where $x_b = 17$ cm yields force data that does not conform to the general trend seen for the other 5 cases. A possible explanation for this may be due to the transition from a relatively disturbed impact where the wave has nearly broken ($x_b = -3.5$ and 7.5 cm), to a less disturbed and more defined impact ($x_b = 25.5, 36$ and 49 cm). The rise-times for the peak force are very similar, ranging from 1.6 to 1.8 msec, except for the case of $x_b = 17$ cm where the rise-time is 2.9 msec. The results from the regular wave impact test yielded a peak slamming force that is approximately 20 times less than the largest impact force due to a breaking wave. The peak horizontal and vertical force components were equal at 2.3 N, and yielded a peak resultant force of 3.3 N that had a rise-time of 6.1 msec.

4.3.3 Cylinder Elevation III

The last set of tests has been conducted with the elevation of the cylinder axis at 12.7 cm above the still water level. At this elevation, the cylinder is subjected to impact only by the crest of the breaking wave. Fig. 4.42 shows a series of images for one of the tests in this set for the case $x_b = 25.5$ cm. The first two frames in the figure show the developing jet at the wave crest and the onset of some spilling on the front of the wave. The 3rd and 4th frames show the impact of the convex tip of the jet with the cylinder. The digitized breaking wave profiles for the test in which the wave breaks at $x_b = 17$ cm are shown in Fig. 4.43. Figure 4.44 shows the force records corresponding to wave breaking at $x_b = 25.5$ cm. The corrected peak forces and rise-times for the tests in this set are presented in Table 4.5. The velocity of the water surface at impact cannot be estimated when $x_b = -3.5$ and 7.5 cm, as the wave crest has already broken. The observed peak forces are then 27.8 N and 24.8 N, respectively and the force vector is directed about 24° above the horizontal. For the remaining tests the velocity at impact increases marginally from 1.7 m/sec to 1.8 m/sec and is about 0.3 m/sec faster than the celerity of the wave. The jet which develops at the wave crest has a convex profile. For $x_b = 17, 25.5,$ and 36 cm, the peak forces show an increasing trend (23.3, 23.4 to 31.1 N respectively). In the latter

two tests the peak force vector is directed approximately 30° below horizontal. The rise-times for all the tests are relatively similar and vary between 2 to 3.2 msec. The tests in regular waves do not indicate the presence of a slamming force for this cylinder elevation and may be explained by the low water particle velocity at impact. In this case, the peak horizontal and vertical force components of 2.5 N and 2.8 N respectively occur after full submergence, and yield a maximum resultant force of 3.8 N.

4.3.4 Slamming Coefficients due to Breaking Wave Impact

The plunging wave impact forces observed at the three different cylinder elevations show significant differences. The dynamics of a plunging wave are considerably more complex than those of a regular non-breaking wave. The geometry of the wave at impact in the vicinity of the cylinder depends on the vertical and horizontal location of the cylinder. The presence of entrained air and splash affect the local water particle kinematics and pressures, and consequently influence the magnitude of the impact force. An analytical treatment which accounts for all these factors is still not feasible using currently available techniques. It may be difficult to formulate a single closed-form expression similar to Eq. 2.22 which can predict the impact force due to the various types of wave impact seen in this study.

Although the force measurements in this study are reasonably accurate, the method used to estimate the water surface velocity at impact has limitations. The video equipment used in this study captures images at the rate of 30 frames/sec, whereas a rate of 80 to 100 frames/sec is desirable in order to record a rapidly moving breaking wave and determine velocities and accelerations from the images with reasonable accuracy. However, the test results reported in this study may provide a useful indication of the general problem.

Table 4.5 shows that the water particle velocity in the vicinity of the cylinder varies with wave breaking location x_b , and the cylinder elevation h . If these velocities are used to determine a peak slamming coefficient based on Eq. 2.22, the values obtained show some scatter and do not reveal any obvious trends. At the lowest cylinder elevation of $h = 4.7$ cm, the peak slamming coefficient C_{s0} based on the local particle velocity varies between 8.0 and 10.7. For the next

case ($h = 8.7$ cm), the slamming coefficient varies from 1.9 to 10.1. At the highest elevation ($h = 12.7$ cm), the slamming coefficient varies from 1.3 to 1.5. A constant velocity equal to the celerity of the breaking wave (1.5 m/sec) has also been used to obtain the peak slamming coefficient based on the test that yields the largest resultant force at each of the three cylinder elevations. The largest values of C_{s0} thus obtained are 2.2, 4.5 and 2.2, for the low, middle and high cylinder elevations respectively. It is seen that the most severe impacts occur when the cylinder is located above the still water level at approximately two-thirds of the wave crest elevation. The combination of large impact velocities and smaller radius of curvature of the wave-front at this elevation can cause impact forces which are significantly larger than those occurring for non-breaking wave conditions.

The issue of using results from model studies of breaking wave impact at prototype scales remains unresolved. Three different types of impact pressures can be caused by breaking waves. These are defined as ventilated shocks, compression shocks, and hammer shocks, and it is expected that all the breaking wave impacts seen in the present study are of the ventilated type wherein any air present between the wave-front and the cylinder is able to escape during impact. Kjeldsen (1981) states that the absolute dimensions and coalescing characteristics of entrained air bubbles differ in sea water and fresh water, and that the damping effect on shock peaks caused by bubble populations with different absolute bubble sizes is unknown, which generally precludes a viable model law for ventilated shocks. Although potential flow theory has been used to obtain a good approximation of the development of a plunging breaker (Vinje and Brevig, 1981), the inability to predict air entrainment and the formation of foam makes it difficult to estimate impact pressures and forces during the early stages of a ventilated impact.

Lundgren (1969) suggests that peak shock pressures and impulses for ventilated shocks might be scaled according to Froude's law, but states that this will yield conservative results since it is expected that relative air entrainment for this kind of impact is expected to be higher in the sea in comparison to laboratory experiments. This conclusion is supported by Alfred Führböter (1986) who compared results for wave impact and run-up from experiments at 1:10 model and prototype scales.

Chapter 5

CONCLUSIONS

The primary objective of this thesis has been to examine the impact loads due to waves interacting with a horizontal circular cylinder located near the still water level. Numerical models have been developed to predict the vertical force on such a cylinder, and these have been extended to the case of a dynamically responding cylinder, and an inclined cylinder. Experiments have been conducted to measure the vertical force on a horizontal cylinder subjected to slamming in regular non-breaking waves. Some experiments have also been carried out with an inclined cylinder. The observed data has been analyzed to obtain peak slamming coefficients and related parameters. The numerical models have been used to examine the behaviour of the maximum vertical force in regular and random waves, and the predicted force has also been compared with experimental observations. Experiments to measure the force due to plunging wave impact on a horizontal cylinder have been conducted for different cylinder elevations and wave breaking locations. The conclusions of the present investigation are presented in two separate sections which represent different aspects of this study.

5.1 Wave Slamming on a Horizontal Cylinder

5.1.1 Experimental Study

Experiments have been conducted to measure the vertical force due to waves incident on a slender horizontal cylinder located near the still water level. The water surface elevation and the corresponding force have been measured over a duration of 20 sec which includes several

slamming events. This data has been analyzed to determine the maximum slamming coefficient C_{s0} , the rise-time for the peak slamming force and related parameters. Corrections to the measured coefficients to account for buoyancy, free surface slope and dynamic response and free surface slope are indicated.

Results from tests in regular waves of various periods and heights and with different cylinder elevations indicate that these coefficients exhibit a considerable degree of scatter, which has also been reported by earlier experimental investigators. The maximum slamming coefficient C_{s0} (with no corrections applied) for each of the 22 tests has mean values which vary from 3.04 to 7.79, and exhibits no noticeable trend with either the incident wave characteristics or the elevation of the cylinder. It is possible that the absence of any such trend in the values of C_{s0} may be due to the limited range of values of the parameters, the relatively low number of observations made, and the possibility of a complex dependence on several of the parameters. The C.O.V. of C_{s0} varies from 0.09 to 0.36 and increases with the steepness of the incident wave. This trend is explained by the likelihood of increased disturbances on the water surface due to the higher water particle kinematics in steeper waves. Individual values of C_{s0} vary from 1.86 to 11.7 and the overall mean of C_{s0} is 4.87. This compares well with the experimental results of Campbell and Weynberg (1980) who reported a mean value of $C_{s0} = 5.15$. The probability density histogram of C_{s0} based on a total of 311 slamming events recorded in the 22 tests is seen to follow a log-normal distribution.

The average value of the measured rise-time T_t for the tests varies from 11.6 to 37.1 msec and its C.O.V. ranges from 0.13 to 0.36. There is a tendency for T_t to increase with the impact velocity v_n/\sqrt{gD} , which may be attributed to the slower rise of impact pressures due to increased presence of entrained air and local disturbances. The rise-time T_t corrected for dynamic effects varies from 10.8 to 37.1 msec for the 22 tests. An average cylinder submergence $(s/a)_0$ of 0.33 (7 mm) was noted when the peak slamming force occurred.

The maximum slamming coefficient corrected for buoyancy, dynamic response and free surface slope, denoted C_{s0}^* , varies between 2.92 and 7.60 with an overall mean value of 4.29, and exhibits no noticeable reduction in scatter in comparison to C_{s0} .

A method of defining slamming as an impulse has been demonstrated, and a corresponding impulse coefficient C_i has been estimated from the experimental data. The mean value of C_i estimated from the 22 tests varies from 0.26 to 1.36, with an overall mean of 0.73; and the C.O.V. of C_i varies from 0.04 to 0.41. The mean value of the impulse coefficient based on the impact velocity corrected for free surface slope C_i^* varies from 0.26 to 1.47 with an overall mean of 0.77, and is higher than the corresponding value of C_i by between 1% and 9%. In general, C_i^* exhibits trends which are similar to those of C_i , and has similar C.O.V.s. The degree of scatter for C_i^* is less than that for C_{s0} by about 25% on average. The estimates of the impulse coefficient did not show any observable trend with respect to incident wave conditions or cylinder elevation.

The dimensionless impulse duration $v_n T_i / a$ which indicates the relative submergence of the cylinder at the end of the impact has a mean value which varies from 0.29 to 1.15, and exhibits less scatter than the quantity $v_n T_r / a$ by about 54%. The overall mean value of $v_n T_i / a$ is 0.69 which corresponds to a submergence of about 1/3rd of the cylinder's diameter at the end of the slamming impulse.

Some experiments in regular waves have also been conducted for the test cylinder inclined at 4.8° and 9.6° with respect to the horizontal. In general, the force records measured during these tests indicate that the slamming force increases more gradually and that the corresponding peak load decreases with inclination, which is similar to the experimental observations of Campbell and Weynberg (1980). There is no obvious evidence of a slamming force maximum for the larger tilt angle of 9.6° , and the rate of increase of the normal force is quite gradual which also results in lower dynamic response of the cylinder. While these force measurements also tend to show scatter in a manner similar to horizontal cylinder tests, the repeatability improves with increasing cylinder inclination which results in smaller slamming forces.

5.1.2 Numerical Modelling

A numerical model based on the use of a slamming coefficient for simulating the vertical wave force acting on fixed, rigid, horizontal circular cylinder located near the still water level is described. Only the two-dimensional case of unidirectional waves propagating in a direction orthogonal to the cylinder axis is considered. The model attempts to account for the limitations of current theory regarding the variation of the slamming coefficient with cylinder submergence, and treats the vertical force during the partial submergence phase in alternate ways. The model has also been extended to include the case of a horizontal cylinder which responds dynamically to the applied wave force, and an inclined cylinder.

Model I (Isaacson and Subbiah, 1990) which uses a C_{s0} value of π and simply assumes a linear variation of the vertical force during partial submergence of the cylinder, and Model II which also uses a C_{s0} value of π but a modified C_{s+d} coefficient, are used to study the variation of the maximum force as a function of the governing non-dimensional parameters in the problem. It is seen that although there are notable differences during periods of partial submergence of the cylinder, both models predict maximum forces which are very close to each other, which indicates that a detailed modelling of the force variation during the stage of partial submergence may be avoided in certain cases

For the case of random waves, the time variation of the force is illustrated both for a narrow-band spectrum and a two-parameter Pierson-Moskowitz spectrum. The probability densities of the force peaks are compared with available analytical predictions which are based on the assumption of a narrow-band spectrum. These probability densities have been obtained using all the force peaks in a record, as well as using a single force peak for each wave, so that the presence of secondary peaks during each wave is accounted for. The latter method provides better agreement with the predictions. In the case of a narrow-band spectrum, the agreement is quite reasonable, with discrepancies due in part to sampling variability. For the case of a broader band spectrum, the agreement is quite poor and indicates that the analytical predictions cannot be directly extended to the case of a broad-band spectrum.

The predictions of the numerical model have also been compared with the experimental data, and results from the simulations indicate that the variation of the slamming coefficient during the early phase of partial submergence is more accurately predicted by Campbell and Weynberg's (1980) expression which is based on a C_{s0} value of 5.15 and has a faster rate of decay in comparison to Taylor's model. It is seen that the proposed method for combining the slamming, buoyancy, drag, and inertia force components works reasonably well when used with appropriate values of the force coefficients, and that the model is able to predict a variation of the vertical force which compares well with the experimentally observed force over the entire wave cycle. The dynamic model which also incorporates a rise-time parameter in the slamming force is seen to perform equally well in predicting the wave force and the resulting response of the cylinder. It is noted that a finite rise-time used in the simulation will give rise to a larger dynamic response for the same value of C_{s0} used with a zero rise-time. Reasonable agreement between simulations and experiments is seen in the case of the inclined cylinder which validates the strip method for estimating the slamming force.

The various methods including an approach based on an impulse coefficient for estimating the maximum response of a cylinder subjected to wave impact, are illustrated in the context of a typical ocean engineering application. In addition to the smaller scatter shown by the experimental estimate of C_i in comparison to C_{s0} , the use of the impulse coefficient method is relatively simple, and appears to be effective in estimating maximum structural element responses for conditions under which this method is applicable.

5.2 Plunging Wave Impact on a Horizontal Cylinder

An experimental study of impact forces due to plunging wave action on a slender horizontal cylinder has been conducted for different cylinder elevations and wave breaking locations. In addition to the horizontal and vertical force components on the cylinder, a video record of the impact has been obtained for the different tests. The maximum values of the force components have been corrected for the dynamic response of the cylinder, and the resultant peak force along

with the impact velocity and radius of curvature of the wave-front which are estimated from the digitized video images, are reported.

As expected, the peak impact force is found to depend on the vertical and horizontal location of the cylinder relative to the breaking wave. The impact is more severe for cases where the radius of curvature of the water surface at impact is similar to the radius of the cylinder. In addition to a significant horizontal force component, the magnitude of the impact force due to a breaking wave is considerably larger than that due to a regular non-breaking wave of the same height and period. The peak slamming coefficient C_{s0} , determined from the recorded force and the corresponding local water surface velocity at impact, exhibits considerable scatter, varying from 1.3 to 10.7. If instead, the wave celerity is used as a basis for calculating C_{s0} , the largest values of C_{s0} obtained are 2.2, 4.5 and 2.2 for the low, middle and high cylinder elevations respectively.

No currently accepted scaling law is available for extending results from model tests on breaking wave forces to prototype scales due to the differing characteristics of the entrained air in the two cases. However, it is expected that the use of Froude's law will lead to results on the conservative side when using model results at large scales.

5.3 Recommendations

Estimation of Design Loads

The results of the present investigation lend support to earlier studies which conclude that the magnitude of C_{s0} is larger than the generally accepted value of π which has been used in design. The nature of the wave slamming phenomenon is such that any departure from 'ideal' conditions, including the presence of disturbances on the water surface, entrained air, compressibility, cylinder roughness, cylinder inclination, and non-normal approach of incident waves tend to result in a reduction of the severity of the slamming force. Other factors such as cylinder motion, and presence of fouling can result in elevated values of the slamming

coefficient. It is currently not possible to use theoretical techniques which can account for the effects of some of these factors.

In the absence of detailed full-scale experimental data, it is recommended that designers use a C_{s0} value between 5 and 6 when calculating slamming forces on a horizontal cylinder in non-breaking regular waves. In cases where the dynamic response of the element is an issue, a time domain simulation to determine the forces and design stresses may be warranted. The modified expression for the combined slamming and drag coefficient based on Campbell and Weynberg's (1980) results used along with the Morison equation and suitable force coefficients is seen to yield reasonable estimates of the vertical force variation with time. For structural elements with natural periods greater than 0.5 sec, the use of an impulse coefficient C_i between 0.8 and 1.2 can also provide a quick estimate of the dynamic response of the element.

The data from the present study shows that the most severe impact forces occur when the underside of the cylinder is close to the still water level for the case of non-breaking wave impact, and the underside of the cylinder is approximately two-thirds of the wave crest elevation above the still water level for the case of plunging wave impact.

Further Study

There are several avenues which can be explored further in the study of wave slamming on cylinders. In addition to a closer examination of the effect of cylinder tilt on the slamming force, oblique wave impact in the case where the wave crest approaches the cylinder at an angle is a problem which merits further study. Laboratory experiments on wave slamming, especially tests involving Froude numbers higher than 1.5, which accurately measure the impact velocity using laser-doppler velocimetry can also help to provide better estimates of the slamming coefficient. Data on the statistical properties of the impact force in experiments using random waves will also be of use to designers.

Since the slamming force is sensitive to a number of parameters which are difficult to reproduce in a laboratory, a valuable contribution to the present understanding of the subject will involve reliable full-scale slamming force data on a platform element in typical sea states. Earlier reported full scale studies have suffered from problems including excessive filtering of force data and the use of inadequate sampling rates. Currently available instrumentation and computer based data collection methods should allow an easier implementation of field measurements.

Forces due to breaking wave impact on a horizontal cylinder are seen to be up to 20 times larger than those due to regular waves of the same period and height. Data from the present study suggests that the maximum force is strongly dependent on the cylinder elevation and wave breaking location. Accurate measurements of the curvature and velocity of the breaking wave-front will allow better correlation between these parameters and the maximum impact force. The unavailability of an accepted scaling law for this problem points to the necessity of conducting similar experiments at large scales which will serve as an important extension to the data gathered in the present study.

References

- Abramowitz, M., and Stegun, I. A. (1970). *Handbook of Mathematical Functions*, 9th edn., Dover Publications, New York.
- Arhan, M., Deleuil, G., and Doris, C. G. (1978). "Experimental Study of the Impact of Horizontal Cylinders on a Water Surface," *Proc. 10th Offshore Tech. Conf.*, Houston, Texas, Paper No. OTC 3107, Vol. 1, pp. 485 - 492.
- Attfield, K. (1975). "Gas Platforms - How Designers Underestimated North Sea," *Offshore Engineer*, pp. 19 - 22, June, 1975.
- Basco, D. R., and Niedzwecki, J. M. (1989). "Breaking Wave Force Distributions and Design Criteria for Slender Piles," *Proc. 21st Offshore Tech. Conf.*, Houston, Texas, Paper No. OTC 6009, pp. 425 - 431.
- Campbell, I. M. C., and Weynberg, P. A. (1980). "Measurement of Parameters Affecting Slamming," *Report No. Report No. 440*, Wolfson Unit for Marine Technology and Industrial Aerodynamics, University of Southampton, Tech. Rep. Centre No. OT-R-8042.
- Chakrabarti, S. K. (1988). *Hydrodynamics of Offshore Structures*, Computational Mechanics Publications, Southampton, U.K.
- Chan, E. S. (1993). "Extreme Wave Action on Large Horizontal Cylinders Located Above Still Water Level," *Proc. 3rd Int. Offshore and Polar Engineering Conf.*, Singapore, Vol. 3, pp. 121 - 128.
- Chan, E. S., and Melville, W. K. (1988). "Deep-Water Plunging Wave Pressures on a Vertical Plane Wall," *Proc. Royal Society of London, Ser. A*, Vol. 417, pp. 95 - 131.
- Chan, E. S., and Melville, W. K. (1989). "Plunging Wave Forces on Surface-Piercing Structures," *J. Offshore Mechanics and Arctic Engineering*, Vol. 111, pp. 92 - 100.

- Chan, E. S., Cheong, H. F., and Gin, K. Y. H. (1991a). "Wave Impact Loads on Horizontal Structures in the Splash Zone," *Proc. 1st Int. Offshore and Polar Engineering Conf.*, Vol. 3, pp. 203 - 209.
- Chan, E. S., Tan, B. C., and Cheong, H. F. (1991b). "Variability of Plunging Wave Pressures on Vertical Cylinders," *Int J. Offshore and Polar Engineering*, Vol. 1, No. 2, pp. 94 - 100.
- Clough, R. W., and Penzien, J. (1975). *Dynamics of Structures*, McGraw Hill, New York.
- Cointe, R. and Armand, J. L. (1987). "Hydrodynamic Impact Analysis of a Cylinder," *J. Offshore Mechanics and Arctic Engineering*, Vol. 109, pp. 237 - 243.
- Dalton, C., and Nash, J. M. (1976). "Wave Slam on Horizontal Members of an Offshore Platform," *Proc. 8th Offshore Tech. Conf.*, Houston, Texas, Paper No. OTC 2500, Vol. 1, pp. 769 - 778.
- Dixon, A. G., Greated, C. A., and Salter, S. H. (1979a). "Wave Forces on Partially Submerged Cylinders," *J. Waterway, Port, Coastal and Ocean Division*, ASCE, Vol. 105, No. WW4, pp. 421 - 438.
- Dixon, A. G., Durrani, T. S., and Greated, C. A. (1979b). "Wave Force Statistics for Partially Submerged Horizontal Cylinders," *Mechanics of Wave Induced Forces on Cylinders*, ed. T. L. Shaw, Pitman, Bristol, U.K., pp. 379 - 392.
- Easson, W. J., and Greated, C. A. (1984). "Breaking Wave Forces and Velocity Fields," *Coastal Engineering*, Vol. 8, pp. 233 - 241.
- Easson, W. J., Greated, C. A., and Durrani, T. S. (1981). "Buoyancy, Drag and Inertial Forces on Partially Submerged Horizontal Cylinders in Random Seas," *Proc. Int. Symp. on Hydrodynamics in Ocean Engineering*, Trondheim, Norway, Vol. 1, pp. 531 - 546.
- Fabula, A. G. (1957). "Ellipse-Fitting Approximation of Two-Dimensional Normal Symmetric Impact of Rigid Bodies on Water," *Proc. 5th Midwestern Conf. on Fluid Mechanics*, University of Michigan Press, Ann Arbor, Michigan, pp. 299 - 315.
- Faltinsen, O., Kjaerland, O., Nottveit, A., and Vinje, T. (1977). "Water Impact Loads and Dynamic Response of Horizontal Circular Cylinders in Offshore Structures," *Proc. 9th Offshore Tech. Conf.*, Houston, Texas, Paper No. OTC 2741, Vol. 1, pp. 119 - 126.

- Funke, E. R., and Mansard, E. P. D. (1984). "The NRCC "Random" Wave Generation Package," *Hydraulics Laboratory Technical Report No. TR-HY-002*, National Research Council, Ottawa, Canada.
- Garrison, C. J. (1978). "Hydrodynamic Loading on Offshore Structures. Three-Dimensional Source Distribution Methods," In *Numerical Methods in Offshore Engineering*, eds. O. C. Zienkiewicz, R. W. Lewis, and K. G. Stagg, Wiley, Chichester, U.K., pp. 97 - 140.
- Greenhow, M. (1988). "Water-entry and -exit of a horizontal circular cylinder," *Applied Ocean Research*, Vol. 10, No. 4, pp. 191 - 198.
- Greenhow, M., and Li, Y. (1987). "Added Masses for Circular Cylinders Near or Penetrating Fluid Boundaries - Review, Extension and Application to Water-Entry, -Exit and Slamming," *Ocean Engineering*, Vol. 14, No. 4, pp. 325 - 348.
- Havelock, T. H. (1929). "Forced Surface Waves on Water," *Philosophical Magazine*, Vol. 8, pp. 569 - 576.
- Isaacson, M., and Subbiah, K. (1990). "Random Wave Slamming on Cylinders," *J. Waterway, Port, Coastal, and Ocean Engineering*, ASCE, Vol. 116, No. 6, pp. 742 - 763.
- Kaplan, P., (1979). "Impact Forces on Horizontal Members," *Proc. Civil Engineering in the Oceans IV*, ASCE, San Francisco, Vol. II, pp. 716 - 731.
- Kaplan, P., and Silbert, M. N. (1976). "Impact Forces on Platform Horizontal Members in the Splash Zone," *Proc. 8th Offshore Tech. Conf.*, Houston, Texas, Paper No. OTC 2498, Vol. 1, pp. 749 - 758.
- Kjeldsen, S. P. (1981). "Shock Pressures from Deep Water Breaking Waves," *Proc. Int. Symp. on Hydrodynamics in Ocean Engineering*, Trondheim, Norway, Vol. 1, pp. 567 - 584.
- Kjeldsen, S. P., and Myrhaug, D. (1979). "Breaking Waves in Deep Water and Resulting Wave Forces," *Proc. 11th Offshore Tech. Conf.*, Houston, Texas, Paper No. OTC 3646, Vol. 1, pp. 2515 - 2522.
- Kjeldsen, S. P., Torum, A., and Dean R. G. (1986). "Wave Forces on Vertical Piles Caused by 2 and 3 Dimensional Breaking Waves," *Proc. 20th Coastal Engineering Conf.*, Taipei, Taiwan, Vol. 3, pp. 1929 - 1942.

- Lundgren, H. (1969). "Wave Shock Forces: An Analysis of Deformations and Forces in the Wave and in the Foundation," *Proc. Symp. on Wave Action*, Delft Hydraulics Laboratory, Delft, The Netherlands, Paper No. 4, pp. 1 - 20.
- Miao, G. (1988). "Hydrodynamic Forces and Dynamic Responses of Circular Cylinders in Wave Zones," Ph.D. Thesis, University of Trondheim, Norway.
- Miao, G. (1990). "Dynamic Response of Elastic Horizontal Circular Cylinders by Wave Slamming," *Proc. 9th Int. Conf. on Offshore Mechanics and Arctic Engineering*, Vol. 1, pp. 239 - 245.
- Miles, M. D. (1989). "User Guide for GEDAP Version 2.0 Wave Generation Software," *Hydraulics Laboratory Technical Report No. LM-HY-034*, National Research Council, Ottawa, Canada, December.
- Miller, B. L. (1977). "Wave Slamming Loads on Horizontal Circular Elements of Offshore Structures," *J. Royal Institution of Naval Architects*, Paper No. 5, pp. 81 - 98.
- Miller, B. L. (1980). "Wave Slamming on Offshore Structures," *Report No. NMI-R81*, National Maritime Institute, Feltham, Middlesex, U.K., March.
- Morison, J. R., O'Brien, M. P., Johnson, J. W., and Schaaf, S. A. (1950). "The Forces Exerted by Surface Waves on Piles," *Petroleum Transactions, American Institute of Mining, Metallurgical, and Petroleum Engineers*, Vol. 189, pp. 149 - 154.
- Nichols, B. D., and Hirt, C. W. (1978). "Hydrodynamic Impact Analysis," *Report No. EPRI NP-824*, Electric Power Research Institute, Palo Alto, California, June.
- Pelletier, D. (1989). "Real Time Control System (RTC) User's Manual," *Hydraulics Laboratory Technical Report No. LM-HY-033*, National Research Council, Ottawa, Canada, November.
- Sarpkaya, T. (1978). "Wave Impact Loads on Cylinders," *Proc. 10th Offshore Tech. Conf.*, Houston, Texas, Paper No. OTC 3065, Vol. 1, pp. 169 - 176.
- Sawaragi, T., and Nochino, M. (1984). "Impact Forces of Nearly Breaking Waves on a Vertical Circular Cylinder," *Coastal Engineering in Japan*, Vol. 27, pp. 249 - 263.
- Taylor, J. L. (1930). "Some Hydrodynamical Inertia Coefficients," *Philosophical Magazine*, Ser. 7, Vol. 9, No. 55, pp. 161 - 183.

- Tuah, H., and Hudspeth, R. T. (1982). "Comparisons of Numerical Random Sea Simulations," *J. Waterway, Port, Coastal and Ocean Engineering*, ASCE, Vol. 108, No. 4, pp. 569 - 584.
- Vinje, T., and Brevig, P. (1981). "Numerical Calculation of Forces from Breaking Waves," *Proc. Int. Symp. on Hydrodynamics in Ocean Engineering*, Trondheim, Norway, Vol. 1, pp. 547 - 565.
- von Karman, T., and Wattendorf, P. L. (1929). "The Impact on Seaplane Floats During Landing," *TN 321*, U.S. National Advisory Committee for Aeronautics, Washington, October.
- Wagner, H. (1931). "Landing of Seaplanes," *TN 622*, U.S. National Advisory Committee for Aeronautics, Washington, May.
- Zhou, D., Chan, E. S., and Melville, W. K. (1991). "Wave Impact Pressures on Vertical Cylinders," *Applied Ocean Research*, Vol. 13, No. 5, pp. 220 - 234.

Investigator	Type of Test	L/D	Froude No.	C_{s0}
Arhan et al. (1978)	Drop test	3.3 - 10	0.6 - 2.6	2.4 - 6.9
Campbell and Weynberg (1980)	Drop test	6 - 16	1.9 - 5.7	3.5 - 6.5
Schnitzer and Hathaway (referred to by Miller, 1980)	Drop test	3.6	1.7	~ 3.5
Sollid (referred to by Miller, 1980)	Drop test	1.1 - 1.5		4.1 - 6.4
Watanabe (referred to by Miller, 1980)	Drop test	0.5	1.4 - 2.1	6.2
Souter et al. (referred to by Miller, 1980)	Drop test	3.6, 4.6	1.6 - 5.1	5.2 - 6.8
Faltinsen et al (1977)	Drop test	23 - 37	0.4 - 1.2	4.1 - 6.4
Miao (1988)	Drop test	0.4, 2, 30	0.1 - 3.8	Avg. 6.1
Bergren (referred to by Miller, 1980)	Regular waves	40 - 100		1 - 3.1
Canham (referred to by Miller, 1980)	Regular waves	15	0.35 - 0.6	
Dalton and Nash (1976)	Regular waves	20	1 - 3.5	1 - 4.5
Holmes et al. (referred to by Miller, 1980)	Regular and Irregular Waves	24 - 108	0.3 - 3.4	0.4 - 2.9
Miller (1977)	Irregular wave packet	15	0.3 - 1.5	1 - 8 (Avg. 3.5)
Webb (referred to by Miller, 1980)	Ocean waves	30		3 - 4
Sarpkaya (1978)	Rising water surface (U-tube)	4.5 - 12	0.5 - 1.3	3.2

Table 1.1 Peak slamming coefficient C_{s0} reported in earlier experimental studies.

Period T (sec)	Height H (cm)	Steepness	Celerity c (m/s)
1.0	9.8	0.064	1.53
1.0	14.6	0.096	1.53
1.1	13.8	0.079	1.61
1.1	17.0	0.102	1.60
1.2	12.1	0.058	1.74
1.2	15.2	0.073	1.74
1.2	19.3	0.092	1.74
1.4	16.5	0.062	1.89
1.4	22.6	0.085	1.89
1.5	13.9	0.048	1.94
1.5	18.4	0.063	1.94
1.5	22.9	0.078	1.94
1.6	16.8	0.053	1.99
1.6	22.4	0.070	1.99
1.8	13.5	0.036	2.06
1.8	17.8	0.048	2.06

Table 4.1 Properties of regular waves used in slamming experiments.

$\dot{\eta}$ (m/s)	C_{so}	v_n (m/s)	C'_{so}	$(s/a)_o$	C''_{so}	T_t (msec)	T_r (msec)	C^*_{so}
0.37	5.06	0.36	5.32	0.33	4.76	19.6	18.8	4.63
0.37	4.71	0.36	4.96	0.44	4.13	25.6	24.9	4.10
0.39	6.22	0.38	6.59	0.33	6.09	18.4	17.7	6.07
0.41	4.88	0.40	5.19	0.36	4.66	19.6	18.8	4.53
0.40	7.20	0.39	7.63	0.30	7.18	17.2	16.9	7.05
0.39	6.63	0.38	7.02	0.33	6.51	18.8	18.1	6.43
0.40	4.05	0.39	4.30	0.51	3.42	27.6	27.1	3.37
0.40	4.87	0.39	5.17	0.31	4.72	17.2	16.9	4.64
0.39	4.69	0.38	4.96	0.29	4.44	19.2	18.5	4.34
0.40	6.28	0.39	6.66	0.36	6.11	20.0	19.4	5.93
0.39	4.36	0.39	4.62	0.40	3.96	22.8	22.1	3.87
0.41	4.52	0.40	4.81	0.30	4.37	17.2	16.9	4.29
0.39	4.57	0.38	4.84	0.40	4.19	22.4	21.7	4.13
Mean	5.16	0.38	5.47	0.35	4.91	20.1	19.4	4.81
C.O.V.	0.16	0.03	0.16	0.14	0.18	0.13	0.13	0.18
Min.	4.36	0.35	4.62	0.29	3.96	17.2	16.9	3.87
Max.	6.63	0.38	7.02	0.44	6.51	25.6	24.9	6.43

Table 4.2 Peak slamming coefficients and related parameters estimated from multiple slamming events in a regular wave test.
 $T = 1.5$ sec, $H = 18.4$ cm, $h = 0.5$ cm.

T (sec)	H (cm)	$\dot{\eta}\sqrt{gD}$		C_{so}		$v_n\sqrt{gD}$		T_t (msec)		T_r (msec)		$v_n T_r/a$		C''_{so}		C^*_{so}
		Mean	C.O.V	Mean	C.O.V	Mean	C.O.V	Mean	C.O.V	Mean	C.O.V	Mean	C.O.V	Mean	C.O.V	
$h = 0.5 \text{ cm}$																
1.0	9.8	0.49	0.02	5.27	0.10	0.48	0.10	14.7	0.18	14.1	0.21	0.20	0.20	5.18	0.12	5.17
1.0	14.6	0.73	0.08	6.51	0.29	0.70	0.29	22.2	0.30	21.6	0.46	0.34	0.34	6.69	0.32	6.62
1.1	13.8	0.73	0.11	4.14	0.25	0.70	0.25	26.8	0.19	26.3	0.56	0.22	0.22	3.85	0.30	3.77
1.1	17.0	0.71	0.06	7.32	0.21	0.68	0.21	20.7	0.31	20.3	0.42	0.33	0.33	7.67	0.24	7.55
1.2	12.1	0.45	0.04	7.79	0.17	0.45	0.17	14.0	0.19	13.6	0.19	0.18	0.18	7.72	0.17	7.60
1.2	15.2	0.70	0.07	5.09	0.18	0.68	0.18	20.1	0.26	19.5	0.40	0.29	0.29	5.02	0.22	4.87
1.2	19.3	0.78	0.09	5.12	0.33	0.75	0.33	20.1	0.36	19.5	0.44	0.37	0.37	5.17	0.35	5.02
1.4	16.5	0.53	0.03	6.65	0.19	0.52	0.19	14.8	0.24	14.2	0.23	0.25	0.25	6.59	0.20	6.57
1.4	22.6	0.71	0.04	4.15	0.36	0.69	0.36	31.3	0.33	31.0	0.66	0.33	0.33	3.55	0.44	3.55
1.5	13.9	0.41	0.04	4.71	0.16	0.41	0.16	16.8	0.13	16.3	0.20	0.13	0.13	4.31	0.17	4.16
1.5	18.4	0.61	0.03	5.16	0.16	0.60	0.16	20.1	0.13	19.5	0.36	0.11	0.11	4.91	0.18	4.76
1.5	22.9	0.72	0.04	3.75	0.24	0.70	0.24	37.1	0.16	37.1	0.80	0.15	0.15	2.91	0.38	2.91
1.6	16.8	0.50	0.04	3.04	0.11	0.49	0.11	18.9	0.20	18.2	0.27	0.19	0.19	2.57	0.15	2.53
1.6	22.4	0.66	0.04	3.55	0.35	0.65	0.35	21.9	0.32	21.3	0.42	0.30	0.30	3.16	0.42	3.14
1.8	13.5	0.37	0.02	3.38	0.09	0.36	0.09	12.6	0.20	11.9	0.13	0.19	0.19	3.07	0.09	2.92
1.8	17.8	0.42	0.06	3.52	0.13	0.42	0.13	11.6	0.25	10.8	0.14	0.21	0.21	3.29	0.14	3.28

Table 4.3 Summary of test conditions and principal results from slamming tests in regular waves.

T (sec)	H (cm)	$\dot{\eta}\sqrt{gD}$		C_{so}		$v_n\sqrt{gD}$		C'_{so}		T_t (msec)		T_r (msec)		$v_n T_r/a$		C''_{so}		C^*_{so} Mean	
		Mean	C.O.V	Mean	C.O.V	Mean	C.O.V	Mean	C.O.V	Mean	C.O.V	Mean	C.O.V	Mean	C.O.V	Mean	C.O.V		
$h = 4.5 \text{ cm}$																			
1.1	17.0	0.75	0.14	3.93	0.31	0.72	0.72	4.45	20.0	0.32	19.4	0.43	0.34	3.89	0.32	3.78			
1.4	16.5	0.54	0.05	4.20	0.15	0.53	0.53	4.42	18.1	0.31	17.6	0.28	0.35	3.87	0.20	3.86			
1.5	18.4	0.75	0.07	3.24	0.13	0.72	0.72	3.53	16.5	0.28	15.9	0.35	0.30	3.11	0.18	2.99			
1.6	16.8	0.55	0.02	4.80	0.07	0.55	0.55	5.03	12.4	0.19	11.7	0.20	0.20	4.72	0.07	4.52			
$h = -4.5 \text{ cm}$																			
1.4	22.6	0.55	0.08	3.72	0.16	0.54	0.54	3.92	21.5	0.33	20.9	0.34	0.41	3.40	0.19	3.38			
1.5	18.4	0.41	0.04	4.54	0.14	0.41	0.41	4.66	21.1	0.23	20.7	0.26	0.25	3.95	0.18	3.92			

Table 4.3 (contd.) Summary of test conditions and principal results from slamming tests in regular waves.

T (sec)	H (cm)	C_i	C_i^*		$v_n T_i/a$	
		Mean	Mean	C.O.V.	Mean	C.O.V.
h = 0.5 cm						
1.0	9.8	0.65	0.68	0.05	0.48	0.08
1.0	14.6	1.08	1.15	0.19	0.88	0.13
1.1	13.8	0.73	0.80	0.15	0.90	0.13
1.1	17.0	1.36	1.47	0.19	0.85	0.13
1.2	12.1	0.74	0.76	0.04	0.41	0.05
1.2	15.2	0.84	0.89	0.14	0.74	0.15
1.2	19.3	1.21	1.30	0.27	1.00	0.15
1.4	16.5	0.90	0.93	0.05	0.54	0.12
1.4	22.6	0.80	0.84	0.30	1.11	0.16
1.5	13.9	0.53	0.54	0.15	0.43	0.07
1.5	18.4	0.72	0.75	0.12	0.68	0.06
1.5	22.9	0.55	0.58	0.41	1.15	0.14
1.6	16.8	0.35	0.38	0.12	0.48	0.08
1.6	22.4	0.64	0.67	0.30	0.76	0.15
1.8	13.5	0.26	0.26	0.04	0.29	0.06
1.8	17.8	0.33	0.33	0.10	0.34	0.07
h = 4.5 cm						
1.1	17.0	0.93	1.01	0.26	0.90	0.12
1.4	16.5	0.61	0.63	0.06	0.57	0.17
1.5	18.4	0.60	0.64	0.09	0.74	0.14
1.6	16.8	0.71	0.73	0.05	0.50	0.07
h = -4.5 cm						
1.4	22.6	0.37	0.47	0.19	0.51	0.21
1.5	18.4	0.34	0.35	0.27	0.40	0.15

Table 4.4 Summary of impulse coefficients and related parameters estimated from slamming tests in regular waves.

x_b (cm)	\hat{F}_x (N)	\hat{F}_z (N)	T_r (msec)	\hat{F}_r (N)	ϕ (deg)	v_n (m/sec)	r_w (cm)
$h = 4.7$ cm							
-3.5	15.0	-4.5	2.6	15.7	-17	-	-
7.5	7.5	10.1	4.4	12.6	53	0.45	> 20
17.0	12.5	13.4	3.6	18.3	47	0.52	> 20
25.5	17.0	16.9	3.8	24.0	45	0.63	> 20
36.0	21.6	18.5	2.6	28.4	41	0.75	> 20
49.0	24.8	17.7	3.9	30.5	36	0.75	> 20
Regular wave	4.5	5.6	15.1	7.2	51		
$h = 8.7$ cm							
-3.5	31.0	8.5	1.6	32.1	15	-	-
7.5	28.0	7.1	1.7	28.9	14	1.4	4.8
17.0	19.0	-14.1	2.9	23.7	-37	1.4	2.8
25.5	61.0	18.4	1.8	63.7	17	1.0	1.7
36.0	56.0	17.0	1.8	58.5	17	1.1	6.7
49.0	50.0	16.3	1.8	52.6	18	1.25	9.7
Regular wave	2.3	2.3	6.1	3.3	45		
$h = 12.7$ cm							
-3.5	25.6	10.8	2.0	27.8	23	-	-
7.5	22.7	9.9	2.0	24.8	24	-	-
17.0	23.0	3.7	3.0	23.3	9	1.7	CONVEX
25.5	18.3	-14.6	3.2	23.4	-39	1.7	CONVEX
36.0	27.3	-14.8	3.0	31.1	-28	1.8	CONVEX
Regular wave	2.5	2.8	25.2	3.8	48		

Notation

\hat{F}_x, \hat{F}_z peak horizontal and vertical impact force components respectively.

$$\hat{F}_r = [(\hat{F}_x)^2 + (\hat{F}_z)^2]^{0.5}$$

$$\phi = \tan^{-1} (\hat{F}_z / \hat{F}_x)$$

v_n normal velocity of the water surface prior to its contact with the test cylinder.

r_w radius of curvature of the water surface prior to its contact with the test cylinder.

-- reasonable estimates of v_n or r_w not possible because water surface was too disturbed.

Table 4.5 Summary of observations from impact tests in breaking waves.

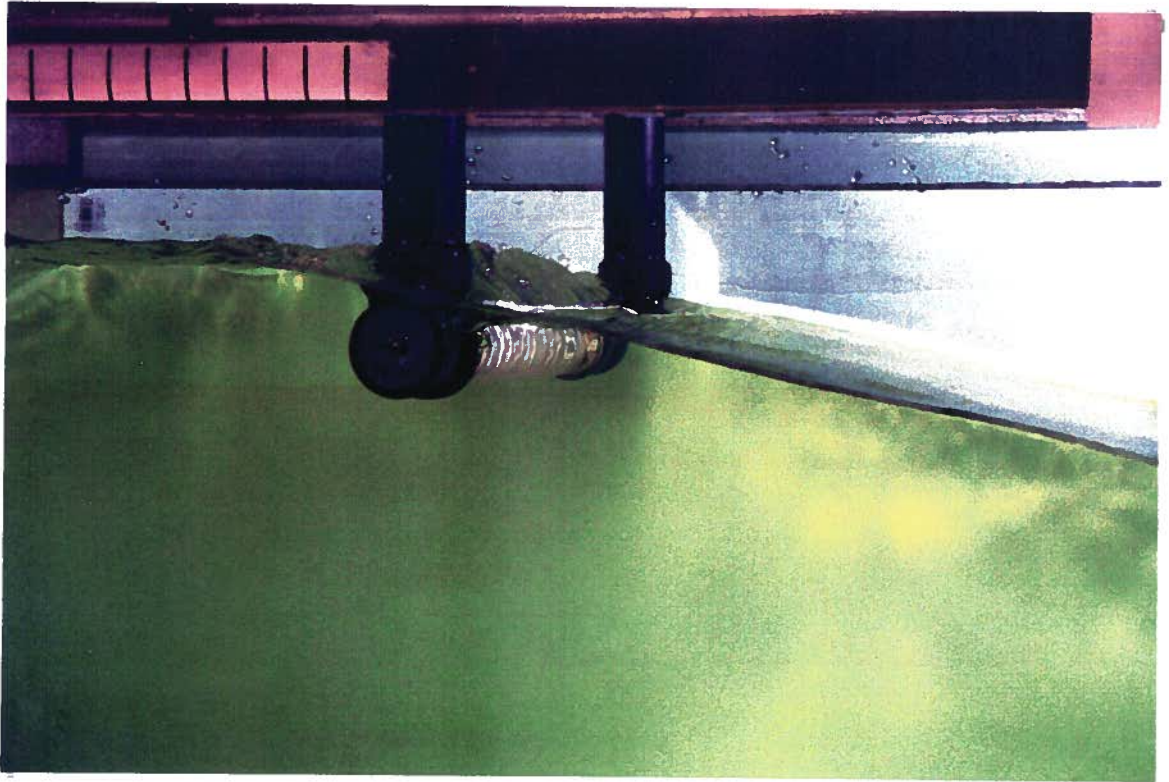


Fig. 1.1 Photograph of non-breaking wave impact on horizontal test cylinder.

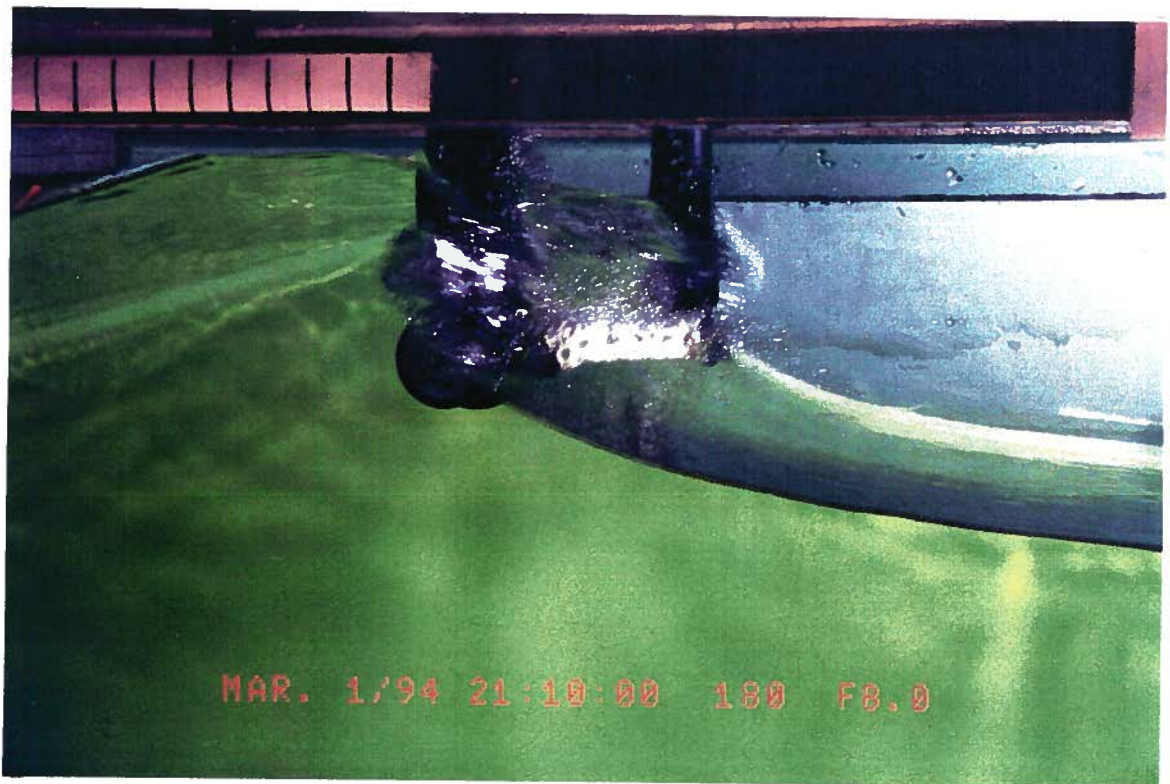


Fig. 1.2 Photograph of plunging wave impact on horizontal test cylinder.

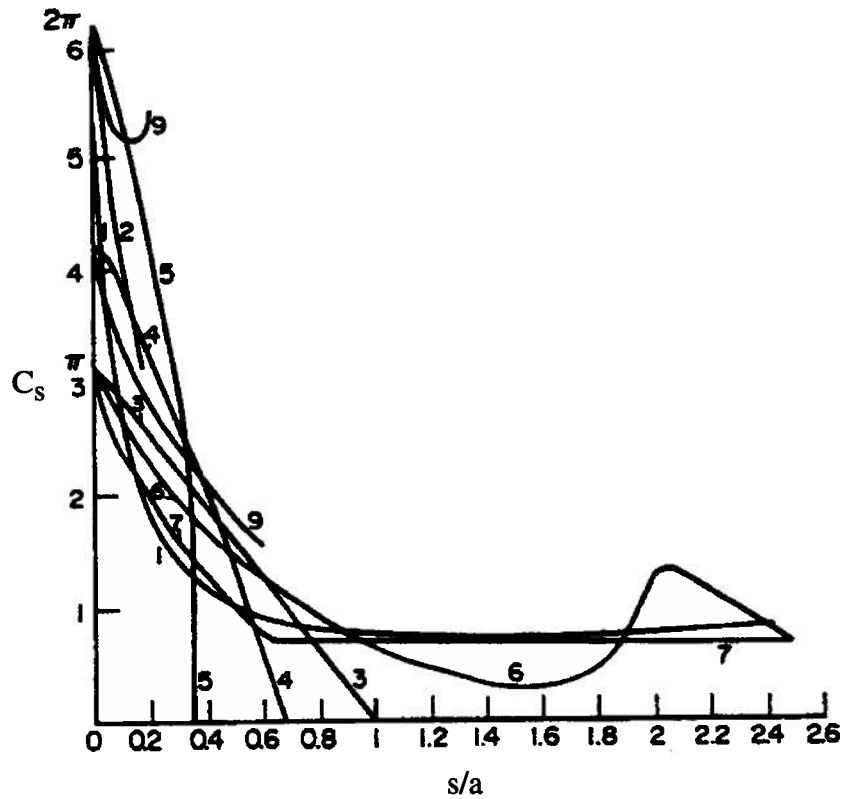


Fig. 1.3 Comparison of analytical and experimental results for the slamming coefficient C_s as a function of relative submergence s/a (Greenhow and Li, 1987). 1, experiments of Campbell and Weynberg (1980); 2, ellipse theory of Fabula (1957); 3, von Karman (1929); 4, semi-Wagner; 5, Wagner's flat plate approach (1932); 6, Taylor (1930); 7, semi-von Karman; 8, semi-Wagner; 9, Wagner's exact body approach.

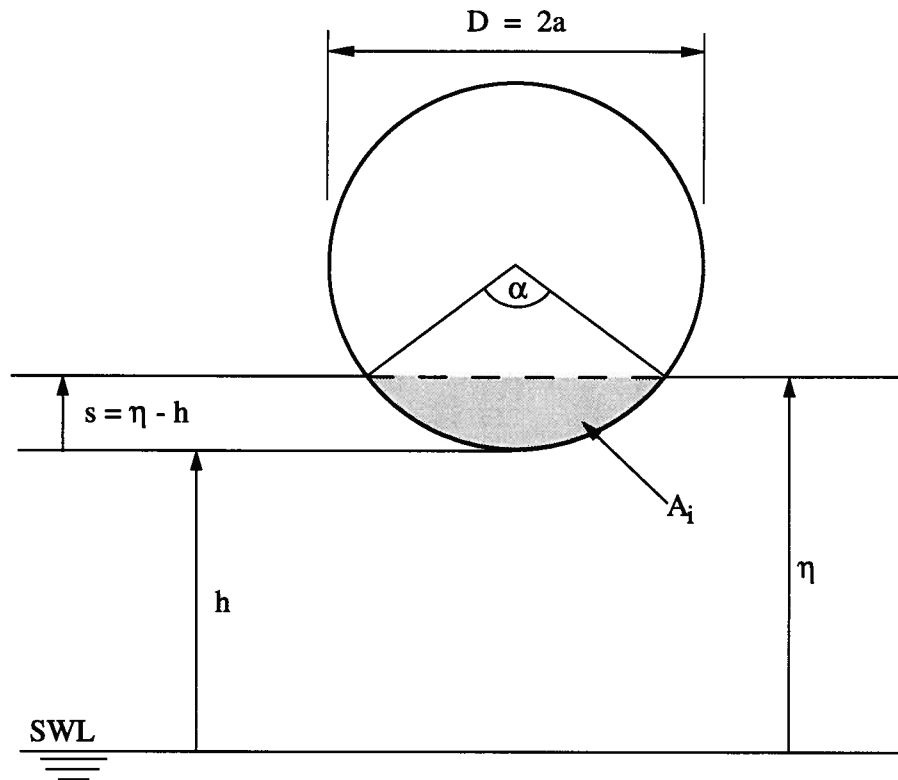


Fig. 2.1 Definition sketch for a fixed cylinder.

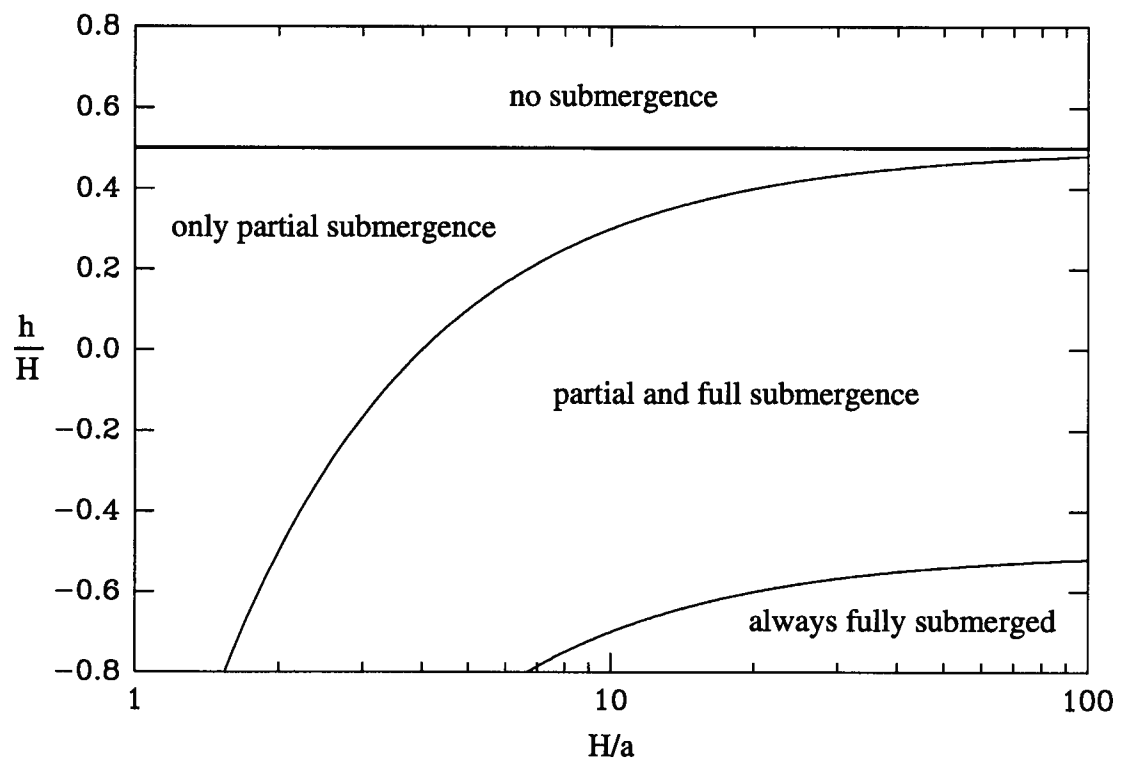


Fig. 2.2 Regimes of cylinder submergence.

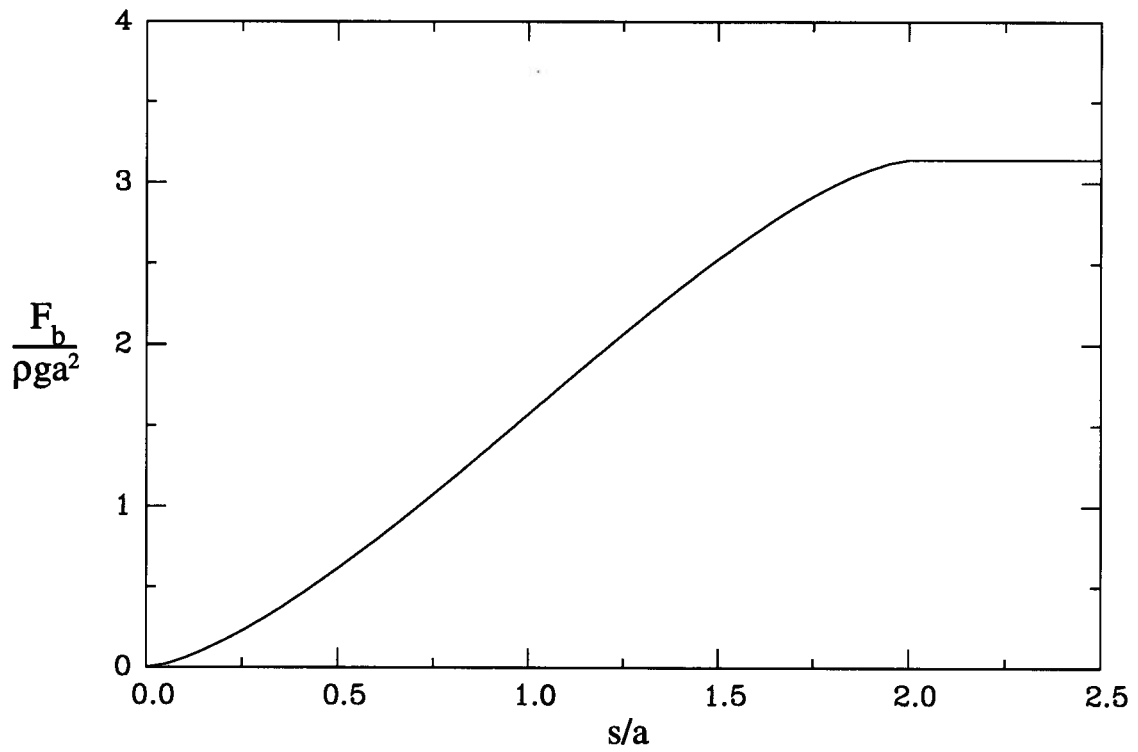


Fig. 2.3 Variation of dimensionless buoyancy force with relative submergence s/a .

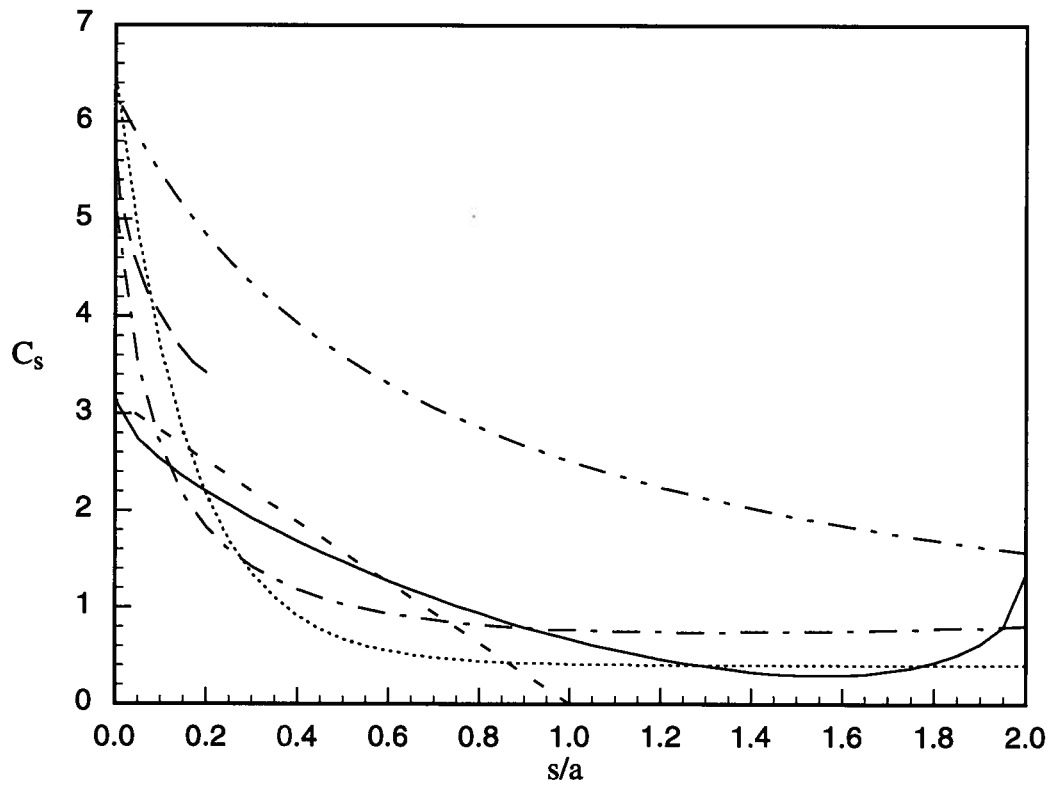


Fig. 2.4 Variation of C_s with submergence s/a - selected results. - - - - -, von Karman; — — — —, Wagner; — — — —, Taylor; — · — · —, Campbell and Weynberg; ·····, Miao; — · — · —, Armand and Cointe.

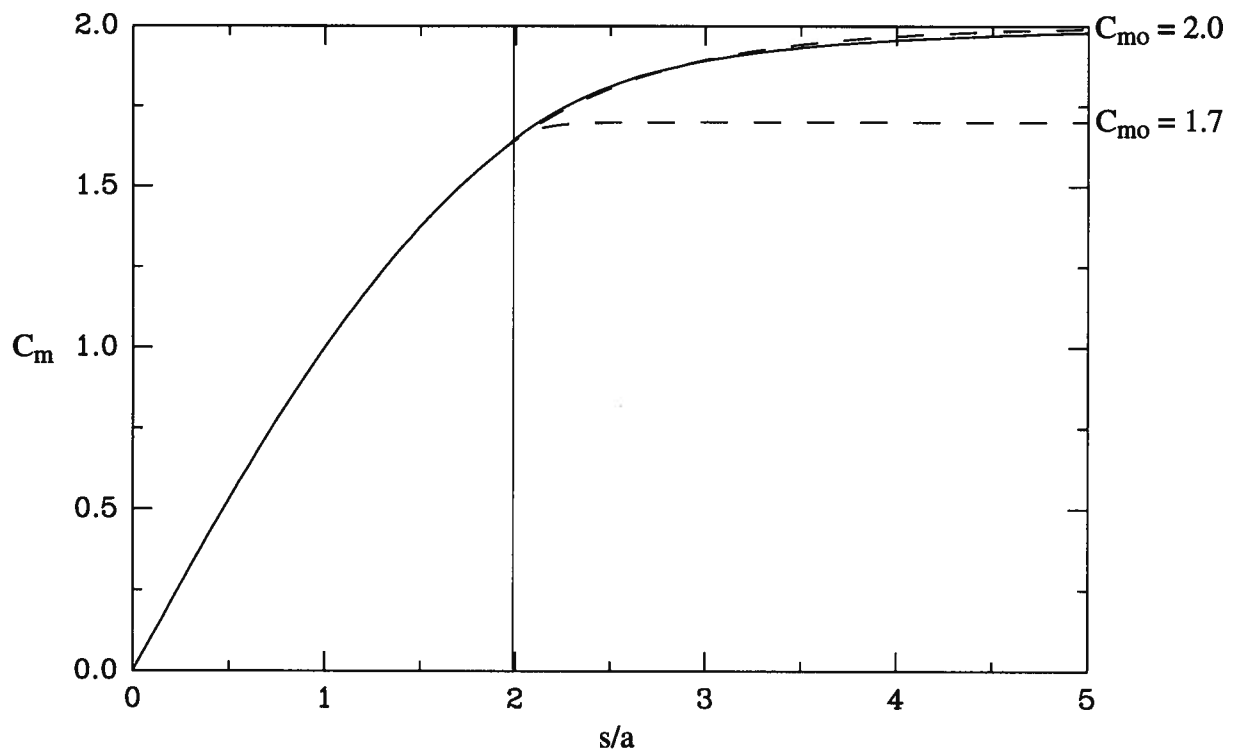


Fig. 2.5 Variation of inertia coefficient C_m with relative submergence s/a . ———, Taylor's solution ($C_{mo} = 2.0$); - - -, approximations for $C_{mo} = 2.0$ and 1.7.

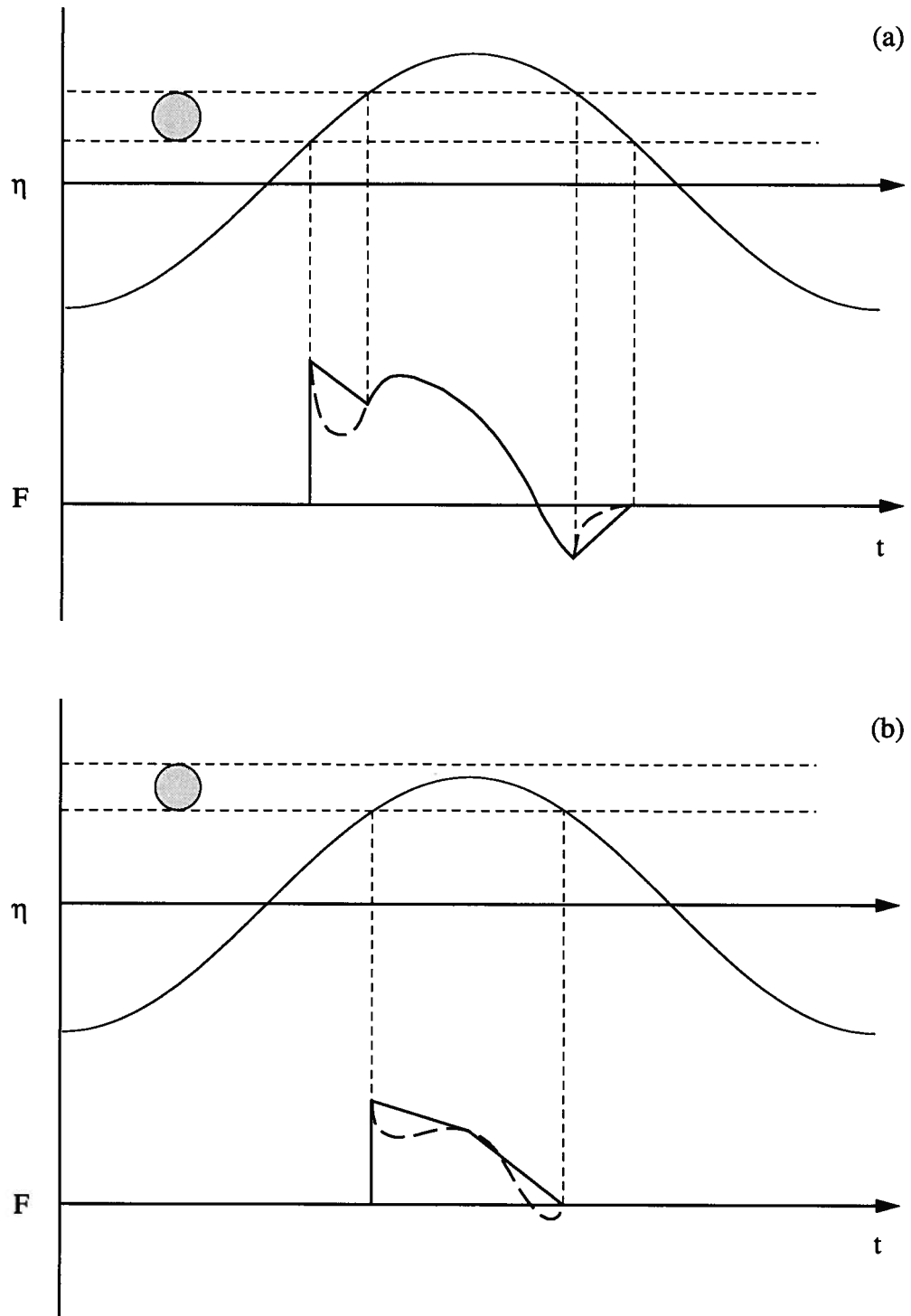


Fig. 2.6 Sketch of free surface elevation and corresponding vertical wave force over one wave cycle. ———, model I; - - -, model II. (a) complete submergence, (b) partial submergence.

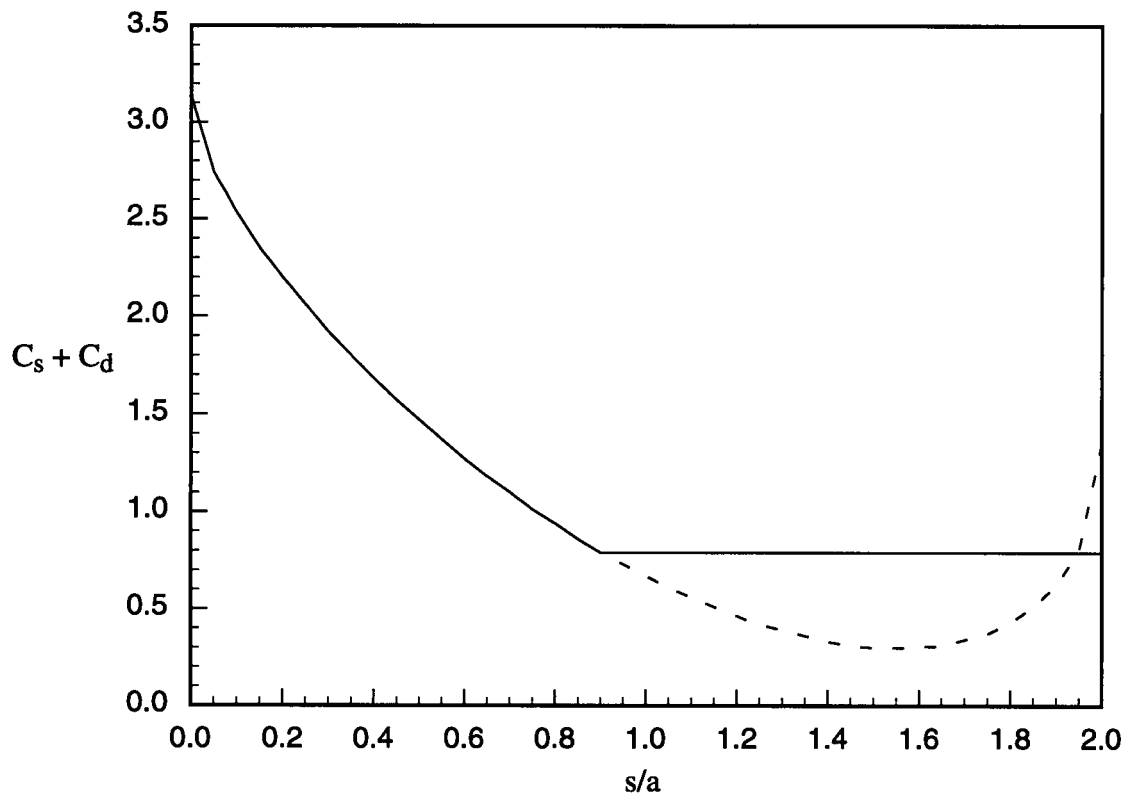


Fig. 2.7 Proposed variation of combined $C_s + C_d$ coefficient with relative submergence s/a for $C_d = 0.8$. ———, $C_s + C_d$; - - - - -, Taylor's solution for C_s .

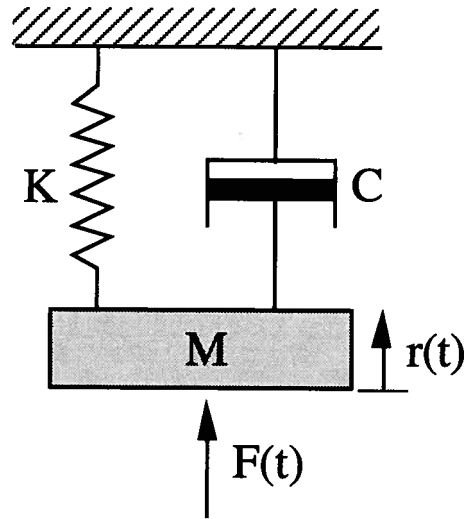


Fig. 2.8 Definition sketch of a single degree of freedom (SDOF) system.

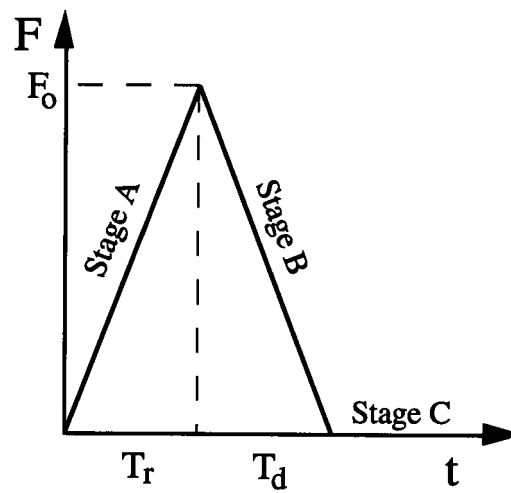


Fig. 2.9 Representation of an idealized impact force with $T_d/T_r = 1$.

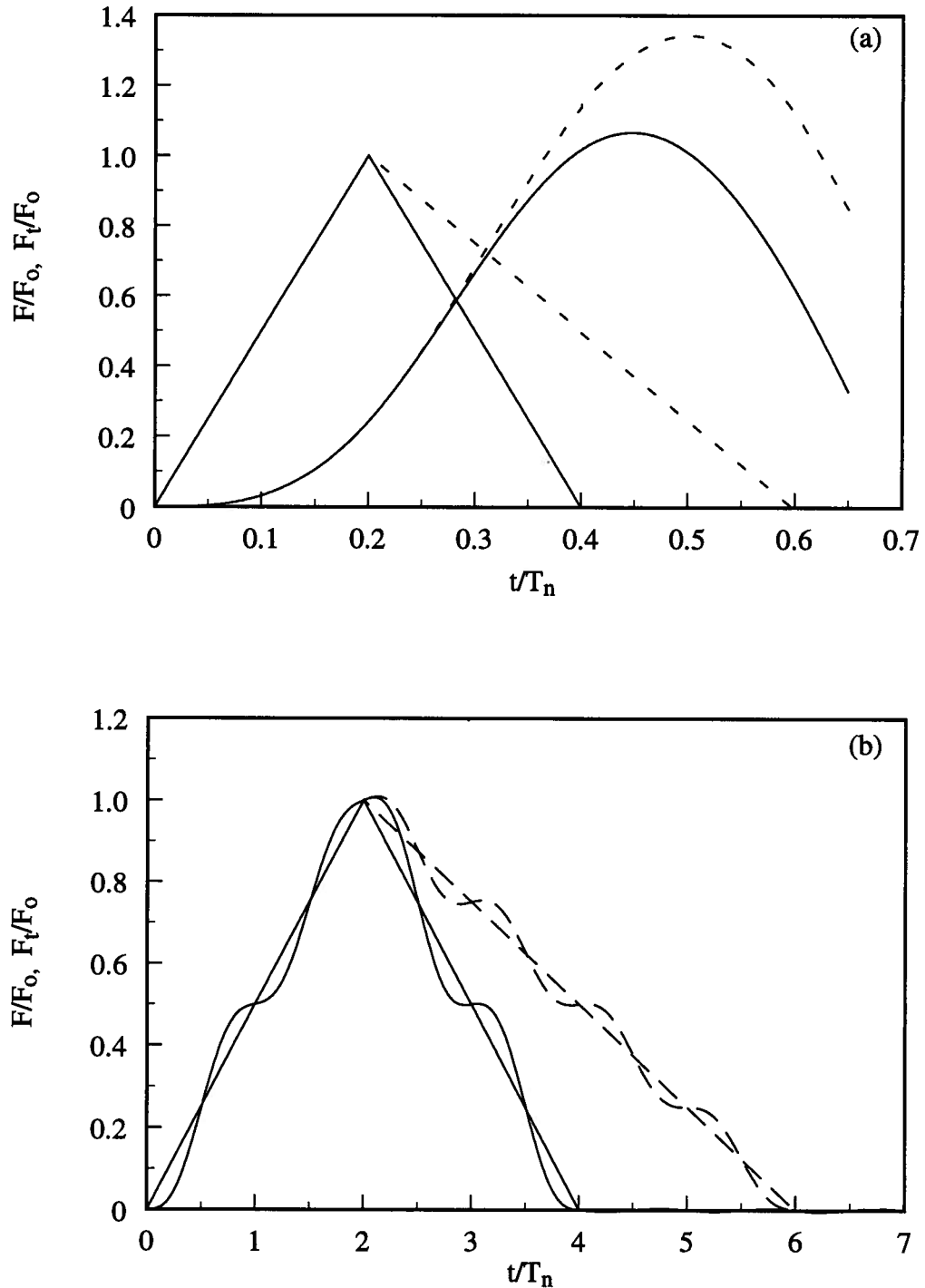


Fig. 2.10 Response F_t/F_0 of SDOF system to an applied impulsive force with different values of T_r/T_n . ———, applied force and response for impact with $T_d/T_r = 1.0$; - - - - -, applied force and response for impact with $T_d/T_r = 2.0$. (a) $T_r/T_n = 0.2$, (b) $T_r/T_n = 2.0$.

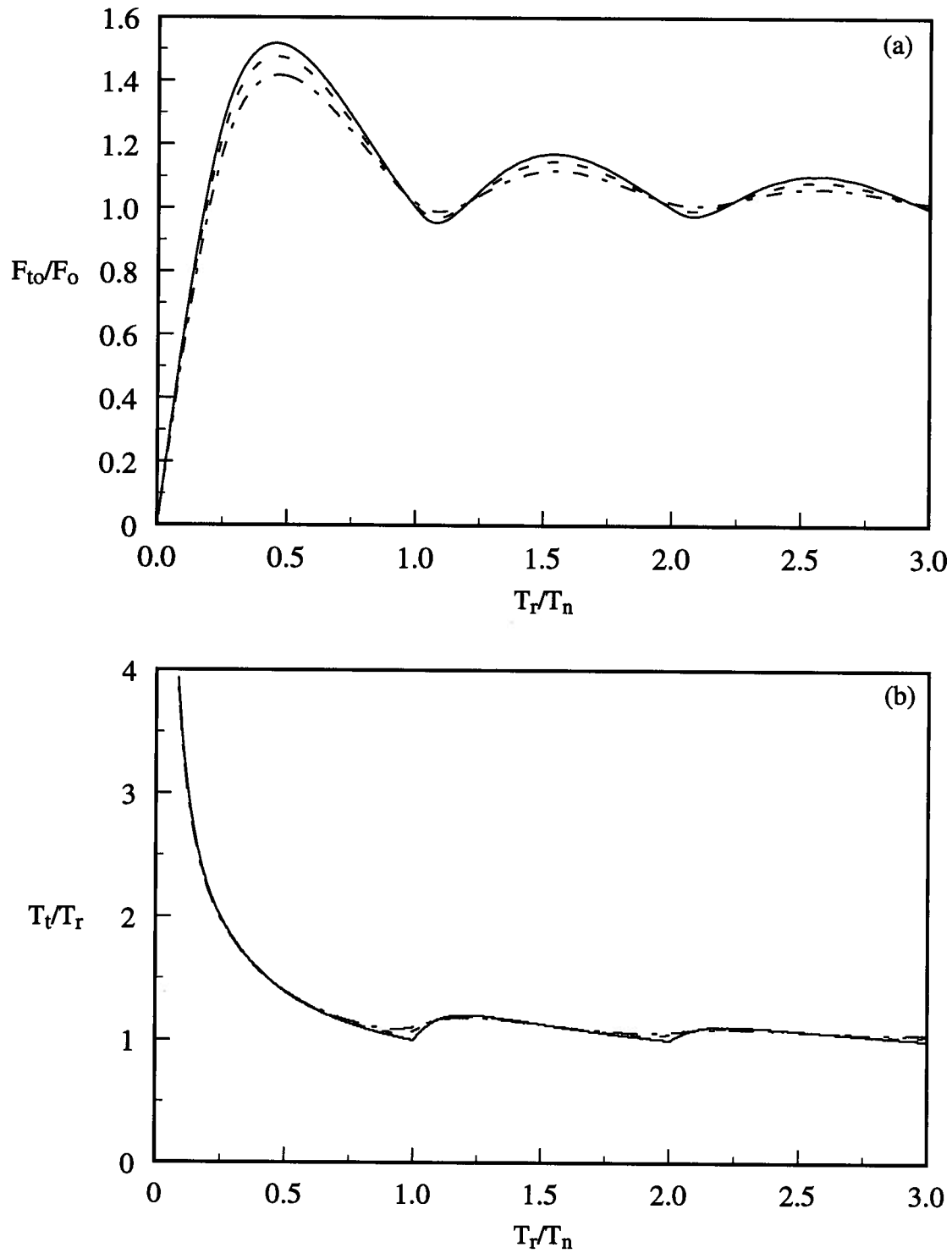


Fig. 2.11 (a) Dynamic amplification factor F_{t0}/F_0 and, (b) relative rise time T_t/T_r as functions of T_r/T_n for an applied impulsive force with $T_d/T_r = 1.0$. —, $\zeta = 0$; ---, $\zeta = 0.02$; - · - ·, $\zeta = 0.05$.

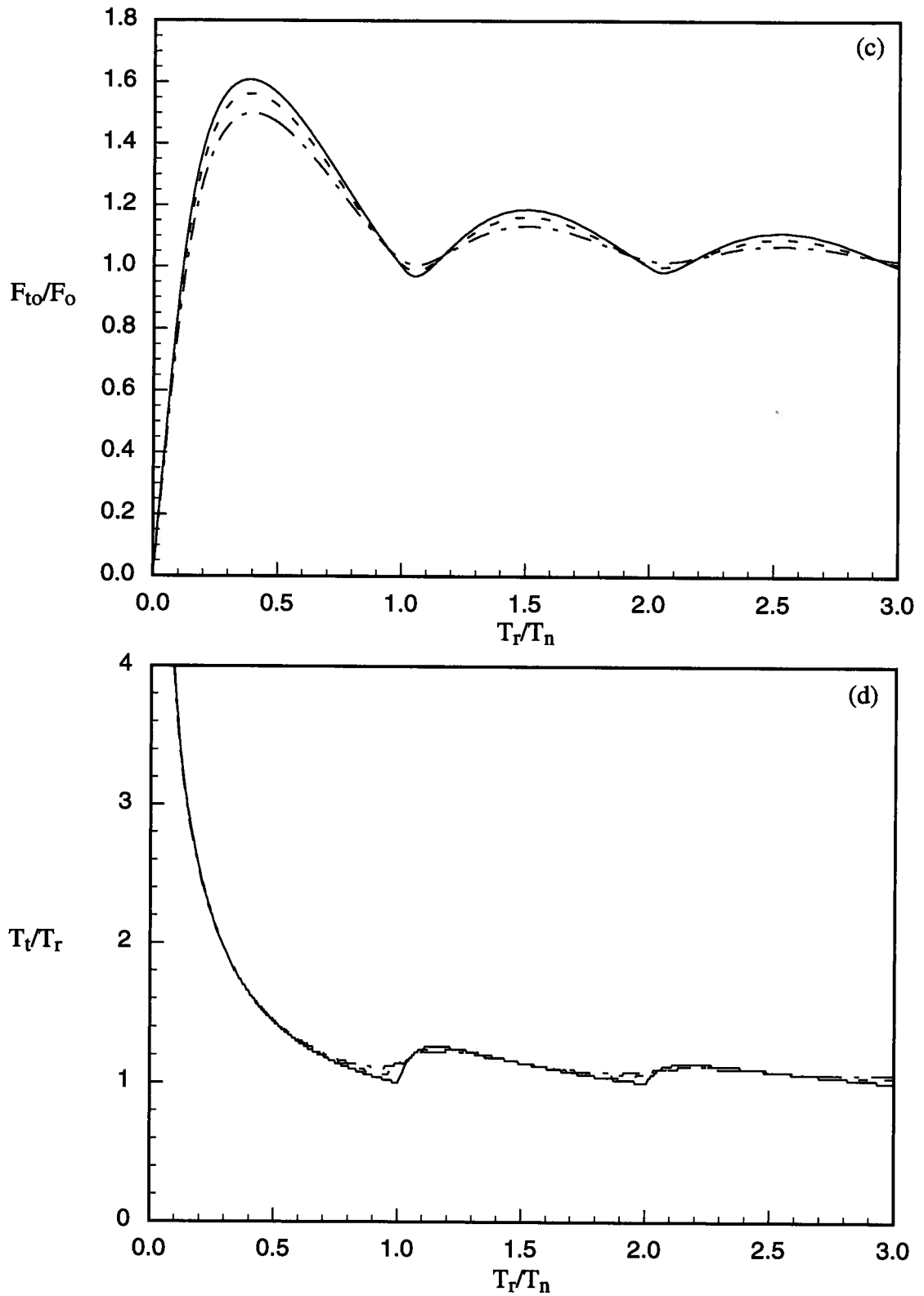


Fig. 2.11 (c) Dynamic amplification factor F_{t0}/F_0 and, (d) relative rise time T_t/T_r as functions of T_r/T_n for an applied impulsive force with $T_d/T_r = 2.0$. —, $\zeta = 0$; ---, $\zeta = 0.02$; - · - ·, $\zeta = 0.05$.

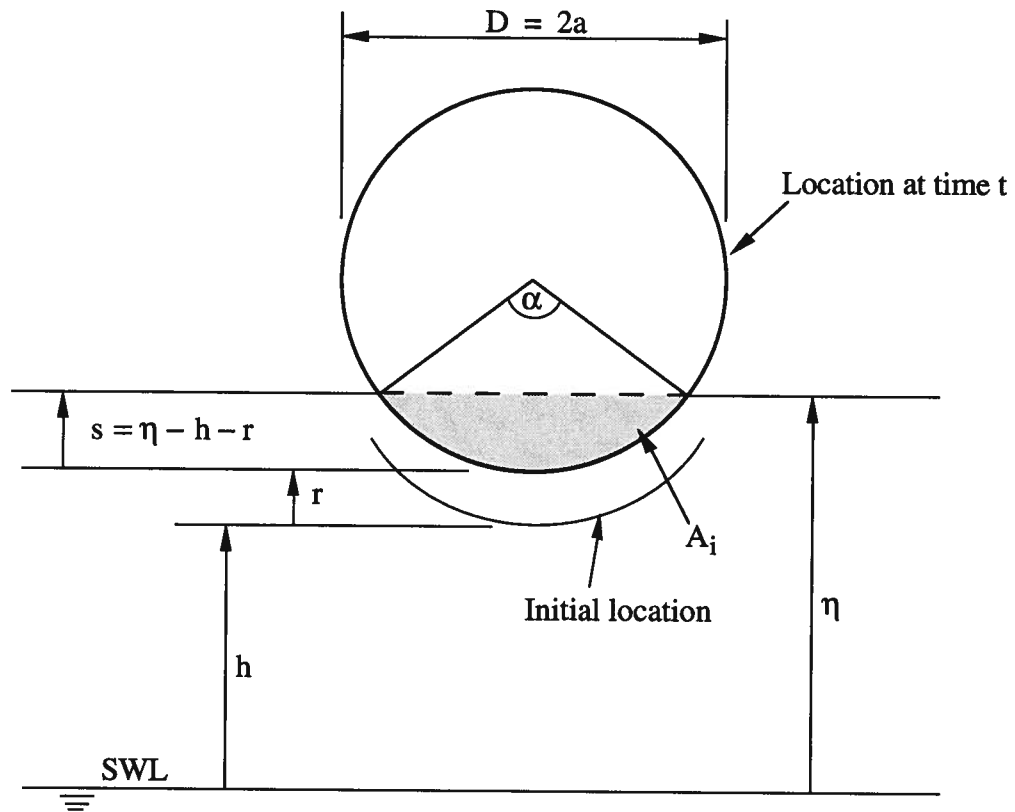


Fig. 2.12 Definition sketch for dynamically responding cylinder.

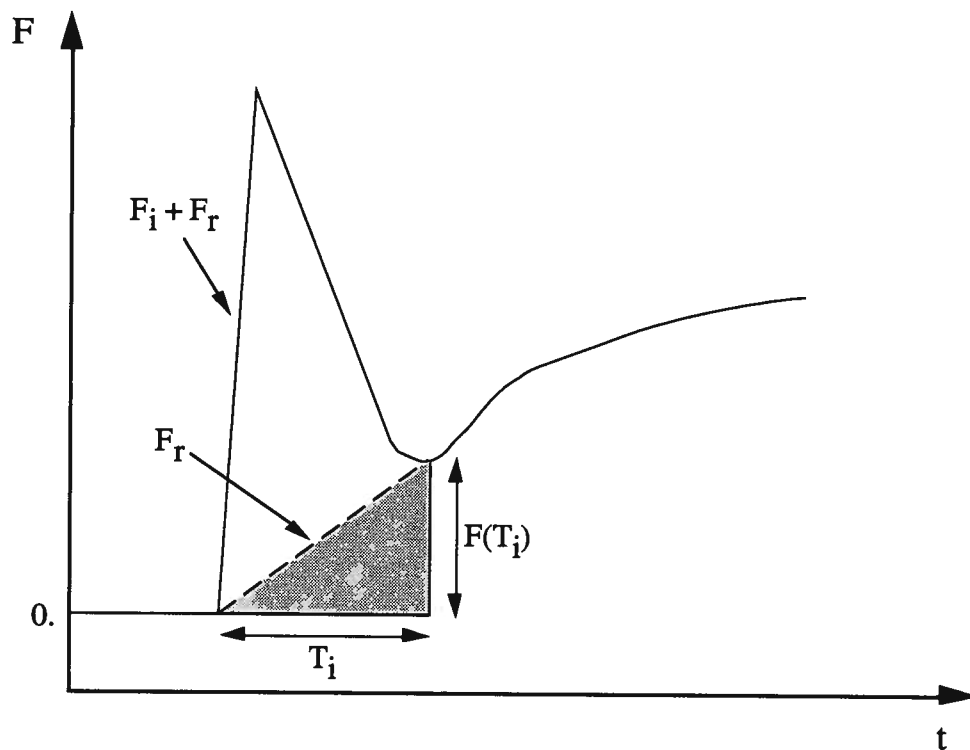


Fig. 2.13 Definition sketch for the computation of the impulse coefficient. ———, combined impulsive and residual force; - - - - -, residual force.

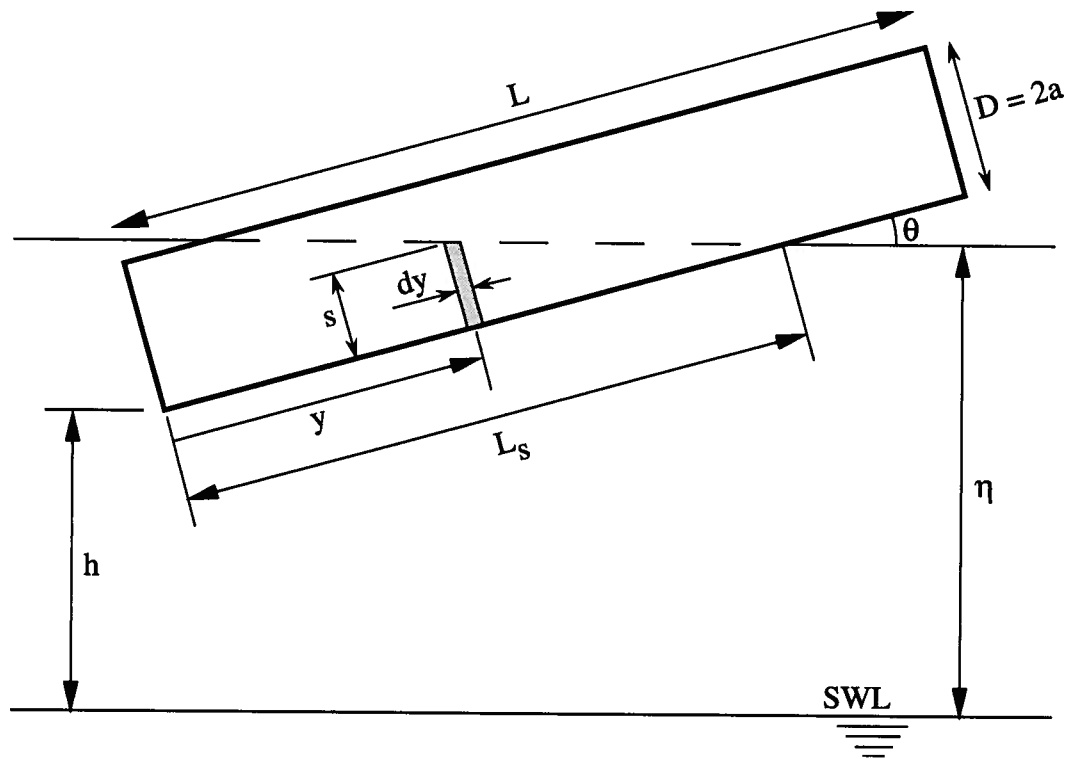


Fig. 2.14 Definition sketch for wave impact on an inclined circular cylinder.

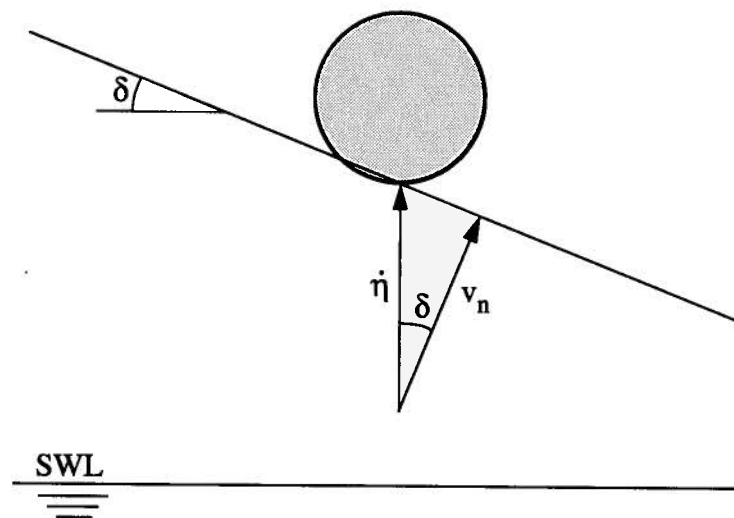


Fig. 2.15 Definition sketch for impact due to a sloping water surface.

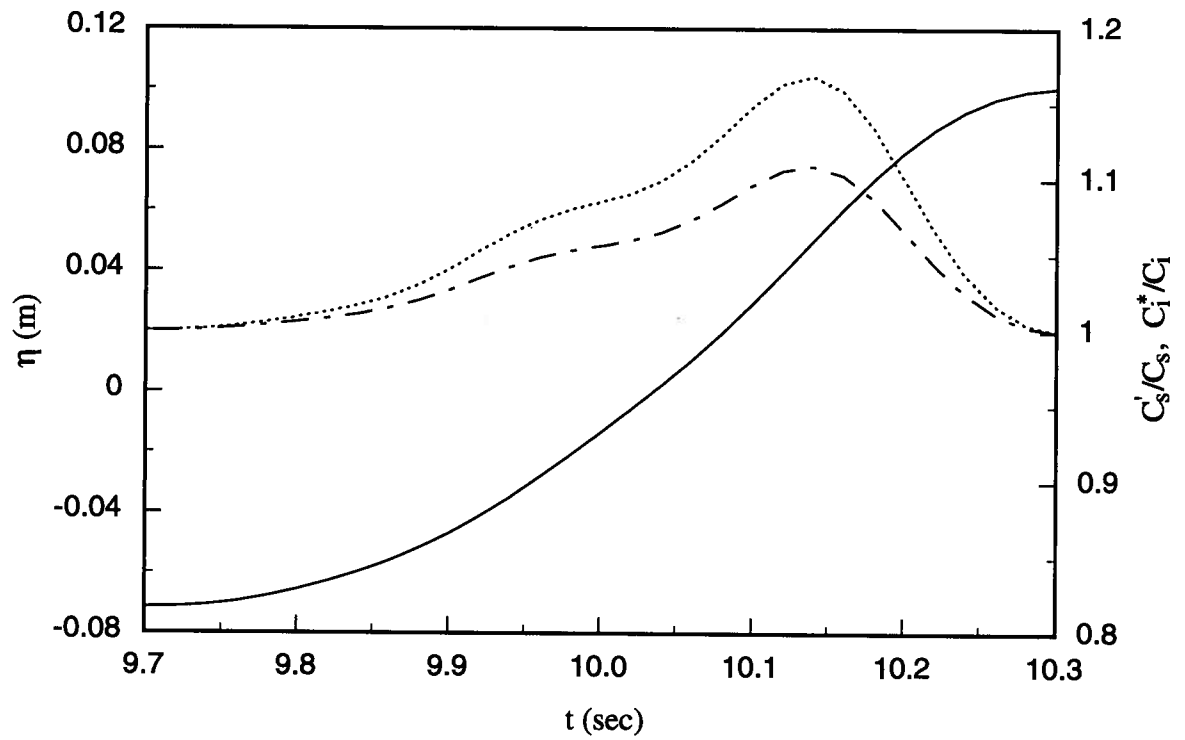


Fig. 2.16 Variation of the free surface slope correction factors C'_s/C_s (.....) and C_i^*/C_i (---) for an experimentally measured wave (—) of period $T = 1.1$ sec, and height $H = 17$ cm.



Fig. 3.1 Photograph of wave flume in the Hydraulics Laboratory.

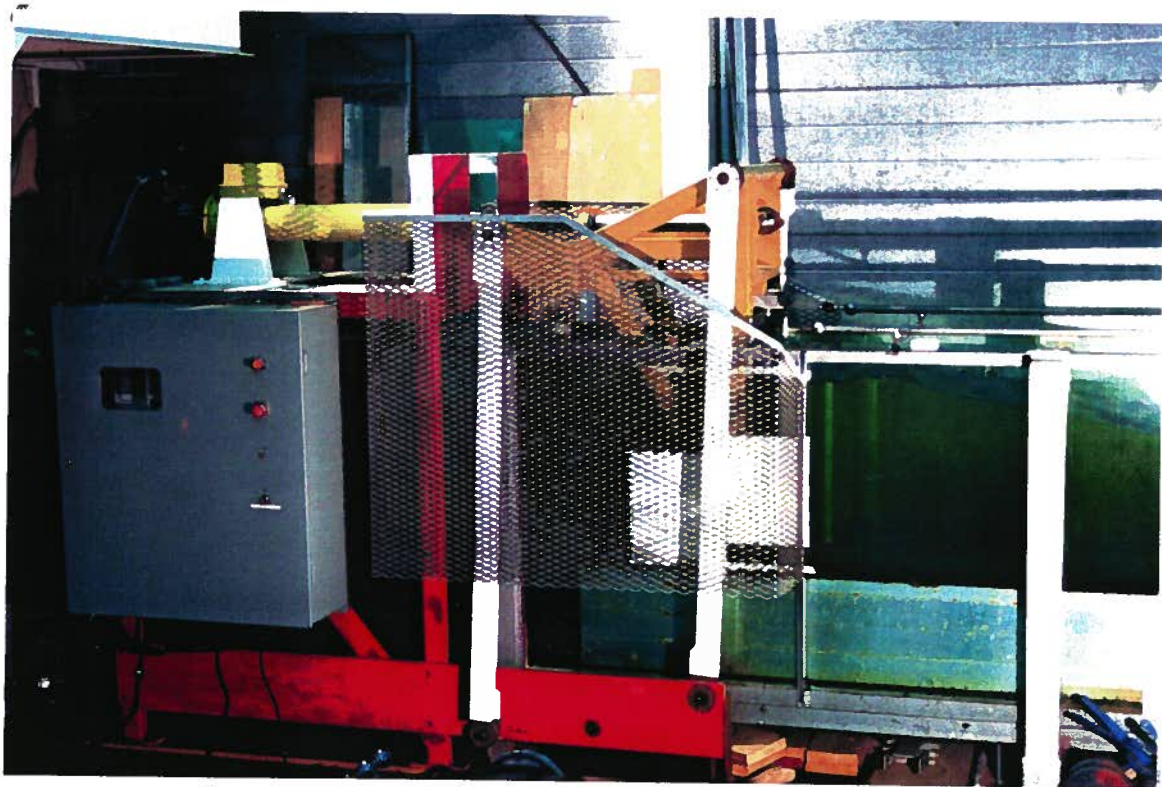


Fig. 3.2 Photograph of computer-controlled wave generator.

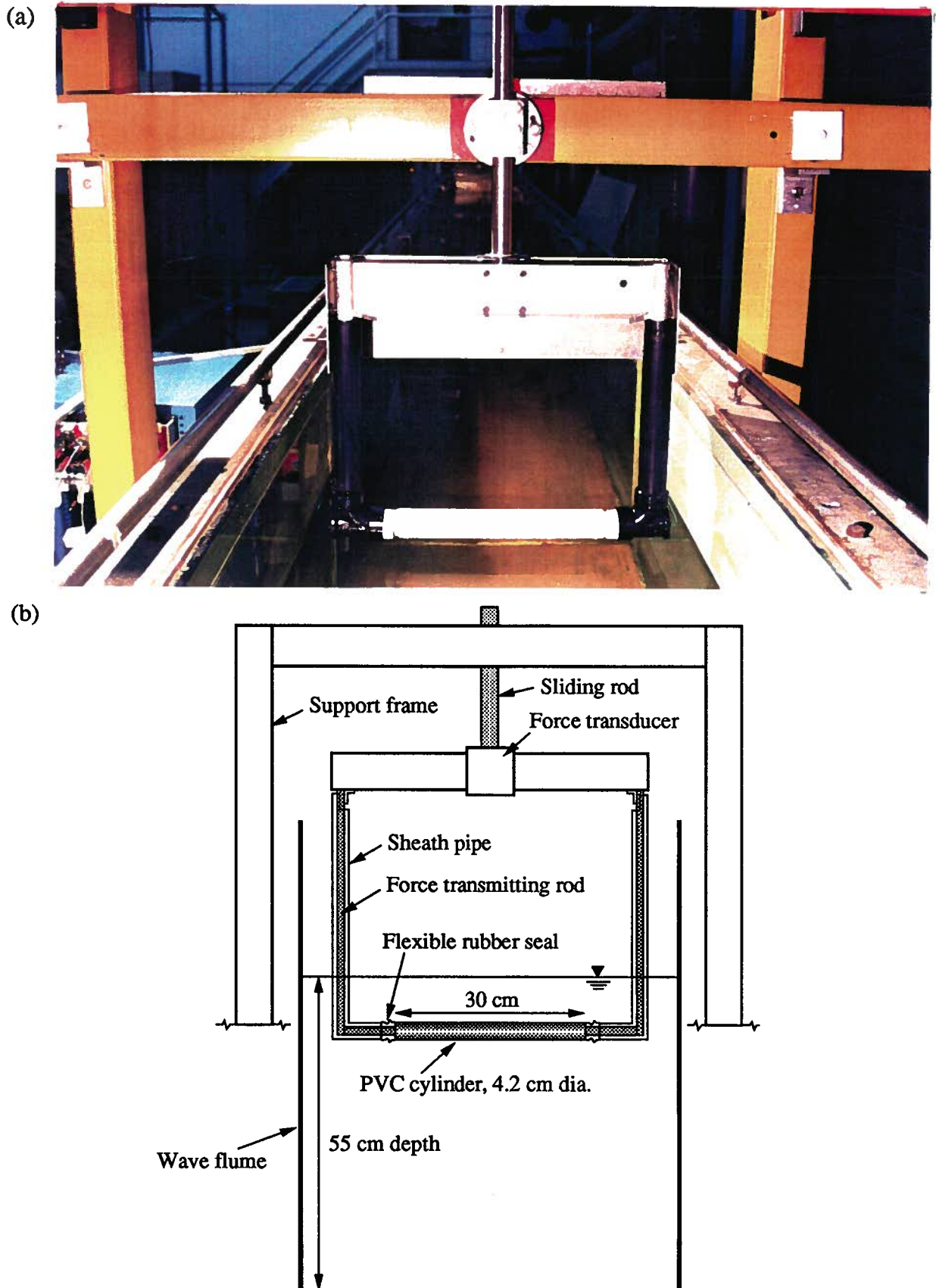


Fig. 3.3 (a) Photograph of test cylinder assembly, (b) Sketch of the experimental setup.

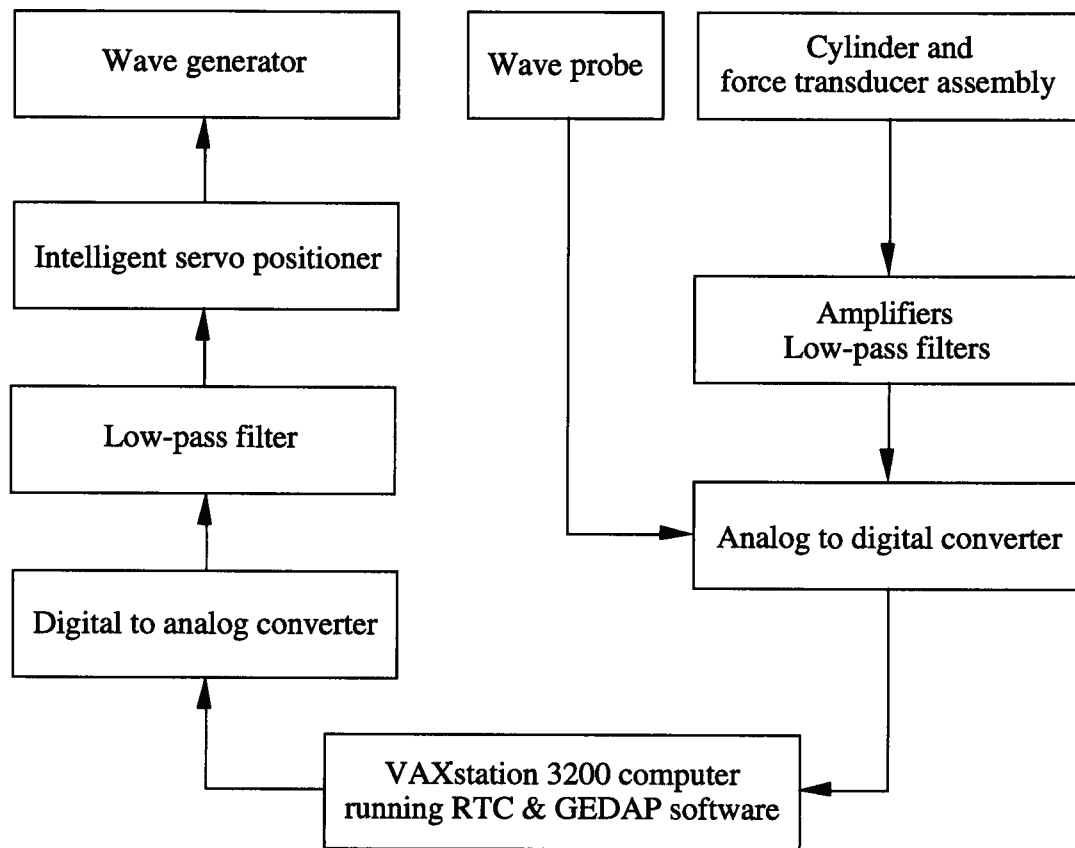


Fig. 3.4 Block diagram of wave generation and data acquisition equipment.

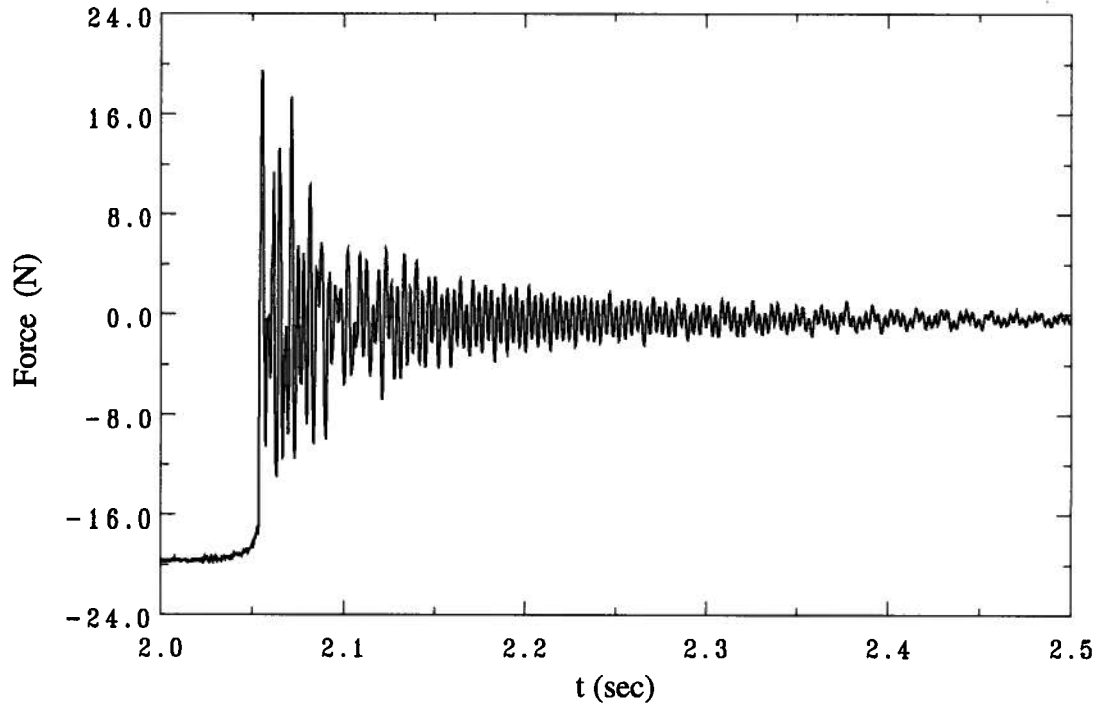


Fig. 3.5 Record of the vertical force due to free vibration of the cylinder induced by an applied step force of -19.6 N (2 kg).

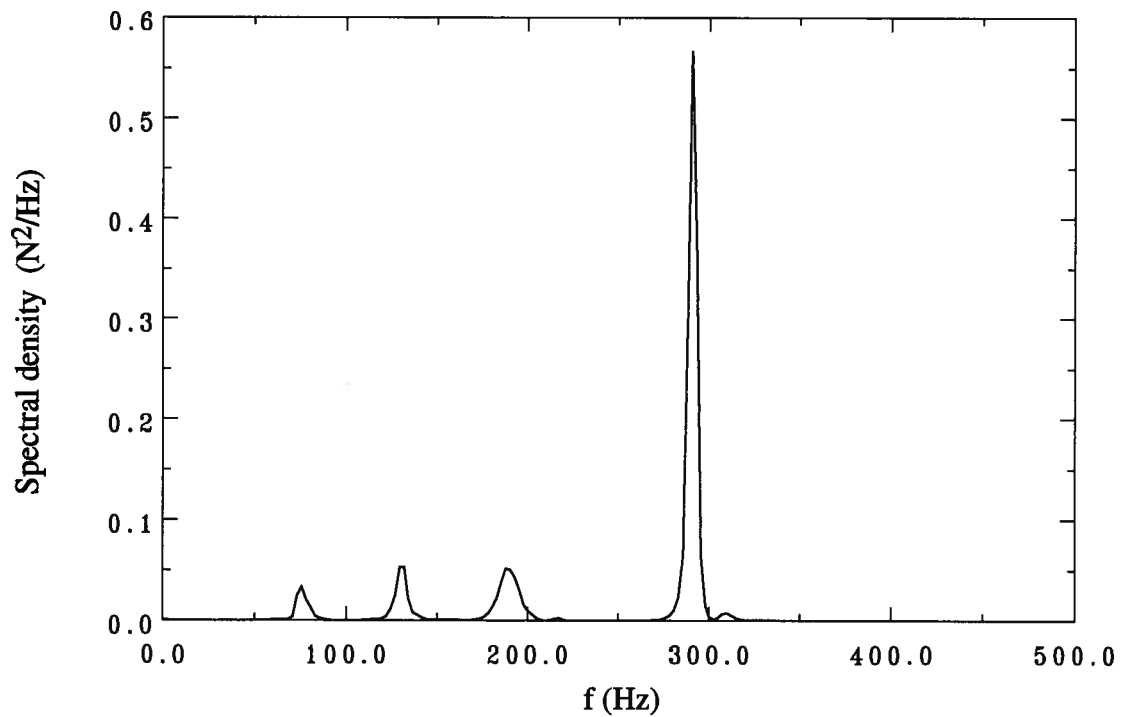


Fig. 3.6 Spectral density of free vibration record in Fig. 3.5.

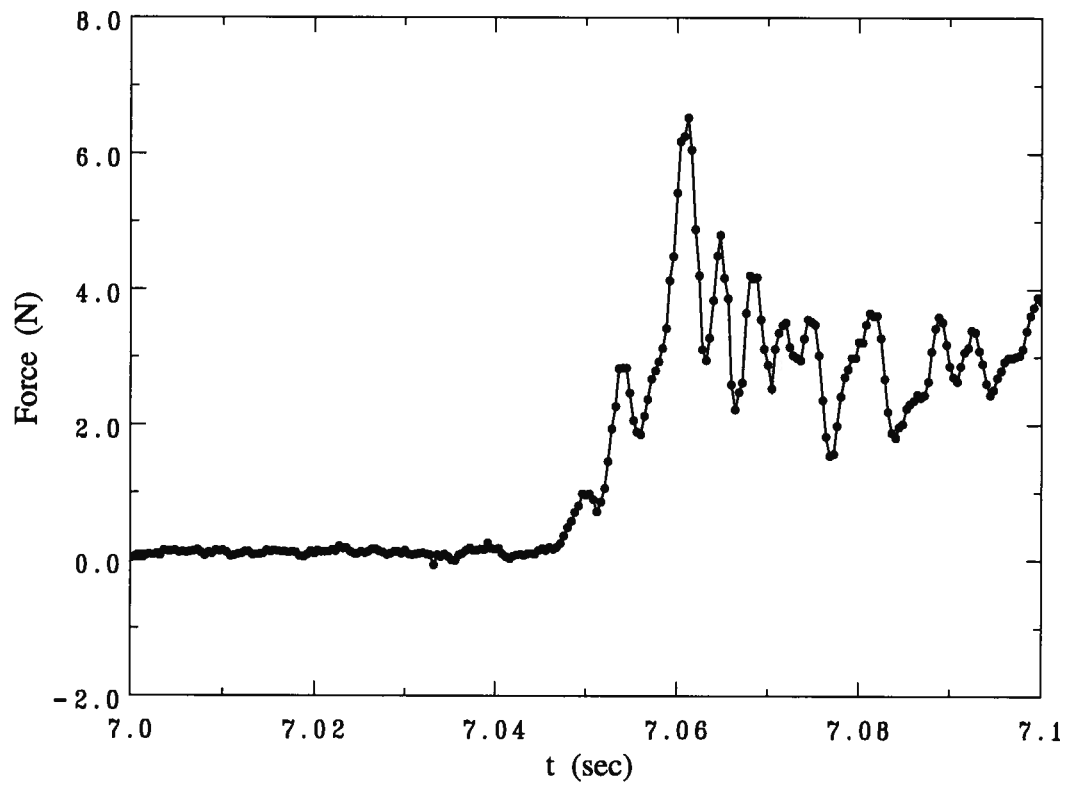


Fig. 3.7 Early stages of the measured vertical force on the test cylinder due to a typical wave slamming event. •, indicates individual force samples.

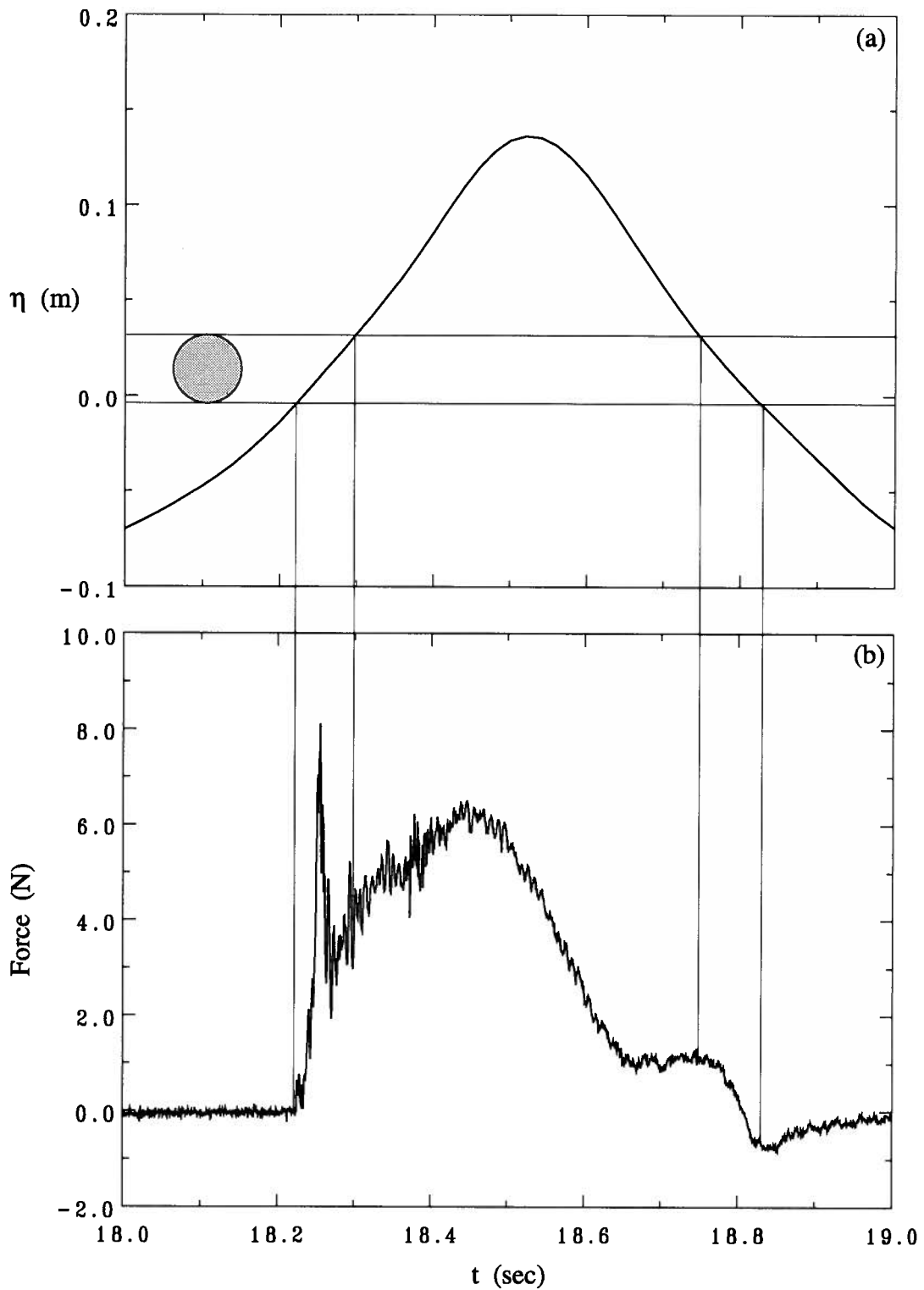


Fig. 3.8 Time histories of free surface elevation and vertical force during a slamming event. $T = 1.4$ sec, $H = 22.8$ cm, $h = 0.5$ cm.

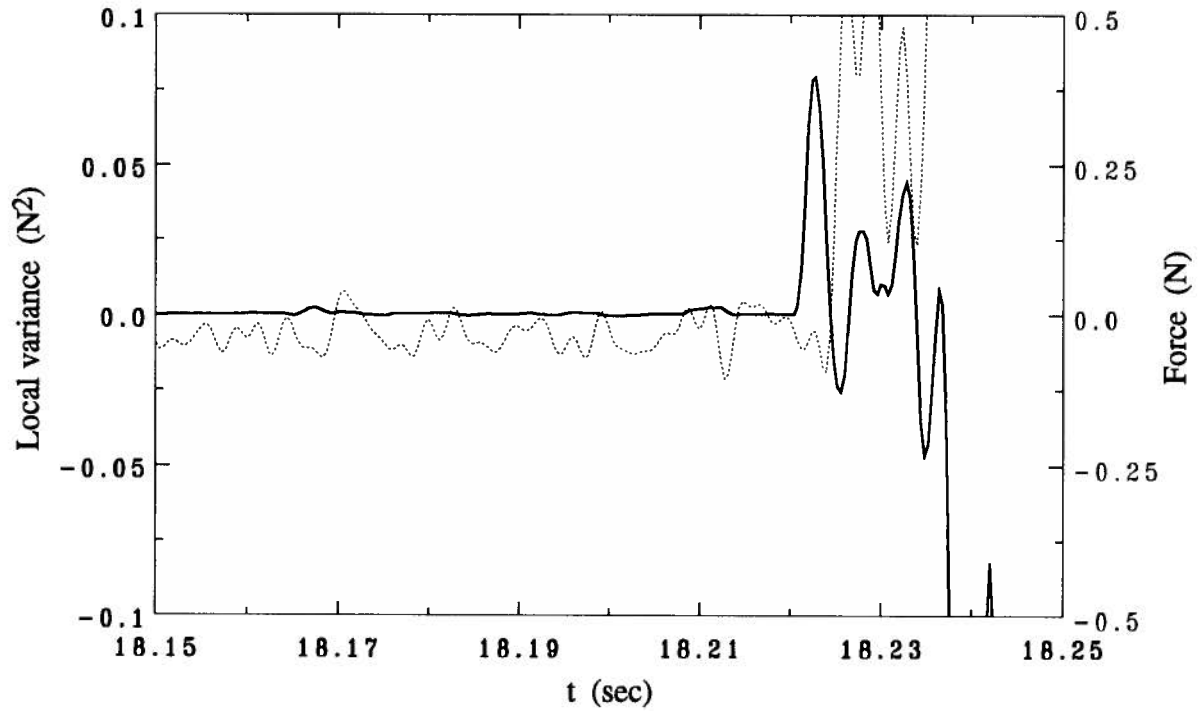


Fig. 3.9 Time series of vertical force (.....) and corresponding local variance (————) used to detect the onset of slamming.

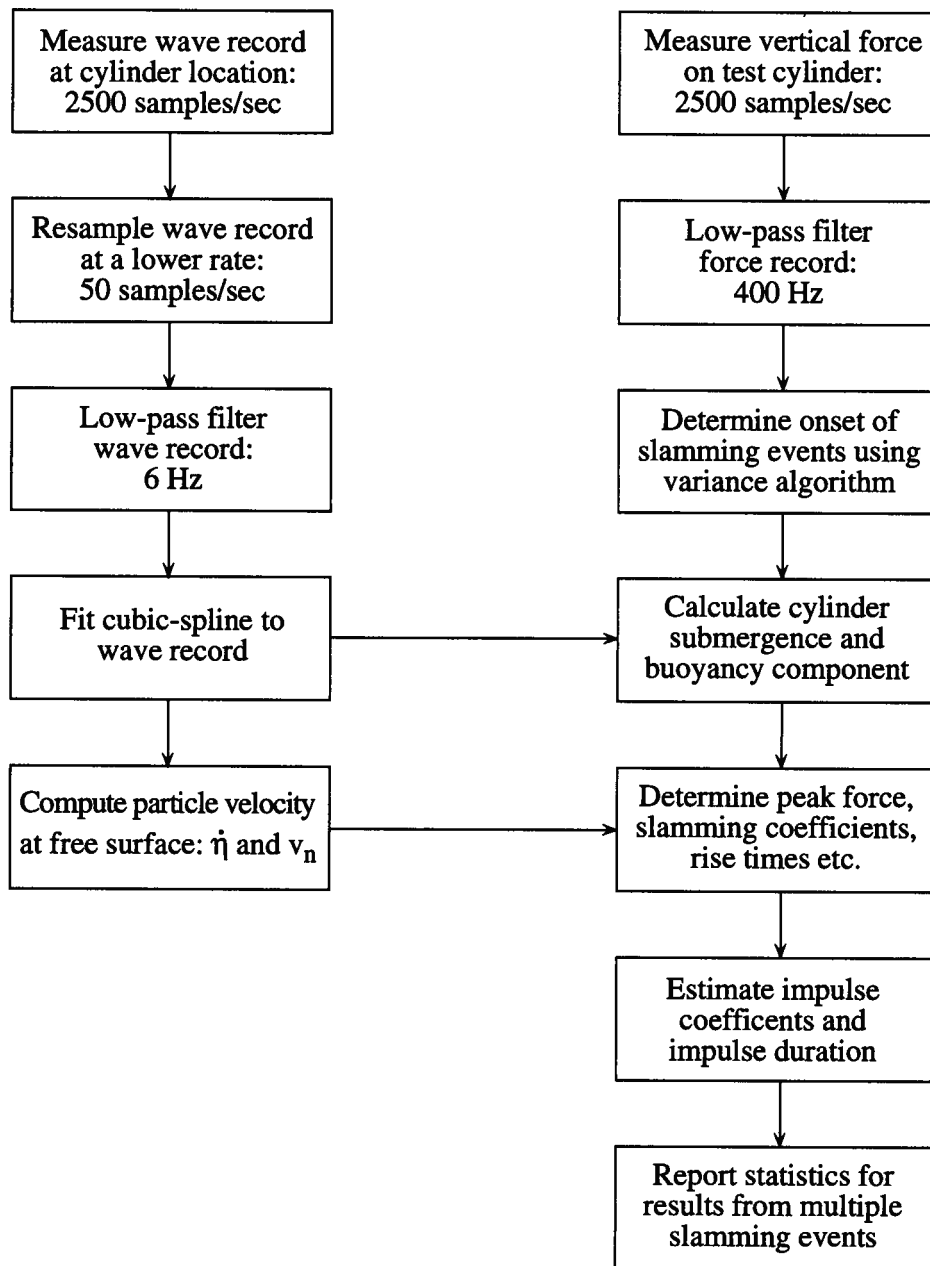


Fig. 3.10 Flow chart showing steps in analysis of experimental data.

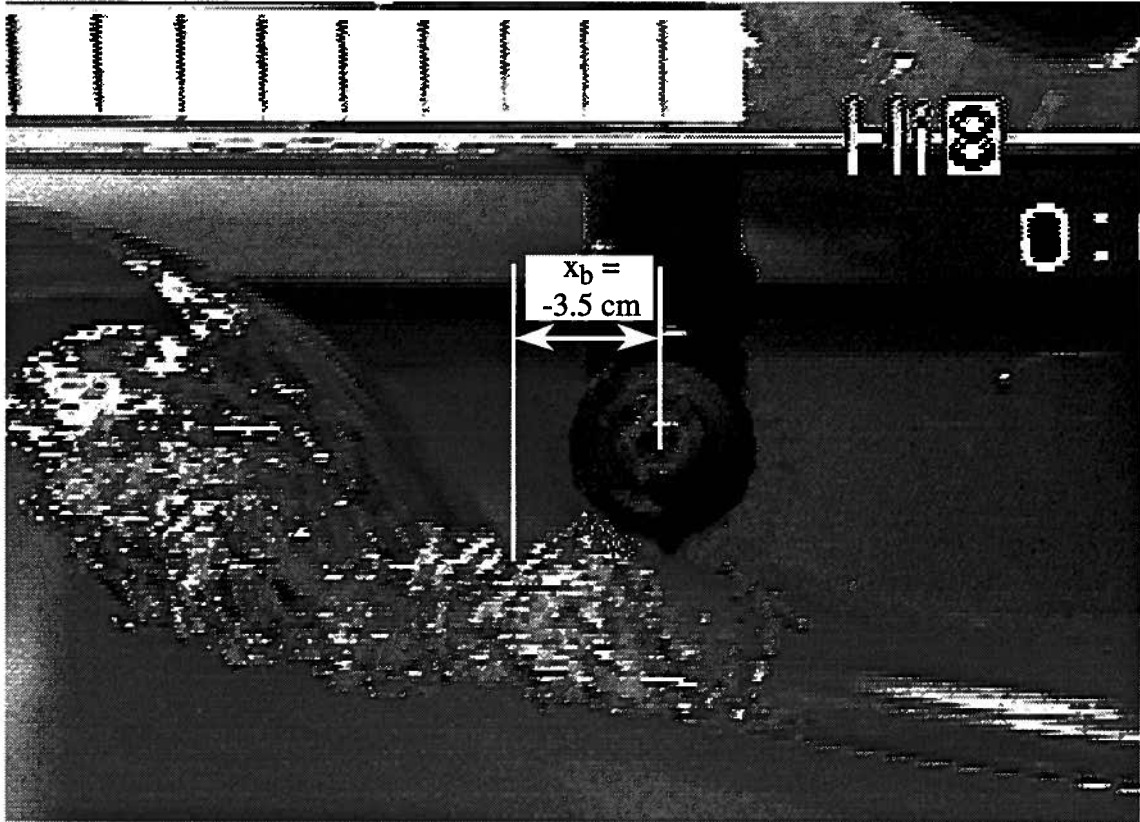


Fig. 3.11 Frame of video record defining the wave breaking location x_b .

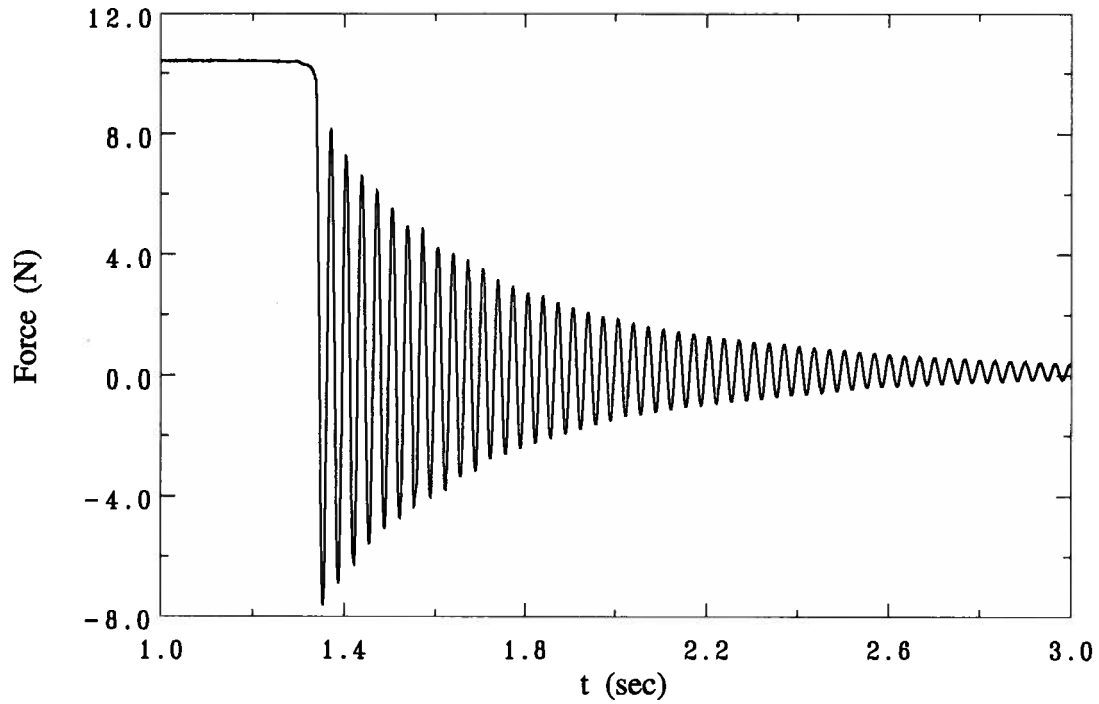


Fig. 3.12 Record of the horizontal force due to free vibration of the cylinder induced by an applied step force of 9.8 N (1 kg).

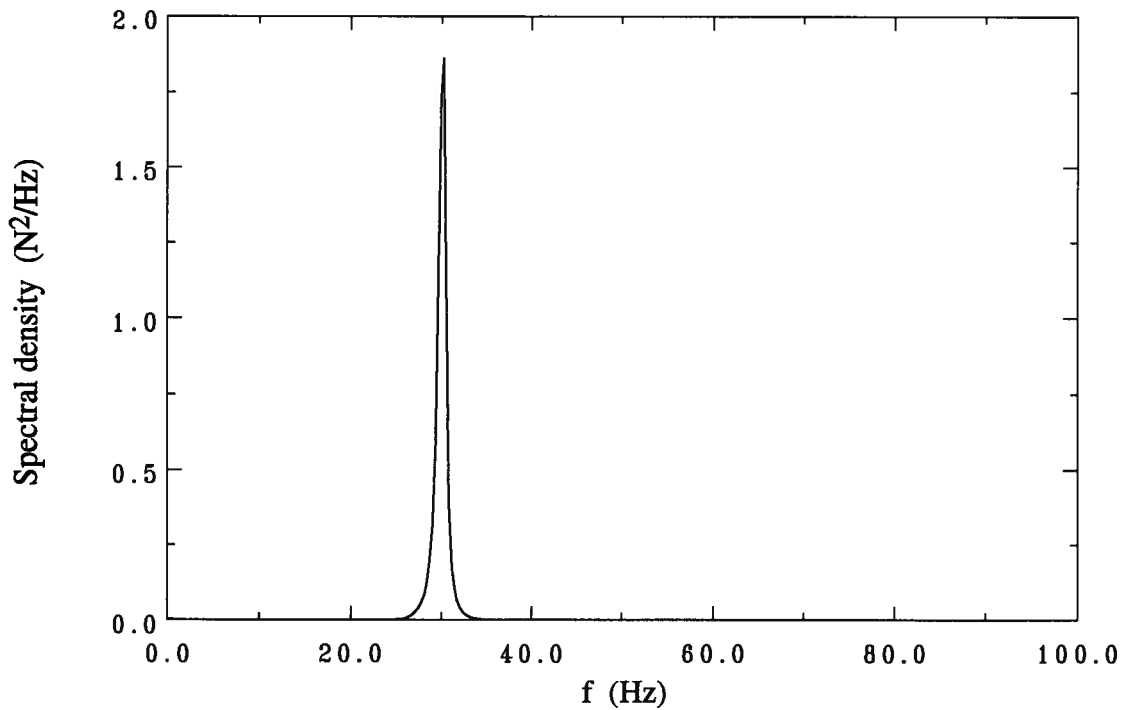


Fig. 3.13 Spectral density of free vibration record in Fig. 3.12.

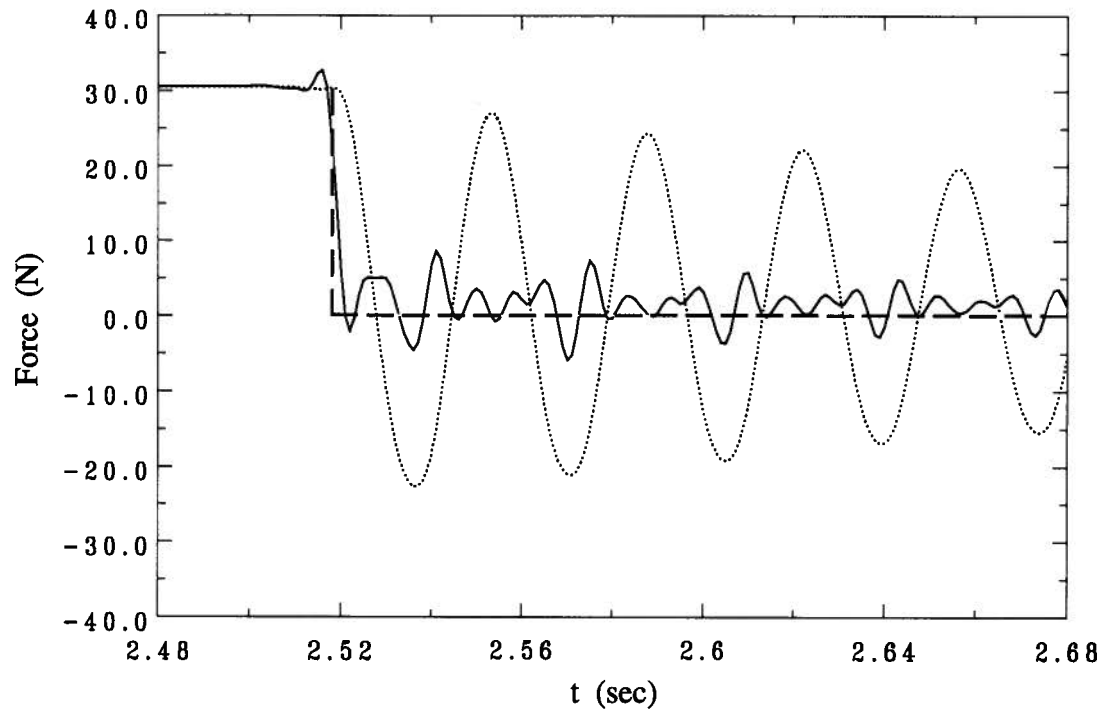


Fig. 3.14 Comparison of corrected horizontal force (————), with recorded horizontal force (······), and applied step force (-----).

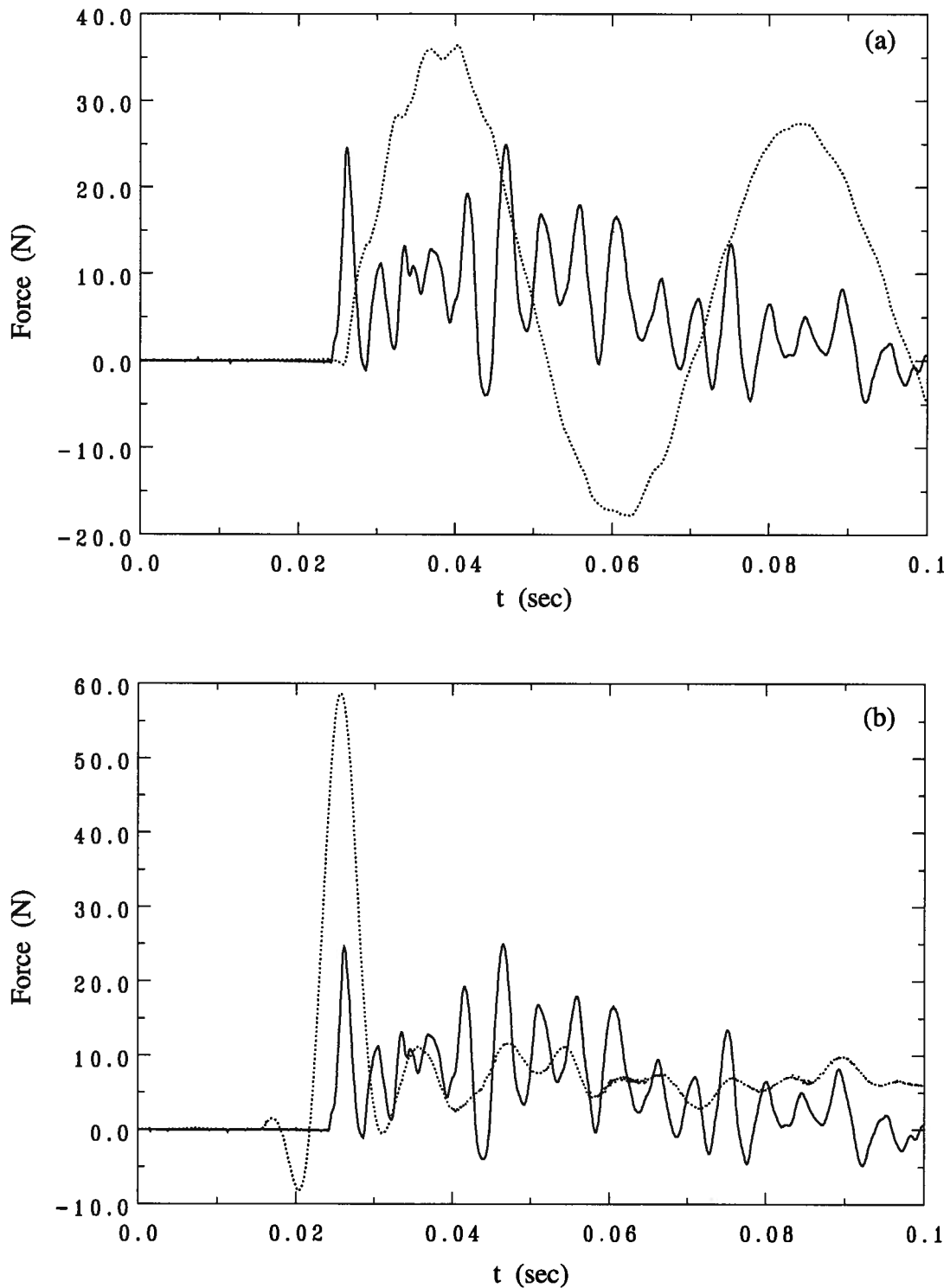


Fig. 3.15 Impact force on the horizontal test cylinder due to plunging wave ($h = 8.7$ cm, $x_b = 36$ cm). (a) ———, recorded vertical force component; ·······, recorded horizontal force component. (b) ———, recorded vertical force component; ·······, corrected horizontal force component.

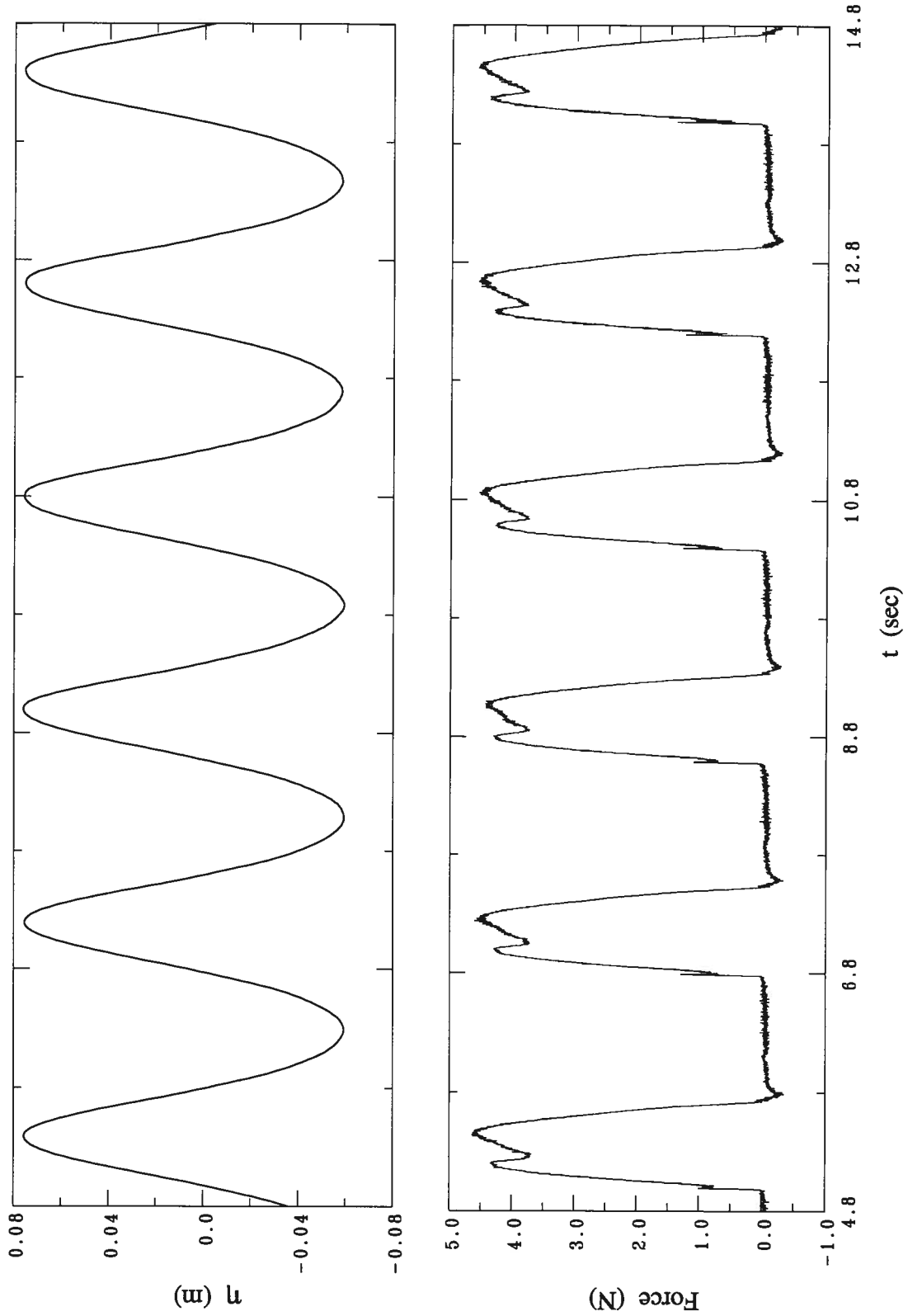


Fig. 4.1 Time histories of the free surface elevation and vertical force over a 10 sec duration for a wave of low steepness. $T = 1.8$ sec, $H = 13.5$ cm, $h = 0.5$ cm.

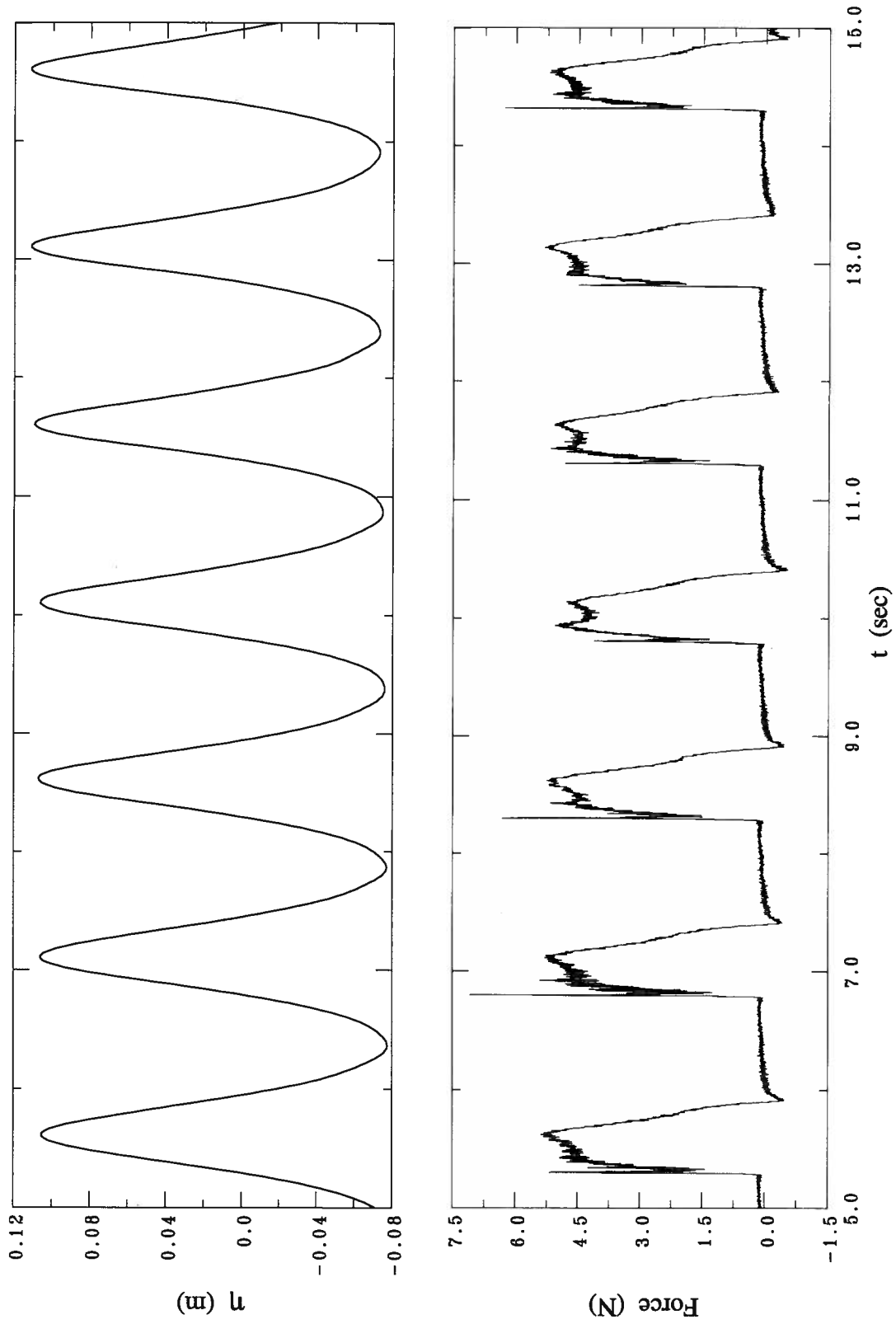


Fig. 4.2 Time histories of the free surface elevation and vertical force over a 10 sec duration for a wave of medium steepness. $T = 1.5$ sec, $H = 18.4$ cm, $h = 0.5$ cm.

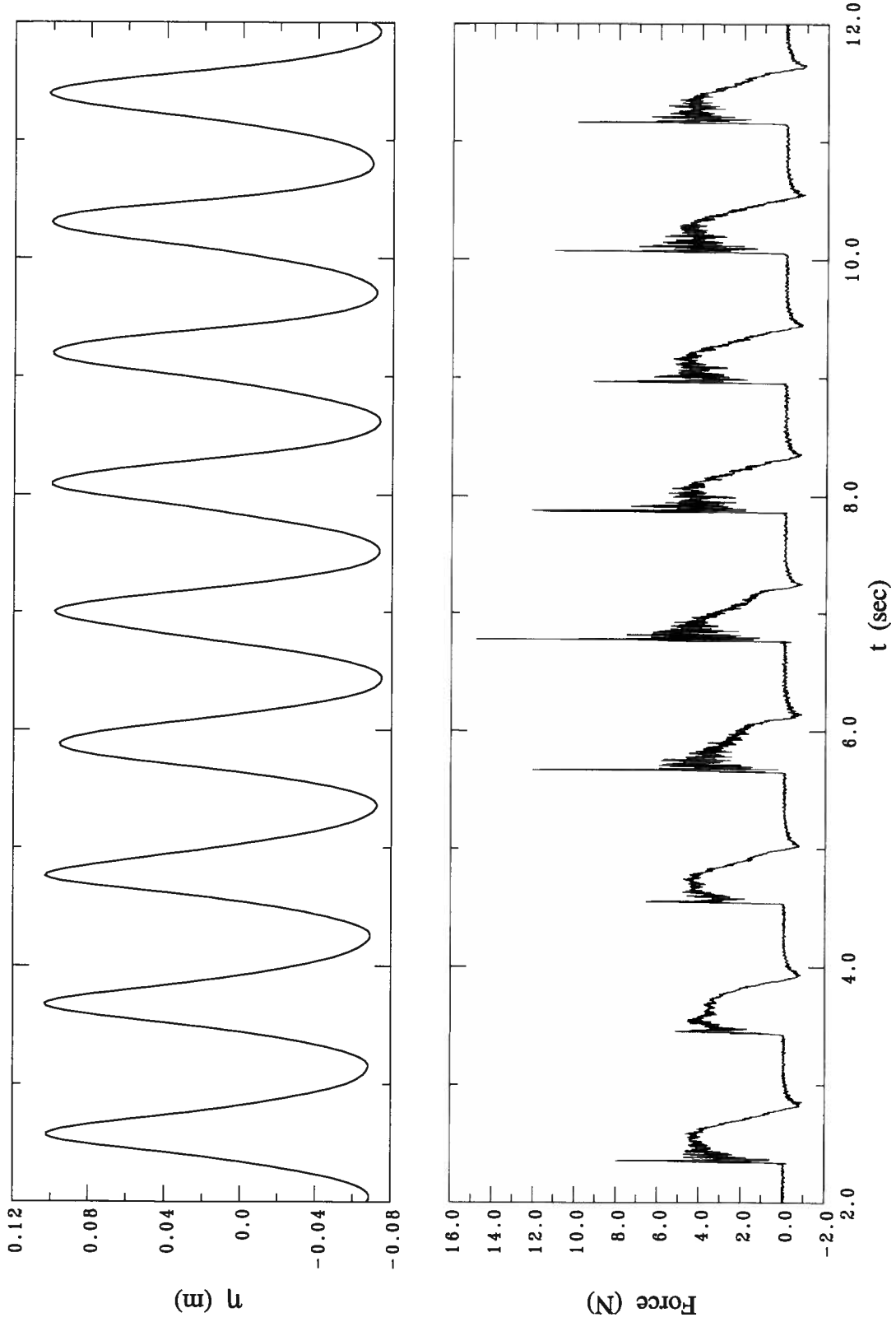


Fig. 4.3 Time histories of the free surface elevation and vertical force over a 10 sec duration for a wave of large steepness. $T = 1.1$ sec, $H = 17$ cm, $h = 0.5$ cm.

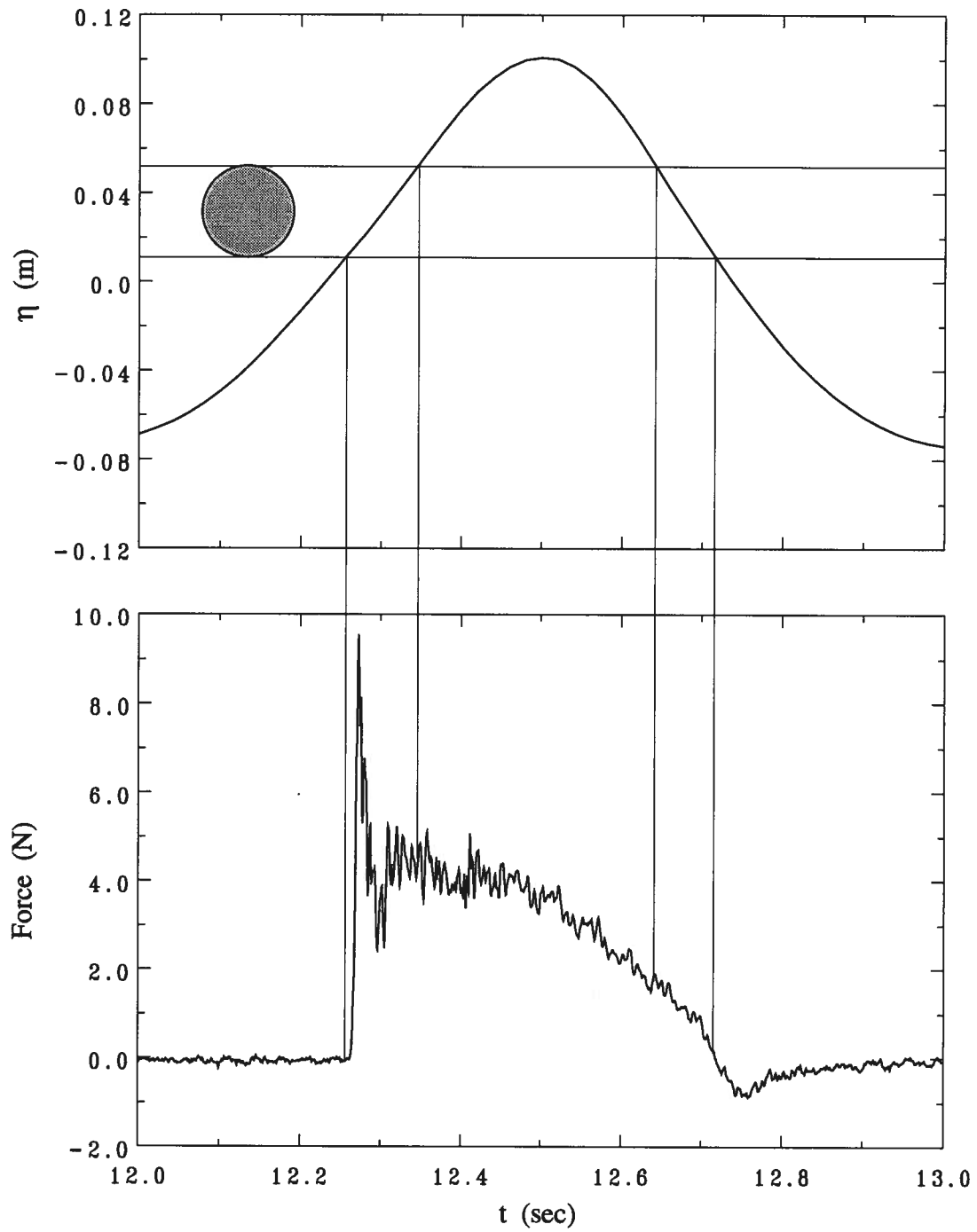


Fig. 4.4 Time histories of free surface elevation and vertical force during a slamming event. $T = 1.1$ sec, $H = 17.5$ cm, $h = 0.5$ cm.

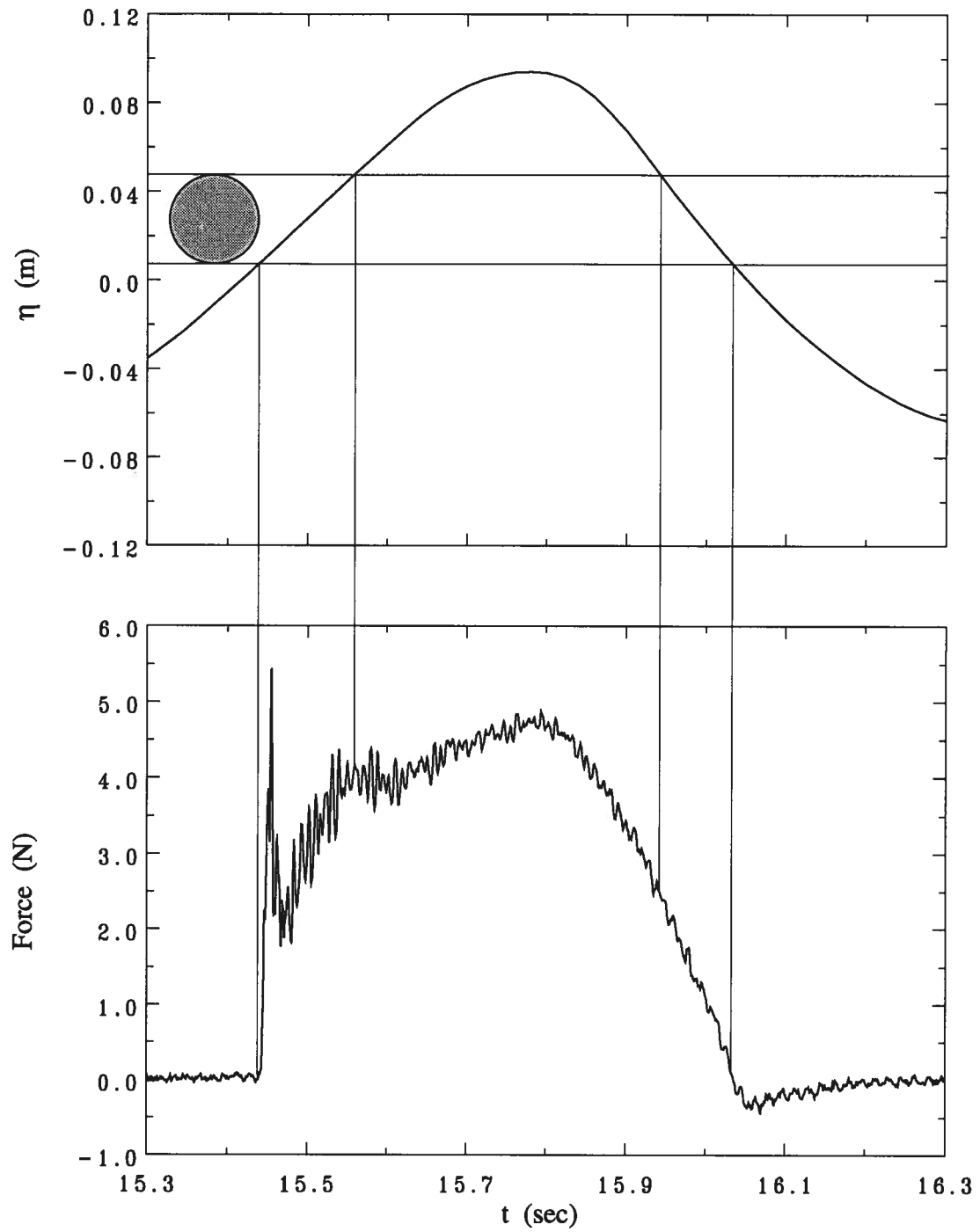


Fig. 4.5 Time histories of free surface elevation and vertical force during a slamming event. $T = 1.4$ sec, $H = 16.5$ cm, $h = 0.5$ cm.

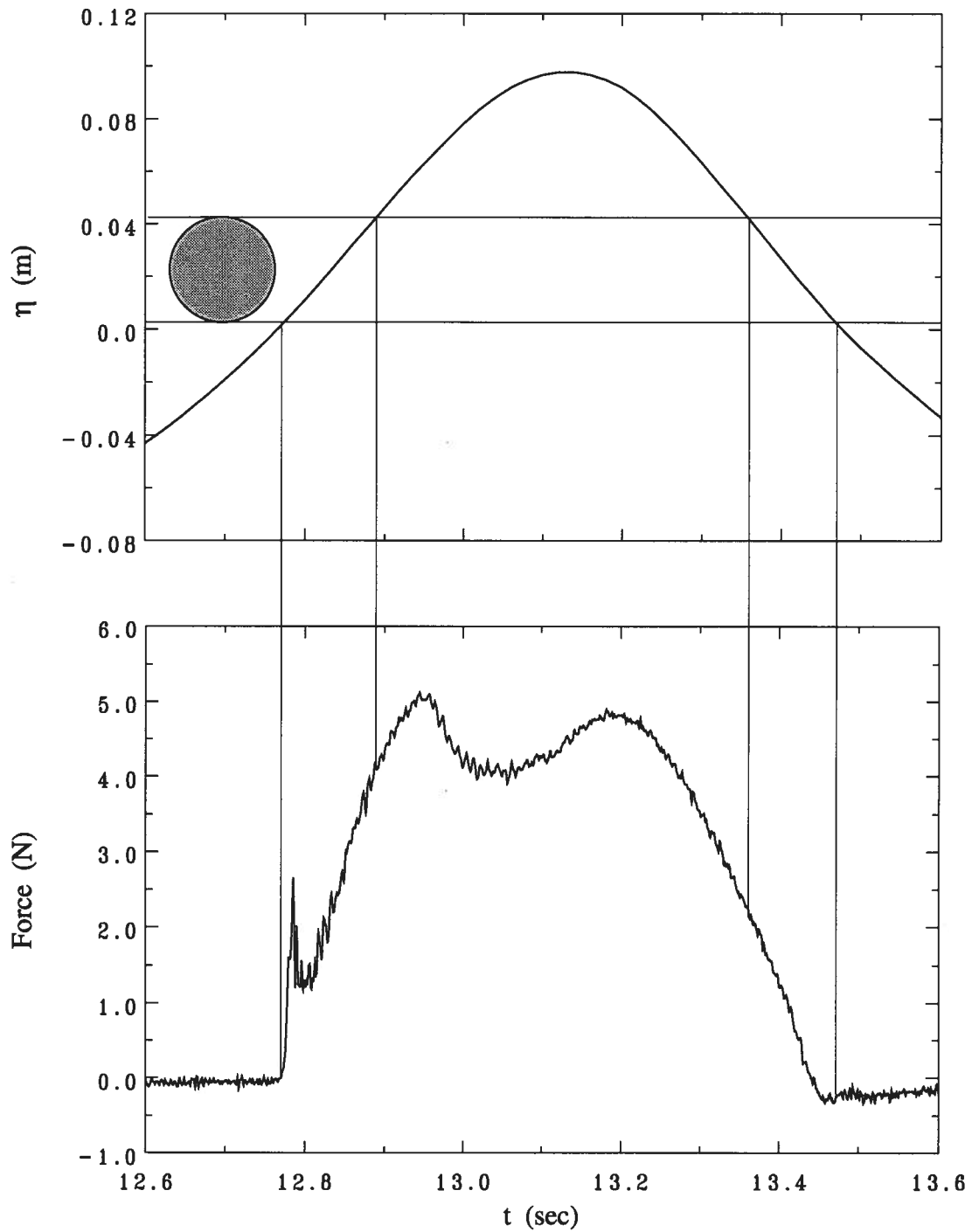


Fig. 4.6 Time histories of free surface elevation and vertical force during a slamming event. $T = 1.6$ sec, $H = 16.8$ cm, $h = 0.5$ cm.

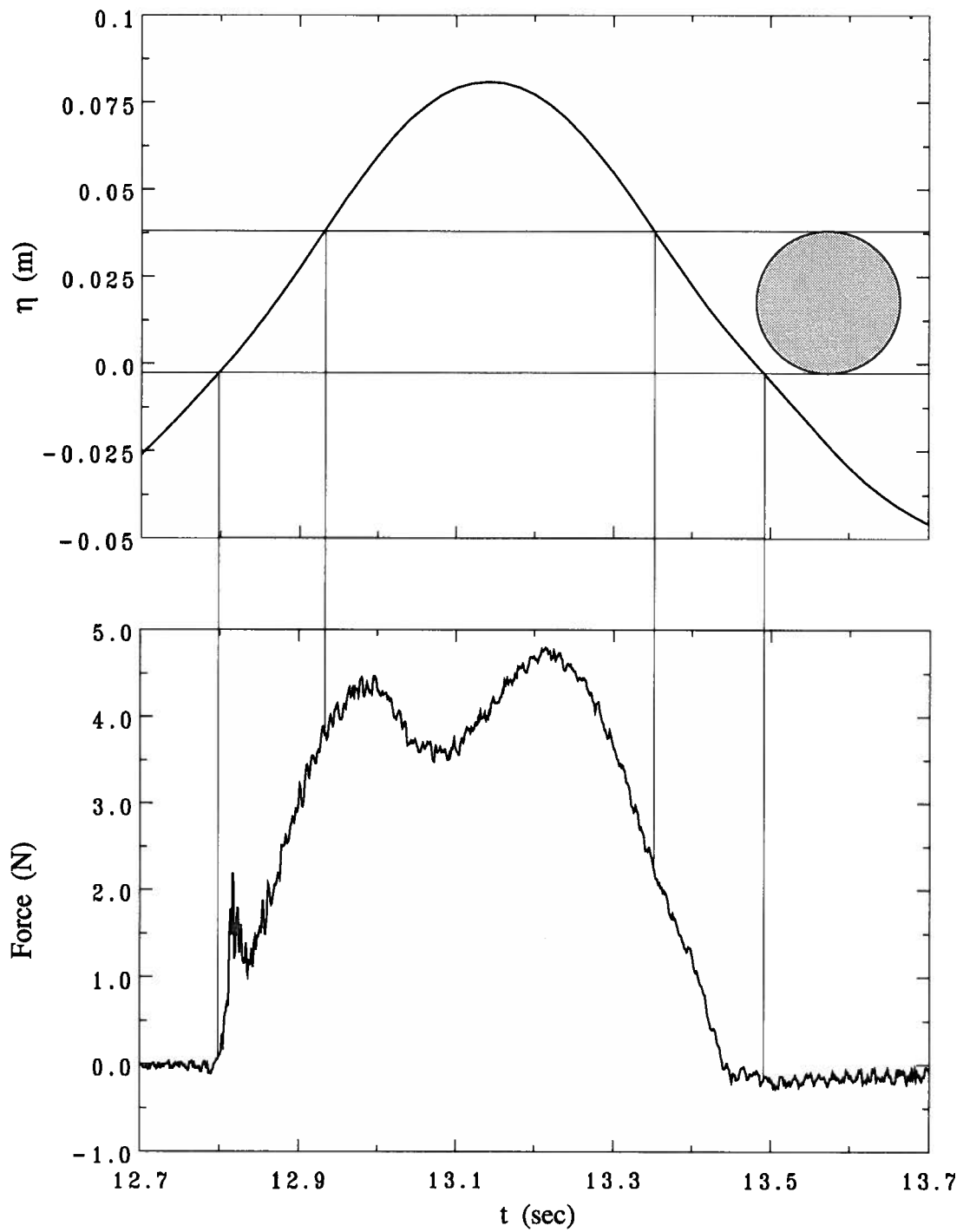


Fig. 4.7 Time histories of free surface elevation and vertical force during a slamming event. $T = 1.5$ sec, $H = 13.9$ cm, $h = 0.5$ cm.

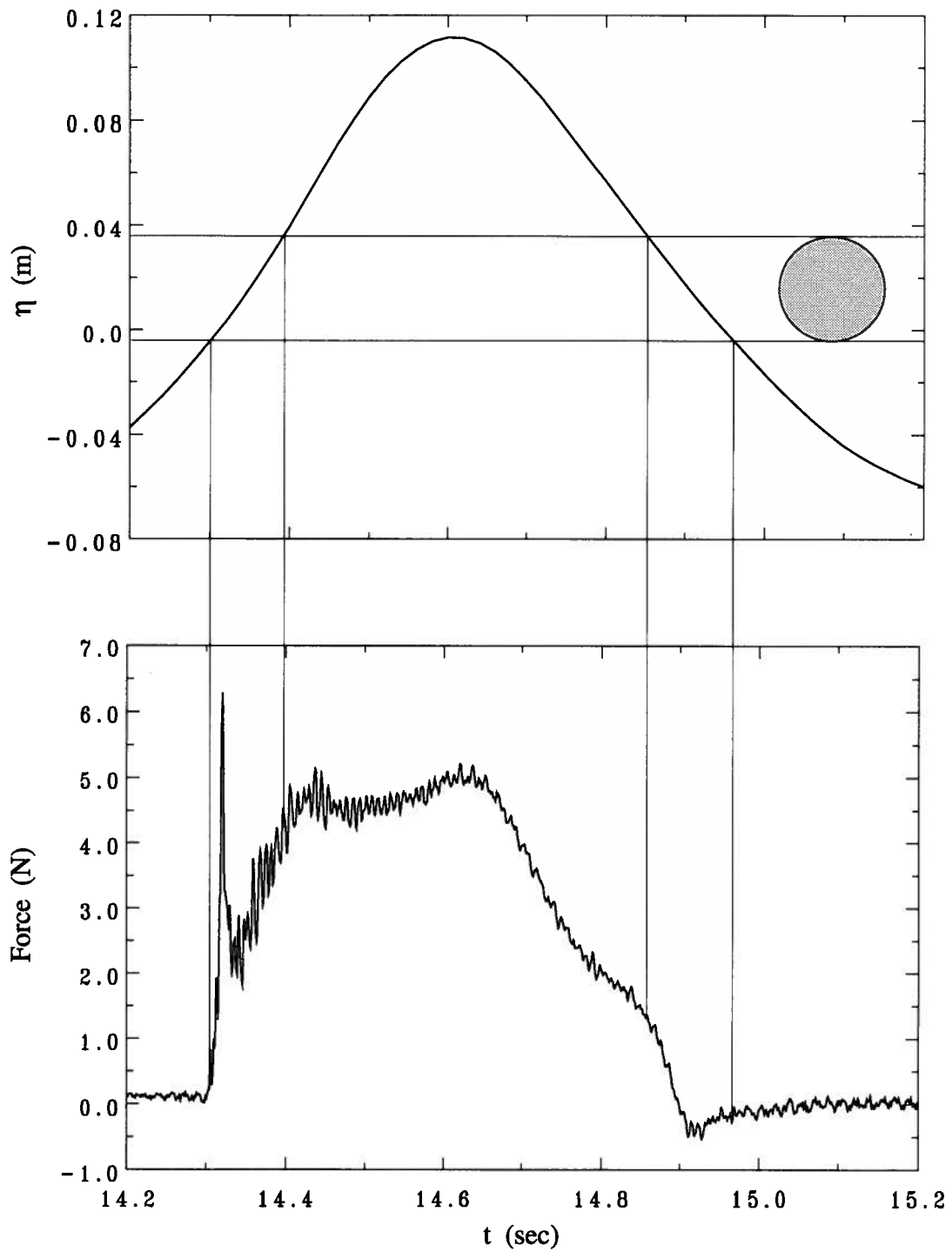


Fig. 4.8 Time histories of free surface elevation and vertical force during a slamming event. $T = 1.5$ sec, $H = 18.4$ cm, $h = 0.5$ cm.

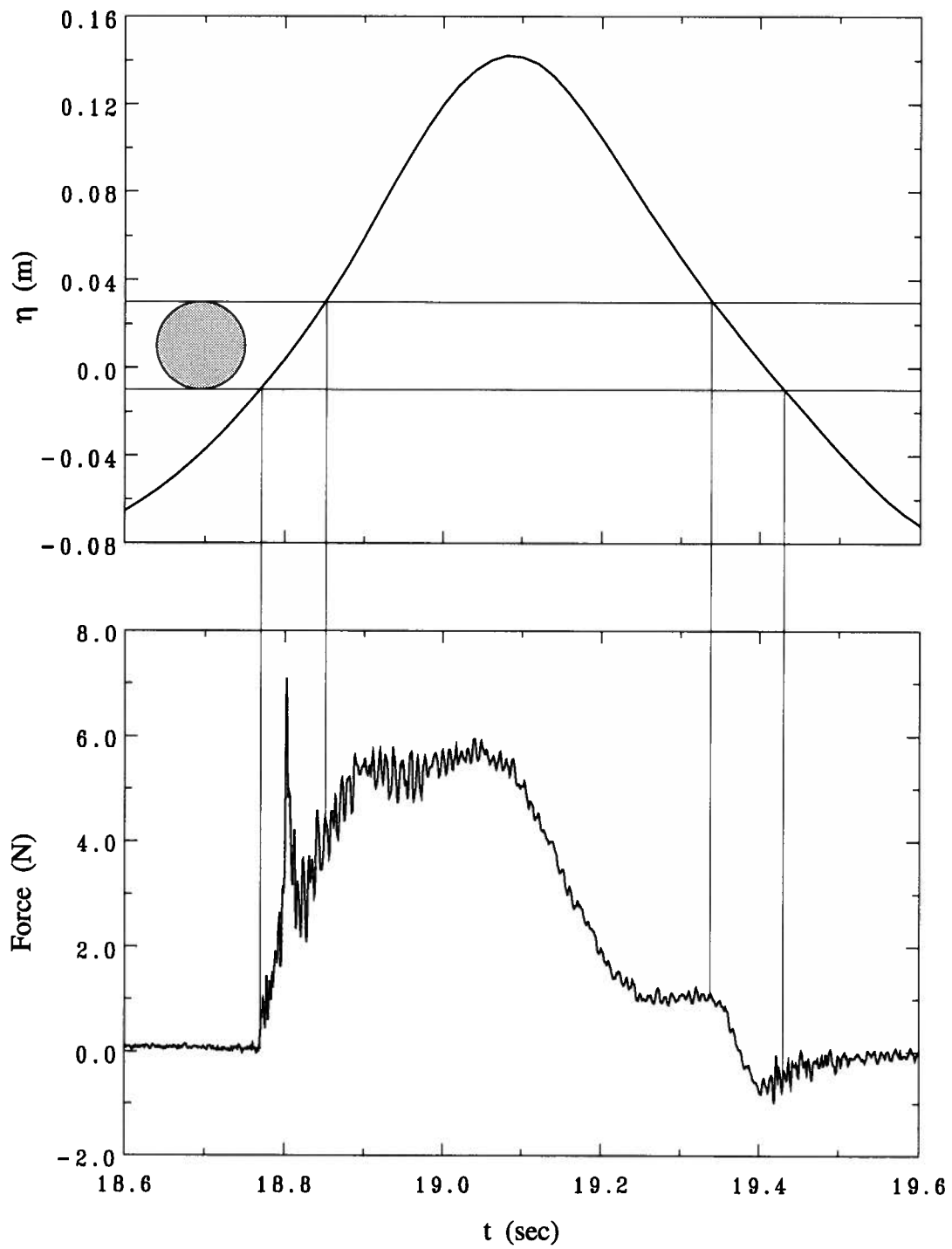


Fig. 4.9 Time histories of free surface elevation and vertical force during a slamming event. $T = 1.5$ sec, $H = 22.9$ cm, $h = 0.5$ cm.

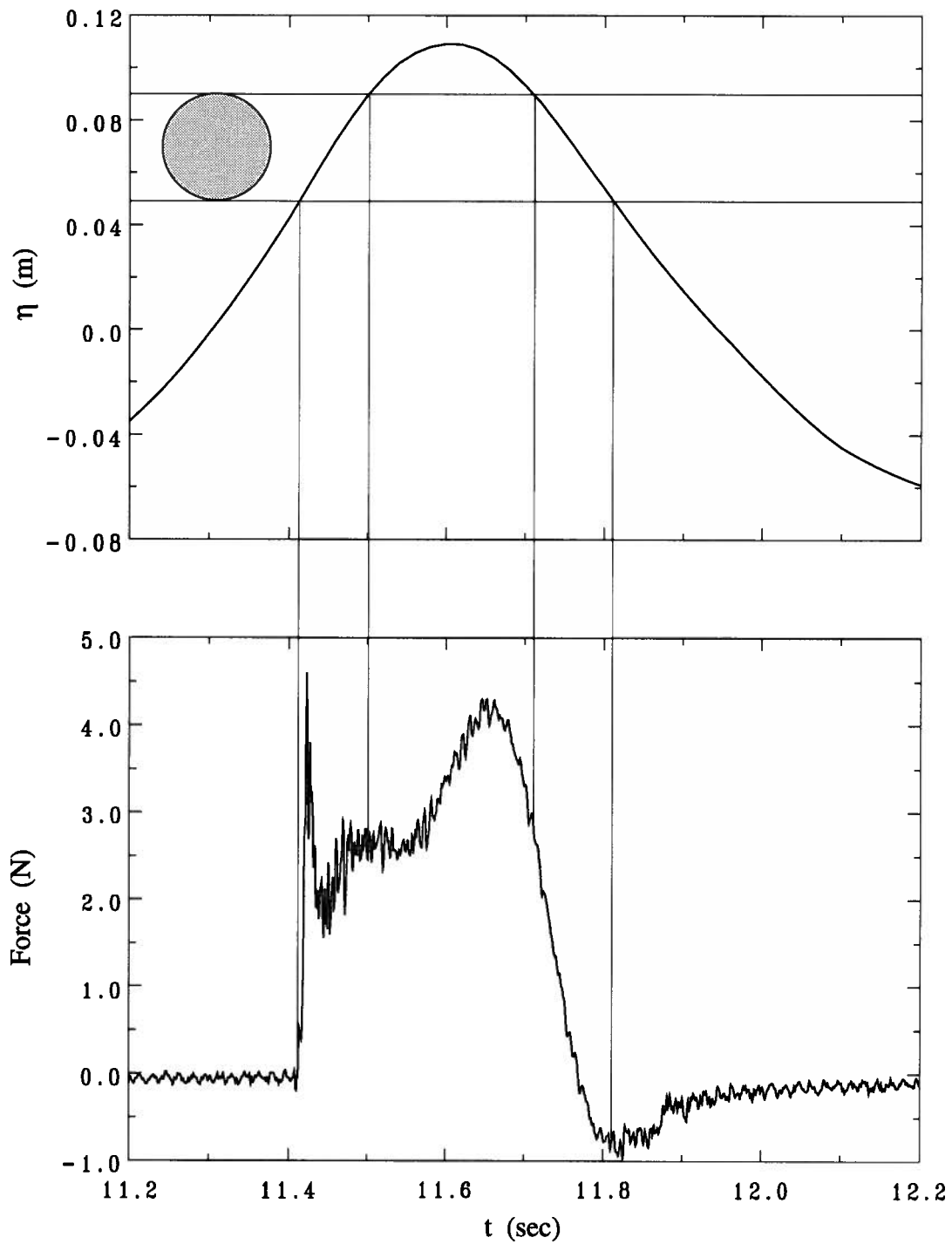


Fig. 4.10 Time histories of free surface elevation and vertical force during a slamming event.
 $T = 1.5$ sec, $H = 18.4$ cm, $h = 4.5$ cm.

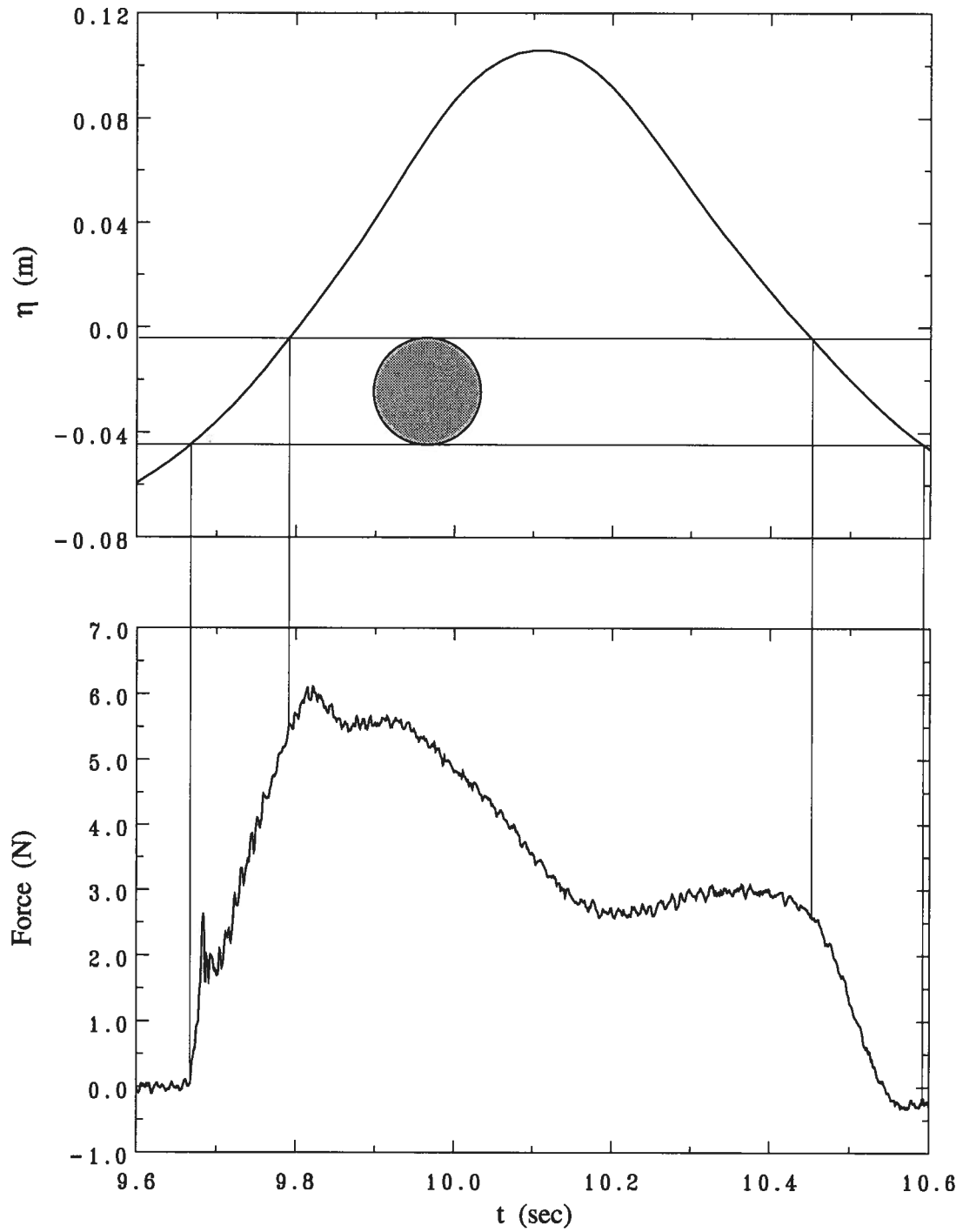


Fig. 4.11 Time histories of free surface elevation and vertical force during a slamming event. $T = 1.5$ sec, $H = 18.4$ cm, $h = -4.5$ cm.

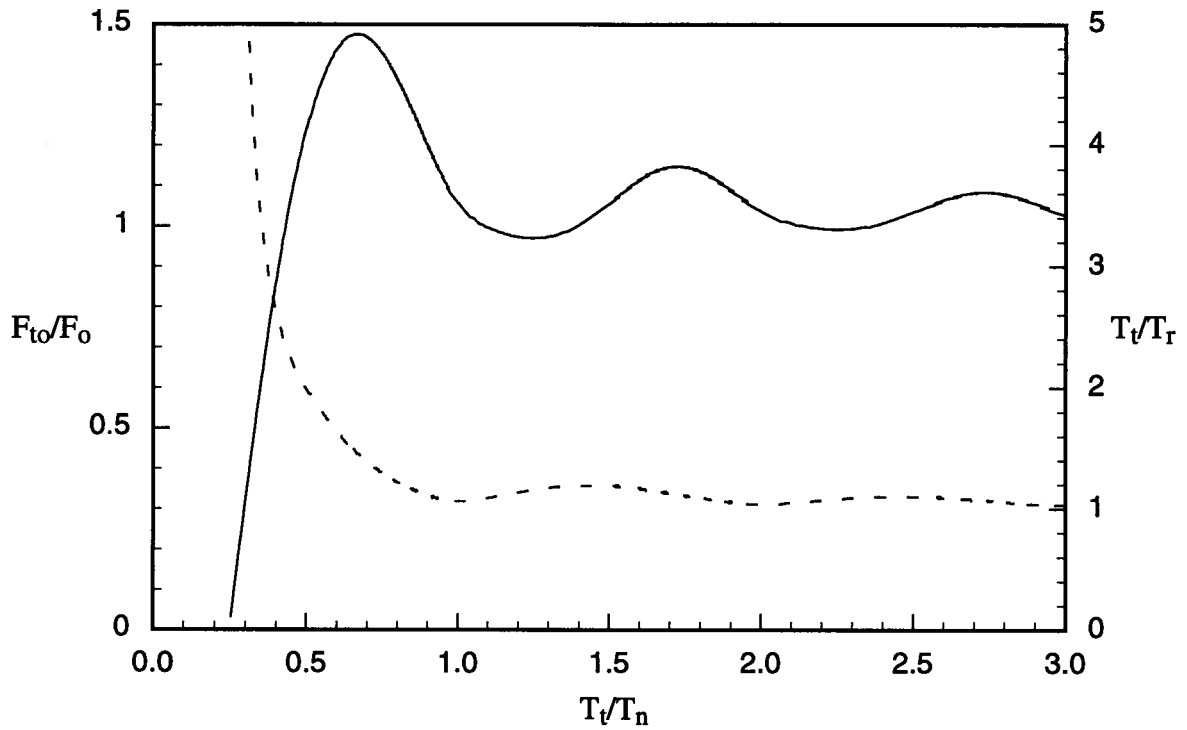


Fig. 4.12 Correction factors for peak slamming force and rise time as a function of the observed rise time ratio T_t/T_n . ———, F_{t0}/F_0 ; - - - - -, T_t/T_r .

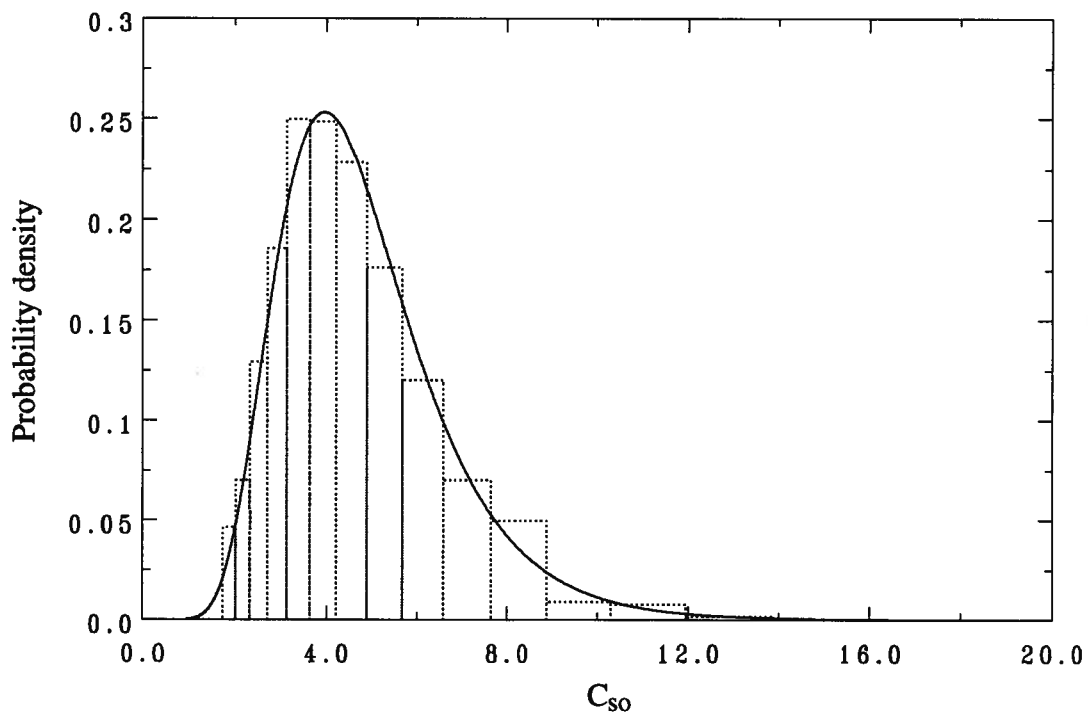


Fig. 4.13 Probability density histogram of C_{so} (- - - - -) based on data collected from entire set of experiments. ———, log-normal probability density.

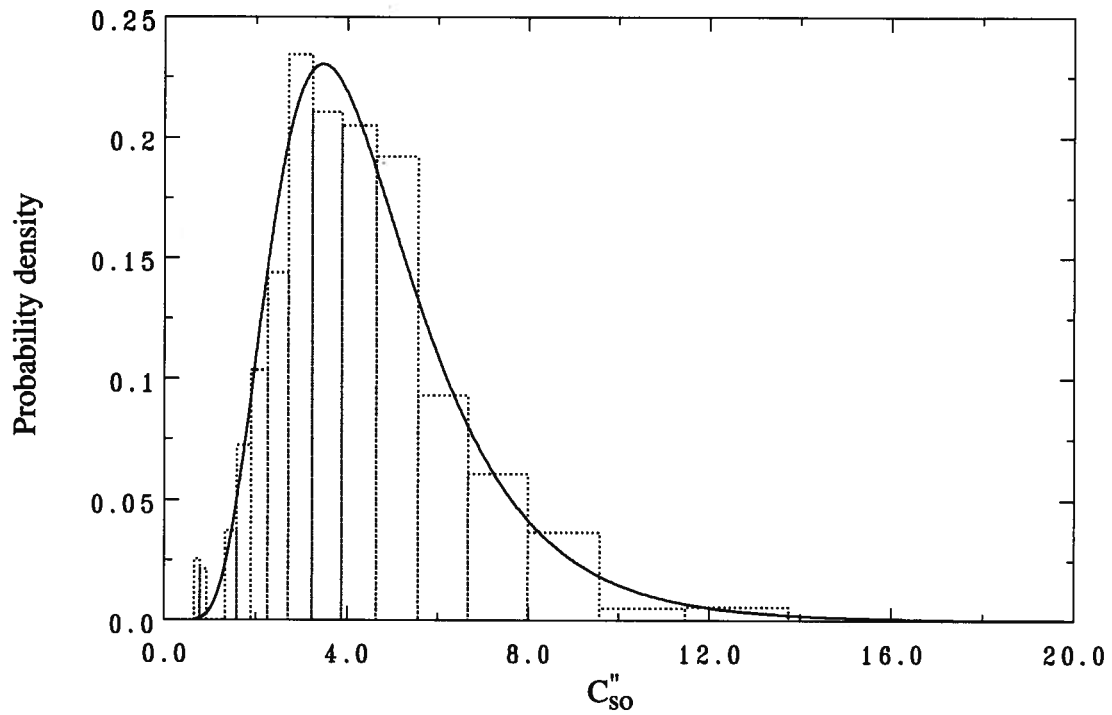


Fig. 4.14 Probability density histogram of C''_{so} (-----) based on data collected from entire set of experiments. ———, log-normal probability density.

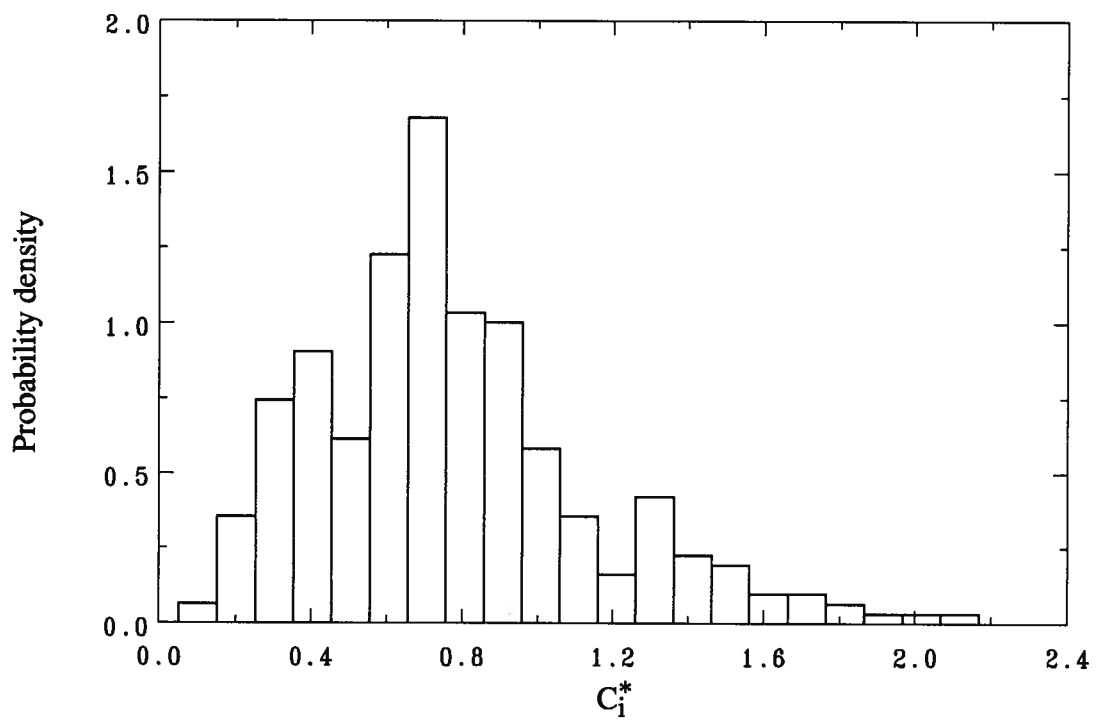


Fig. 4.15 Probability density histogram of C^*_1 based on data collected from entire set of experiments.

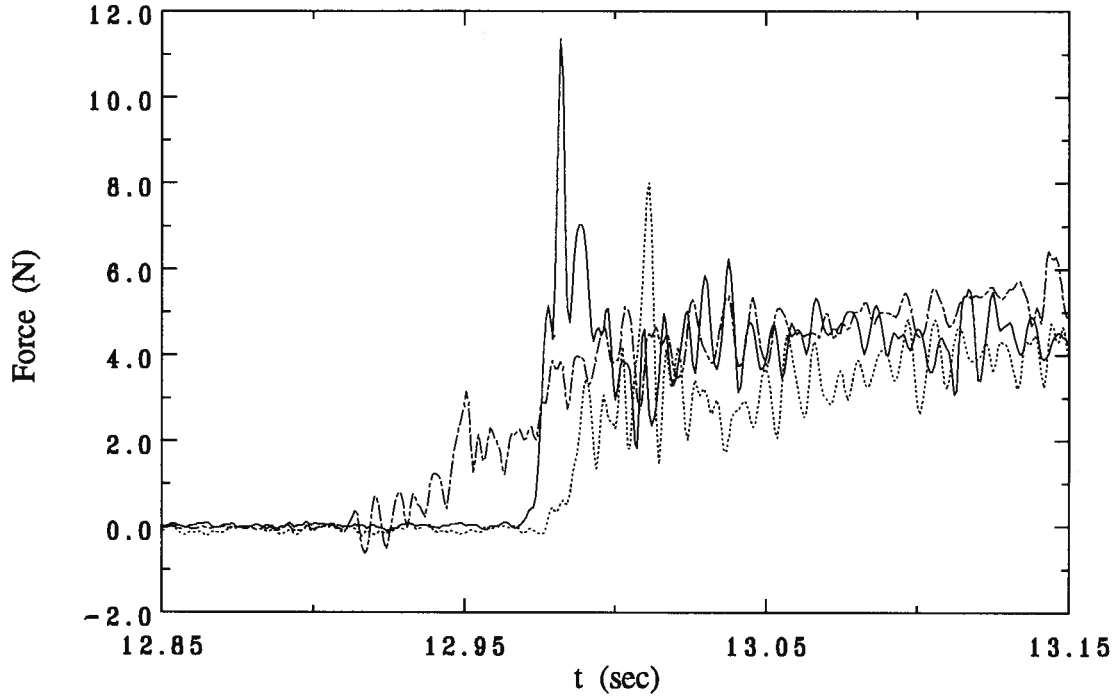


Fig. 4.16 Comparison of slamming force time histories for different cylinder inclinations, $T = 1.2$ sec, $H = 19.3$ cm. —, $\theta = 0^\circ$; ·····, $\theta = 4.8^\circ$; - - - -, $\theta = 9.6^\circ$.

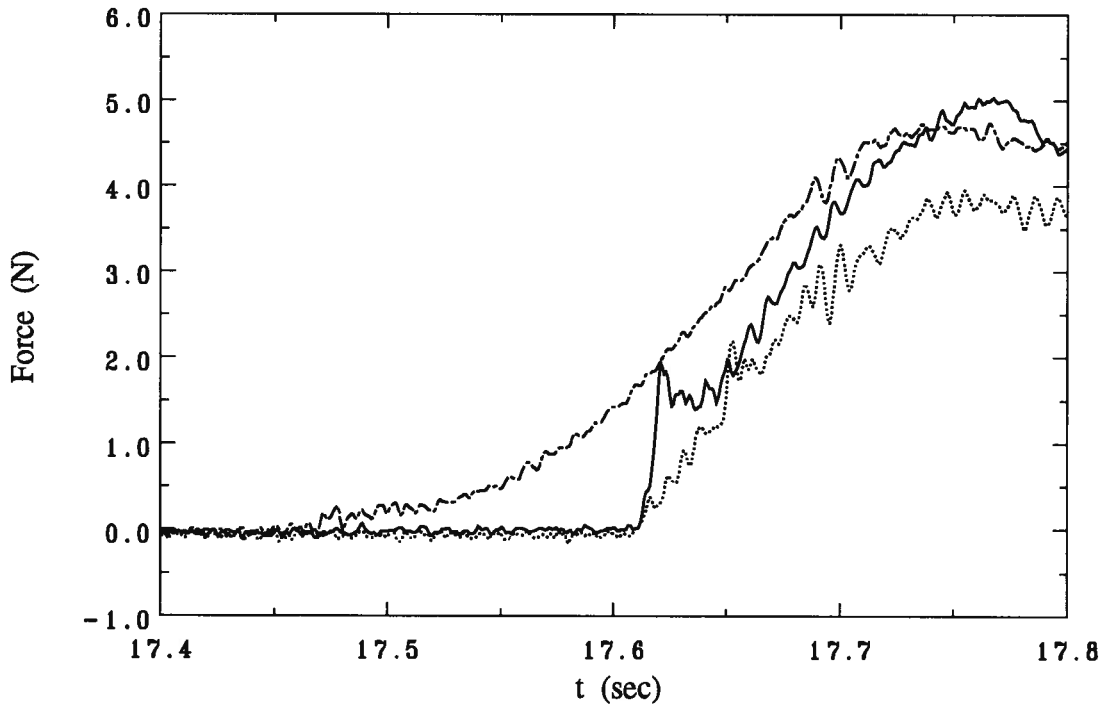


Fig. 4.17 Comparison of slamming force time histories for different cylinder inclinations, $T = 1.8$ sec, $H = 17.8$ cm. —, $\theta = 0^\circ$; ·····, $\theta = 4.8^\circ$; - - - -, $\theta = 9.6^\circ$.

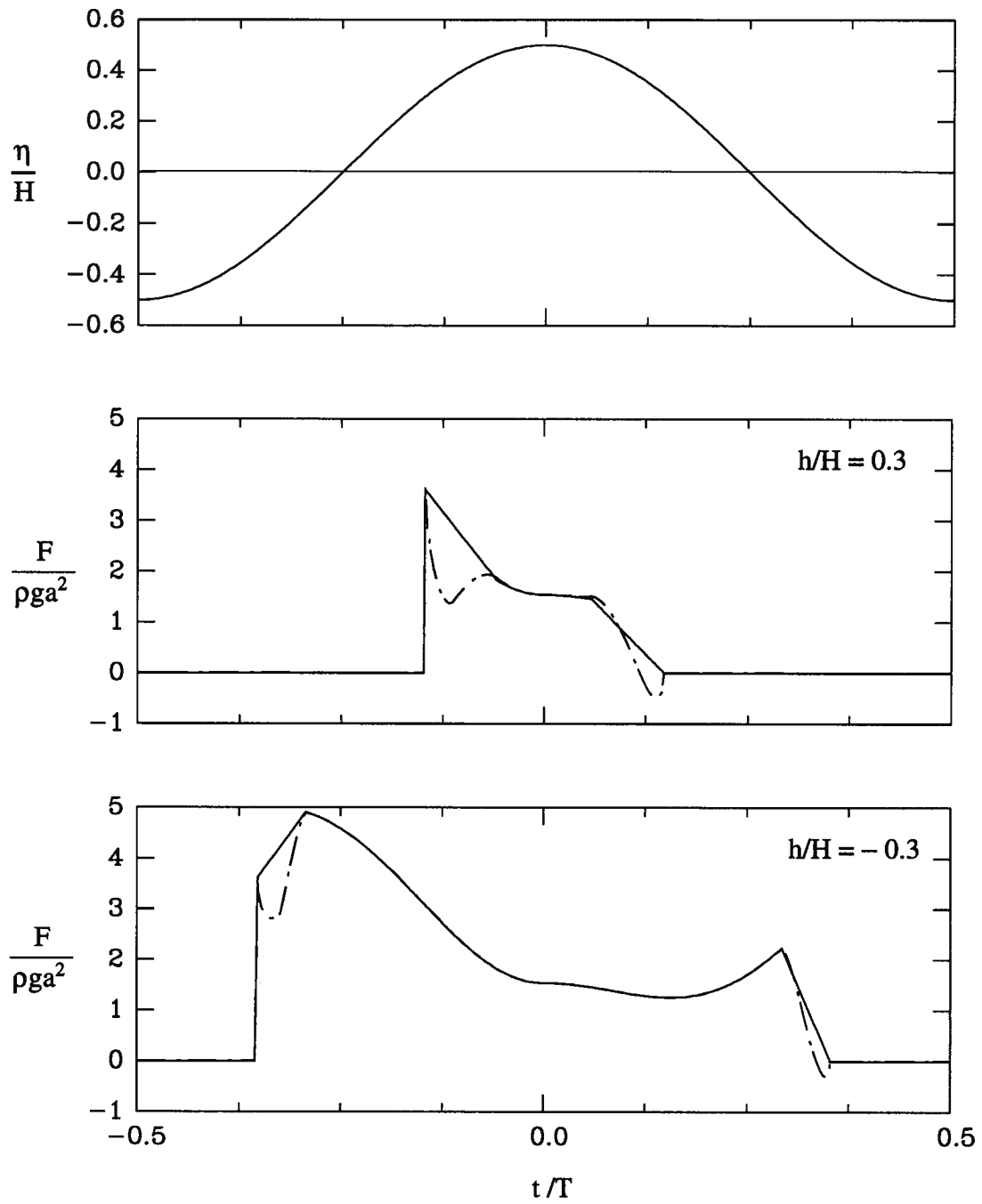


Fig. 4.18 Time variation of free surface elevation and simulated vertical force for $\omega^2 a/g = 0.05$, $\omega^2 H/g = 0.6$, and different cylinder elevations. ———, Model I; - - - - -, Model II.

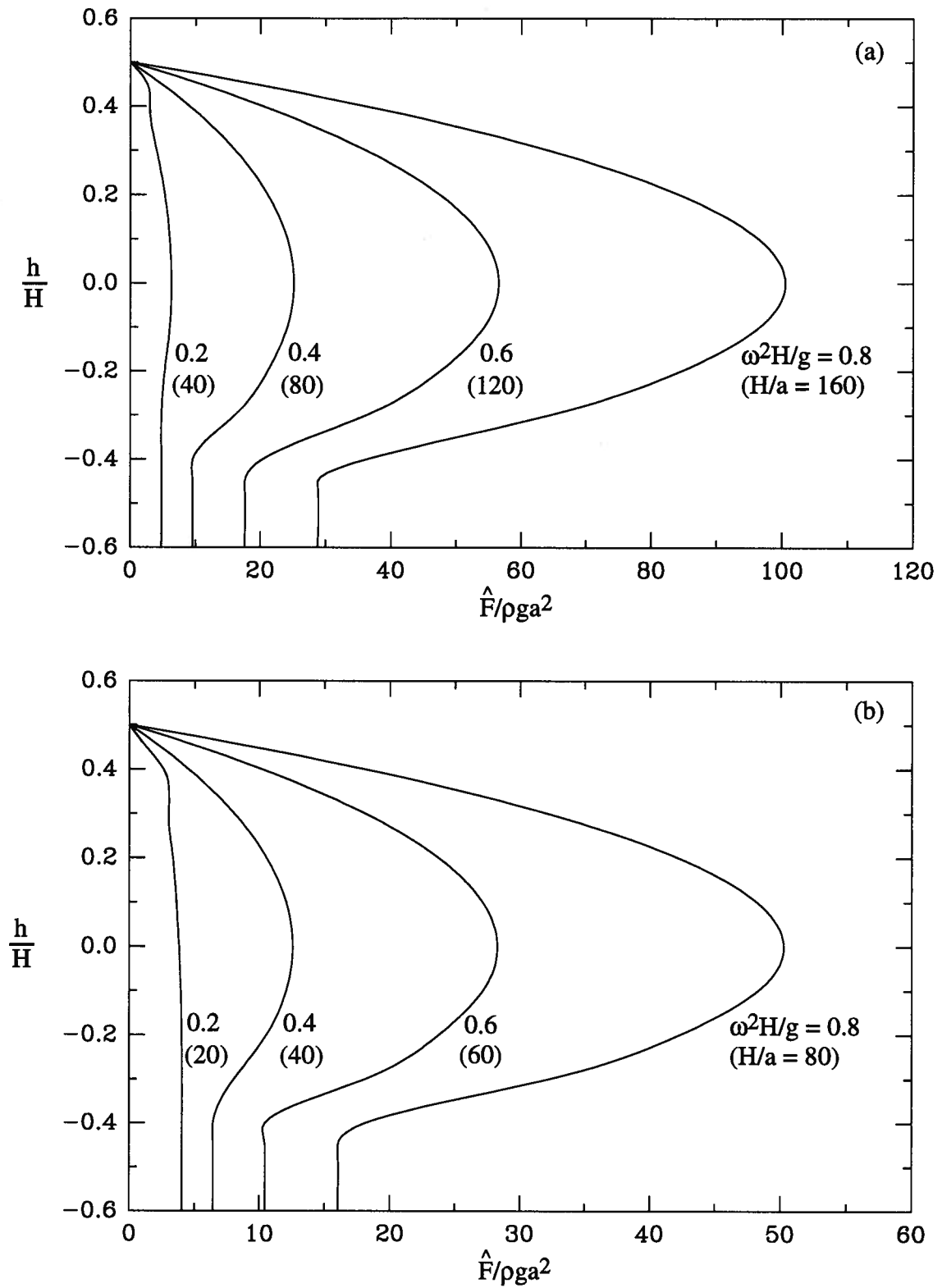


Fig. 4.19 Distribution of the non-dimensional maximum vertical force as a function of cylinder elevation and $\omega^2 H/g$. ———, Model I; - - -, Model II. (a) $\omega^2 a/g = 0.005$, (b) $\omega^2 a/g = 0.01$.

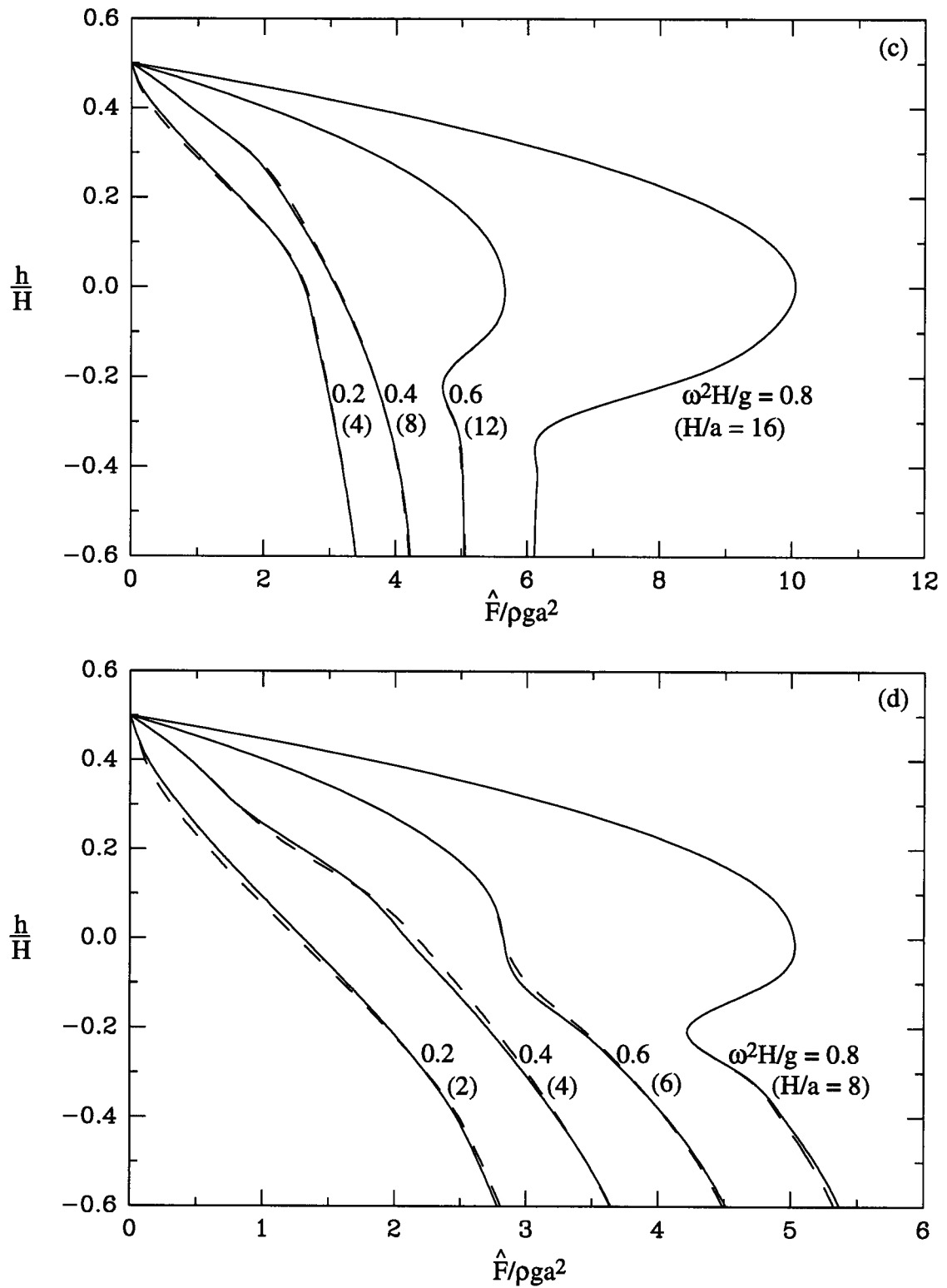


Fig. 4.19 Distribution of the non-dimensional maximum vertical force as a function of cylinder elevation and $\omega^2 H/g$. ———, Model I; - - - -, Model II. (c) $\omega^2 a/g = 0.05$, (d) $\omega^2 a/g = 0.1$.

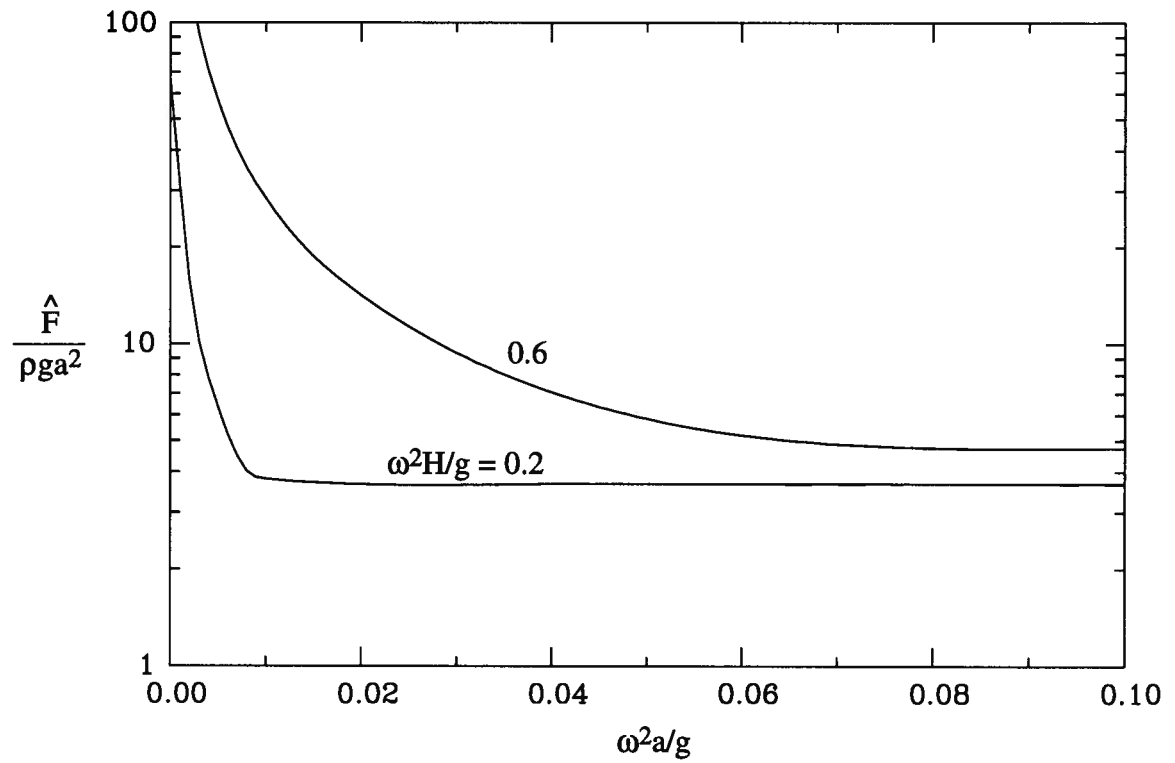


Fig. 4.20 Variation of the non-dimensional maximum vertical force as a function of $\omega^2 a/g$ for different values of $\omega^2 H/g$. ———, model I; - - -, model II.

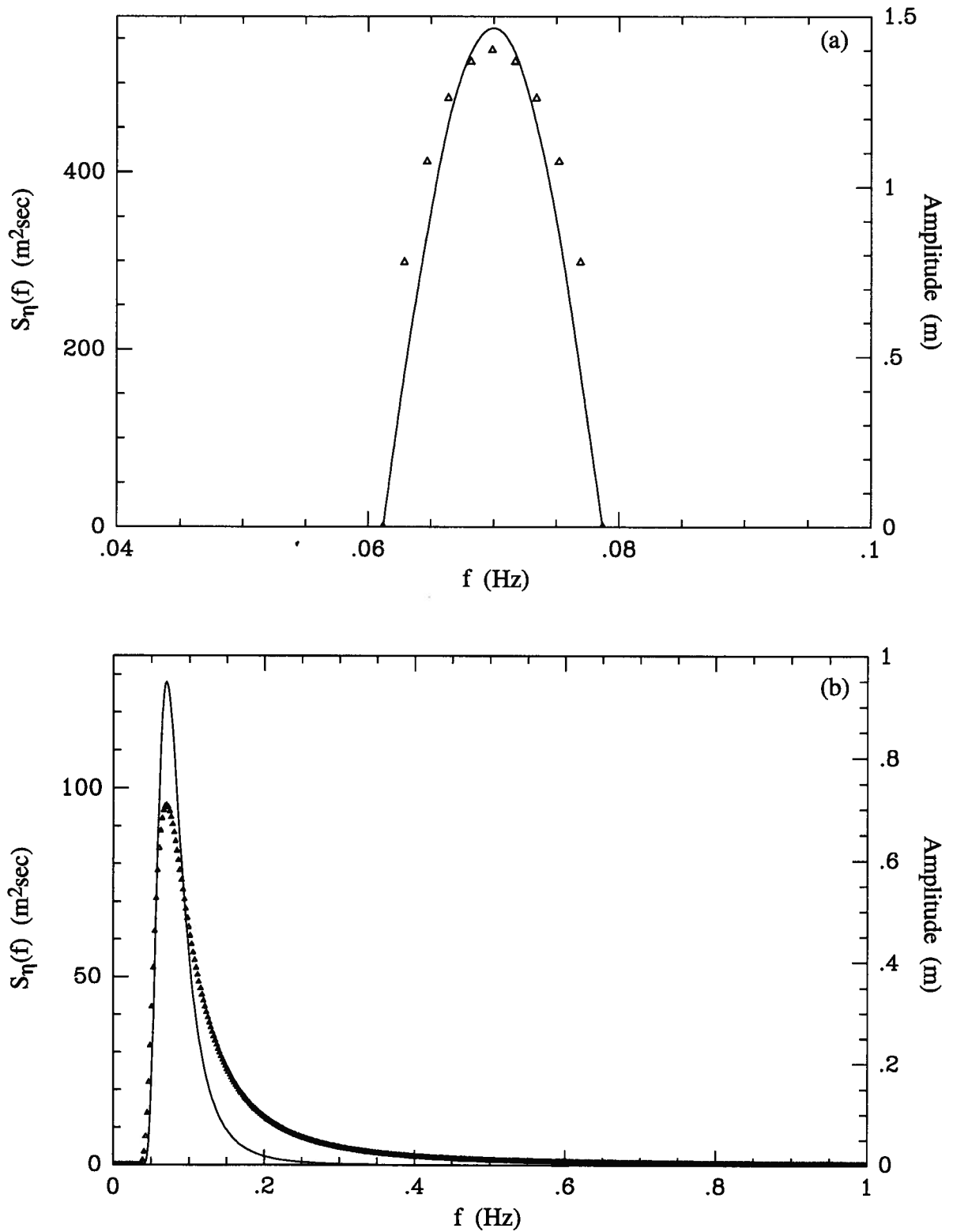


Fig. 4.21 Spectral density (—) and corresponding amplitude spectrum (Δ) with $H_s = 10$ m, and $T_p = 14.3$ sec, used in the numerical simulation of random waves. (a) Narrow-band spectrum, (b) Pierson-Moskowitz spectrum.

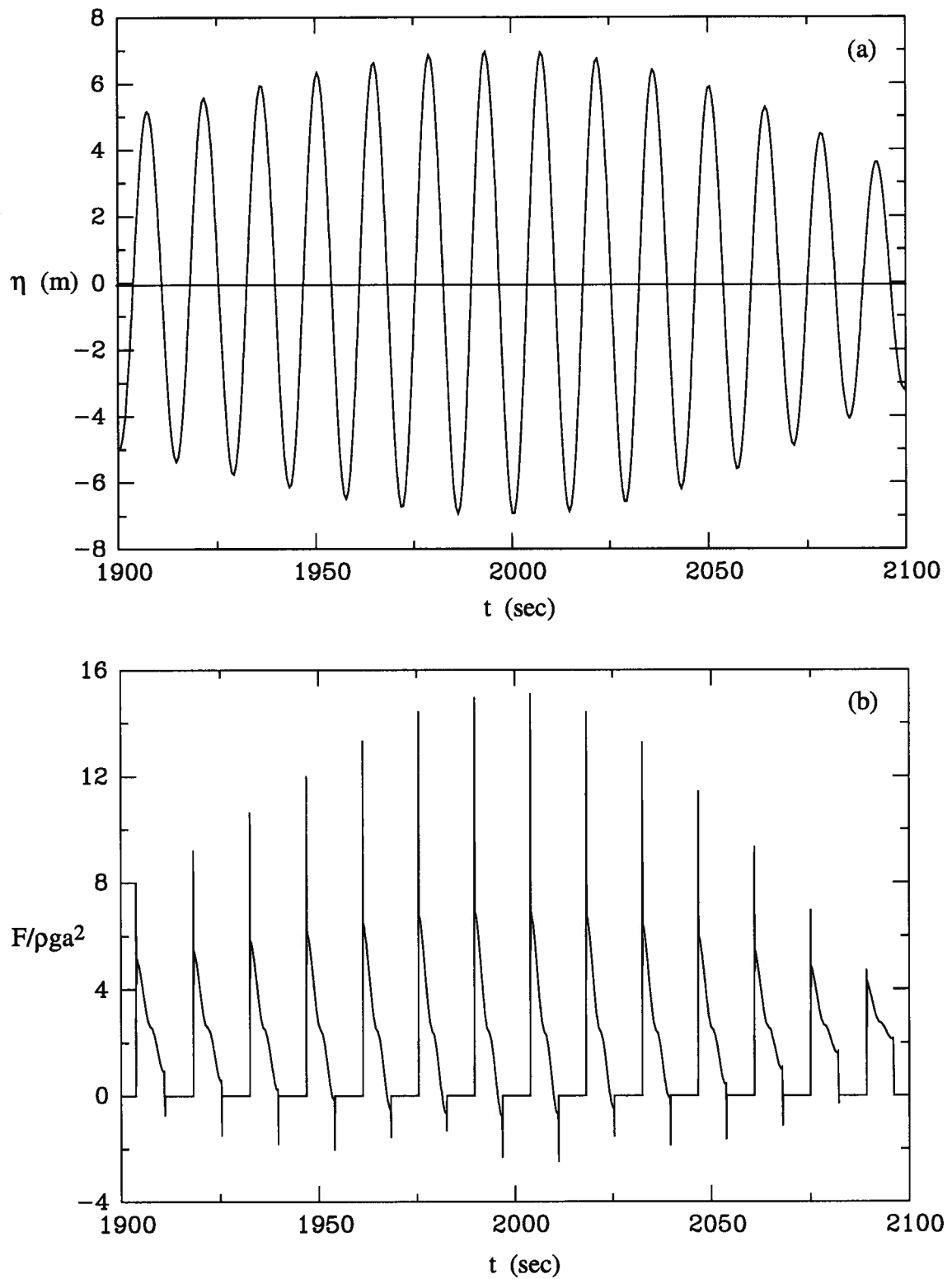


Fig. 4.22 Segment of numerically simulated time series of (a) free surface elevation and, (b) non-dimensional vertical force for a narrow-band spectrum.

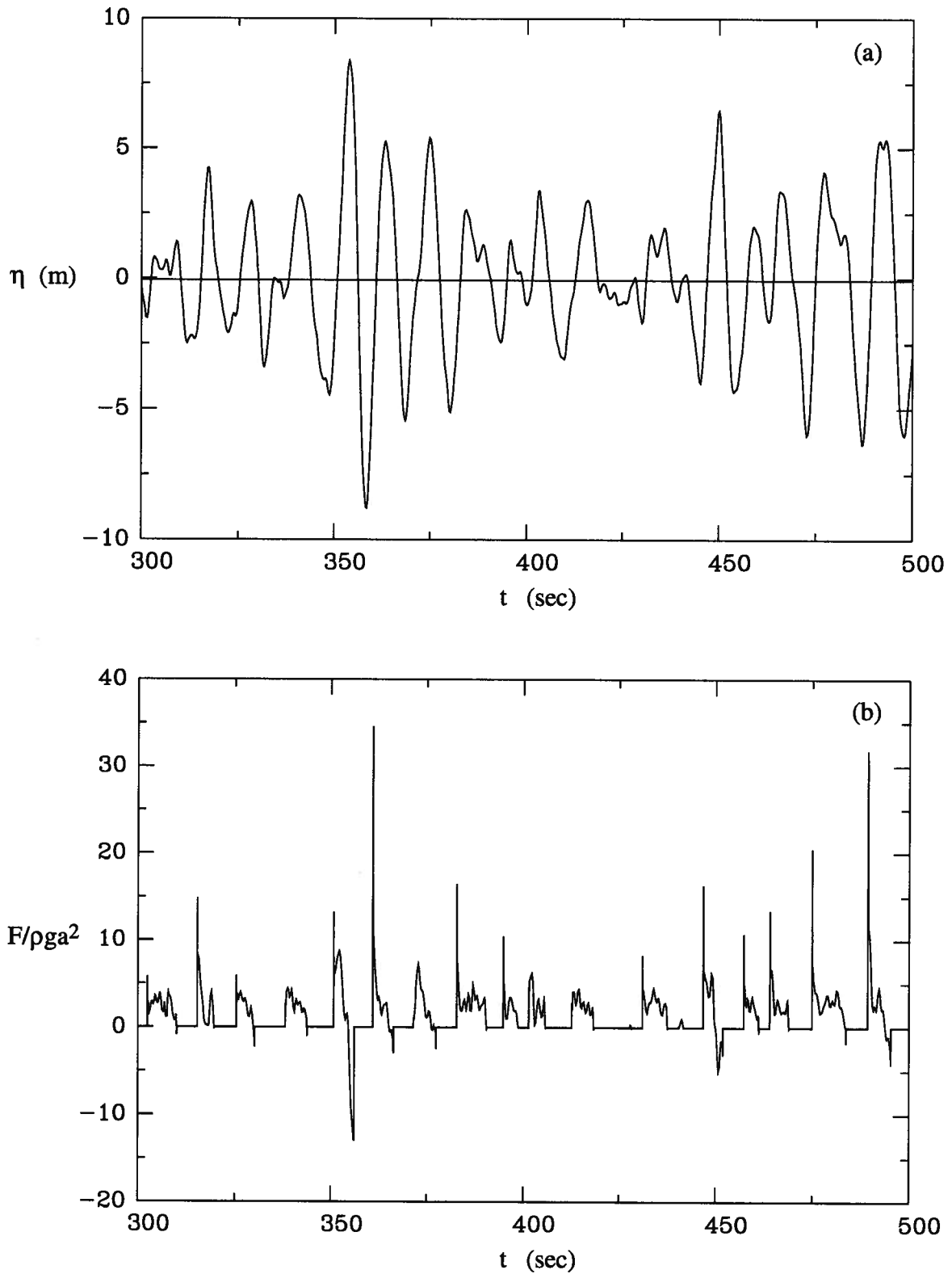


Fig. 4.23 Segment of numerically simulated time series of (a) free surface elevation and, (b) non-dimensional vertical force for a two-parameter Pierson-Moskowitz spectrum.

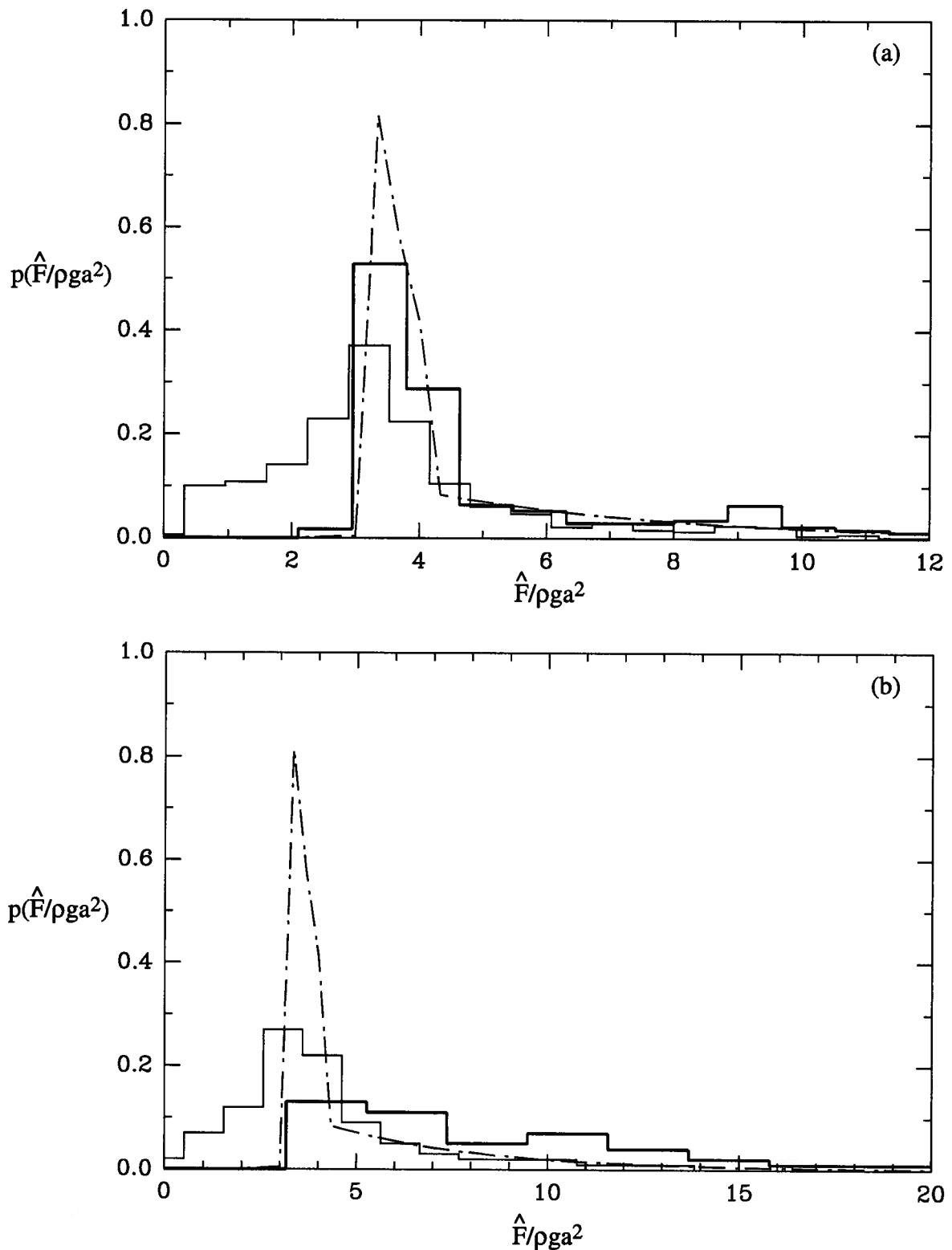


Fig. 4.24 Comparison of probability density of force maxima on a horizontal cylinder located at $h = 0$. - - - - -, analytical prediction (Isaacson and Subbiah, 1990); ————, numerical simulation, method A; ————, numerical simulation, method B. (a) narrow-band spectrum, (b) two-parameter Pierson-Moskowitz spectrum.

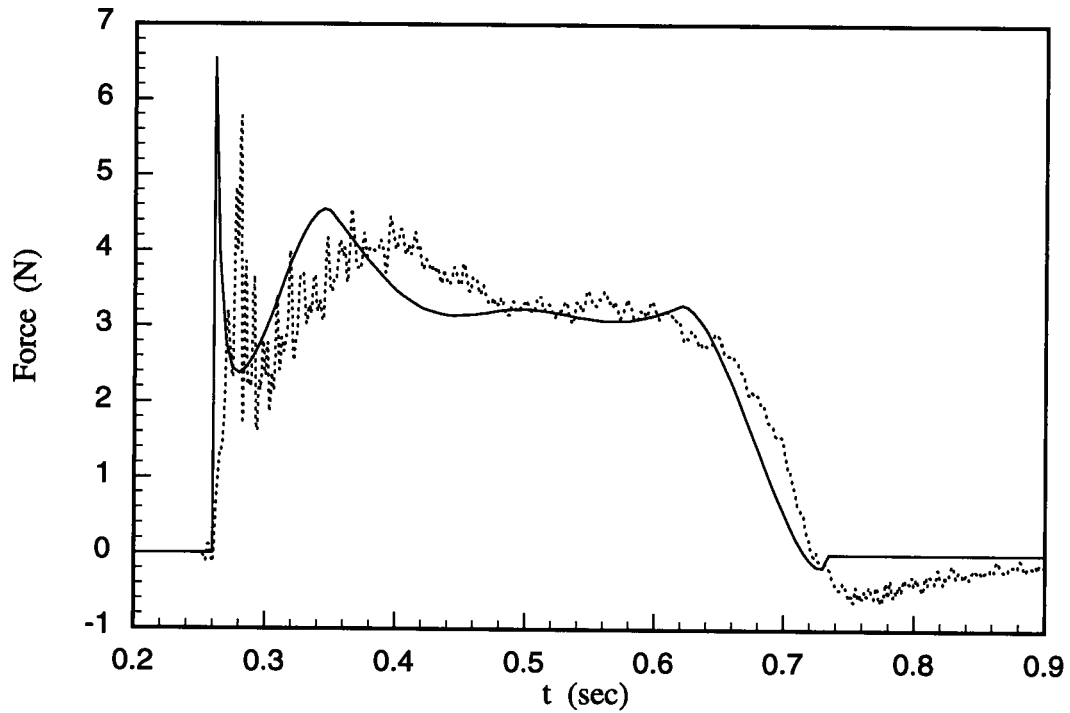


Fig. 4.25 Comparison of vertical force predicted by rigid cylinder model (————) with the measured force (······). $T = 1.2$ sec, $H = 15.2$ cm, $h = 0.5$ cm.

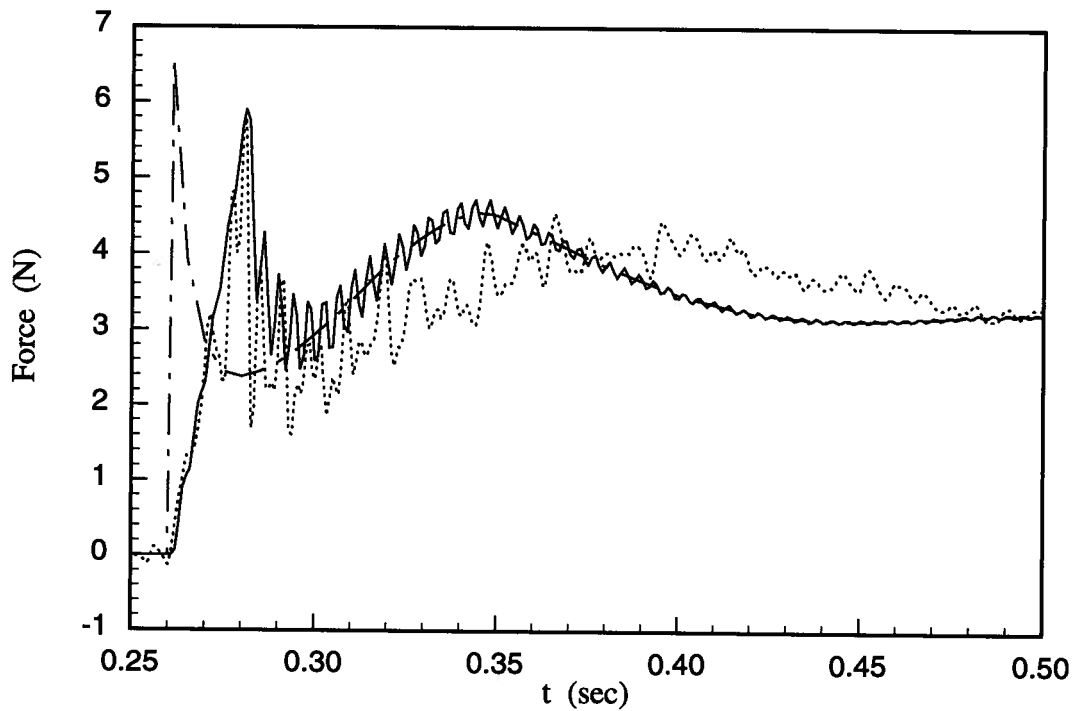


Fig. 4.26 Early stages of slamming force predicted by dynamic cylinder model (————) compared with rigid cylinder model estimate (— - — -) and the measured force (······). $T = 1.2$ sec, $H = 15.2$ cm, $h = 0.5$ cm, $T_n = 290$ Hz, $T_r = 20$ msec.

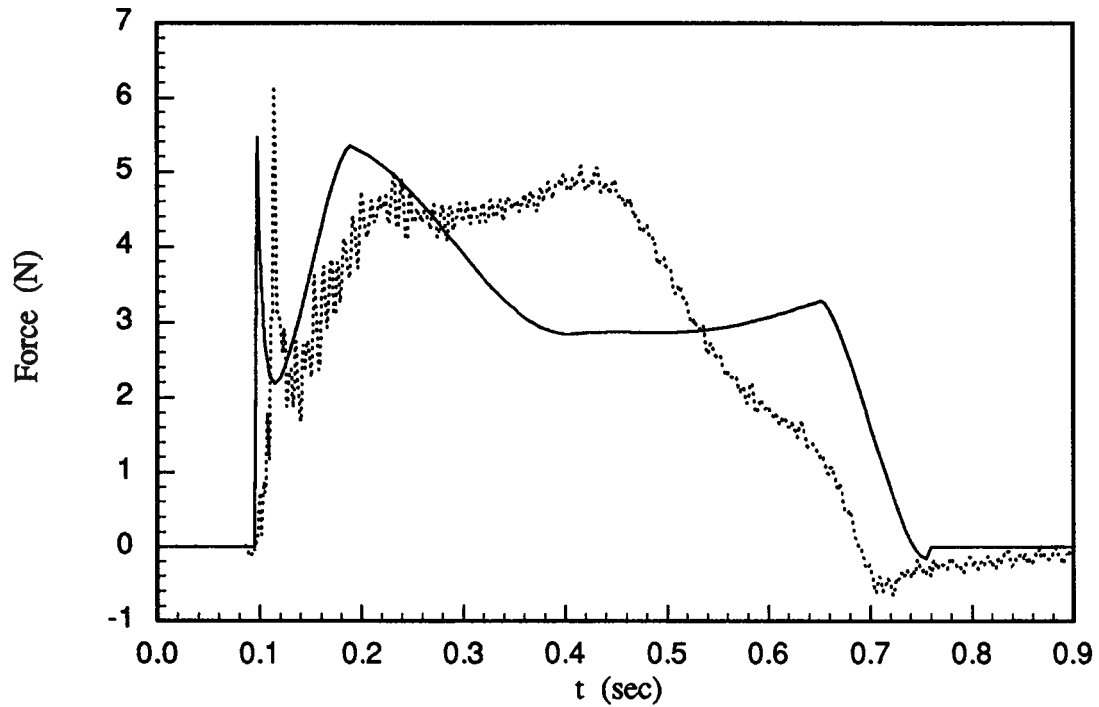


Fig. 4.27 Comparison of vertical force predicted by rigid cylinder model (————) with the measured force (·····). $T = 1.5$ sec, $H = 18.4$ cm, $h = 0.5$ cm.

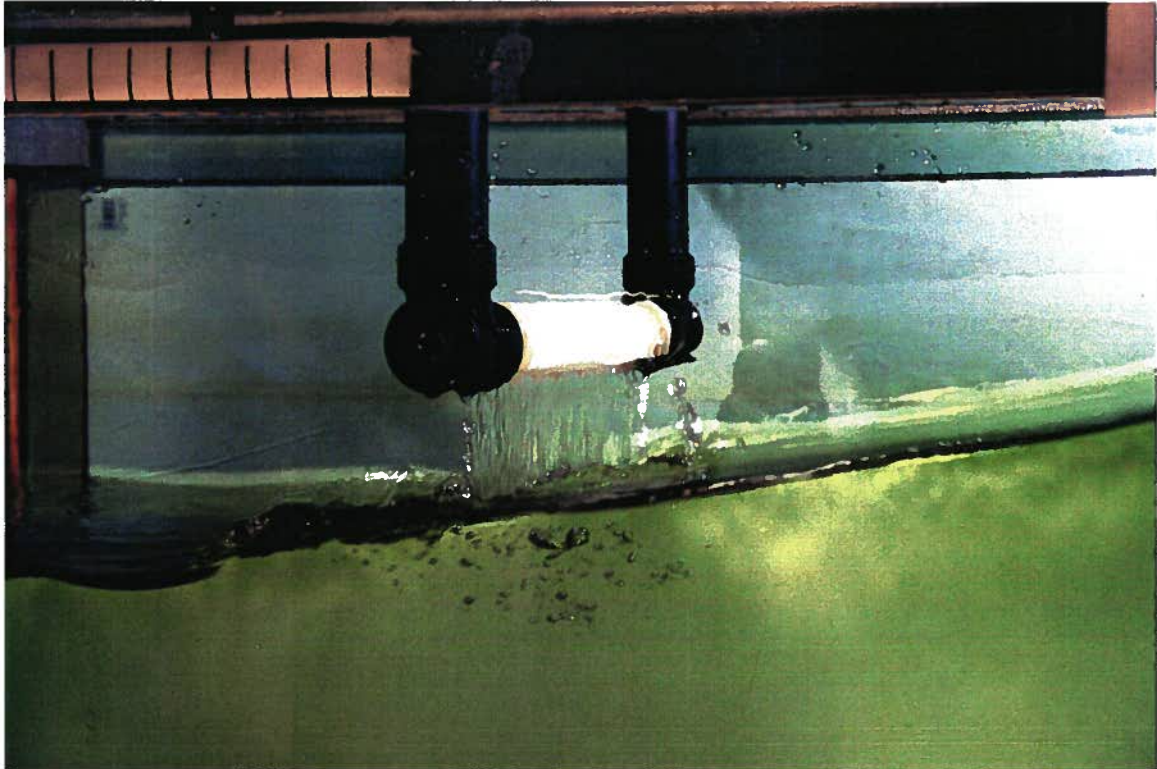


Fig. 4.28 Photograph showing mass of water suspended from test cylinder after recession of incident wave.

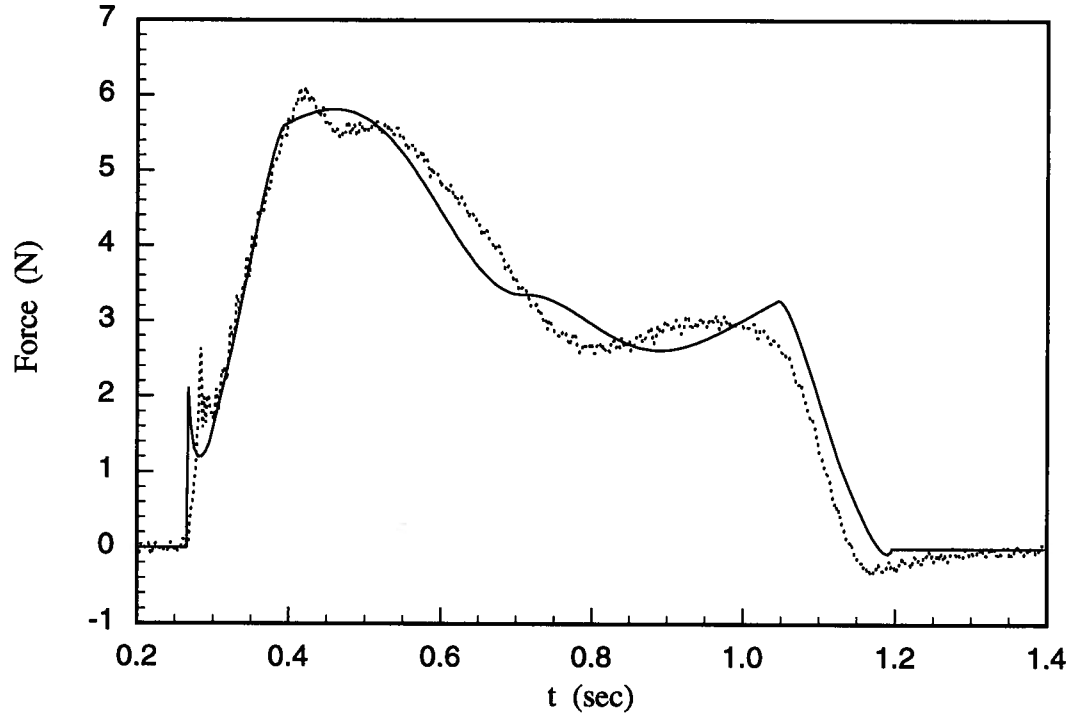


Fig. 4.29 Comparison of vertical force predicted by rigid cylinder model (————) with the measured force (·····). $T = 1.5$ sec, $H = 18.4$ cm, $h = -4.5$ cm.

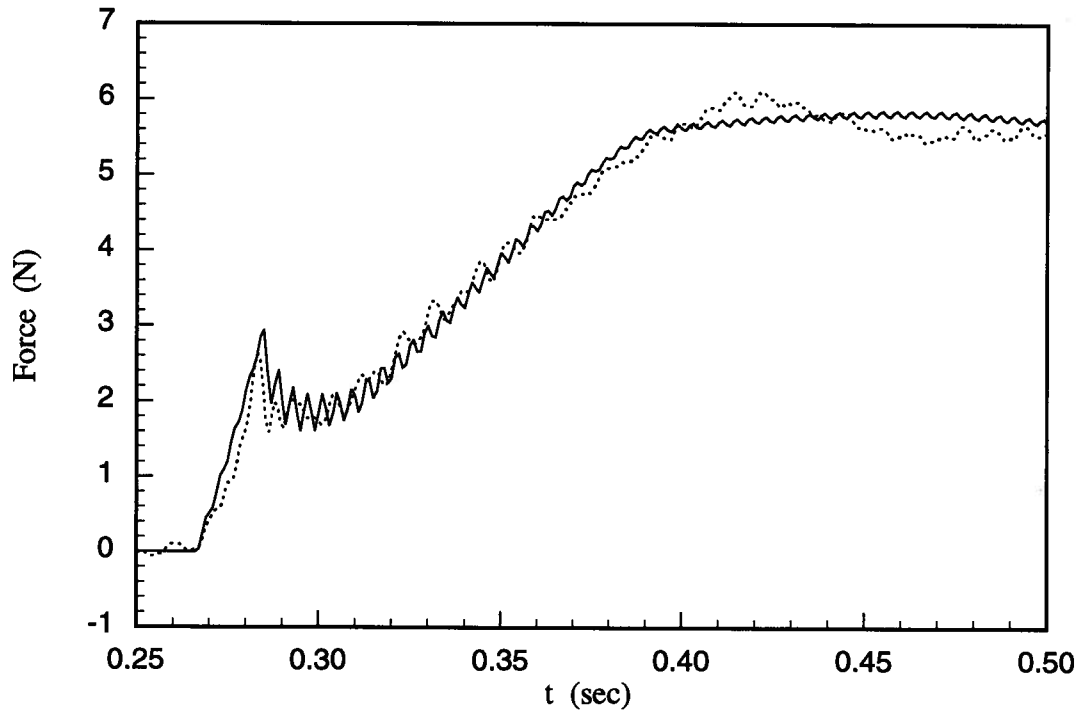


Fig. 4.30 Early stages of slamming force predicted by dynamic cylinder model (————) compared with the measured force (·····). $T = 1.5$ sec, $H = 18.4$ cm, $h = -4.5$ cm, $T_n = 290$ Hz, $T_r = 18$ msec.

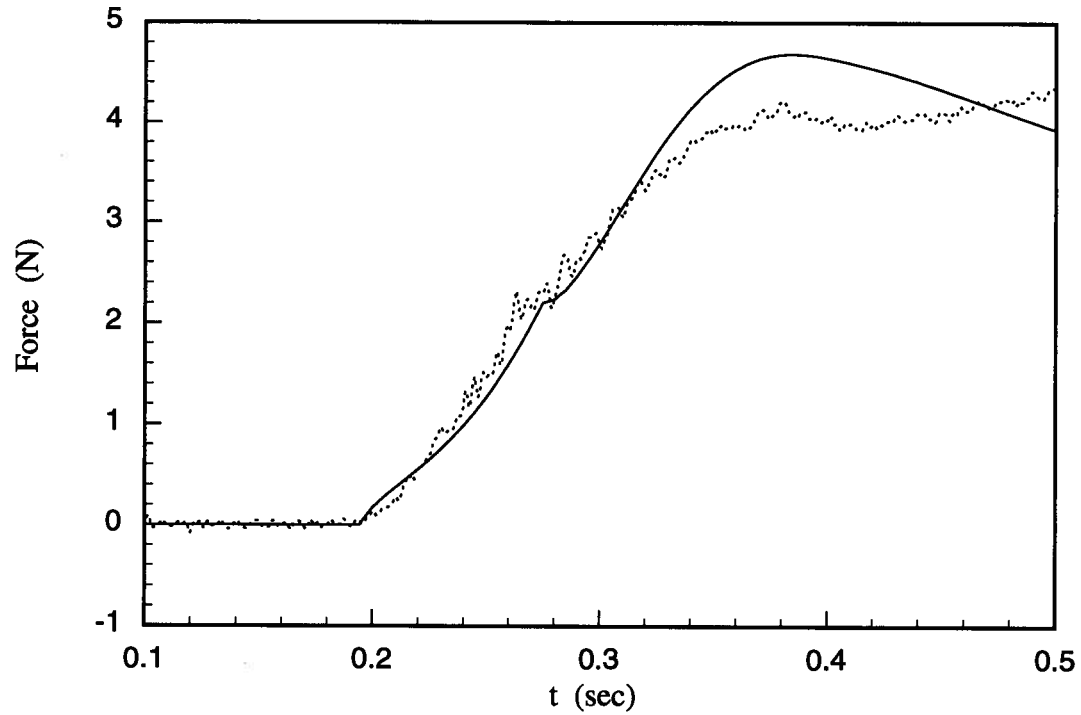


Fig. 4.31 Comparison of force on inclined cylinder predicted by numerical model (————) with the measured force (·····). $T = 1.8$ sec, $H = 17.8$ cm, $\theta = 4.8^\circ$.

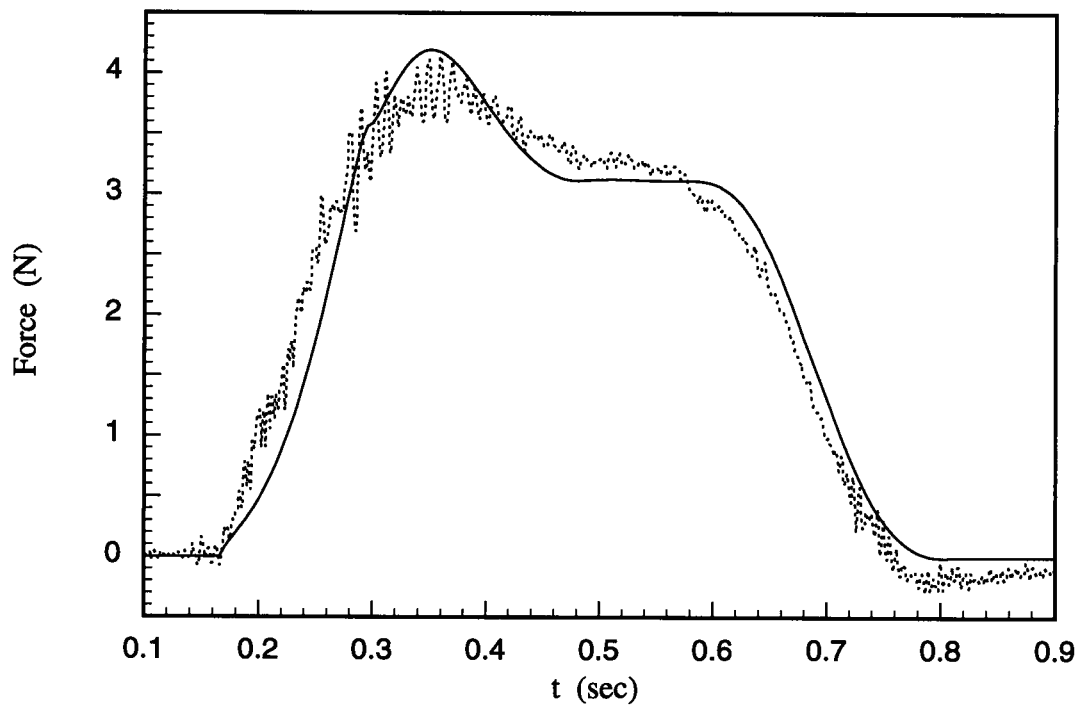


Fig. 4.32 Comparison of force on inclined cylinder predicted by numerical model (————) with the measured force (·····). $T = 1.2$ sec, $H = 15.2$ cm, $\theta = 9.6^\circ$.

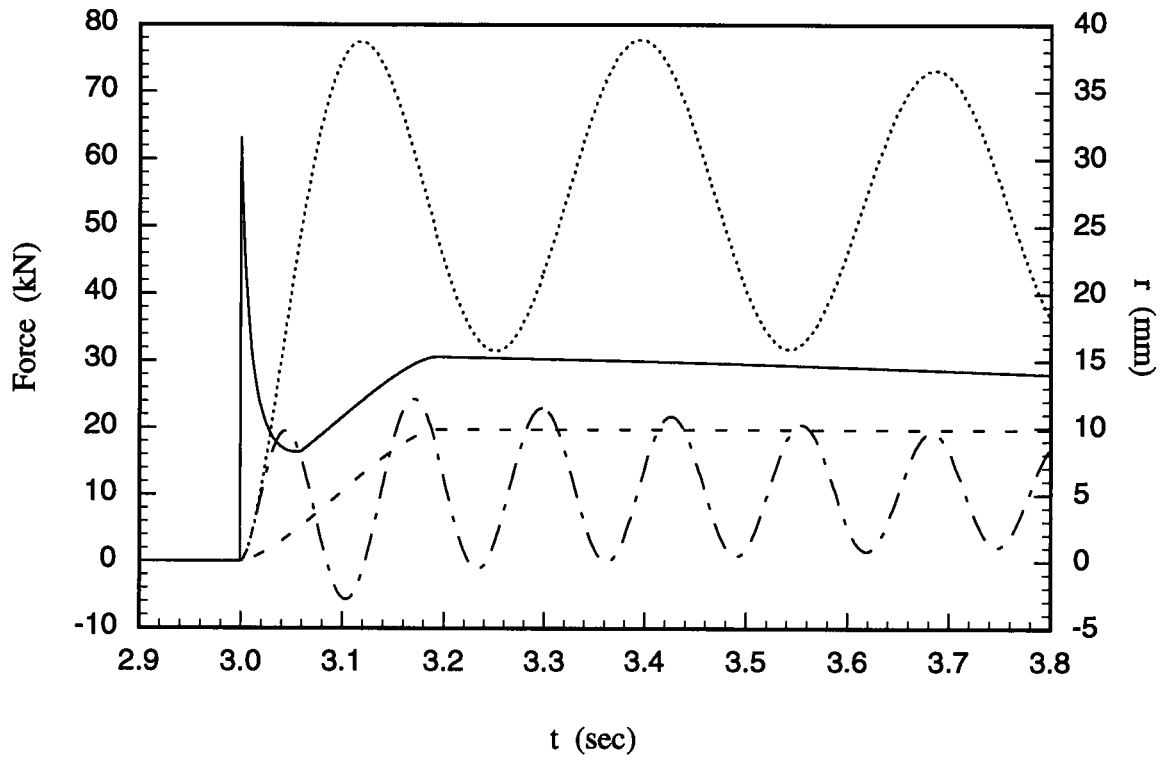


Fig. 4.33 Predicted time history of the vertical force on the cylinder for the example application. ———, total force on rigid cylinder; - - - - -, buoyancy force component; — · — · —, mid-span cylinder response for fixed-end condition; ·····, mid-span cylinder response for pinned-end condition.

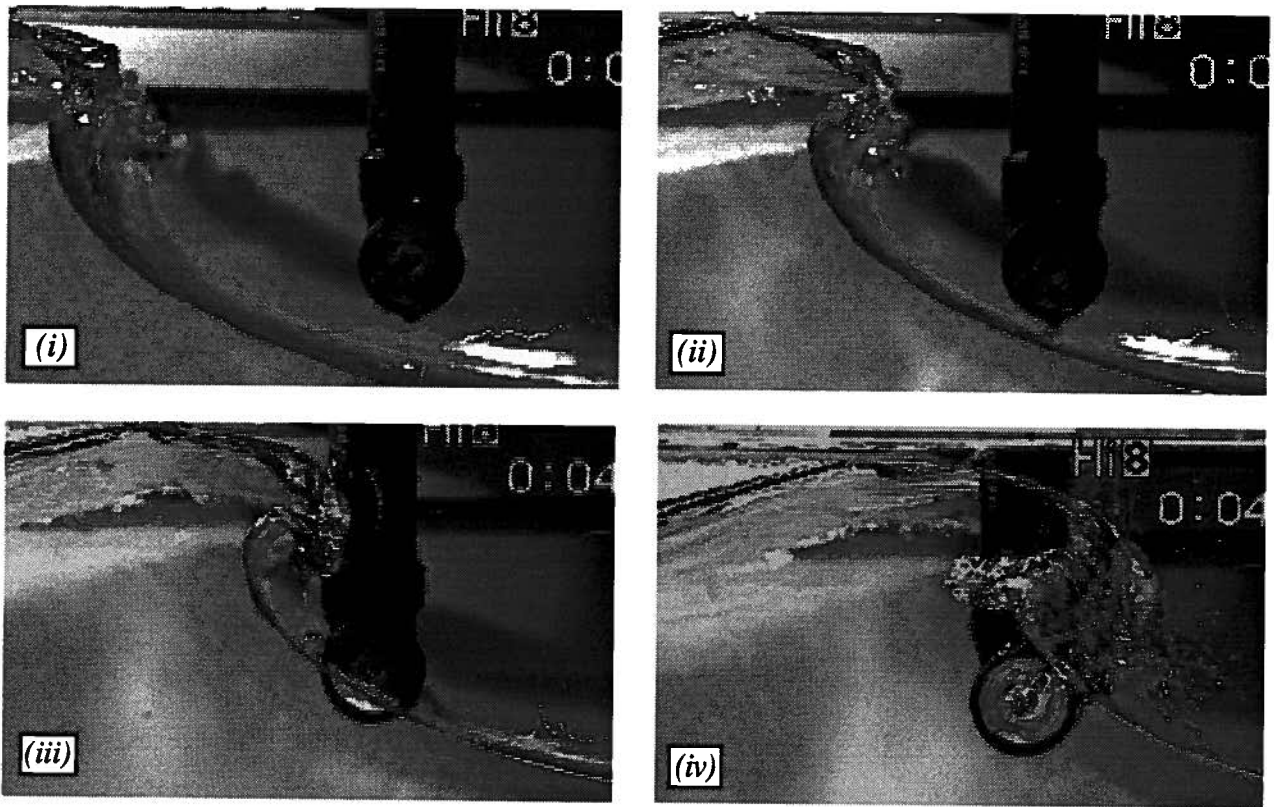


Fig. 4.34 Sequence of video frames showing plunging wave impact on horizontal test cylinder.
 $h = 4.7$ cm, $x_b = 25.5$ cm.

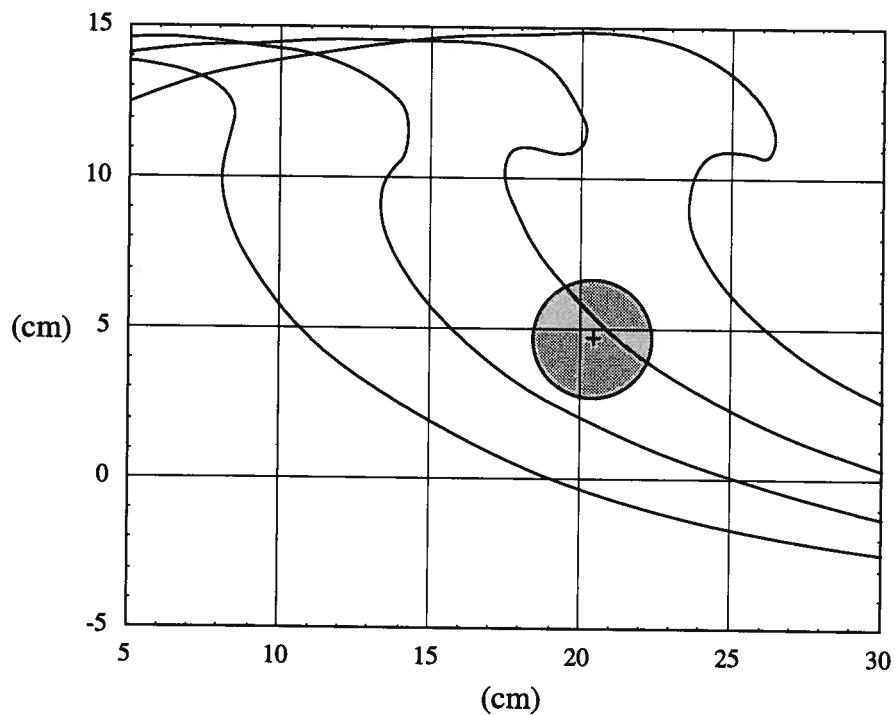


Fig. 4.35 Digitized profiles of plunging wave in the vicinity of the horizontal test cylinder.
 $h = 4.7$ cm, $x_b = 36$ cm.

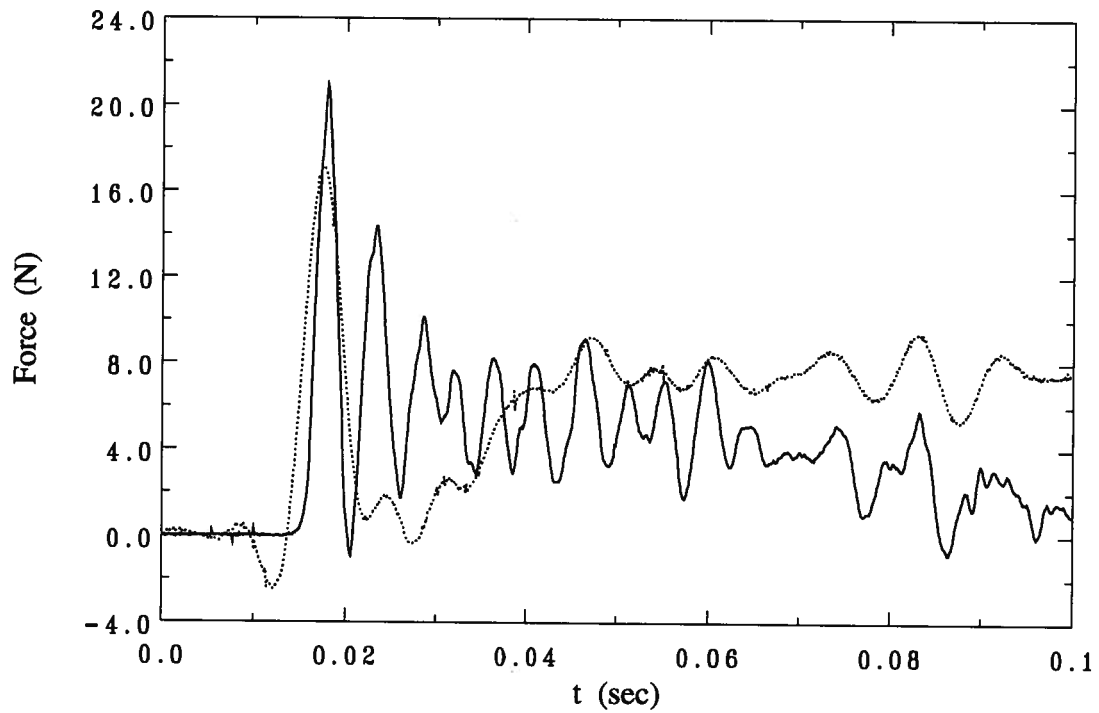


Fig. 4.36 Time histories of recorded vertical force (—) and corrected horizontal force (·····) on horizontal test cylinder due to breaking wave impact. $h = 4.7$ cm, $x_b = 25.5$ cm.

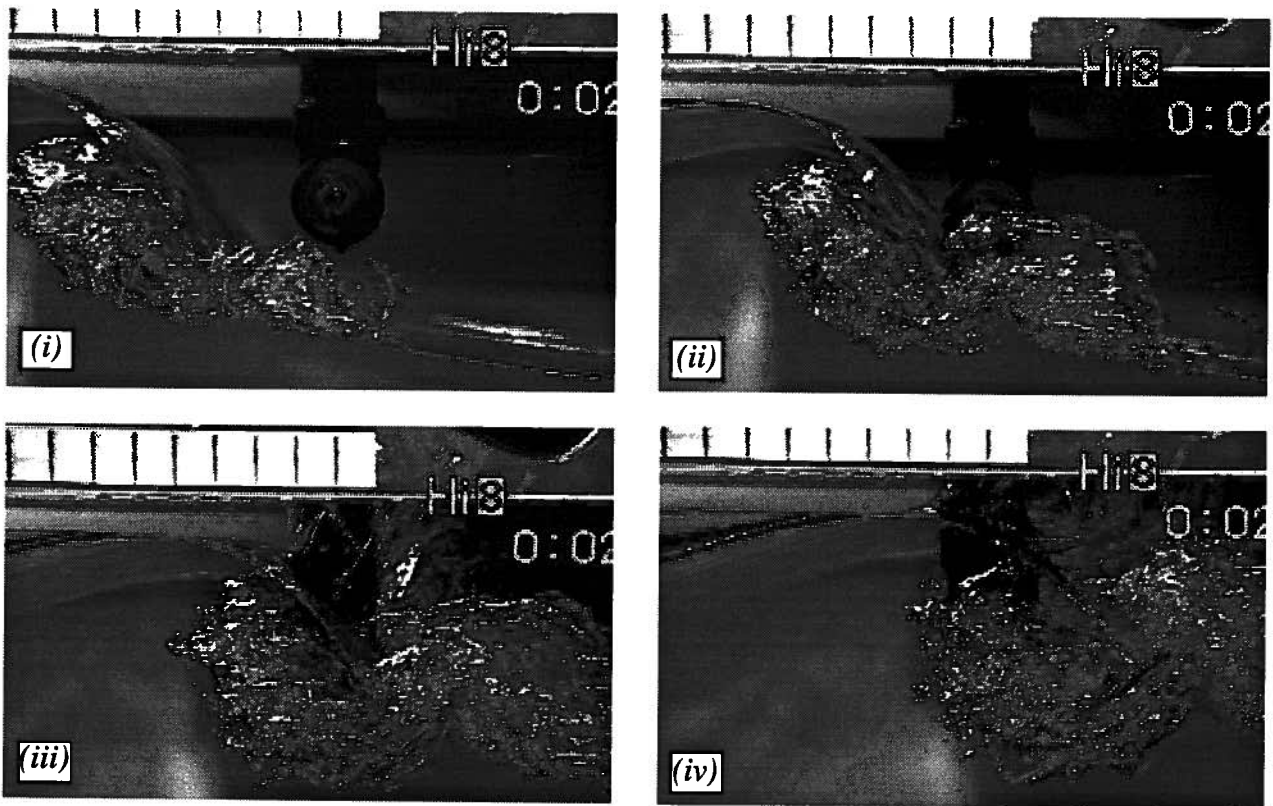


Fig. 4.37 Sequence of video frames showing plunging wave impact on horizontal test cylinder. $h = 8.7$ cm, $x_b = -3.5$ cm.

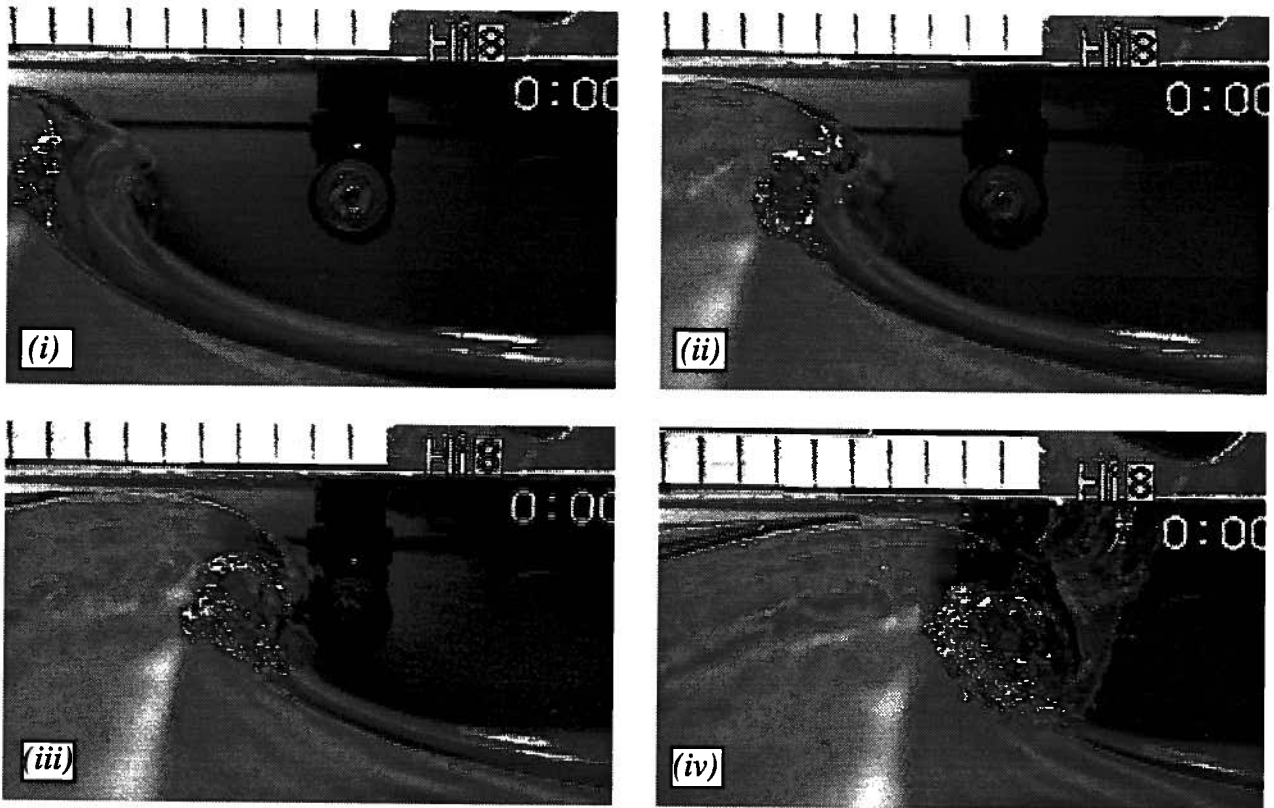


Fig. 4.38 Sequence of video frames showing plunging wave impact on horizontal test cylinder.
 $h = 8.7$ cm, $x_b = 25.5$ cm.

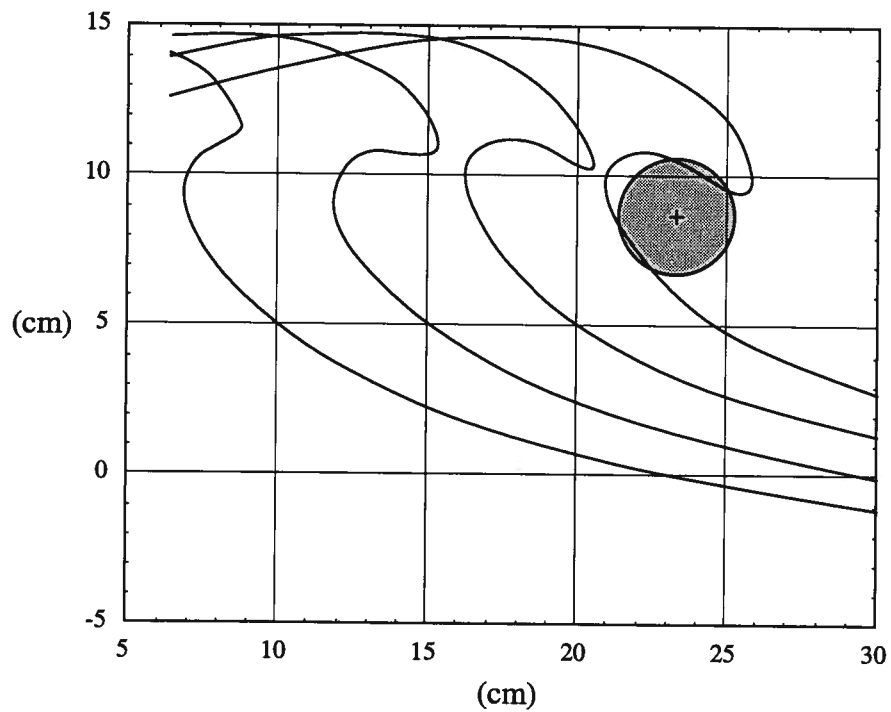


Fig. 4.39 Digitized profiles of plunging wave in the vicinity of the horizontal test cylinder.
 $h = 8.7$ cm, $x_b = 25.5$ cm.

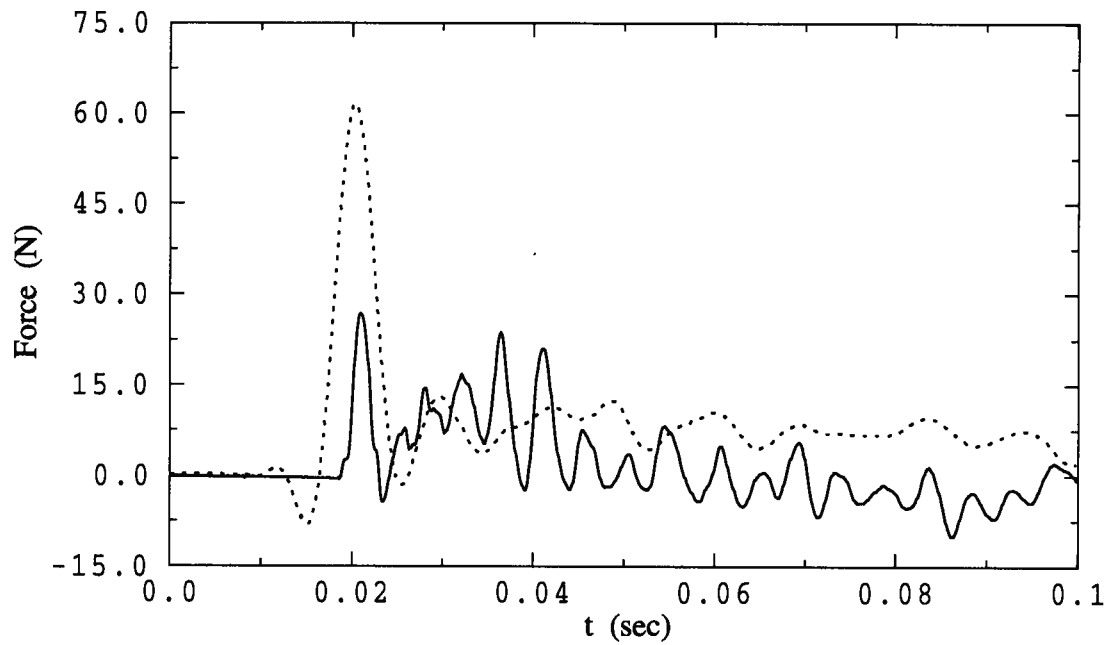


Fig. 4.40 Time histories of recorded vertical force (—) and corrected horizontal force (·····) on horizontal test cylinder due to breaking wave impact. $h = 8.7$ cm, $x_b = 25.5$ cm.

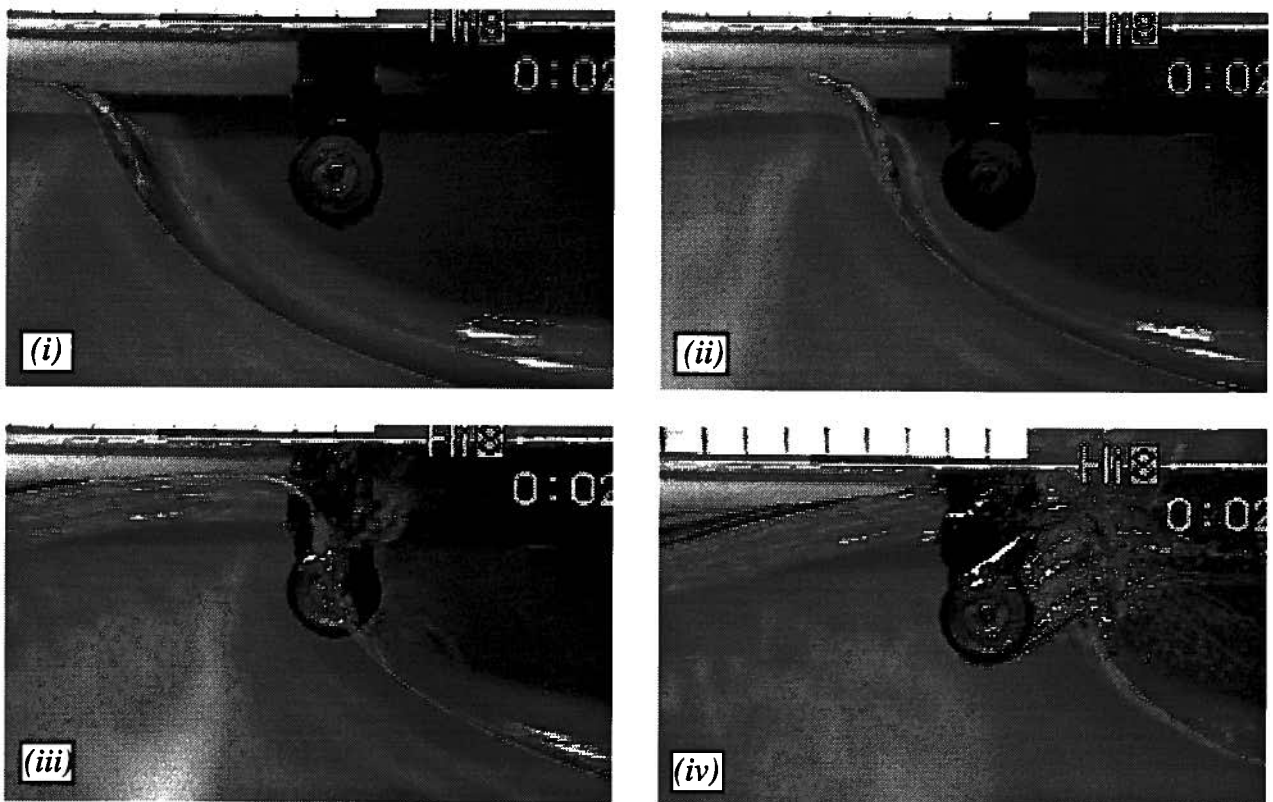


Fig. 4.41 Sequence of video frames showing plunging wave impact on horizontal test cylinder. $h = 8.7$ cm, $x_b = 49$ cm.

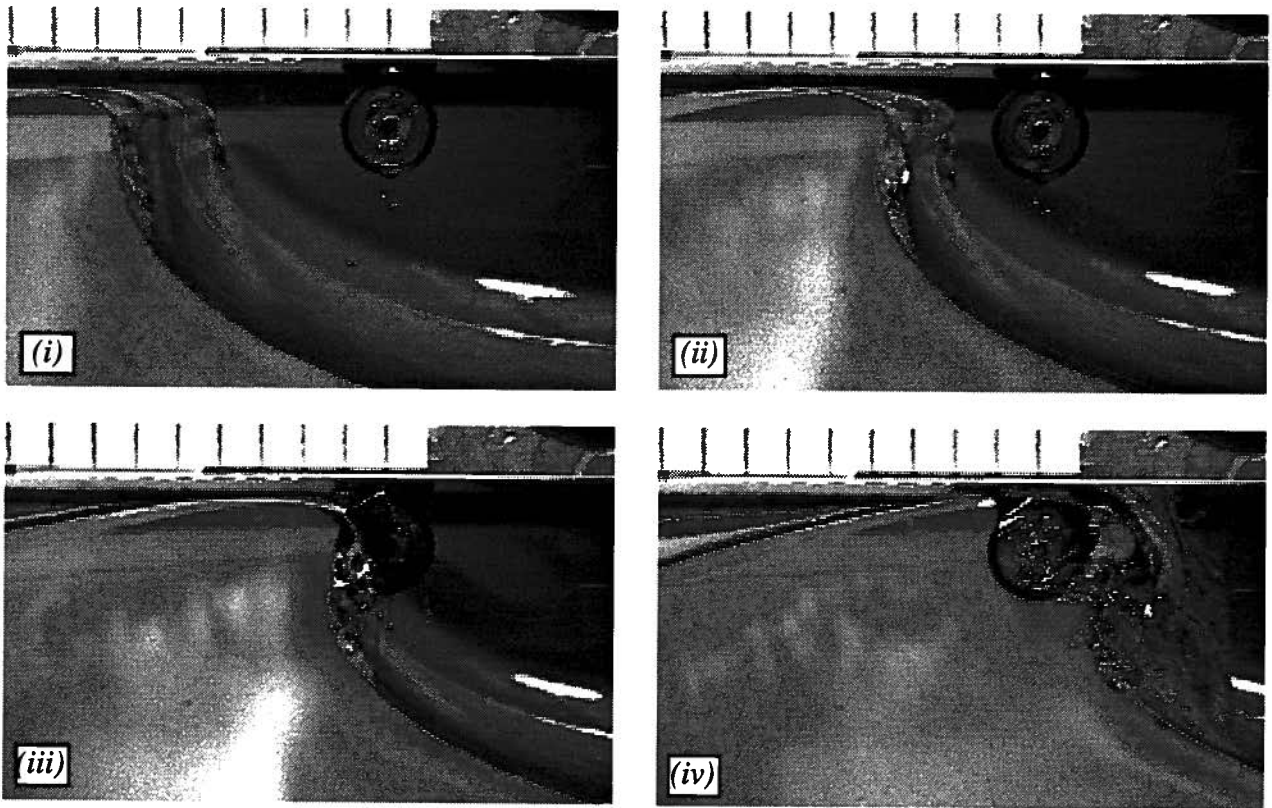


Fig. 4.42 Sequence of video frames showing plunging wave impact on horizontal test cylinder.
 $h = 12.7$ cm, $x_b = 25.5$ cm.

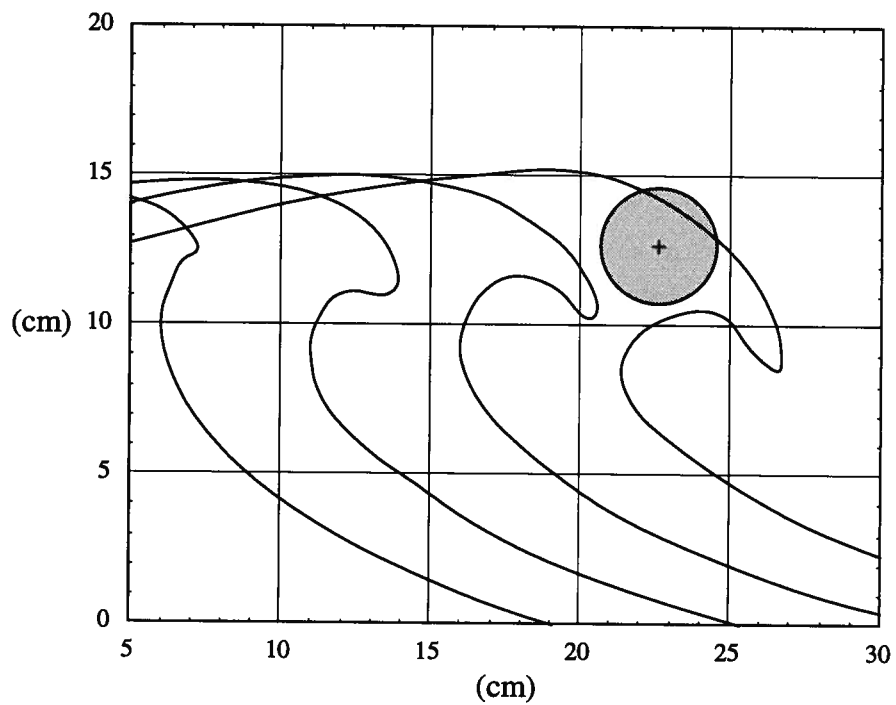


Fig. 4.43 Digitized profiles of plunging wave in the vicinity of the horizontal test cylinder.
 $h = 12.7$ cm, $x_b = 17$ cm.

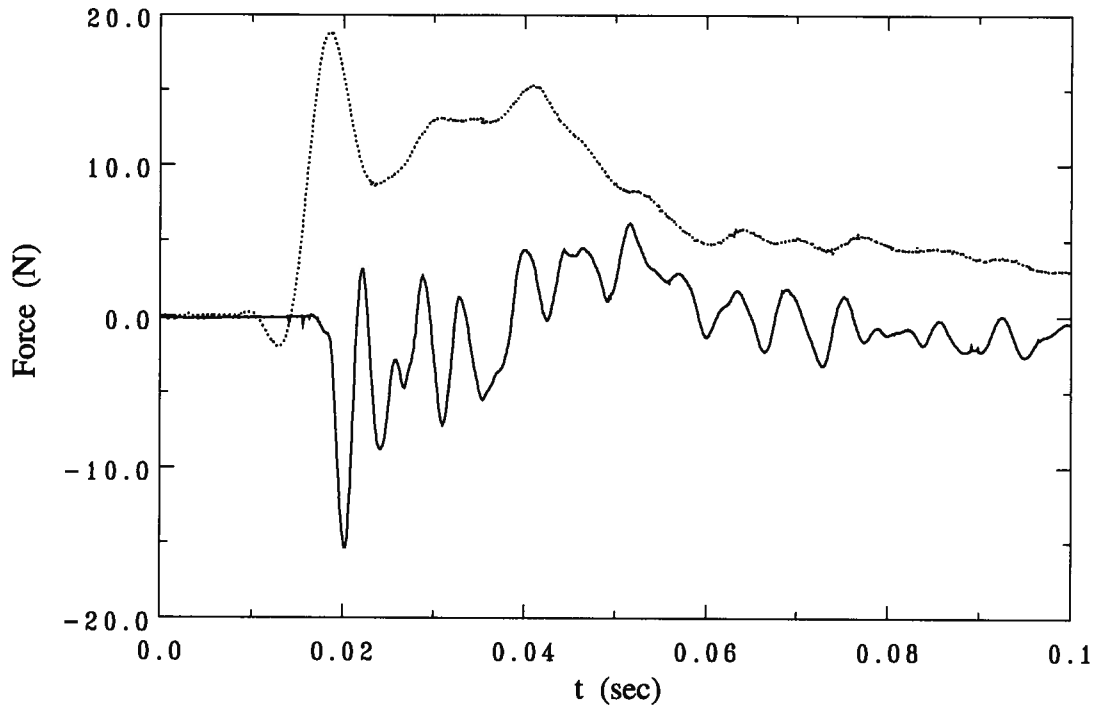


Fig. 4.44 Time histories of recorded vertical force (————) and corrected horizontal force (······) on horizontal test cylinder due to breaking wave impact. $h = 12.7$ cm, $x_b = 25.5$ cm.